UNIVERSITÉ DE LORRAINE

Ecole Doctorale C2MP (Chimie - Mécanique - Matériaux- Physique)

Thèse

Présentée et soutenue publiquement pour l'obtention du titre de

DOCTEUR DE l'UNIVERSITE DE LORRAINE

Mention : « Chimie »

par Elena YUNDA

Conception de surfaces chimio-structurées pour l'étude de l'adhésion bactérienne et la formation contrôlée des biofilms bactériens

1er octobre 2019

Membres du jury :

Rapporteurs :	Sophie LECOMTE	Directrice de recherche, CNRS, Bordeaux
	Yves BLACHE	Professeur, Université de Toulon, Toulon
Examinateurs :	Karine GLINEL	Professeure, Université catholique de Louvain, Louvain-la-Neuve
	Frédéric BORGES	Maître de conférences, Université de Lorraine, Nancy
	Fabienne QUILES	Chargée de Recherche, CNRS, Nancy, directrice de thèse
	Halima ALEM-MARCHAND	Maître de conférences, Université de Lorraine, Membre Junior Institut Universitaire de France, co-directrice de thèse

A c k n o w l e d g e m e n t s

Abstract

Biofilm formation by pathogenic bacteria brings concerns, particularly in food and medical sectors, and is associated with high sanitary risks and economic losses. Therefore, preventing their growth is of great importance. The biofilms of probiotic bacteria can potentially be used to prevent the surface contamination by pathogenic species. Therefore, this work was focused on the investigation of the development of biofilms of probiotic *Lactobacillus rhamnosus* GG (LGG) and the possible control of their formation by combining surface functionalisation processes and physico-chemical approaches. The effect of different environmental conditions on the kinetics of the biofilm growth and on its biochemical composition was analysed by *in situ* and real time measurements with infrared spectroscopy in attenuated total reflection mode (ATR-FTIR) under flow conditions. These data were complemented by epifluorescence images providing information on the surface distribution and the shape of bacterial cells at specific stages of the biofilm development. Compatible with ATR-FTIR measurements zinc selenide (ZnSe) crystal was chosen as a substrate, bare or functionalised with self-assembled monolayers (SAMs). SAMs were formed from alkanethiols terminated by methyl ($-CH_3$), hydroxyl ($-OH$) or amine ($-NH_2$) groups to obtain hydrophobic, hydrophilic and positively charged substrates, respectively. The examination of the physico-chemical properties of ZnSe, alkanethiol SAMs and cultivated LGG biofilms was performed successively. The kinetics of self-assembly of the alkanethiols onto ZnSe, the organisation of molecules, their areal density and the surface energy of thus obtained surfaces were studied preliminarily to the biofilm cultivation by means of ATR-FTIR spectroscopy, high energy Rutherford backscattering spectrometry, and contact angle measurements. The results were compared with SAMs formed onto gold-coated ZnSe (Au/ZnSe) crystals, as the properties of SAMs on gold, unlike on ZnSe, have been widely described. Substrates with a well-defined surface chemistry were obtained on both ZnSe and Au/Znse, on which bacterial cells behaved similarly. The analysis of the ATR-FTIR spectra of LGG biofilms recorded continuously revealed an important role of the nutritive medium in the biosynthesis of nucleic acids, phospholipids, polysaccharides and lactic acid. The surface coverage with bacteria and the shape of LGG cells were also medium-dependent. Substrate properties had low impact on the biochemical composition and

shape of LGG cells, but had a critical role in the strength of attachment of cultivated biofilms. The adhesive forces between LGG and the different alkanethiol molecules were increasing in the order -OH < -CH$_3$ << -NH$_3^+$. The changes in the mechanical stress conditions have thus provoked a total removal of the biofilm from substrates with –OH and -CH$_3$ groups, whereas the retention was high on the substrate with –NH$_3^+$ groups. On the latter substrate, the cells were not damaged and provided a fully covered surface after 26.5 hours of cultivation. Finally, the potential of LGG to prevent the growth of pathogenic biofilms was estimated using as a model a strain of *Escherichia coli*. The results of the preliminary assays have shown a penetration of *E. coli* in the LGG biofilm, suggesting more complex mechanisms of LGG antipathogenic action, than a simple prevention of the adhesion. The findings of this multidisciplinary work provide a fundamental understanding of how the direct environment, including a support surface, influences the properties of bacterial biofilms at the molecular and cellular scales, based on which favourable conditions for the enhancement or inhibition of biofilm growth and its mechanical stability can be chosen. The potential of the ATR-FTIR method in the research of bacterial adhesion is highlighted through the development of ZnSe substrates with controlled surface properties.

Résumé

La formation de biofilms avec des bactéries pathogènes est un problème important, particulièrement dans les secteurs médicaux et agro-alimentaires. Ils sont associés à des risques sanitaires ainsi qu'à des pertes économiques. La formation contrôlée de biofilms du probiotique *Lactobacillus rhamnosus* GG (LGG) est sélectionnée ici comme méthode potentielle pour prévenir la contamination de surfaces par des bactéries pathogènes. Nous avons donc étudié le développement de biofilms de LGG ainsi que leur possible contrôle en combinant des approches physico-chimiques et de fonctionnalisation de surface. L'impact des conditions environnementales sur la cinétique de croissance des biofilms et sur leur composition biochimique a été analysé par des mesures *in situ* et en temps réel par spectroscopie infrarouge à transformée de Fourier en réflexion totale atténuée (ATR-FTIR) sous conditions de flux. Ces données ont été complétées par des images de microscopie en épifluorescence permettant d'obtenir des informations sur la distribution et la forme des cellules bactériennes sur la surface à des étapes clé du développement du biofilm. Compatible avec les mesures ATR-FTIR, un cristal de séléniure de zinc (ZnSe) a été choisi comme substrat, nu ou fonctionnalisé avec des monocouches auto-assemblées d'alcane-thiols (SAMs). Différents groupes fonctionnels ont été étudiés : méthyl (-CH$_3$), hydroxyle (-OH) ou amine (-NH$_2$) pour obtenir respectivement des substrats hydrophobe, hydrophile ou chargé positivement. Une étude physico-chimique approfondie de la surface du ZnSe, des SAMs et de leur impact sur la croissance des biofilms cultivés de LGG a été successivement effectuée. La cinétique d'auto-assemblage des SAMs, leur organisation et l'énergie de surface ont été étudiées en combinant ATR-FTIR, spectroscopie de rétrodiffusion de Rutherford à hautes énergies et mesures d'angles de contact. Les résultats ont été comparés avec ceux des SAMs formées sur un cristal de ZnSe couvert d'une couche d'or, déjà largement décrits dans la littérature. Des surfaces chimiquement bien contrôlées ont été obtenues sur les deux types de substrat, sur lesquels le comportement des bactéries a été similaire lors de la croissance des biofilms. L'analyse des spectres ATR-FTIR des biofilms de LGG enregistrés pendant 24 heures a montré un rôle important du milieu nutritif sur la composition biochimique et le métabolisme bactériens. Le recouvrement de surface par les bactéries et la forme des cellules de LGG sont aussi affectés par les conditions

nutritives. Les propriétés du substrat ont un impact faible sur la composition biochimique et la forme des cellules de LGG, mais ont un rôle crucial sur la force d'attachement des biofilms. Les forces d'adhésion entre LGG et la surface fonctionnelle sont croissantes dans l'ordre : OH < -CH$_3$ << -NH$_3^+$. Des conditions de stress mécanique ont ainsi provoqué un lessivage complet des biofilms cultivés sur les SAMs avec les fonctions -OH et -CH$_3$, contrairement au NH$_3^+$ qui permet une adhésion bactérienne importante. Sur ce substrat, les cellules n'étaient pas endommagées et le recouvrement total de la surface a été observé après 26,5 heures de croissance. Dans un dernier temps, la capacité de LGG à empêcher la croissance de biofilms pathogènes a été estimée avec une souche d'*Escherichia coli*. Les résultats d'essais préliminaires ont montré la pénétration d'*E. coli* dans le biofilm de LGG. Ce résultat suggère des mécanismes plus complexes d'action anti-pathogène de LGG que de simples propriétés anti-adhésives. Finalement, ce travail a fourni des informations sur l'influence de l'environnement, et particulièrement des caractéristiques du support, sur les propriétés des biofilms aux échelles moléculaire et cellulaire. Nous avons mis en évidence les capacités de la méthode ATR-FTIR dans le domaine de la recherche sur l'adhésion bactérienne à travers le développement de substrats dont les propriétés de surface sont contrôlées.

Résumé en français

Lactobacillus rhamnosus GG (LGG) est une bactérie probiotique en vente libre. Un probiotique est un micro-organisme vivant, qui, administré ou consommé en quantité suffisante, exerce des effets positifs sur la santé de l'individu hôte. LGG est reconnue pour son efficacité dans la prévention et la lutte contre plusieurs types de diarrhées et certaines infections du système digestif. Dans ce cadre, l'adhésion de LGG aux cellules épithéliales de l'intestin est un facteur important contribuant à sa protection. Ainsi, une stratégie prometteuse consiste à développer des surfaces artificielles qui favorisent la colonisation de LGG sur des matériaux d'intérêt pour bénéficier de son activité de lutte contre la colonisation par des bactéries pathogènes, notamment sur des surfaces en contact avec des produits alimentaires. Développer des surfaces à chimie contrôlée permettra de comprendre les interactions entre la bactérie et une surface. Il sera possible par la suite d'optimiser ces surfaces afin de promouvoir la croissance de biofilms bénéfiques dans le cadre de futures applications industrielles. Le paramètre clé de cette étude est l'influence de la chimie de la surface considérée sur l'adhésion et la colonisation bactériennes. Une fois l'adhésion irréversible de biofilms de LGG réalisée, sera-t-il possible d'empêcher grâce à l'ingénierie de surface développée l'adhésion d'une bactérie concurrente comme *Escherichia coli*, souvent impliquée dans les contaminations alimentaires ?

L'adhésion de différentes bactéries sur des surfaces modifiées chimiquement a déjà fait l'objet de quelques études. Elles testent l'influence de l'hydrophilie/hydrophobie, la charge de surface ou encore l'organisation à l'échelle nanométrique de la surface (nano-structuration) par des méthodes de la microbiologie classique et de microscopie en fluorescence. Dans ce projet, nous proposons l'utilisation d'approches physico-chimiques combinées à des méthodes de microbiologie classique pour l'étude de biofilms bactériens. L'impact des conditions environnementales sur la cinétique de croissance des biofilms et sur leur composition biochimique a été analysé par des mesures *in situ* et en temps réel (c'est-à-dire directement dans leur milieu et de manière non destructive) par spectroscopie infrarouge à transformée de Fourier en réflexion totale atténuée (ATR-FTIR) sous conditions de flux. Ces données ont été complétées par des images de microscopie en épifluorescence permettant d'obtenir des informations sur la distribution et la forme des cellules bactériennes sur la surface

à des étapes clé du développement du biofilm. Compatible avec les mesures ATR-FTIR, le séléniure de zinc (ZnSe) a été choisi comme substrat. Pour élaborer les surfaces à chimie contrôlée, les monocouches auto-assemblées (SAMs) d'alcane-thiols sont sélectionnées car elles permettent de donner une fonctionnalité à la surface avec une grande stabilité. Les propriétés des SAMs d'alcane-thiols sur l'or ont déjà été largement décrites dans la littérature ces trois dernières décennies, alors que très peu d'études se sont intéressées à l'adsorption d'alcane-thiols sur les cristaux de ZnSe. Nous avons donc réalisé une étude approfondie des propriétés de ces SAMs sur le ZnSe nu ou recouvert par une couche mince d'or (~3 nm). Différents groupes fonctionnels terminaux ont été étudiés : méthyl (-CH₃), hydroxyle (-OH) ou amine (-NH₂) pour obtenir respectivement des substrats hydrophobe, hydrophile ou chargé positivement. L'influence de la nature de la nouvelle fonctionnalité de surface sur l'adhésion et la croissance des biofilms a ensuite été étudiée et mise en évidence.

Une étude physico-chimique de la surface du ZnSe, des SAMs et de leur impact sur la croissance des biofilms de LGG a été effectuée. Les étapes successives de cette étude sont rassemblées dans le schéma de la figure 1 et sont décrites ci-dessous.

1) Effet du milieu nutritif sur le développement des biofilms LGG.

Comme les bactéries sont des objets vivants, leur comportement dépend fortement de la disponibilité et de la qualité des nutriments. Les nutriments consommés par les bactéries influencent la composition de leurs cellules, ce qui conduit directement à la variation de leurs propriétés physiologiques. Par conséquent, le premier chapitre de ce manuscrit porte sur l'étude de l'influence de trois milieux nutritifs sur le développement des biofilms de LGG. Deux de ces milieux sont recommandés pour la culture des lactobacilles (MRS, AOAC), et le troisième est compatible avec la croissance de nombreuses de souches bactériennes (mTSB). Pour les expériences sur les biofilms, ces milieux ont été utilisés à une dilution au dixième par rapport aux recommandations du fabricant (ils sont notés ci-après MRS/10, AOAC/10 et mTSB/10). Cette faible concentration en nutriments permet de réduire les interférences liées au milieu de culture dans le spectre infrarouge des biofilms pendant leur culture, tout en conservant la croissance bactérienne. L'analyse des spectres ATR-FTIR enregistrés pendant 24 heures lors du développement des biofilms de LGG a montré un rôle important du milieu nutritif sur la biosynthèse des acides nucléiques,

des phospholipides, des polysaccharides et de l'acide lactique. De plus, la synthèse de l'acide lactique a été observée en fonction du temps dans le milieu MRS/10 et AOAC/10. La production maximale de polysaccharides a été observée dans le milieu mTSB/10, et les biofilms obtenus sont les plus denses. D'importants changements dans la forme des bactéries ont aussi été observés, ils sont liés à la mauvaise qualité nutritionnelle (mTSB/10) ou à l'acidité induite (AOAC/10) des milieux nutritifs. Malgré ses pauvres qualités nutritives, le milieu mTSB/10 a été conservé pour la culture ultérieure des biofilms de LGG car il présente les conditions les plus favorables pour un fort recouvrement de la surface.
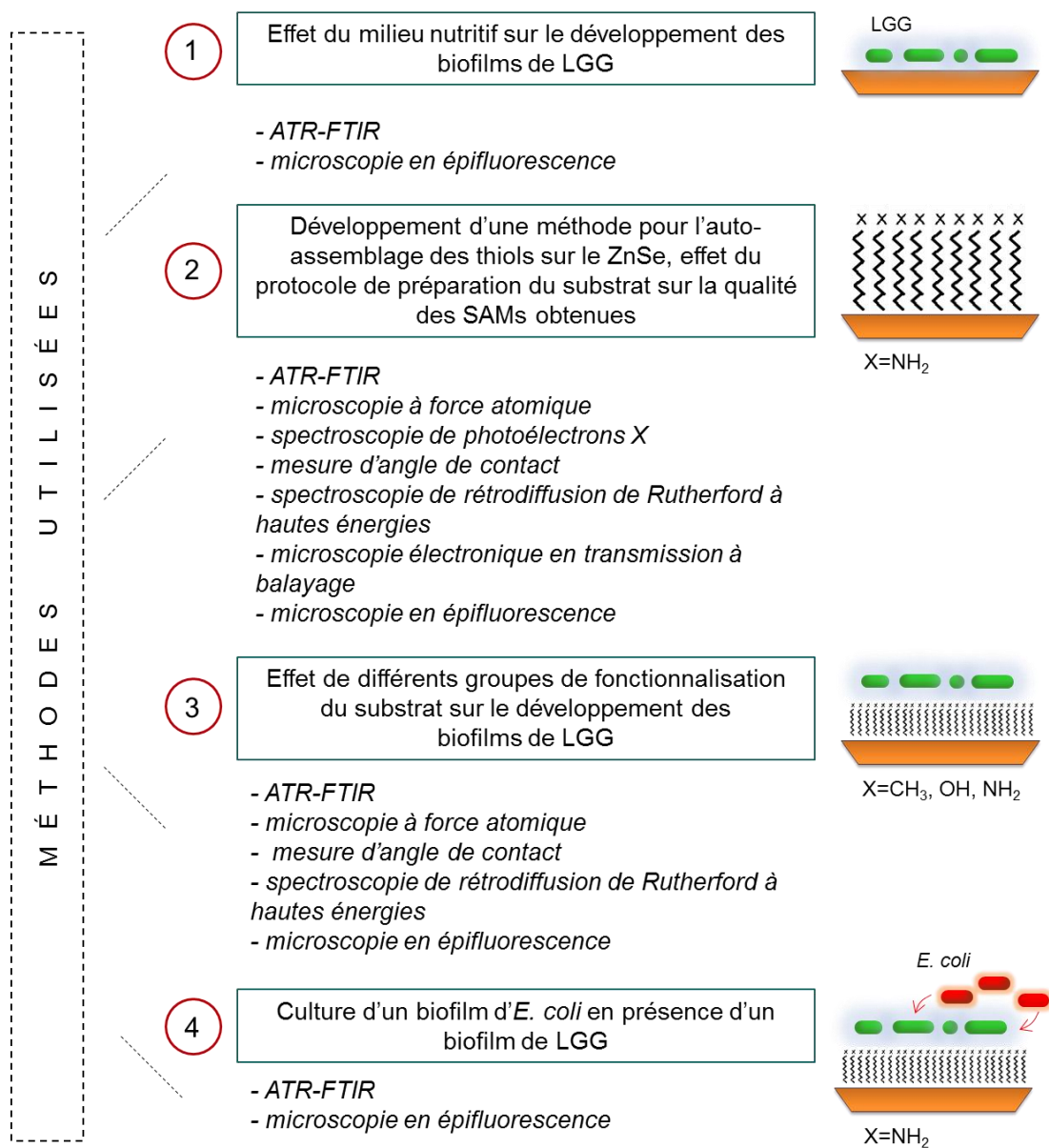

Figure 1. Schéma de l'organisation du projet

2) Développement d'une méthode pour l'auto-assemblage de thiols sur le ZnSe : effet du protocole de préparation du substrat sur la qualité des SAMs obtenues.

Après avoir établi le rôle du milieu nutritif sur la croissance de LGG sur le ZnSe, nous avons porté notre attention sur le rôle du substrat sur la croissance de LGG sous forme sessile. La stratégie de ce projet inclue la fonctionnalisation chimique par un thiol, nous avons donc étudié l'importance des propriétés du substrat sur l'organisation des SAMs. Notamment, nous avons montré que la procédure de préparation de la surface du cristal préalablement à la réaction chimique avec le thiol est une étape importante à considérer. Les résultats obtenus nous ont permis de conclure que les SAMs étaient plus organisées et plus denses sur le ZnSe recouvert d'or que sur le ZnSe nu. Ces différences n'ont, en revanche, pas de conséquences notables sur les caractéristiques finales des biofilms de LGG. Par conséquent, nous avons synthétisés les différentes SAMs directement sur le ZnSe, c'est-à-dire sans dépôt d'une couche d'or préalable.

3) Influence des différents groupes fonctionnels du substrat sur le développement des biofilms de LGG.

L'influence des propriétés fonctionnelles du substrat sur la composition biochimique et la force d'attachement des biofilms de LGG sur les groupes fonctionnelles ont été abordées ensuite dans ce travail. Nous avons montré que LGG peut adhérer et croître sur les surfaces modifiées avec différents groupes fonctionnels. Cependant, des conditions de stress mécanique appliquées aux différents biofilms ont montré que leur rétention est fortement dépendante de la surface sur laquelle ils sont cultivés. En effet, les valeurs mesurées des forces d'interaction entre LGG et les différents thiols sont les plus grandes avec les groupements $-NH_3^+$. Un biofilm dense avec un recouvrement complet de la surface a été obtenu sur ce substrat après 26,5 heures d'incubation. De plus, nous avons montré que la membrane des cellules de LGG reste intacte malgré la forte interaction électrostatique observée sur ce substrat.

4) Culture d'un biofilm d'*E. coli* en présence d'un biofilm de LGG.

Le dernier chapitre est dédié à l'estimation du potentiel de LGG pour la prévention de la croissance d'un biofilm pathogène. *E. coli* est un bon modèle de bactéries d'intérêt sanitaire d'origine fécale. La souche d'*E. coli* utilisée ici a une forte capacité d'adhésion sur les surfaces grâce à la présence de fimbriae de type 1. Elle exprime aussi la

protéine fluorescente *gfp*. Pour distinguer les deux bactéries sur les images obtenues avec le microscope en épifluorescence, nous avons utilisé la même souche de LGG mais modifiée génétiquement pour exprimer une autre protéine fluorescente (*mTag*). Les résultats de ces essais préliminaires ont montré que le milieu nutritif lui-même joue déjà un rôle important sur la croissance d'*E. coli* sous forme sessile. Cette observation montre l'importance du choix du milieu dans des essais d'interférences bactériennes. Les résultats obtenus ont montré la pénétration d'*E. coli* dans le biofilm de LGG, suggérant des mécanismes plus complexes d'action anti-pathogène de LGG que de simples propriétés anti-adhésives. Nous avons montré ici, qu'il est aussi intéressant d'associer les résultats obtenus par spectroscopie ATR-FTIR à ceux obtenus par microscopie à épifluorescence pour analyser des biofilms composés de deux souches bactériennes. Ces résultats suggèrent des interactions particulières entre cellules bactériennes qui méritent des études supplémentaires à conduire dans le futur.

Pour conclure, ce travail a fourni des informations sur l'influence de l'environnement, et particulièrement des caractéristiques du support, sur les propriétés de biofilms bactériens aux échelles moléculaires et cellulaires. Ainsi, des conditions favorables pour la promotion de la formation de biofilms stables ou l'inhibition de leur développement peuvent être contrôlées. Nous avons mis en évidence la puissance de la spectroscopie ATR-FTIR dans l'étude du suivi de l'adhésion bactérienne à travers le développement de substrats dont les propriétés de surface sont contrôlées. Dans cette perspective, il serait intéressant d'étudier les interactions de LGG *in situ* avec des molécules plus complexes, comme par exemple des protéines du lait. De plus, une étude avec d'autres espèces bactériennes comme modèles d'organismes pathogènes peut offrir un aperçu du potentiel de LGG dans la préservation des surfaces envers la contamination par d'autres espèces. Des résultats prometteurs ont été obtenus dans ce travail dans le cadre de cette stratégie, car le biofilm de LGG obtenu ici est stable mécaniquement, physiologiquement actif, et il présente une distribution bactérienne de surface très homogène.

Table of contents

General introduction

Bacterial adhesion to surfaces with subsequent development into closely linked populations (biofilms) is of great concern, particularly, in food industries and medicine fields. The sanitary risks and economic losses are especially associated with contamination of surfaces of food and medical equipment with biofilms of pathogenic species. On the other hand, biofilms composed of non-pathogenic bacteria might be beneficial. Thus, probiotic bacteria (i.e. live microorganisms that when administered in adequate amounts confer a health benefit on the host) play an important role in the protection of human intestinal epithelial cells. The adhesion of probiotic bacteria to biological tissues is considered as prerequisite for such protection mechanism, and in particular for the inhibition of the development of biofilms of pathogens. Inspired by mechanisms of probiotic action in the human intestine, the strategy to protect abiotic surfaces from contamination with unwanted microorganisms using probiotics as bio-protective coating has emerged recently. To advance this strategy, it is of great importance to understand the properties of probiotic biofilms and their support surfaces, as well as interactions occurring at their interface. What types of interactions with the substrate would lead to the formation of a dense and mechanically stable biofilm of probiotics? Are the cells physiologically active in these biofilms? Could they act, under those conditions, against adhesion and growth of pathogenic species? The research strategy selected in this PhD project was driven by these questions.
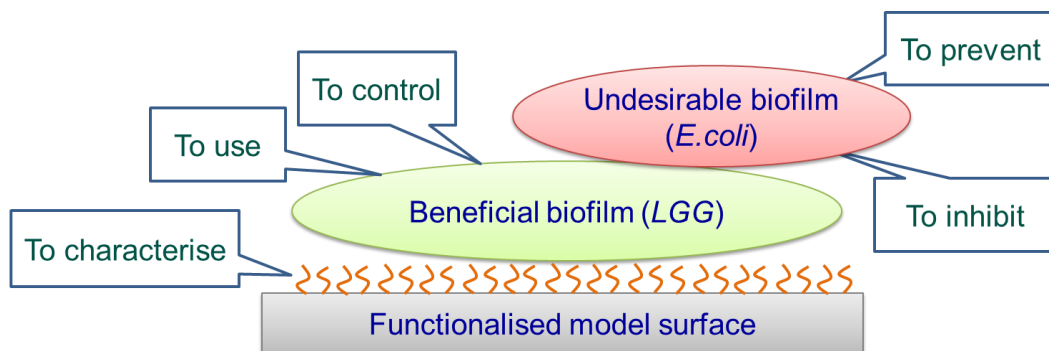
Figure 2. Graphical abstract of the concept of this project

As it is shown in figure 2, we selected two bacterial strains as models to carry out this work. *Lactobacillus rhamnosus* GG (LGG) is one of the best-studied probiotics in the clinical field, and widely used in food products and supplements. *Escherichia coli*, a

commensal bacterium that, depending on the strain, may present a virulence action, was chosen as a model of challenging biofilm to test the antipathogenic properties of LGG. Several nutritive conditions and substrates with different functional properties were studied in this work for the possible promotion of LGG adhesion and biofilm growth to understand the role of the environment in these two processes. The major attention was paid on the role of the support surface in the development of LGG biofilm. Chapter I describes the state of the art on the concerns associated with the formation of biofilms, the strategy for the prevention of pathogenic biofilms with the focus on the action of probiotics, as well as the methods for the analysis of biofilms and the role of the support surface in a biofilm life cycle. In chapter II, the materials and methods used in this work are presented. Chapter III presents the role of the nutritive medium in the development of LGG biofilm. Chapter IV is dedicated to the description of the effect of the substrate surface properties on the process of the substrate surface functionalisation and on the attachment of LGG. Chapter V reveals the impact of the functional groups on the substrate surface on the development of LGG biofilms. Finally, in chapter VI, the preliminary results of the assays estimating the antagonistic potential of LGG against *E. coli* adhesion and growth are discussed.

I. Scientific context

1.1 Introduction to biofilms

1.1.1. Biofilm – what is it made of and how does it form?

It is widely accepted now that in majority bacteria do not live alone, but prefer to gather in groups and accumulate at interfaces [1], [2]. Although, it took some time to realise it, truly accept it and integrate in research. That is somewhat ironic, as biofilms are everywhere around us. First, they are on us and in us. The teeth, the skin, and especially the intestine – we find there up to fifty percent (or more, the debates are still on [3]) of cells that originate from the foreign environment. Next, we shall look around. One way to start is by taking a bath. Basins, bathtubs and drains, shower shelves and curtains have all been reported as niches for biofilm growth [4]. A recent study on the "dark side" of bathtub toys has revived a broad attention to the topic [5]. Fundamentally, it is not so surprising. All organisms are vitally in need for water. It might well be expected then – wherever there is water biofilms will form easily. Luckily for us, water is abundant in nature with most of it found in oceans. It is clear then that a vast amount of research is directed on marine biofilms appearing both on biotic and abiotic surfaces. Regarding the latter ones, we often want to avoid biofouling as it leads to fast material wear and, associated with it, costs for a change or repair. However, sometimes it helps to clean the environment, for example by degradation of plastic [6]. Biofilms are found not only in sea, but also in contact with drinking water. They are harboured on pipes of the water systems even after disinfection treatments [7]. Understanding of biofilms is a key for providing safe water and, in its essence, a step towards better knowledge of anything that resides in an aqueous system.

Biofilms can be defined as communities of microorganisms embedded in a self-produced matrix of extracellular polymeric substances (EPS) and adherent to each other and/or a surface [8]. The first description of a biofilm is attributed to Antonie Von Leeuwenhoek (1632 – 1723) when he observed the microbes taken from his dental plaque under a self-constructed microscope. The term of biofilm as we know it today was introduced only in the 20th century, first, in environmental microbiology and few decades after in the medical field [9]. Biofilms can be single-species or multispecies,

bacterial or fungal. Importantly, a large part of a biofilm (up to 90 %) is represented by the extracellular matrix, the role of which in its lifestyle cannot be underestimated (figure 1.1). The matrix of a biofilm is a complex environment that is largely represented by polysaccharides, but also include proteins (enzymes, lectins and proteinaceous adhesins), lipids, nucleic acids and water, the latter being the major substance [10].
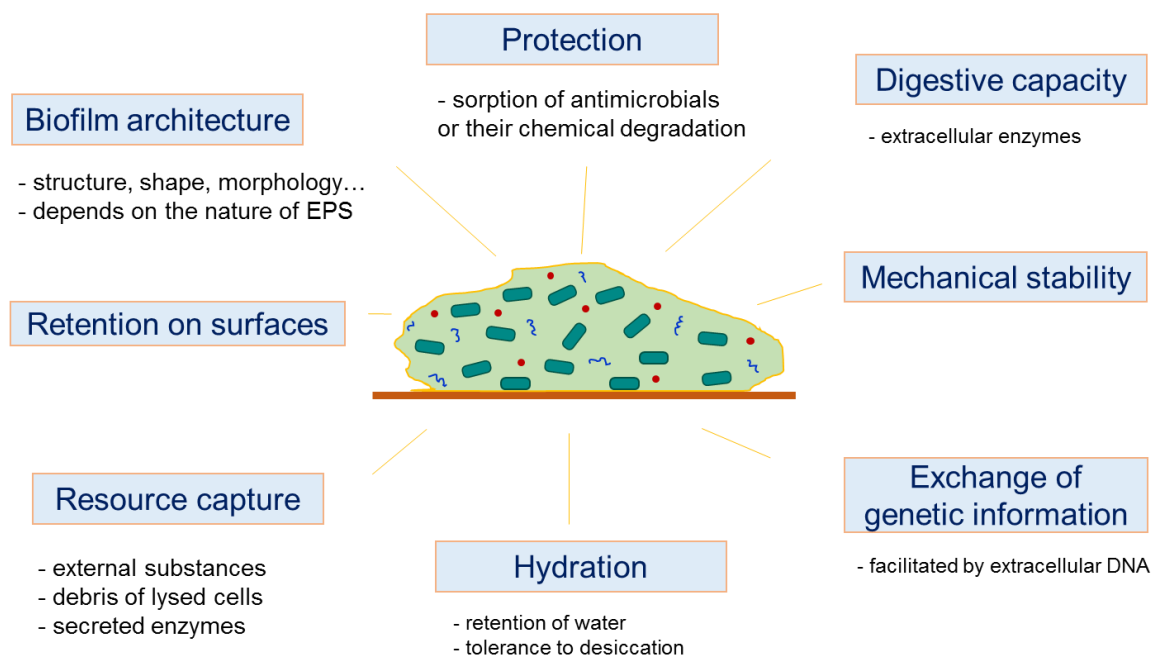
Figure 1.1. Functions of the extracellular matrix in a biofilm

Owing to a diverse composition of its matrix, biofilms are able to adapt to ever-changing environment making them extremely versatile inhabitants. However, the likeliness of biofilm growth and even more of its initiation is affected by many factors, i.e. microorganisms involved, surrounding nutrients, the nature of the substrate, and physico-chemical properties of the environment. Biofilms cultivated from specific bacteria are in the focus of this work.

Bacteria are prokaryotic (no membrane-defined nucleus) single-celled organisms that are varying in shapes (rod, sphere, curved, etc.) and have an average size of a few micrometres. Based on the features of the cell wall, bacteria are divided in two groups – Gram-positive and Gram-negative. This classification is based on the membrane differences which were observed in coloration tests with bacteria by Hans Christian Gram (1853 – 1938). In brief, the difference of two groups is in the thickness of the peptidoglycan layer, which is high in Gram-positive bacteria and much lower in Gram-

negative ones. In addition, the outer membrane composed mainly of lipopolysaccharides is present only in Gram-negative cells.

Many bacteria are motile thanks to the presence of extracellular appendages named flagella, common especially for rod-shaped bacteria. In addition, bacteria can possess surface appendages (pili in both types or fimbriae in Gram-negative cells), which help them adhere to substrates and keep them from washing away with a liquid flow. They also act as sensors for substrates aiding the cell to "realise" that it arrived to its proximity [11]. From here, given the substrate and nutrient conditions are suitable, the process of biofilm formation begins (figure 1.2).

planktonic cells

planktonic cells

sessile cells

EPS

arrival to the surface, reversible attachment

start of EPS production, transition to irreversible attachment

biofilm maturation

dispersion of cells
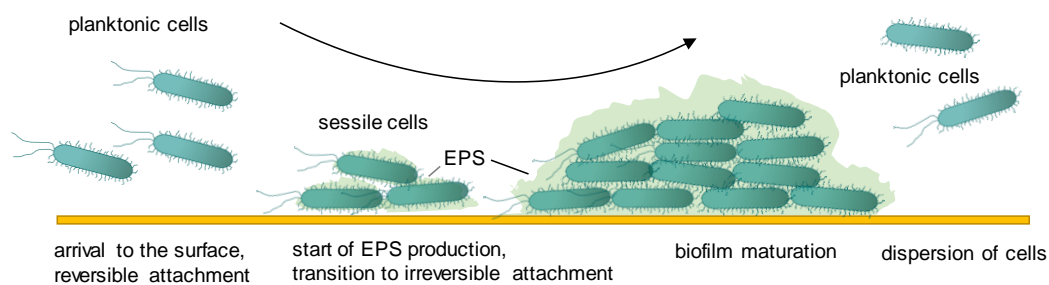
Figure 1.2. Schematic representation of biofilm development. Modified from [12]

Upon arrival to a surface, a cell will start to synthesise EPS. In the beginning, bacterial attachment is considered as reversible as gentle forces applied for example during rinsing flow will result in removal of the young biofilm from the surface. Later, the EPS layer will thicken up leading to the enhancement of mechanical stability of the biofilm. At this point, a biofilm has reached its maturation and its attachment to the surface is considered as irreversible. The further biofilm evolution will generate complex structural architecture, from which some cells eventually will be dispersed into surrounding environment. These planktonic cells will free-float in the medium until finding a new spot on the surface where they can join or initiate a biofilm again.

1.1.2. Sanitary risks associated with biofilms and strategies of their prevention

a) Nosocomial infections

Despite biofilms are so well integrated in nature, some of them bring sanitary concerns. This is especially the case in the medical field as up to 80 % of human bacterial infections are associated with biofilms [13]. Several bacteria, such as *Pseudomonas*

aeruginosa (*P. aeruginosa*), *Staphylococcus aureus* (*S. aureus*), and *Escherichia coli* (*E. coli*) are main causes of concern in hospital environment. For example, some strains of *P. aeruginosa,* develop persistent biofilms using the mechanism similar to "walking" as pili move across biotic and abiotic surfaces and producing thick alginate matrix [14]. Alginate is a very strong virulence factor affecting children with cystic fibrosis [15]. Critically ill people are, in general, of special consideration due to increased risk of bacterial infection associated with potentially contaminated devices used for health care. For example, ventilator-associated pneumonia (VAP) is the most common infection among the critically ill, whereas *P. aeruginosa* and *S. aureus* are its most frequent causes [16]. VAP is a major clinical and economical problem owning to significant mortality and prolonged hospital care, the latter resulting in elevated health care costs up to US$40,000 per episode [17]. Other nosocomial infections can be acquired through uropathogenic strains of *E. coli*. These strains use special proteinaceous adhesins (type 1 fimbriae) for specific binding to mannose sites on the uroepithelium, provoking an inflammatory response of the tissue [18]. For instance, urinary infections are the most common healthcare-associated infections in the United States, 75 % of which are associated with biofilms on a urinary catheter [19]. An additional risk of bacterial infection, especially for people with compromised health, is associated with the presence of biofilms of opportunistic pathogens in water distribution systems, which have only recently appeared as a subject of investigation. For example, mycobacterial populations were found to grow on hospital shower pipes, including strains provoking pulmonary and disseminated (spreading) infections in immunocompromised individuals [20]. *Legionella* strains are other representatives of pathogens that can be located in water distribution systems [21], [22]. These microorganisms are at the origin of life-threatening pulmonary diseases. Hence, it is of major importance to take timely measures to effectively eliminate or prevent biofilm appearance, especially in places with high level of risks of bacterial infections such as hospitals.

b) Contamination of food

Food-processing equipment is another potential source of pathogenic contamination, in case of which a large population of people may be affected. Some of the most frequent pathogens that contaminate food, the consumption of which results in an infection, include *Salmonella* strains, *E. coli*, *Listeria monocytogenes*

(*L. monocytogenes*) and *S. aureus.* In France for example, over 1000 cases of collective food poisoning occur annually affecting more than 10000 people sometimes with a fatal result [23]. In these outbreaks, pathogens were found in meat, fish, poultry, eggs, dairy products and ready-to-eat meals. Herein, more than half of reported poisoning cases that have occurred in catering establishments were contributed by contamination from equipment (figure 1.3). Thus, currently employed methods for cleaning and disinfection procedures or the awareness of maintaining hygiene of surfaces are not sufficient to eliminate pathogenic biofilms. For example, a study of Latorre et al. of the samples from a real milk farm have reported the presence of *L. monocytogenes* species on the equipment surface despite routine cleaning procedures with water, salts and acidic solutions [24]. The observation of the presence of pathogens in bulk tank milk for several months was consistent with the authors' hypothesis that continuous sloughing of cells from a biofilm on the used equipment could result in a subsequent continuous milk contamination. *L. monocytogenes* can be a cause of serious health disorders like gastroenteritis in healthy individuals or spontaneous abortion in pregnant women [25]. Of course, the process of milk pasteurisation would result in elimination of danger from pathogen presence. However, the consumption of raw milk is increasingly popular in recent years [26] with consequent raise of alarm towards sanitary risks in dairy industry.
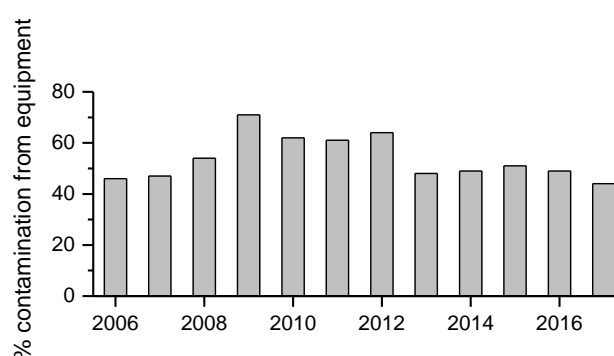
Figure 1.3. Percentage of collective food poisoning in catering establishments caused by pathogen source from equipment with respect to a total number of cases from 2006 to 2017 in France (data collected from the annual epidemiological reports of French National Public Health agency [23])

E. coli is also frequently reported as a contaminant of food products appearing there from animal sources and as a result of poor hygiene conditions. It should be mentioned that some *E. coli* strains are naturally present in the intestine constituting the human microbiome. However, some strains of *E. coli* are recognised as pathogenic due to virulence factors including production of potent toxins and/or invasion into epithelial

cells. These factors may provoke severe damage of the intestine and other organs such as kidneys [27]. The infection with *E. coli* is primarily associated with eating undercooked meat, but dairy products and other food may also be potential transporters [23], [28]. For example, a very recent case of collective poisoning in France has occurred owning to the presence of pathogenic *E. coli* in several types of cheese [29]. It led to at least 13 paediatric episodes of haemolytic-uremic syndrome, the symptoms of which include bloody diarrhoea, fever, vomiting, and weakness. The ultimate concern associated with *E. coli* biofilms is that only a slight contamination of surfaces (few hundreds organisms) may result in development of infection [30]. *E. coli* strains form biofilms in a very wide range of conditions – stainless steel, glass or polystyrene at 12, 20, or 37°C [31]. It is therefore clear that finding efficient treatment for disinfection of surfaces remains a difficult task.

c) Strategies to fight with pathogenic biofilms

The challenge associated with biofilm infections is due to the fact that most of research characterising the physiology of bacteria, including studies of response to antibiotics, has been performed on planktonic cells. However, bacteria in biofilms have higher resistance to antimicrobial treatment supported by extracellular matrix (figure 1.1), genetic adaptation and reduced metabolic and growth rates of bacteria [32]. The concentration of antibiotics required to inhibit or stop pathogen growth in biofilms can be 10 to 1000 times higher compared to their planktonic counterpart [33]. Hence, methods to inhibit bacterial growth developed using batch cultures cannot be directly applied for elimination of biofilms, and new strategies of antibacterial treatment are progressively developed, which are listed below.

Solving a problem of pathogenic biofilm formation involves two main directions that are referred here as "prevention from bottom" and "elimination from top" (figure 1.4). The former approach is based on the treatment of surfaces for avoiding or diminishing bacterial adhesion. Many treatments of such kind render the surface extremely hydrophobic. In such condition, the surface gains self-cleaning properties similar as exhibited by the leaves of some plants in nature, e.g. those of the lotus flower. Other types of surfaces are designed to release antimicrobial substances thus preventing bacterial development through a range of mechanisms as diffusion to the aqueous phase, erosion/degradation of loaded matrices (collagen, poly-dl-lactic acid, chitosan),

hydrolysis of covalent bonds (functionalised polymers), etc. [34]. The active compounds used in this kind of substrates inhibiting pathogen growth include silver, chlorhexidine, antibiotics, antimicrobial peptides – individually or as a mixture. Coatings releasing oxidizing agents such as hydrogen peroxide and other reactive oxygen species (ROS) were also reported as promising substrates for diminishing bacterial growth as a result of the damage of bacterial cell wall through lipid peroxidation [34]. In particular, photoactive materials like titanium dioxide (TiO_2) or zinc oxide (ZnO) possess antimicrobial potential due to ROS production induced especially by UV, but also visible range light (related to their photo-catalytic activity) [35], [36].

The second strategy involves the use of molecular compounds that disrupt physiological processes in bacterial cells. Quorum sensing (QS) is an important mechanism in biofilm formation, which coordinates gene expression in bacteria in accordance with their density and takes part in the regulation of virulence factors [37]. The use of synthetic molecules, e.g. metabromo-thiolactone, appear to inhibit QS receptors in *P. aeruginosa* and consequently biofilm formation and virulence [38]. Naturally available molecular compounds from garlic [39] and ginseng [40] were also shown to decrease QS and promote faster recovery from *P. aeruginosa* infection. Interestingly, in some cases natural QS peptides produced by bacterial cells are able to kill their own cells at higher concentration [41].
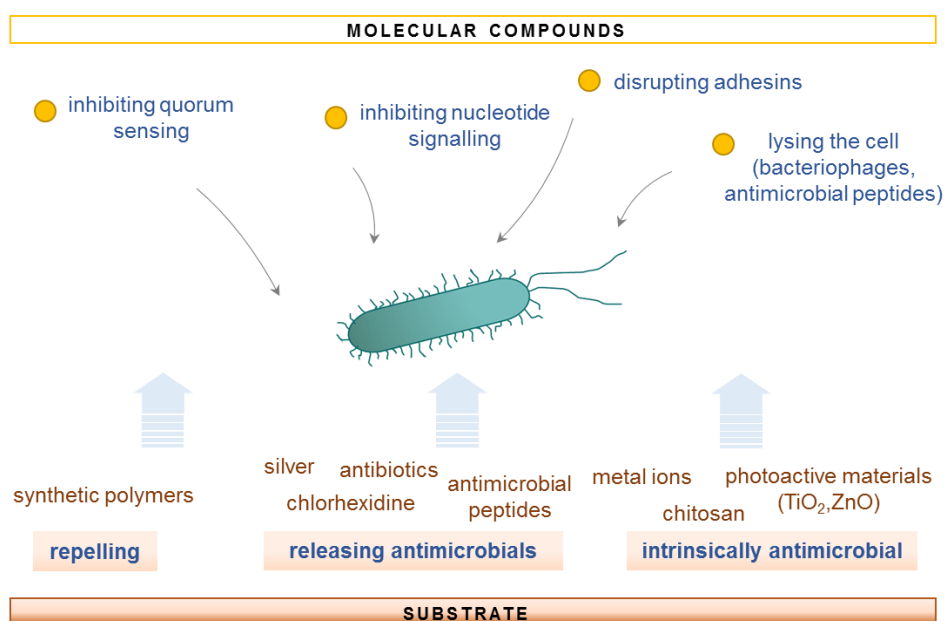
Figure 1.4. Summary of strategies for inhibition of pathogenic biofilm formation and growth: two main approaches involve substrate modification ("prevention from bottom"), or addition of molecular compounds in the medium to disrupt physiological processes in the installed biofilm ("elimination from top")

Some nucleotides, i.e. monomers of DNA and RNA biomolecules, participate in the transformation of the bacterial cell from motile to sessile form of life, particularly in Gram-negative bacteria [42]. Thus, the drugs targeting nucleotides signalling will also inhibit biofilm growth. In addition, disruption of bacterial adhesins, such as pili and curli, and introducing bacteriophages, i.e. viruses infecting bacteria, are alternative routes to inhibit the growth or kill bacteria in a biofilm, respectively [37], [43].

Despite a wide range of strategies explored for inhibiting the growth of pathogenic biofilms, there is no consensus on the method that would be the most efficient in preventing or eliminating the risk of pathogens growth at surfaces. The development in the area of research for fighting the surface-associated pathogenic bacteria is relatively nascent, and as such many interesting routes are investigated for their potential to aid in this field. One very exciting strategy to control pathogen growth is based on the phenomenon of bacterial interference and has been gaining attention in recent years. In nature, microorganisms typically form multispecies biofilms benefiting from each other's presence. For example, degrading of nutrients by one bacterium may give a source of food through by-products for another species, while the presence of both species contributes to biofilm stability [44]. Otherwise, one organism may outcompete the other one thanks to a more suitable adjustment to environmental conditions and synthesis of molecules provoking the damage of other bacteria [45]. Our intestine is a good example of complex bacterial relationship, in which beneficial organisms (probiotics) regulate the presence of non-beneficial ones on the epithelial cells. Bacterial interactions of such kind lay the base of the promising route for prevention and inhibition of pathogenic biofilm growth also on abiotic supports.

1.1.3. Probiotic bacteria as a tool to fight biofilms of pathogens

Probiotics are defined as live microorganisms that, when administered in adequate amounts, confer a health benefit on the host [46]. The definition implies no limit to the route of administration (e.g. oral, vaginal, topical, rectal), however more ordinarily probiotics are used as parts of food and drugs consumed orally and delivered to the intestine as site of action [47]. The term probiotics commonly refers to bacteria, especially lactobacilli, but other bacterial species, e.g. *E. coli* Nissle 1917 [48]–[51], or yeast (*Saccharomyces cerevisiae*, *Issatchenkia occidentalis* [52]) also exist. The idea of consuming beneficial live microorganisms to improve health was first suggested by

the immunologist Élie Metchnikoff in the early 1900s [53]. Unlike many others at that time, he assumed that intestine microbiome *per se* is a part of a normal healthy human, whilst the population of "putrefactive" bacteria can be reduced with the aid of lactate-producing bacteria consumed for example with yogurts. He also speculated that life expectancy can be increased when, among others, sour milk is consumed regularly since childhood [54]. Metchnikoff's recommendations have gained higher industrial and public interest during the 20th century. The first commercial product with probiotics was made by Japanese company Yakult in 1935. The first lactic acid bacteria brand in Europe was opened in 1990s by Valio company (Finland) with introduction into their dairy products a probiotic bacterial strain *Lactobacillus rhamnosus* GG (LGG). Since then, the interest in using probiotics as part of food or medical supplements has been continuously increasing, which has resulted in a multi-billion worldwide industry nowadays [55].

It is known today that beneficial effects related to the probiotic presence for example on epithelial cells include the function of protective barrier, inhibition of pathogen activity and modulation of the immune system [56]. More precisely, antivirulence action occurs through inhibition of adhesion of pathogens and of quorum sensing in pathogenic biofilms, competition for nutrients, release of antimicrobial substances and neutralisation of toxins ([57], figure 1.5). Despite clear evidence of clinical benefits of probiotic species and its ability to eliminate pathogen-associated symptoms, it is only recently that studies deciphering interactions between probiotic and pathogens in biofilms started to appear (figure 1.5).
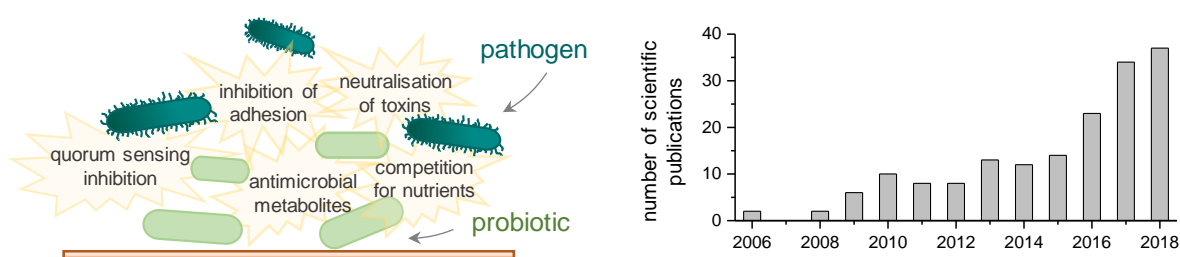
Figure 1.5. Antivirulence action of probiotics, left, and number of annual scientific communications cited in Web of Science in the field combining "probiotic" and "biofilm" and "pathogen" (search parameters), right

Table 1.1 lists examples of studies of antagonistic action of probiotics towards pathogenic bacteria. Overall, the works reported positive results regarding inhibition effect of probiotics on pathogens. Most of studies revealing mechanisms of

antipathogenic action of probiotic bacteria have been performed in medically relevant field, i.e. utilising cells that provoke infections in human urine tract, lungs, mouth and skin [48], [49], [51], [58]–[65] . Notably, the community of probiotics investigated for its antipathogenic potential is very broad and the protocols for conducting the experiments are varying significantly. Antipathogenic potential of probiotics was evaluated either by studying the impact of antimicrobial substances released into the culture medium during the incubation of probiotics (cell-free culture supernatants, CFCS) [50], [58], [59], [61]–[63], [65]–[69] or by using probiotics as whole cells to inhibit pathogenic biofilms [48], [49], [51], [60], [63], [64], [67], [70]–[72]. The former approach is easier in practice, as there is no need for methods to distinguish bacterial species in the analysis (e.g. multiple agar plates for counting colony forming units or fluorescence in situ hybridization), which might be tedious and time-consuming to elaborate. However, the dynamic changes in the important mechanisms of bacterial interplay (co-aggregation, adhesins interaction, competition for nutrients) are omitted in this experimental set-up. More complex picture on the antipathogenic action can be obtained when probiotics used as whole cells to prevent, outcompete, or displace pathogenic biofilms. The latter three mechanisms of action are fundamental for three possible scenarios that are evaluated in so called exclusion (when probiotic biofilm is formed preliminarily to addition of pathogenic cells for further incubation), competition (when the surface is exposed to pathogens and probiotics in the co-culture simultaneously) and displacement (when pathogenic biofilm is formed preliminarily to addition of probiotic cells for further incubation) assays. The choice of assay depends on the application field and the investigated hypothesis. In case of a disease, pathogenic biofilms formed on the organ cells are of expectance, and the idea of their disruption (displacement test) is likely first to arise. Nonetheless, at early stages of clinical infections or even for prophylactic purpose the competition and exclusion, respectively, are also relevant processes.

Table 1.1. Examples of studies of antipathogenic action of probiotic bacteria

Probiotics	Pathogens	Method of evaluation of inhibition of pathogenic biofilms	Temp., ºC	Time, h	Relevance	Ref
		Biofilms formed on the bottom of microtitre plates				
Lactic acid bacteria (LAB) isolated from food	15 various pathogenic strains	co-incubation with probiotic **cell-free culture supernatants (CFCS)** - *XTT[a] assay*	37	24	Suppression of oral pathogens	[58]
L. acidophilus, *L. sakei*	*E. coli* O157:H7	co-incubation with **CFCS** - *crystal violet[b] staining*	30	48	Reduction of virulence of foodborne pathogens	[66]
LAB isolated from chicken and calves	*K. pneumonii*, *E. coli*	co-incubation with **CFCS** or co-incubation with acids produced by LAB or co-incubation with probiotic cells (**competition assay**) - *crystal violet staining + FISH[c] staining*	37	24	Use of probiotics as growth promoters in animal feed	[67]
L. acidophilus, *L. fermentum*, *L. plantarum*, *L. rhamnosus* and Bio-Kult® (commercially available mixture of probiotics)	*E. faecalis* and *E. coli*	co-incubation with **CFCS** - *crystal violet staining*	37	18	Treatment of urinary tract infections	[59]
S. oralis and *S. salivarius*	*S. pyogenes*	co-incubation with probiotic cells (**competition assay**) - *imaging with scanning electron and confocal laser scanning microscopies*	37	72	Protection of respiratory tract epithelial cells by probiotics	[60]
E. coli Nissle 1917	other *E. coli* strains	co-incubation with probiotic cells (**competition assay**) - *recovery of the biofilm and plating on appropriate agar plates for CFU[d] counting*	37	overnight	Prevention of intestinal infections	[48]
L. acidophilus, *L. casei*, *L. paracasei*, *L. rhamnosus*	*S. Typhimurium*, *L. monocytogenes*	co-incubation with probiotic cells (**competition assay**) or formation of probiotic biofilm preliminarily to addition of pathogenic cells for further incubation (**exclusion assay**) or formation of pathogenic biofilm preliminarily to addition of probiotic cells for further incubation (**displacement assay**) - *recovery of the biofilm and plating on appropriate agar plates for CFU counting*	37	24	Inhibition of biofilms of foodborne pathogens	[70]
L. casei Shirota, *L. rhamnosus*	*L. monocytogenes*	- formation of probiotic biofilm preliminarily to addition of pathogenic cells for further incubation (**exclusion assay**) - *recovery of the biofilm and plating on appropriate agar plates for CFU counting*	30	24	Inhibition of biofilms of foodborne pathogens	[71]
14 various probiotic strains	*P. acnes*, *S. aureus*, *E. coli*, *P. aeruginosa*	co-incubation with **CFCS** (8h) or incubation without (4 h) and then with **CFCS** (24 h) - *crystal violet staining*	37	See details in method description	Treatment of skin disorders	[61]
LAB isolated from Tunisian traditional fermented food	*L. monocytogenes*	co-incubation with **CFCS** (24 h) or incubation without (24 h) and then with **CFCS** (24 h) - *crystal violet staining*	37	See details in method description	Inhibition of biofilms of foodborne pathogens	[68]
L. sakei, *L. lactis*, *L. curvatus*, *L. helveticus*, *W. viridescens* isolated from food	*L. monocytogenes*, *E. coli O157:H7*, *S. Typhimurium*	Formation of probiotic biofilm (48 h) preliminarily to addition of pathogenic cells for further incubation for 24, 48 or 72 h (**exclusion assay**) - *recovery of the biofilm and plating on appropriate agar plates for CFU counting*	30	See details in method description	Inhibition of biofilms of foodborne pathogens	[72]

[a] XTT – tetrazolium-based chemical reagent that is reduced by mitochondrial enzymes in live cells forming water-soluble orange-coloured product; it enables determination of the quantity of live cells.
[b] crystal violet is a cationic dye, which binds to proteins and DNA; the degree of colourisation after staining is proportional to biomass quantity
[c] FISH refers to Fluorescence In Situ Hybridization, a staining technique that is specific to particular DNA, hence enabling identification of different species in a mixed biofilm
[d] CFU – colony forming units

		Biofilms formed on other types of surfaces (glass, titanium, hydroxyapatite, falcon tubes, functionalised surfaces, enamel)				
L. fermentum	*S. aureus*, *P. aeruginosa*	co-incubation with **CFCS** (48 h) in microtitre plates or on glass slides or incubation without (4 h) and then with **CFCS** (24 h) - *crystal violet* staining and *confocal laser scanning microscopy*	37	See details in method description	Treatment of clinical infections	[62]
L. rhamnosus, *L. paracasei*	*S. mutans*, *S. oralis*	co-incubation with **CFCS** on titanium disks (24 h) or co-incubation with probiotic cells for 24 h (**competition assay**) or formation of pathogenic biofilm (1 h) preliminarily to addition of probiotic cells for further incubation for 24 h (**displacement assay**) or formation of probiotic biofilm (0.5 h) preliminarily to addition of pathogenic cells for further incubation for 24 h (**exclusion assay**) - *recovery of the biofilm and plating on appropriate agar plates for CFU counting*	37	See details in method description	Suppression of oral pathogens	[63]
E. coli Nissle 1917	*P. aeruginosa*	formation of pathogenic biofilm (24 h) on pegs of a modified polystyrene microtitre lid preliminarily to addition of probiotic cells for further incubation for 4 h (**displacement assay**) - *crystal violet* staining and - *recovery of the biofilm and plating on appropriate agar plates for CFU counting* and - *confocal laser scanning microscopy*	37	See details in method description	Prevention of gut infection	[49]
22 various probiotic strains	*S. mutans*	incubation without (1 h) and then with **CFCS** on hydroxyapatite discs for 24 or 48 h - *crystal violet* staining and - *recovery of the biofilm and plating on appropriate agar plates for CFU counting*	37	See details in method description	Suppression of oral pathogens	[65]
E. coli Nissle 1917	*E. coli* O157:H7, *P. aeruginosa*, *S. aureus*, *S. epidermidis*	co-incubation with **CFCS** in Falcon culture tubes - *recovery of the biofilm and plating on appropriate agar plates for CFU counting*	37	24	Prevention of pathogenic biofilms in general	[50]
L. rhamnosus GG, *S. salivarius K12*	*S. aureus*, *S. epidermidis*	co-incubation with **CFCS** in mictotitre plates coated with fibronectin for 48 h or incubation without (4 or 24 h) and then with **CFCS** (for total 48 h) - *safranin*[e] staining	37	See details in method description	Prevention of pathogenic biofilms in general	[69]
8 various probiotic strains	*S. mutans*	formation of probiotic biofilm in flow conditions on bovine enamel slabs preliminarily to addition of pathogenic cells for further flow (**exclusion assay**) or formation of pathogenic biofilm in flow conditions on bovine enamel slabs preliminarily to addition of probiotic cells for further flow (**displacement assay**) - *recovery of the biofilm and plating on appropriate agar plates for CFU counting*	37	Various times depending on flow conditions	Use of probiotics for caries prevention	[64]
E. coli Nissle 1917	*E. faecalis*	formation of probiotic biofilm (5 days) on mannoside-functionalised PDMS preliminary to addition of pathogenic cells for further incubation for 11 days (**exclusion assay**) - *optical microscopy* and - *recovery of the biofilm and plating on appropriate agar plates for CFU counting*	37	See details in method description	Treatment of urinary tract infections	[51]

[e] Safranin is positively charged dye that binds to negatively charged parts of cells; alternative to crystal violet for biomass estimation [73]

Pre-forming probiotic biofilms can be a very efficient strategy to inhibit pathogenic biofilm formation. For example, in the work of Trautner et al. the development of biofilm by *Enterococcus faecalis*, an urinary pathogen, was impeded by non-pathogenic *E.coli* biofilm formed on mannose-functionalised surface [74]. Herein, the stability of the non-pathogenic *E. coli* biofilm was ensured thanks to specific interaction between fimbriae type 1 present on the *E. coli* cell wall and mannose grafted on the substrate. Similarly, *E. faecalis* biofilm formation was inhibited by *E. coli* Nissle 1917 on the substrates functionalised with mannosides in exclusion assay that was conducted for as long as 11 days [51]. More commonly however, experiments (table 1.1) are carried for shorter periods of time – from 24 to 48 hours. For example, in the study of Gómez et al. potential probiotic lactic acid bacteria (LAB) formed a biofilm within 48 hours and reduced significantly formation of the biofilm by foodborne pathogens *E. coli* O157:H7, *Listeria monocytogenes*, and *Salmonella typhimurium* [72]. Biofilms of the latter two pathogens were also inhibited by LAB in exclusion and competition assays in the study of Woo and Ahn [70]. Interestingly, in their work *Lactobacillus rhamnosus* had the most enhanced biofilm formation among other lactobacilli, and in both exclusion and competition assays more probiotic cells were counted than when probiotics were incubated alone. This indicates potential growth advantage of *L. rhamnosus* over *S. typhimurium* and *L. monocytogenes* and makes prominent a promising route to enhance surface hygiene by utilising probiotic biofilms in food industry. It also shows that strong adhesive capacity of probiotic cells is a beneficial factor for elimination of pathogenic biofilms. In fact, it is considered as a prerequisite for biofilm formation and concomitant beneficial mechanisms [56].

One strain of *L. rhamnosus* – LGG – has particularly remarkable adhesive properties compared to other lactobacilli strains and probiotic species [75]; it is even used as a reference in adhesion assays for other bacterial species [76]. It is a Gram-positive rod-shaped bacterium that attaches strongly to both epithelial cells and abiotic surfaces through the mediation by cell wall adhesins, LGG-specific SpaCBA pili [77]. The name refers to three units comprising the LGG pilus – the major pilin spaA exerting structural function (as a backbone) and covering it minor pilins SpaB and SpaC playing functional role (spaC predominantly), i.e. adhesion to mucus. Interestingly, it was found that pili on the LGG cell reinforce interaction also with an abiotic surface [78], on which LGG is able to form biofilm [79]. In addition to outstanding adhesion properties, LGG was

shown to produce antimicrobial substances active against a range of Gram-positive and Gram-negative bacteria [80], [81] and more recently yeast [82]. The clinical benefits from LGG consumption in form of dairy products or food supplements have been provided in massive research owning to its early place on the market of probiotics (Valio Ltd, Finland). These benefits are mainly associated with the promotion of gastro-intestinal health, such as treatment and prevention of diarrhoea [83]. There is also an evidence of LGG immunomodulatory action against allergic diseases [84]–[86], prevention of caries [87], [88], and treatment of pulmonary diseases [89], [90]. In addition, some studies suggest a promising potential of LGG to induce tumour regression [91], [92] and prevent obesity [93]. The consumption of this strain in a form of dairy products, juices, cheeses, and capsules in over 40 countries worldwide has proven its safe use. It thus appears as a perfect candidate for combatting with pathogenic biofilms, yet the studies evaluating LGG potential against pathogenic biofilms only recently began to appear [64], [82], [94]. For example, Schwendicke et al. showed the effect of LGG and a range of other probiotics against growth and biofilm formation of cariogenic bacteria (*Streptococcus mutans*) on bovine enamel slabs in exclusion and displacement assays [64]. In another work, *S. mutans* and a mix of other pathogens (*S. sanguinis*, *C. albicans*, *A. actinomycetemcomitans*, and *F. nucleatum*) formed also less dense biofilms in presence of LGG on saliva-coated hydroxyapatite in competition assay [95]. Besides oral cavity, LGG (in particular its lectin domains) inhibit biofilms of pathogens of the intestine (*Salmonella enterica* serovar typhimurium) and urinary tract (uropathogenic *E.coli*) [81]. Recently, it was also reported that LGG is able to inhibit biofilms of fungal pathogen *Candida albicans* by breaking down chitin, the main polymer in the hyphal cell wall of *C. albicans* [82]. The mechanisms of how LGG inhibit pathogens growth remain not fully understood. It is apparent that lectin-like proteins secreted by LGG are able to destabilise the structure of a pathogenic biofilm by selective binding to the components of its matrix (such as glycosylated colanic acid in the matrix of *S. typhimurium* and *E. coli*) [81]. Herein, the extracellular matrix in biofilms is varying in composition depending on bacterial species, which can explain the strain-specific differences in the antimicrobial action of LGG. In addition, some studies have revealed lactic acid as being the main antimicrobial component [96], [97], although it is clearly not specific for LGG. It is plausible that its role is to permeabilise the membrane of Gram-negative cells, thus facilitating the antibacterial action of other compounds [75]. As the antimicrobial action depends on metabolic

bacterial activity, both pathogens and probiotics, a nutritive medium is of major importance. Interestingly, even the concentration of nutrients appear to be a significant factor. Indeed, Petrova and co-authors [81] showed that lectin domains isolated from LGG inhibit planktonic cultures of *Salmonella* only in non-diluted nutritive medium, whereas, surprisingly, in 20-fold diluted medium the antipathogenic effect was absent. As authors suggested, *Salmonella* is able to degrade LGG lectins in poor medium and use them to grow, or lectins promote sugar uptake. LGG biofilms are also affected by the nutritive medium properties. Thus, Lebeer et al. reported inverse correlation between the density of LGG biofilms on the abiotic surface (polystyrene) and the concentration of fermentable sugar (glucose) in the nutritive medium [79]. Altogether, this highlights the significance of the choice of suitable experimental conditions in antipathogenic assays using LGG and other probiotics.

1.2 Strategies for biofilm investigation

1.2.1. Methods used for biofilm analysis

The diversity in biofilm nature, as well as its complex structure and composition demand the use of multiple methods for gaining subtle knowledge on its properties. Various characterisation techniques complement each other for studying biofilms from chemical, physical and microbiological perspective enabling identification of microbiological species in the biofilm, studying of its biochemical composition and evaluation of its structural properties (figure 1.6). Overall, the techniques for biofilm examination can be separated into two categories – those that allow direct observation and the ones requiring preliminary removal of the biofilm from the surface.

a) Direct observation of biofilms by imaging methods

The methods allowing direct observation of biofilms are represented by various microscopic techniques, such as optical, scanning electron and atomic force microscopy.

Optical microscopy is one of the most classical methods used for biofilm analysis. It is a relatively low-cost and easy to use imaging technique that demands little sample preparation. Using epifluorescence, the microscope detects the light emitted by fluorochrome molecules that are used to stain the sample. It can also be performed in

the confocal mode, in which images are reconstructed into three-dimensional picture of the biofilm architecture. This method is effective to obtain information on the distribution of different components within the biofilm owing to specific binding between chosen fluorochrome and certain molecules, such as nucleic acids, proteins or polysaccharides.
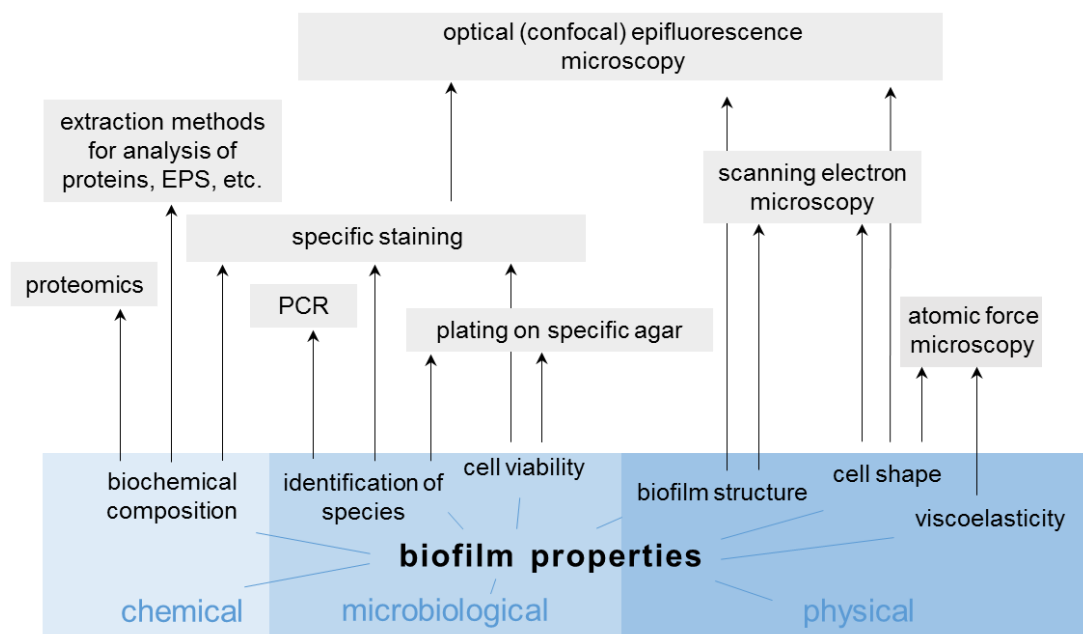
Figure 1.6. Examples of methods used for the analysis of physical, chemical and microbiological properties of biofilms

Thus, DAPI, Syto 9, SYBR Green are examples of commercially available dyes that bind to nucleic acids, and they are commonly applied for biofilm staining ([98]–[101]). As nucleic acids are more concentrated inside the cells than in the biofilm matrix these fluorochromes will typically enable visualisation of the shapes of bacterial cells. For staining polysaccharides of the matrix, lectins can be used, i.e. proteins that links with carbohydrate moieties, conjugated with fluorochromes. An example of such lectins is Concanavalin A that binds to glucose and mannose residues [102], [103].

In addition to component localisation, staining techniques allow recognition and localisation of physiologically active bacteria in a biofilm. This is achieved through a biochemically induced reaction. The examples are tetrazolium salts such as CTC (5-Cyano-2,3-di-(p-tolyl)tetrazolium chloride) and XTT (2,3-Bis-(2-Methoxy-4-Nitro-5-Sulfophenyl)-2H-Tetrazolium-5-Carboxanilide) reduced by cellular respiration chain and mitochondrial enzymes in live cells, respectively [58], [104], [105]. In case of CTC, the reduction induces the formation of insoluble and fluorescent formazan crystallised

and trapped in the membrane enabling the assess on a per cell basis with the fluorescence microscope (excitation / emission: 540 / 630 nm). When XTT is used, however, the formed product is soluble and orange-coloured formazan molecules that absorb at 490 nm are detected by UV-Vis spectrometry [104]. In principle, a formation of the coloured product can be measured *in situ* as it is released to the buffer medium during cells proliferation. Nonetheless, tetrazolium salts are generally cytotoxic, which significantly limits the conduction of time-course experiments [106], [107]. This issue can be alleviated using other molecules reducing the environment of the living cells, such as resazurin–based Alamar Blue, which is not cytotoxic and permits continuous assay of cell metabolic activity [107].

Alternatively to redox potential, cell membrane integrity is generally perceived as a marker of cell viability [98]. The most commonly used dyes in this regard comprise a *Bac*Light™ kit that contains Syto 9 and propidium iodide fluorochrome molecules. The green-fluorescent Syto 9 penetrate all cell membranes, whereas larger in size red-fluorescent propidium iodide will stain only the cells having compromised membrane replacing Syto 9 and thus enabling to distinguish the cells. Attention must be paid however when analysing thick biofilms as the penetration of the dyes might be limited [108].

Using fluorescently labelled oligonucleotide probes one can also localise the species within the biofilm. The technique, named fluorescence in situ hybridization (FISH), is based on molecular hybridization between target DNA or RNA sequences and an artificially constructed and fluorescently-labelled probe matching the sequence under question. The process is occurring as a result of formation of hydrogen bonds between helices of the molecules, target and fluorescent probe, after a preliminary denaturation step. It must be noted that the intensity of the observed fluorescence depends on the ribosome content and thus, the physiological status of bacterial cells will affect the staining [98]. FISH is a powerful method to distinguish bacterial samples in a large variety of species that can be found in human and environmental biofilms. For instance, LGG spatial distribution within other lactobacilli species was analysed *in vivo* on the samples of the human, murine and avian gastrointestinal tract by FISH with specific probes [109].

Although optical microscopy techniques are valuable and powerful, they do have limitations. The major limitation is in their resolution limited by the visible range of the electromagnetic spectrum. This precludes distinguishing structural components of the biofilm as well as morphological features of bacterial cells below a threshold of 200-300 nm. Closer look on the structure of a biofilm can be made by means of scanning electron microscopy (SEM). SEM is an imaging technique based on the interaction of electrons with the sample. Since the wavelength of electrons is much smaller than that of photons of visible and UV light, the resolution of SEM is about a few nanometres. A great advance in understanding biofilms has been made with the invention of SEM and application to its research. In particular, the localisation areas where bacteria adhere on relevant substrates, like epithelial tissues [110], industrial equipment [24] and food matrix [111] was possible to assess using SEM with nanometre scale resolution. The data on the structure of the extracellular matrix have also become accessible with a higher precision. However, a strong disadvantage of SEM is the demand of complete sample dehydration before the analysis under vacuum. Considering that biofilms are mainly composed of water [10], the image obtained with SEM omits the information on the actual biofilm structure that can be seen in aqueous environments [98]. In addition, the sample for analysis with SEM must be conductive. Therefore, biofilms must be coated with a thin layer of metal such as gold or platinum, which requires the use of additional equipment and increase the time necessary for sample preparation.

As alternative to SEM method that allows nanoscale imaging of samples and does not require systematic sample dehydration is atomic force microscopy (AFM). In AFM the image is obtained as a consequence of the interaction between a bacterial surface and a sharp (1-10 nm) probe attached to a flexible cantilever. The forces arising between the sharp probe and the sample surface will cause the cantilever to bend, and cantilever bending is detected by focusing the laser beam at the cantilever edge. Thus, the information on the morphology of bacterial cells and surrounding matrix are obtained. In addition, the interactions forces between bacteria and the probe provide also the information on viscoelastic properties of the cells. It is of special interest in case of bacterial samples, as the majority of cells have various adhesins on their walls. In this regard, AFM has proven to be a very powerful method to study bacterial adhesins interaction. An example is the study of mutants of *E.coli* having various adhesins, in which elasticity of the cell was shown to be simultaneously dependent on

the nature of adhesins and ionic strength of the aqueous medium [112]. LGG was also a subject of many AFM studies, which revealed important function of LGG cell wall pili as mediators with the surrounding environment [78], [113]–[115]. A very important feature of AFM is the feasibility to assess processes occurring at the bacterial interface at the molecular level in the direct bacterial environment, i.e. in an aqueous medium.

b) Non-direct observation of biofilms

The second family of methods in biofilms research deals with the cells extracted from the support surface preliminarily to the analysis. Essentially, the examination of the cells in such set-up is not different from studying bacteria in planktonic cultures. Ordinarily used techniques, in this regard, are chemical extraction methods for determination of biochemical nature of the biofilm components (proteomics methods, extraction of nucleic acids and EPS), and genetical methods (e.g. polymerase chain reaction, PCR) for determination of biochemical composition and identification of species in a biofilm. More precisely, proteomics methods are aimed to identify protein content of the cell. For this, the proteins should be, first, extracted from the cell by cell disruption or lysis, and then analysed using separation or mass spectrometry techniques. One of the most commonly used methods for separation of protein samples is sodium dodecyl sulfate polyacrylamide gel electrophoresis (SDS-PAGE). Here, the separation of protein molecules occurs through electrophoresis due to binding of proteins with negatively charged SDS. The quantity of SDS linked with protein varies as a function of the protein mass. As the electrophoresis process takes place in polyacrylamide gel, larger protein molecules move to a positively charged electrode slower than smaller molecules. The migration distance of the protein thus can be measured after staining the proteins in the gel with appropriate dyes [116]. By virtue of this analysis, one can determine the relative abundance of major proteins in a sample. Additionally, using antibodies specific for the protein of interest it is possible to identify proteins in the sample (so-called Western blotting technique) [117]. Thus, two major proteins secreted by LGG were separated and identified by Claes and co-workers [118]. SDS-PAGE can be also combined with gel electrophoresis based on separation of proteins according to their isoelectric point. First, the proteins are separated in one dimension based on their net charge; then, the separation is performed in the second dimension based on their masses (proportional to linked

SDS). The method can be further upgraded by labelling proteins from different samples under study (e.g. control sample and analytical sample) by different dyes that allow comparing the protein quantities directly in one assay. The latter technique gained its own name as two-dimensional fluorescence difference gel electrophoresis (2D-DIGE) [119]. For example, 2D-DIGE was used by Koponen et al. to study effect of acid stress on protein expression by LGG [120], and by Koskenniemi et al. to study the impact of the nutritive medium chosen for cultivation of planktonic cultures on the proteome of LGG [121].

Generally, SDS-PAGE and 2D-DIGE make part of the family of electrophoresis methods that are very frequently used in molecular biology. With some variations in extraction procedure [122], electrophoresis of nucleic acids is performed in polyacrylamide or agarose gel to separate macromolecules that can be further identified using for example mass spectrometry or gas chromatography. If the amount of extracted nucleic acids are too small, their quantity can be increased using an amplification step such as PCR [123], [124]. Using PCR, one can also identify bacterial species based on features of its specific gene (16S gene) that can be compared with references from the DNA database of bacteria [125]. The use of PCR for identification of LGG among other strains was validated [126], and examples of PCR and other genetic methods applied for LGG research include studies aimed to identify LGG and surrounding microbiome in mammary gland of mice fed with probiotics during pregnancy [127], and detection of LGG in human faecal samples [128].

Regarding EPS, as some quantities of proteins and nucleic acids are present in its composition [10], electrophoresis methods are useful for their analysis, whereas the carbohydrates fraction can be estimated using colorimetric methods (e.g. breaking carbohydrates with sulfuric acid and subsequent linking to phenol to give yellow-coloured product) [129]. However, the extraction of EPS from the biofilm is somewhat a less trivial task due to the necessity to maintain the cells maximally intact and avoid destruction of EPS. Various methods of EPS extraction exist, including dialysis, alcohol precipitation, enzyme digestion (selective removal of proteins and nucleic acids by proteases and nucleases), incubation in EDTA (ethylenediaminetetraacetic acid), etc. [130]. The extraction efficiency varies as a function of the chosen method. Moreover, some extraction methods may interfere with analytical measurements and give non-

consistent results, thus demanding time to find an appropriate method for a specific bacterial sample [131]. Often the techniques mentioned above for EPS extraction are combined in order to ensure the highest purity of the obtained sample (e.g. absence of proteins and other "contaminating" molecules). For example, Allonsius et al. studied the impact of LGG EPS in its antagonistic action towards *Candida* species [132]. The authors implemented incubation in EDTA, ethanol precipitation, dialysis and incubation in trichloroacetic acid to extract and purify EPS from LGG, the carbohydrate fraction of which was further analysed using phenol-sulfuric acid method. It must be noted that the authors faced some difficulties with purification of the EPS, as they stated the presence of unexpected components, originating from the filters and membranes used during extraction in the Nuclear Magnetic Resonance (NMR) spectra obtained to check the purity of the sample. Additional optimisation of extraction procedures helped to eliminate unwanted substances.

Altogether, this indicates that despite molecular biology techniques are undoubtedly of great value in biofilm analysis, they are associated with multiple steps of operation, use of multiple reagents and disposable equipment, each being a potential source of contamination that might generate misleading or ambiguous results. The demand on large number of supplies and the need to use multiple analytical tools for proof-checking the data is associated with a high cost of experimental work. The strong need to optimise extraction methods to a specific sample among numerous existing procedures make it difficult to compare the results between studies, and more importantly, engender higher risk of associated lack of reproducibility and reliably of the results if the study is not well designed. With this in mind, one must consider the additional risk of implementing non-direct observation methods for biofilm research. The critical issue in this regard is a recovery of the biofilm from the surface, which may appear as trivial due to simplicity of operating procedures (sonication, vortex or and/or scraping), but in fact is associated with a strong risk of underestimating the biofilm content and potential damage of bacteria during dispersion steps [133]. Thus, additional (laborious and time-consuming) calibration steps are mandatory to ensure that bacterial cells are optimally extracted, dispersed and left intact. Besides, in some cases (e.g. porous substrates) the full biofilm recovery may simply not be achievable [98]. Consequently, alternative approaches to molecular biology techniques that allow

more rapid, simple, reagentless and non-invasive analysis of biofilm components are of greatest interest.

c) Two particular methods frequently used for studying mixed probiotic-pathogen biofilms

It is worth mentioning aside that the works aimed to evaluate antipathogenic action of probiotics in biofilms, in particular, are frequently associated with the use of crystal violet staining and colony forming units (CFU) counting. Their abundant use may be estimated from the examples of studies presented in table 1.1 ([48]–[51], [59], [61]–[67], [70]–[72]). Crystal violet staining allows estimating the quantity of biofilm, whereas CFU counting serves for determination of the number of cultivable cells in the biofilm. The advantage of these methods is in their relatively easy accessibility. CFU are counted by recuperation of the biofilm from the surface (using sonication, vortex and/or scraping) and plating resuspended cells from the biofilm on specific agar. It is thus available as a method for biofilm characterisation in every microbiological laboratory. However, a strong disadvantage of CFU counting method is a high probability of not recovering all cells from the surface and damaging of cells, hence associated drawbacks as aforementioned for methods of non-direct biofilm observation [104], [133], [134]. More precisely, an assumption is made that each colony derives from one original cell, which might not be the case as often bacterial cells tend to aggregate [135], [136].

Crystal violet staining is a facile method for qualitative assay of biofilm formation as it can be viewed by the naked eye. It can also give quantitative information with the aid of a spectrophotometer by measuring the absorbance at 595 nm, which is proportional to the biomass quantity. For instance, LGG biofilm formation was assessed on an abiotic surface (polystyrene) in different nutritive media using crystal violet stain by Lebeer and co-workers [79]. The results of that study showed variation in LGG biofilm formation capacity from zero to complete surface coverage depending on the nutrient conditions. It must be noted, however, that biofilms were examined only after 72 hours of cultivation after reaching the mature stage. Indeed, thin early-stage biofilms are difficult to analyse using spectrophotometry due to large variability of measurement data [137]. Hence, crystal violet staining does not provide the information on how bacterial cells adapt to a sessile condition from early stages of biofilm development.

The major limitation of CFU counting, crystal violet stain and other methods listed above (with few exceptions) is a non-feasibility of monitoring the biofilm formation process continuously and *in situ*, i.e. from the beginning to mature stages directly in the aqueous environment. However, the knowledge of the process of bacterial attachment and early stages of growth on the surface is of fundamental importance for understanding biofilms. Few reports have shown surface plasmon resonance spectroscopy, a technique based on the sensitivity of the electromagnetic surface wave to boundary conditions, as a useful method for the determination of binding kinetics of bacteria [138]–[140]. However, this method does not provide structural information on the sample as the data reflect only absorption in terms of changes in the mass on the surface. In this regard, a valuable tool to gain the information on both quantities and molecular structure changes *in situ* is Attenuated Total Reflectance-Fourier Transform Infrared (ATR-FTIR) spectroscopy that is illustrated with examples below.

1.2.2. Vibrational spectroscopies for in situ monitoring of biofilm formation

Vibrational spectroscopy methods employ molecular vibrations to elucidate molecular structure of the material. The main vibrational spectroscopy methods are infrared (mid-IR and near-IR) and Raman spectroscopies. Although both methods measure vibrations of molecules, IR and Raman spectroscopies arise from different processes and different selection rules apply for the absorption of radiation energy [141].

In Raman spectroscopy, the signal is induced by a non-resonant process of oscillation of the electric field and is a function of the molecule polarizability, i.e. deformability of the electron cloud about the molecule by an external electric field. It therefore works best for measuring non-polar molecular groups. The samples in the aqueous environment can be analysed with Raman spectroscopy due to low absorption of polar water molecules. Raman process is a scattering process, in which a photon of a monochromatic laser beam is scattered with slight change in energy, which was given to provoke the vibration of the molecule. The use of a laser beam allows obtaining high spatial resolution (≈ 1 μm^3). In terms of the analysis of bacterial samples, this is a valuable feature for example for determining molecular structures on a per cell basis [142]. The utility of Raman spectroscopy was shown also in the study with LGG

reporting conformational changes in DNA upon rehydration of bacterial cells after freeze-drying process and the effect of microencapsulation on these changes [143]. It must be noted, however, that fluorescence of the sample will perturb the obtaining of an informative spectrum, which represents a drawback to the analysis of microorganisms by Raman spectroscopy.

IR spectroscopy is based on the absorption of infrared radiation at frequencies resonant with the natural frequency of a particular mode of molecular vibration. In order for the energy to be absorbed, the molecular vibration must cause a change in dipole moment of the molecule. Thus, IR gives high signal intensity in the spectra of polar molecular groups. The fluorescence of microorganisms does not arise under infrared radiation, hence IR spectroscopy is routinely applied to study biological samples such as wood, cells, tissues and bacteria [144]–[146]. It is especially attractive when used in ATR mode as it allows to study samples in aqueous media. This mode is sensitive to the support-sample interface meaning that the spectra will reflect the information only for the first 1-2 µm above the surface of the infrared crystal (see materials and methods for details). Given the size of the bacterial cell is in order of a few µm, ATR-FTIR enables the early stages of biofilm formation to be monitored as well as how sessile bacteria at the base of biofilms response to environmental changes. The main advantage of this approach is the fact that there is no need of specific sample preparation (extraction/purification) to obtain chemical information on biofilms. This helps to avoid biases in identification of the nature and the quantity of the native components. It is a non-invasive technique that permits evaluating changes in biomolecular composition of live bacterial cells without perturbing their health status. It is especially useful for comparison of the evolution of the main components of the biofilms (proteins, phospholipids, nucleic acids, polysaccharides) in response to changes in environmental conditions.

Moreover, the data can be collected in flow, which is relevant to physiological and industrial conditions bacteria are exposed to. Indeed, hydrodynamic conditions are very important in life cycle of bacteria. In flow systems the mass transport occurs faster leading to a faster adhesion of bacteria despite present shear forces [147]. There is a force threshold, however, after which adhesion will be prevented and adhered bacteria will be detached. The value of forces sufficient to prevent bacterial adhesion or provoke

its removal from the surface is highly depended on the bacterial species and support surface properties. The adhesion of *Pseudomonas fluorescens* to stainless steel was prevented at shear forces of 6-8$\times 10^3$ nN, and at 12$\times 10^3$ nN cells were prone to detach [147], [148], whereas adhesion of *S. aureus* was decreased already at forces of 0.5$\times 10^3$ nN [147], [149]. Surprisingly, the increase of shear forces may also cause higher strength of the bonds between bacteria and the support, as was reported in a study with *E. coli* [150]. Besides, shear stress exerted in flow conditions critically affect metabolism of bacteria. For example, Qi et al. [151] reported that in higher shear stress longer time for adaptation to environmental changes is required. EPS production is also influenced by flow conditions. Indeed, Qi et al. [151] and Hou et al. [152] reported higher EPS production at higher shear stress, possibly as a result of self-protection mechanisms induced in bacterial cells. In addition, flow conditions influence resistance of bacteria in a biofilm against chemical and mechanical treatments [153]. Nonetheless, the majority of works investigating probiotic/pathogen interactions are performed in static conditions. Indeed, the studies listed in table 1.1 include only one example where probiotic antipathogenic action was assessed in flow conditions [64].

The attempts to use infrared spectroscopy for microorganisms characterisation have been made as early as in 1950s [154], [155]. However, the most significant findings have been achieved with the improvement of experimental facilities in late 20th century. The great advance in implementing ATR-FTIR for biofilm research have been performed by joint effort of many scientific groups in the last three decades (table 1.2). The main actors in pioneering research of biofilms with ATR-FTIR were Nivens [156]– [158], Schmitt [159], Suci [160], [161], Donlan [162], and Quilès [100], [163]. Their selected works as well as other illustrative examples of the use of ATR-FTIR for biofilms characterisation are listed in table 1.2.

Table 1.2. Illustrative examples of works utilising ATR-FTIR for biofilm characterisation in last decades

Authors	First author affiliation	Bacterial strain	Field of the study
1990s			
Nivens et al. [156]	University of Tennessee (USA)	*Caulobacter crescentus*	Monitoring of the biofilm under various conditions
White et al. [157]	University of Tennessee (USA)	*Pseudomonas* spp.	Monitoring biofilm formation, succession and stability under various conditions
Schmitt et al. [159]	IWW Water Centre (Germany)	*Pseudomonas putida*	Degradation of toluene by bacterial cells in the biofilm
2000s			
Nivens et al. ([158])	University of Tennessee (USA)	*Pseudomonas aeruginosa*	Role of alginate in biofilm formation
Suci et al. [160]	Montana State University (USA)	*Candida albicans*	Transport of antimicrobials in the biofilm
Donlan et al. [162]	Centers for Disease Control and Prevention (USA)	*Streptococcus pneumoniae*	Assessment of EPS production
Parikh and Chorover [164]	The University of Arizona (USA)	*Pseudomonas putida GB-1*	Biofilm formation and MnO production by bacterial cells
Delille, Quilès and Humbert [100]	Nancy-Université (currently University of Lorraine, France)	*Pseudomonas fluorescens*	Development of the biofilm in low-nutrient conditions
Ojeda et al. [165]	The university of Sheffield (UK)	*Pseudomonas putida*	A role of hematite coating in biofilm formation
2010s			
Quilès, Humbert and Delille [166]	University of Lorraine (France)	*Pseudomonas fluorescens*	Changes in bacterial metabolism at early stages of biofilm development
Huang et al. [167]	Institute of Biogeochemistry and Pollutant Dynamics (Switzerland)	*Shewanella putrefaciens*	Bioremediation of arsenic at hematite surfaces
Lorite et al. [168]	Universidade Estadual de Campinas (Brazil)	*Xylella fastidiosa*	The role of conditioning film in biofilm formation
Lorite et al. [169]	Universidade Estadual de Campinas (Brazil)	*Xylella fastidiosa*	The influence of EPS on biofilm formation
Giotta et al. [170]	University of Salento (Italy)	*Rhodobacter sphaeroides*	Reversible Binding of Metal Ions onto biofilms
Wang et al. [171]	Nanjing Agricultural University (China)	*Salmonella* spp.	Impact of nutritive medium on biochemical composition of biofilms
Parikh et al. [172]	University of California (USA)	*Pseudomonas* spp., *Escherichia coli*	Biomolecular groups responsible for bacterial adhesion to hematite
Quilès et al. [173]	University of Lorraine (France)	*Pseudomonas fluorescens*	Impact of antimicrobial peptides on biofilm formation
Kumari, Mangwani and Das [174]	National Institute of Technology (India)	*Pseudomonas pseudoalcaligenes*	Interaction of EPS with Pb ions during biofilm formation
Hou et al. [152]	University Medical Center Groningen (Netherlands)	*Staphylococcus aureus*	Influence of shear forces on EPS production during biofilm formation
Freudenthal, Quilès and Francius [175]	University of Lorraine (France)	*Escherichia coli*	Impact of antimicrobial peptides on biofilm formation
Zhou et al. [176]	Southwest University of Science and Technology (China)	*Kocuria rosea*	Bioremediation of As-U tailings
Fanesi et al. [177]	University of Lorraine (France)	*Pseudomonas putida G7*	Impact of soil particles on metabolism of bacteria
Pousti and Greener [178]	Université Laval (Canada)	*Pseudomonas fluorescens*	Impact of surface plasma treatment on biofilm accumulation rate

Overall, the works listed in table 1.2 are represented mainly by categories dealing with bioremediation [159], [167], [170], [174], [176], response to antimicrobials [160], [173], role of EPS [152], [158], [162], [169], [174] and support surface[165], [168], [172], [178] in biofilm formation. It can be noticed that since early studies implementing ATR-FTIR spectroscopy for biofilm research, the geography of laboratories as well as diversity of investigated microorganisms have expanded, highlighting the versatility of the method in terms of variety of applications. It is noteworthy, that commonly ATR-FTIR is applied for one-species biofilms. Nonetheless, Gram-positive and Gram-negative bacteria can potentially be distinguished based on differences in their membrane. In particular, presence of thick peptidoglycan layer in Gram-positive cells (40-80% by weight versus 10% in Gram-negative cells [179]) might lead to enhanced bands for polysaccharides, whereas lipopolysaccharides in the membrane of Gram-negative cells should be associated with the growth of bands corresponding to lipids. A recent work of Kochan et al. combining IR and AFM in the one technique (IR-AFM) illustrated the differences in the spectra between Gram-positive and Gram-negative cells using second-derivative analysis [180]. Another potentially useful approach for spectra differentiation is based on chemometric tools such as Bayesian positive source separation (BPSS) method of curve resolution allowing the estimation of spectra of pure components and their relative contribution to a biofilm spectrum [181], [182].

Of interest, the signal in infrared spectrum can be enhanced by deposition of metal islands on the ATR crystal surface. This method has grown into a separate technique named surface-enhanced infrared absorption spectroscopy [183]. The origin of increase in sensitivity is still a subject of investigation, but in majority, it is agreed that it arises from local electromagnetic field enhancement due to plasmon resonance of nano-structured metal thin film [184]. In addition, a possible enhancement effect can be caused by chemical changes due to chemisorption of a molecule on the metal surface [185]. In biofilm research, this technique took its place, thus far, for elucidation of electrochemical properties of bacteria due to electron transfer between metal surface and the cells [186], [187].

Despite clear evidences of wide range of advantages of ATR-FTIR method, main of which are non-invasiveness, sample preparation simplicity, and real-time sensitivity to changes in molecular structure of the sample, this method is highly underexploited in

biofilm research. Notably, probiotic bacteria were only scarcely addressed in planktonic cultures [188]–[190], and, to the best of our knowledge, no biofilms of probiotic bacteria were studied by this method. Probiotic biofilms bring forth a promising strategy for preservation of surfaces against pathogenic contamination that appeared as the subject of investigation only recently. In this regard, ATR-FTIR is a method of great interest because it can help to elucidate the mechanisms behind CFU counts and crystal violet observations in antipathogenic assays (e.g. table 1.1) at molecular level, being a fast and simple alternative tool with respect to molecular biology techniques. Generally, biofilms are constantly subjected to various stresses being in the human body, ecological field or industrial environment. With this in mind, ATR-FTIR is a powerful analytical technique to determine the changes in molecular structures of biofilms as a function of environmental stress, as it allows to perform measurements directly in the aqueous environment and on substrates that can be functionalised according to the needs. The latter subject is of special interest for the current project and is developed in detail in the following chapter.

1.3 Biofilm formation as a function of surface properties

1.3.1. Bacterial interactions with surfaces

The partner of bacterial cells in biofilm formation process is a surface. If the support is represented by biological cells, the interaction occurs through recognition mechanisms between adhesin molecules from the bacterial cell wall and receptor molecules on the tissue. This binding mechanism is generally conceived as a first step in virulence of pathogens [191], [192], but also helps beneficial microbiome to persist in its niche [75]. Non-specific interactions occur when bacteria approach abiotic surfaces like glass, polystyrene, stainless steel, metals and alloys, etc. These interactions display a complex process guided by physical and chemical properties of both a substrate and a bacterial cell. Hence, in order to understand the bacteria-surface interactions, they both should be carefully characterised.

a) Bacterial cell wall and surface interactions

Bacteria have on their surface multiple functional groups including carboxylate, hydroxyl, phosphate, and amine moieties [193]. Typically, negatively-charged groups

predominate on the cell wall of bacteria resulting in an overall negative charge. In addition, for most of bacteria it is characteristic to possess surface adhesin structures such as pili and curli, which will mediate the interaction with the surrounding environment. For example using the AFM technique, LGG pili were shown to bind to milk proteins [114], CH_3-terminated abiotic surface and to mucus of epithelial cells [78]. It is therefore a relevant topic in each area of bacterial life circle – from *in vivo* and *in vitro* laboratory studies to industrial applications. *E. coli* do also possess surface adhesins, as fimbriae type 1, which include in their structure mannose-binding lectin (FimH) [194]. Surface appendages of *E. coli* are of major importance in adhesion phenomena. For example, Ryu et al. have demonstrated that the presence of curli was crucial for biofilm formation on stainless steel by using curli-deficient and curli-overproducing strains of *E. coli* [195]. Curli presence or absence may even affect electrophoretic mobility of *E. coli* and therefore must be considered when evaluating electrostatic forces arising between bacterial cell and the substrate [112].

b) Substrate role in biofilm development: impact of surface energy

The nature of the bonds established with an abiotic substrate depends on the quantity of polar and non-polar groups on its surface (that reflect surface energy), and its surface charge. As such, there have been many investigations on how particular surface energy or surface charge (and its density) affects bacterial adhesion, development and retention on abiotic surfaces. For instance, knowing the exact surface energy of the surface is advantageous for an easier removal of pathogenic biofilms at washing. This fact was illustrated with *P. aeruginosa*, when the bacterial cells retained on substrates as a function of their surface energy values [196].

Surface energy is related to surface hydrophilic or hydrophobic properties, which can be evaluated with contact angle measurements (see part 2.1.4 for more details). It is thus often assessed on which substrate, hydrophilic or hydrophobic, bacterial adhesion is preferential. There is a substantial number of works showing that bacteria have stronger interaction forces with hydrophobic surfaces. It was suggested that hydrophobic surfaces are favourable for bacterial adhesion due to removal of water from the interphase of the interacting bacterial cell and a substrate enhancing the possibility of bridging [197]. For example, stronger interaction on hydrophobic (dimethyldichlorosilane-coated glass) relatively to hydrophilic (non-coated glass)

surfaces, was illustrated on six various bacterial strains (two strains of *Staphylococcus epidermidis*, two strains of *P. aeruginosa*, *Raoultella terrigena*, and *Streptococcus thermophilus*) [197]. Hydrophilic (activated with various siloxane molecules) surfaces also showed the greatest resistance to the adhesion of *L. monocytogenes*, *S. typhimurium*, S. *aureus*, and E. *coli* [198]. Li and Logan [199] have studied eight bacterial strains on eleven different surfaces (3 types of glass and 8 different metal oxides). In case of all bacterial strains several times higher number of cells were attached on the most hydrophobic surface among studied (Fe_2O_3) compared to the most hydrophilic one (Si-Sn glass), and on other nine tested surfaces the number of cells also increased with the increase of surface hydrophobic properties. Dou et al. [200] observed extremely low adhesion of Gram-positive bacteria *Micromonospora purpurea* on superhydrophilic and superhydrophobic surfaces presenting micron-sized hierarchical structures duplicated from rose petals, and attributed this effect to peptidoglycan-surface interaction. The authors also suggested that the adhesion of bacteria can be very low on superhydrophillic surfaces due you to tightly bound to the surface water layer, whereas on superhydrophobic surface the adhesion might be low due to trapped air in the irregularities of petal-like features. Similar findings represented by an increased adhesion of *E. coli* onto moderately hydrophobic surface, but very low adhesion onto superhydrophillic and superhydrophobic polystyrene-based polymers were later reported by Yuan et al. [201]. Superhydrophobic surfaces are known for their self-cleaning properties as for example a surface of a lotus flower that is very resistant to fouling due to its hierarchical micro/nanostructure and presence of waxes [202]. On such irregular surface the air is trapped in the vicinity of the leaf surface preventing its wetting and provoking an easy rolling off of the water droplet, which results in taking away also the dirt particles [202], [203].

The polarity of the substrate and its wettability properties are also relevant factors due to the fact that bacteria are surrounded by an aqueous environment. Water is a crucial participant in the substrate-cell interplay, the affinity of which to the substrate can drastically modulate bacterial adhesion and, even more, bacterial retention at surfaces. Several studies pointed on the importance of air-liquid interphase in the mechanisms of bacterial attachment stability [147], [197], [204]–[206]. Interestingly, the implication of forces arising at air-liquid boundary can be an issue also before actual removal of the substrate with the biofilm from an aqueous medium. This can be due to an air

bubble unintendedly introduced into flow cells or on surfaces of superhydrophobic nature and irregular topography due to air trapped in the surface defects, as listed with aforementioned examples [200]. In this regard, *in situ* methods (as AFM or ATR-FTIR spectroscopy, see part 1.2.2) enabling the observation directly in the aqueous medium are extremely valuable to understand the role that a particular surface has on biofilm stability, as kinetics of detachment can be followed in real time. Nonetheless, very few authors have attempted to modify the substrate surface for studying *in situ* the effect of the surface modification on the interaction between a substrate and a bacterium and its possible biofilm development. A very recent example is the AFM study comparing adhesive forces of *E. coli* and *S. aureus* onto sophorolipids, methyl- and hydroxyl-terminated alkanethiols in phosphate buffered saline [207]. Using the AFM mode, in which a single living bacterium is attached to an AFM probe (single-cell force spectroscopy), the authors demonstrated very low adhesive forces to sophorolipids compared to interactions with alkanethiols. The same technique was applied in the study of Sullan et al. to elucidate interactions between LGG pili and methyl-terminated gold-coated glass surface [78]. AFM can also be used for estimating the strength of bacterial attachment by gradual increase of the force with which, in this case, a bare AFM probe scans bacterial cells placed on the substrate. At a certain threshold force bacterial cells will detach from the surface and will disappear from the area of the image. An example is a study on the role of surface topography in the attachment *S. aureus* cells to the surface [208]. Flow-chamber set up does also permit the impact of the surface on bacterial attachment *in situ* to be studied. Thus, hydrophilic (non-coated) and hydrophobic (dimethyldichlorosilane-coated) glass substrates were used as substrates and their influence on the attachment and detachment of six different bacterial strains was demonstrated [197]. ATR-FTIR spectroscopy, however, to the best of our knowledge, has not yet been reported to employ chemically functionalized substrates for studying surface dependent bacterial adhesion and biofilm development. An exception, perhaps is the implication of ATR crystals coated with elements that differ in composition with respect to the crystal itself, such as hematite [165], [167], [172], [209] and titanium dioxide [210]. Nonetheless, functionalized with different molecules, ATR crystals were successfully used to investigate protein adsorption mechanisms [211], [212], DNA hybridization [213] and surface-dependent affinity of metal ions [214].

c) Substrate role in biofilm development: impact of the surface charge

With some exceptions [215], most of bacteria are characterised with an overall negative charge on their cell wall and therefore will be electrostatically attracted towards positively charged surfaces. Indeed, the adhesion of *P. aeruginosa* was found to be twice faster on positively charged methacrylate copolymers when compared in situ in a flow chamber with negatively charged methacrylate copolymers [216]. However, the relationship between surface charge and surface-associated bacteria is not evident to predict. Thus, within the first hour of adhesion ~4 times higher number of cells was counted on the positively charged substrates with respect to negatively charged ones. But when the flow of bacterial suspension was switched to the sterile nutritive medium, the growth was absent on the positively charged polymer, whereas on negatively charged surface it was exponentially increasing. In another work based on layer-by-layer self-assembly of cationic polyvinylamine / anionic cellulose nanofibril onto the cellulose surfaces the correlation between the density of positive charges and its inhibiting effect towards *E. coli* growth was recently reported [217]. Similarly, the results on reduced viability of bacterial cells (*E. coli* and *Bacillus subtilis*) after contact with positively charged substrates (ethylamine and diethylamine modified polyethylene membranes) were shown [218]. However, it is important to note that after 8 hours of a contact time with these surfaces, a higher number of viable *B. subtilis* cells compared to *E. coli* cells were counted, and this effect was attributed to a possible protection with a thick layer of peptidoglycan present in Gram-positive cells (*B. subtilis*). This result was in accordance with the study of Gottenbos et al., in which positively charged poly(methacrylate) surfaces prevented the growth of Gram-negative cells (*E. coli, P. aeruginosa*), but not Gram-positive cells (*S. aureus*, *S. epidermidis*) [219].

c) Substrate role in biofilm development: impact of the surface topography and composition

It should also be noted that the surface topography and surface composition are also determining factors in bacterial development. Some materials are intrinsically antibacterial as silver [220], copper [221] and photocatalytic materials (ZnO, TiO_2) [35], [36] (see part 1.1.2). The viability of bacterial cells on such surfaces is an adequate concern that should be considered, in particular also in reports of antipathogenic assays using probiotics (an example of such study is [63]). As for surface topography,

there have been several works conducted for its impact on bacterial adhesion and growth to be revealed. Using *S. aureus* and *P. aeruginosa* species, Whitehead et al. [222] showed that a titanium-coated silicon surface patterned in order to present valleys with the width corresponding approximately to the size of bacterial cells retained efficiently bacterial cells into these valleys. The preferential retention of bacteria on surfaces presenting scratches of microbial dimensions was later confirmed by the same group with *L. monocytogenes* and *Staphylococcus sciuri* species on titanium coated substrates [223]. Perera-Costa with colleagues demonstrated using three different bacterial genera having either rod (*Bacillus subtilis*, *E. coli*) or sphere (*S. epidermidis*) shapes that, irrespective of the shape, bacteria preferentially adhere onto receding features of the patterned surface, given the size of these receding features is slightly larger than the size of bacterial cells (5–10 µm) [224]. Similar findings were reported by Lorenzetti and co-workers using *E.coli* and titanium-based substrates with surface topography having features varying in the size from 0.4 µm (lower adhesion) to 3 and 5 µm (higher adhesion) [225]. However, nanoscale surface pores of certain size seem to reduce the attachment of bacterial cells. Indeed, four different species of bacteria (*E. coli*, *L. monocytogenes*, *S. aureus*, *S. epidermidis*) attached with significantly lower efficiency onto nanoporous aluminium oxide when the pores were 15 and 25 nm, but the attachment was stronger when the size of pores was 50 and 100 nm [226]. These results jointly demonstrate major implications of surface features in the infection outbreaks occurring as a result of contamination of the equipment with pathogens. Indeed, micron-sized scratches on the surface can be a niche for bacterial growth in the industrial equipment, as was seen for instance during the examination of the contamination case of real milking equipment with *Listeria monocytogenes* [24]. Interestingly, by tuning the surface topography one can drastically change the growth of bacteria in a multispecies biofilm. For example, by fabricating a surface with pillars of different length Bhattacharjee et al. succeeded to attribute probiotic properties to a commensal strain of *E. coli* in a sense that it was able to inhibit the biofilm growth by *P. aeruginosa* [227].

d) DLVO theory to model bacteria-surface relationship

Bacterial adhesion is often modelled with Derjaguin, Landau, Verwey, and Overbeek (DLVO) theory originally developed for explanation of colloidal aggregation in aqueous

dispersions [228], [229]. In accordance with this theory, the interaction between the bacterial cell and the surface is determined by long-range electrostatic repulsive forces and short-range attraction forces, the latter known as Van der Walls forces. In particular, the influence of the distance between two interacting particles on these forces is considered, as well as the charges of the particles and the presence of counter ions (with the charge opposite to the surface charge of the particles) present in the medium. In addition, extended DLVO theory (XDLVO) has been developed to include the contribution from acid-base interactions [230]. However, both DLVO and XDLVO theories assume the interaction between smooth particles, whereas bacterial surface is not smooth and overall far more complex compared to a colloidal particle. Surface appendages (e.g. pili, flagella) may project up to several micrometres from the cell wall. In addition, bacteria are surrounded by a thick wall (0.2–0.4 µm) of protein and polysaccharide fibres [133]. Consequently, care should be taken when predicting bacterial adhesion using DLVO theory and its limited application must be considered.

e) Conclusions

Taken together, these numerous examples illustrate how important is the role of the surface in bacterial adhesion and biofilm formation phenomena. Nonetheless, biofilms of probiotics on abiotic surfaces were very poorly addressed in literature. Limited examples include only studies that provide evidence to the ability of probiotics to form biofilms on abiotic substrates such as polystyrene and glass [79], [231], [232]. However, to our awareness, studies on the effects of substrates with well-defined surface chemistry on biofilm formation by probiotics, and in particular LGG, were not reported thus far. This subject is, yet, of great interest to investigate due to promising strategy utilizing biofilms of probiotics against pathogenic growth (as described in part 1.1.3), and for fundamental knowledge on the behaviour of probiotics in the surface-associated form. This knowledge would be of special practical use for understanding *in vitro* laboratory tests of biofilm formation with probiotics, including those that evaluate their antipathogenic effect. Indeed, it seems as a common practice to perform only short-time adhesion tests on biological cells, whereas longer-term biofilm formation assays are made in microtitre plates or other relevant abiotic substrates [59], [60], [66] (see also table 1.1). To develop the surface with well-defined chemistry it is necessary to graft onto the surface molecules with well-defined functional groups. In

this regard, a simple and fast route to obtain stable and homogeneously distributed functionalisation is self-assembly of alkanethiol monolayers that is discussed below.

1.3.2. Control of surface properties using functionalisation chemistry

Surface can be functionalised using two main families of functionalisation methods – supramolecular chemistry and covalent bonding.

a) Grafting by supramolecular chemistry methods

Supramolecular chemistry concentrates on the interactions that are weaker than covalent bonding and reversible, such as hydrogen bonding, electrostatic interaction and Van der Waals bonds. A well known example of supramolecular grafting methods is the layer-by-layer (LbL) technique, in which films of controlled composition and arrangement are formed by alternating layers of oppositely charged macromolecules [233] (figure 1.7a). The LbL method is versatile and practical in many applications owing to the possibility of tailoring the surface properties (planar surfaces but also sphere capsules of micron and nanoscale dimensions) through the choice of the polyions. Usually, polymers are used as constituting layer such as poly(ethylenimine), poly(dimethyldiallyl ammonium chloride), poly(allylamine), poly(lysine), etc. as polycations, and poly(styrenesulfonate), poly(vinylsulfate), poly(acrylic acid), etc. as polyanions. The resulting film properties will depend on the chosen combination of molecules. LbL deposition technique has proven its utility in many domains [234], but has a limitation of being dependent on the electrostatic forces that can be weaken in the presence of salts and alternated by pH changes [235]. Both issues are adequate concerns when studying bacterial suspensions. Indeed, bacteria, especially *lactobacilli*, are able to lower the pH of the medium drastically (down to 4–4.5 and even lower for some species) because of their ability to release lactic acid as a result of glucose fermentation, as well as other organic substances [236].
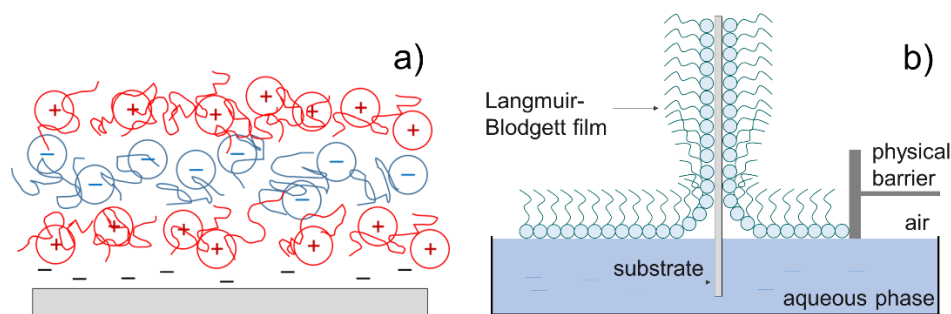
Figure 1.7. Non-covalent chemistry for surface functionalisation: a) schematic representation of layer-by-layer deposition depicting adsorption of charged materials to an oppositely charged surface (modified from [233]), and b) schematic representation of the procedure for obtaining Langmuir-Blodgett films (modified from [237])

Another technique for surface functionalisation based on non-covalent bonding is fabrication of Langmuir-Blodgett (L-B) films (figure 1.7b). The L-B technique allows grafting monolayer structures by pulling a solid substrate through a monolayer of amphiphilic molecules at the air-water interface [237], [238]. The molecules that are desired to graft are first diluted in a volatile organic solvent (e.g. chloroform, hexane), and the drop of this solution is carefully spread on the aqueous surface. After evaporation of the organic solvent, the amphiphilic molecules are reorganised at the air-water interphase in such a way that non-polar tails rise against the aqueous surface, whereas polar groups are directed towards water phase. In order to make a dense film of these molecules, the aqueous surface is compressed by moving a physical barrier. The compressed film of organic molecules is further transferred onto the solid substrate that can be of various nature (glass, metals, metal oxides, mica etc.) by immersing the substrate into the aqueous media. The process of grafting is driven by lowering surface free energy of the solid substrate with surfactant molecules. The L-B technique is an attractive method for obtaining monolayer structures, in particular for mimicking biological membranes. Indeed, the effect of drug action, membrane permeability and chain reactions in such a set up can be successfully followed [239]. However, the disadvantage of the L-B method is a poor chemical and mechanical stability of obtained films [240], the need to use toxic solvents and critical importance of keeping the device exceptionally clean [241].

b) Surface modification by covalent functionalisation

To perform a robust and homogeneous functionality, a covalent bonding between a surface and a grafting molecule is very preferential and advantageous, and was in primary focus of the present work. There are two main routes that have been widely

applied for covalent surface grafting that employ silanization or alkanethiol self-assembly chemistry (figure 1.8).

In silanization, the general experimental procedure represents the grafting of silane molecules (alkyltrichlorosilanes, alkylalcoxysilanes, alkylaminosilanes, etc.) onto hydroxylated surfaces (SiO_2/Si, Al_2O_3/Al, TiO_2/Ti, mica, glass, etc). In particular, the reaction of alkyltrichlorosilanes with -OH terminated surface occurs as a result of hydrolysis of trichlorosilane groups after physical adsorption of molecules on the water layer present on the surface. The presence of a thin water film permits in-plane reorganization of organosilanes at the surface, and eventually covalent siloxane bonds are formed at the surface providing formation of stable densely packed monolayer [242]. It must be noted, however, that an actual monolayer structure is relatively difficult to obtain due to high interlinking between silane molecules leading to a disorganised surface finish. This has major implications in the investigation of bacterial attachment efficiency, as the level of surface organisation will affect the number of the molecular groups exposed to bacterial cells, ultimately varying surface charge and surface energy of the substrate [198], [243]. For a reproducible reaction gas-phase grafting in an evacuated glove box is a better choice, but make the process laborious and time-consuming. Alternatively, with a various success in terms of homogeneity of monolayer structure [244], the reaction can be carried in organic solvents (e.g. toluene), that should be handled with care due to their toxicity.

Figure 1.8. Schematic view of SAM supported on a substrate: a case of silanized surface on the example of (3-Aminopropyl)trimethoxysilane (left) and thiolated surface on the example of decanethiol (right)

An easier and faster route to obtain reliable surface chemistry is represented by alkanethiol self-assembly. Self-assembled monolayers (SAMs) are organic assemblies spontaneously formed into (semi)crystalline structures by the adsorption of molecular constituents from the solution or the gas phase on the surface of solids (or liquids such as mercury) [245]. SAMs consist of three fundamental units: an anchor group that

provides binding to the substrate surface, a functional group determining final surface properties and a linker between those two (e.g. sulphur bridging atom, alkanethiol chain and methyl terminal group in figure 1.8).

The process of self-assembly of alkanethiols in liquid media is typically initiated by an immersion of the suitable substrate in a solution of thiol-derived molecules. Ethanol is a common solvent because it solvates a variety of alkanethiols and has low toxicity. Nonetheless, depending on the type of organic compounds, other solvents, such as acetone, water, dichloromethane, etc. can be considered [246]. Upon immersion of the substrate, the molecules adsorb onto the surface in seconds, first, forming a loosely packed monolayer, and eventually developing dense flawless structures within several hours of exposure (usually overnight). The minimum concentration for forming a dense SAM is 10^{-2} mM, but low concentrations require longer immersion times, therefore in practice dense monolayers are obtained with the typical concentration of 1 mM [247]. The process of monolayer formation is self-terminated as the anchor group is chosen to have affinity to the substrate, but not to the terminal group of the formed monolayer.

The formation of SAMs undergoes easily owing to the thermodynamic favorability of the process. Bare surfaces of metals have high surface energy, which is readily lowered with the adsorption of organic substances. Due to a high affinity of thiols for surfaces of noble and coinage (Au, Ag, Cu) metals, most studied SAMs are those formed by the adsorption of alkanethiols on gold, silver, copper, platinum, palladium, and mercury; these systems are thoroughly described in a large number of reviews [245], [246], [248]–[254].

Most studied and well-characterised systems are SAMs of alkanethiols on gold. This substrate became a sort of a standard for SAM formation due to several reasons including (i) inertness of gold, (ii) facility of preparation of gold films with physical and chemical methods, (iii) its use in many characterisation techniques (e.g. surface plasmon resonance (SPR) spectroscopy, quartz crystal microbalances, infrared reflection-absorption spectroscopy, electrochemical methods, etc.), and (iv) compatibility of gold with biological samples [245]. The monolayer is covalently bonded to the Au surface via S atom and stabilized by Van der Waals interactions between alkane groups of hydrocarbon chains, oriented at 30⁰ with respect to the plane of the surface (figure 1.9).
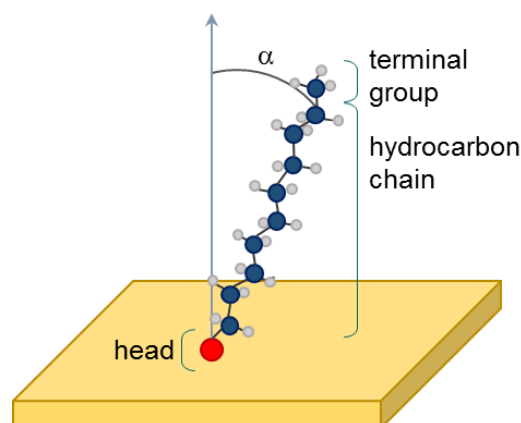
Figure 1.9. Scheme of a decanethiol molecule adsorbed onto gold crystal in a standing up configuration. $\alpha = 30°$. Red: sulfur atom; blue: carbon atom; white: hydrogen atom. Drawn based on [248]

The energy of the S-Au bond is ~50 kcal/mol, whereas the energy of methylene-methylene bond between hydrocarbon chains is equal to ~1–2 kcal/mol. Therefore, the binding to the surface is stable at temperatures up to ~60 degrees [255]. During the process of adsorption, the thiol molecule loses S-bonded H atom, converting itself in a thiolate. The process is expected to comply the following reaction [248]:

$$CH_3(CH_2)_n SH + Au \rightarrow (CH_3(CH_2)_n SH)_{phys} Au \tag{1.1}$$

$$CH_3(CH_2)_n SH_{phys} Au \rightarrow CH_3(CH_2)_n S\text{-}Au + 1/2\,H_2 \tag{1.2}$$
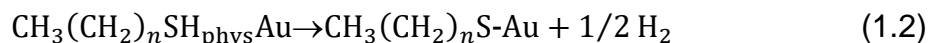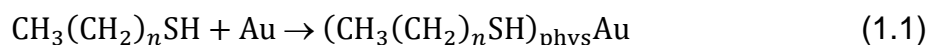
where (1.1) and (1.2) correspond to thiol physisorption and chemisorption, respectively. However, the nature and mechanism of the chemisorption reaction is not completely understood. Particularly, it remains unknown whether the adsorption of alkanthiol involves ion or radical species. Furthermore, the fate of released hydrogen atom is not determined unambiguously. While in a vacuum it probably exists in the form of dihydrogen, in solution another possibility occurs, that is formation of water molecules due to presence of oxygen in the medium [245].

Physical and chemical properties of SAMs and hence, of the functionalized surface, depend in a large extend on the choice of the terminal group. The interactions of terminal groups with respect to each other must be carefully considered. Notably, functional tails containing carboxyl or amine groups may link to each other via hydrogen bonding resulting in the formation of a bilayer (figure 1.10).
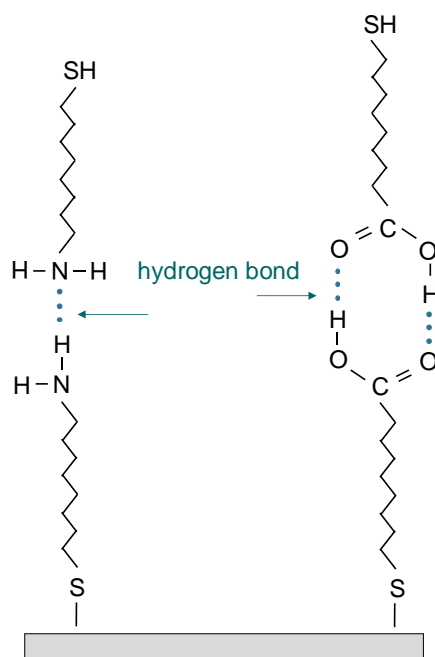
Figure 1.10. Illustration of a possible bilayer formation of carboxyl- and amino-terminated SAMs. Modified from [256]

Various attempts have been made in order to extend thiol chemistry on surfaces of other compositions. In particular interest for the present work the study of Noble-Luginbuhl and Nuzzo illustrating the feasibility of SAM formation on ZnSe [257]. Zinc selenide (ZnSe) is a material transparent in the infrared range and therefore suitable for ATR-FTIR measurements and *in situ* monitoring of biofilm formation. Nonetheless, the feasibility of its chemical functionalisation were extremely scarcely addressed in literature. Indeed, besides alkanethiol chemistry presented by Noble-Luginbuhl and Nuzzo, silanization and photoactivation routes were considered in two studies [213], [258]. Noble-Luginbuhl and Nuzzo performed the adsorption of alkanethiols $HS(CH_2)_nCH_3$ of different chain length (n = 7, 11, 15, 17) and an alkanethiol with hydroxyl terminal group $HS(CH_2)_{12}OH$ [257]. Alkanethiols formed well-organized monolayers, whereas the number of conformational defects decreased with growth of the number of carbons in the chain. The hydrophobic character of SAMs with the methyl terminal group increased with increasing length of hydrocarbon chain, in line with the earlier observations of Bain et al. on gold [247]. Hence, different wetting properties of monolayers make them a suitable model system for studying surface interactions at the molecular level, including bacterial biofilms [139], [140], [259].

A great variety of organothiols with different functional groups provides numerous options for SAM applications. In regard with biofilm studies, a common model system

is based on SAMs terminated with –CH$_3$, -OH, -COOH, -NH$_2$ functional groups, where first two represent hydrophobic/hydrophilic surfaces, and second two bring negative/positive charge to the surface. For instance, microbial (*B. subtilis*) attachment and adsorption–desorption kinetics was studied on these model surfaces using SPR spectroscopy [139]. Of interest, the rate of attachment was higher on NH$_2$-terminated surface owing to electrostatic interaction with negatively charged bacteria. However, the quantity of attached cells were eventually higher on CH$_3$-terminated surface, indicating, as suggested by the authors, a stronger contribution of hydrophobic forces in the bonding mechanism of this bacterium. Although it must be noted that, as it is described in part 1.3.1, the resulting lower biomass quantity can be due to inhibiting effect of positive charges [216]–[219]. SPR spectroscopy does not allow further elucidate these aspects, and other methods enabling *in situ* characterisation should be used.

1.4. Aim of the present work

The goal of this PhD project was to study *in situ* the development and possible control of bacterial biofilms by *Lactobacillus rhamnosus* GG on surfaces with controlled physico-chemical properties, and subsequently the possible inhibiting action of LGG biofilm against *E. coli* adhesion and growth.
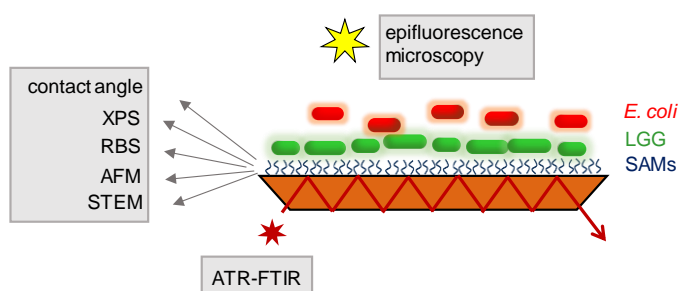
Figure 1.11. Schematic representation of the concept of the project and used characterisation techniques

Several steps summarised in figure 1.11 were performed in order to accomplish the aim:

(i) functionalization of nude ZnSe and gold coated ZnSe using self-assembly of alkanethiols HS(CH$_2$)$_n$X (X=CH$_3$, OH, NH$_2$, n = 11 or 10); these surfaces are suitable for the ATR-FTIR method that is used for the *in situ* monitoring of biofilms development;

(ii) characterisation of obtained surfaces by means of infrared spectroscopy, contact angle measurements, Rutherford backscattering spectrometry, X-ray photoelectron spectroscopy, and atomic force microscopy to confirm the control of the surface chemistry and its physico-chemical properties;

(iii) LGG biofilms formation on functionalized surfaces with *in-situ* spectroscopic analysis of their molecular fingerprints at different stages of their development; ATR-FTIR measurements of LGG biofilms were accompanied by epifluorescence microscopy and single-molecule force spectroscopy for a better understanding of LGG interactions with the functional groups and the impact of surface properties on the biofilm development;

(iv) finally, the substrates with functional groups leading to the highest LGG coverage that maintain LGG alive and metabolically active were chosen to test LGG efficiency against *E. coli* adhesion and growth; a mutant strain of *E. coli* that specifically express adhesins on its surface was used for a closer imitation to a real pathogen; several methods were tested to distinguish LGG and *E. coli* on the functionalised substrates.

The use of probiotics as a bio-tool to preserve surfaces and control pathogen growth is a promising strategy. It is of importance to consider the effect of the environmental conditions on probiotic bacteria when estimating their antipathogenic properties. The range of methods used in the present work will help to elucidate the mechanisms of LGG biofilm formation on abiotic surfaces and to have a better knowledge of its antipathogen potential, of interest for further research and use of LGG biofilms.

II. Materials and methods

2.1 Preparation of substrates and their characterisation

2.1.1. Magnetron sputtering of gold onto ZnSe crystal

Magnetron sputtering is a physical vapour deposition method used for the deposition of thin films on different types of substrates. The process is based on the ionisation of a gas by flowing electrons between two electrodes (the target, i.e. material to be deposited, and a sample holder (figure 2.1), and sputtering of the material by the newly formed ions. The flow of electrons is generated by high voltage, and electrons leave the target at high speed. These electrons will hit the atoms of the gas filling the chamber (argon in figure 2.1), leading to removal of electrons from the gas atom shell (ionisation). Positively charged ions of the gas (plasma) directed by electromagnetic field will strike the negatively charged target. As the speed of ions is very high, their kinetic energy is sufficient to eject the atoms from the target. These atoms are then condensed on the substrate placed in the proximity of the target. The control of electric and magnetic fields in the chamber allows regulating the rate of the deposition, while the duration of the voltage supply will affect the film thickness.
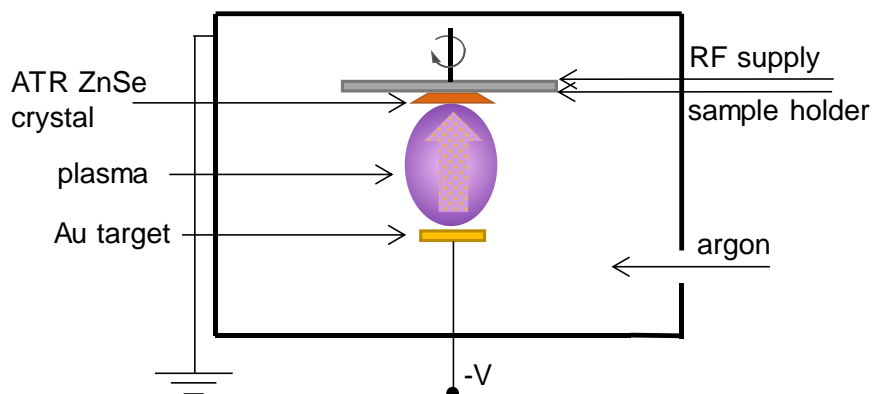
Figure 2.1. Scheme of plasma vapour deposition process of gold onto zinc selenide

The surfaces of trapezoidal ATR ZnSe crystals (6.8×1×0.6 cm, Eurolabo) and ZnSe disks (Ø 1.8 cm, Crystran) were coated with a thin layer of gold at a rate of 3 nm/min in a home-built apparatus. The crystals were mounted on a rotating holder with the distance of 5 cm to the gold target. The argon flow in the deposition chamber was 50 cm^3/min, whereas the total pressure was 0.4 Pa. The charge voltage was set at 333 V (Pinnacle Plus DC power supply, Advanced Energy) and the current was 11 mA.

The samples were etched with argon using radio frequency (RF) supply for 1 minute, which was instantly followed by the deposition of gold for 1 minute.

2.1.2. Self-assembly of alkanethiols onto bare and gold-coated ZnSe crystal

a) ZnSe substrate preparation

In this work, three methods to prepare the surface prior to functionalisation with SAMs were tested (figure 2.2):

(i) exposure of ZnSe to ozone/UV (15 min) followed by rinse with isopropanol [257];

(ii) dipping of surface of ZnSe into H_2O_2 (10 %, 30 s) and HCl (10 %, 1 min) (v/v) solutions [213];

(iii) coating of ZnSe with Au followed by ozone/UV treatment (15 min) and rinse with isopropanol.
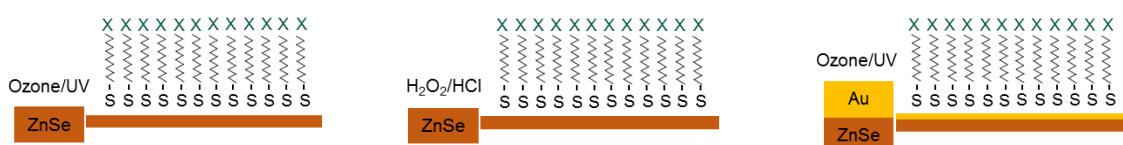
Figure 2.2. Schemes of substrates used for SAM functionalisation, X=CH$_3$, OH or NH$_2$

b) Alkanethiol self-assembly

Freshly cleaned ZnSe or Au/ZnSe crystals (figure 2.3a) were mounted into the infrared flow cell (Specac, figure 2.3b).
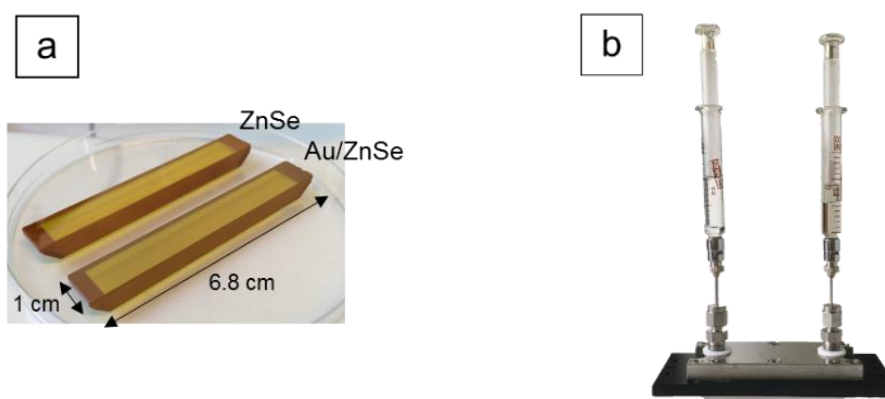
Figure 2.3. ZnSe and gold-coated ZnSe ATR crystals (a) and mounted infrared cell filled with alkanethiol solution (b)

The mounted infrared cell was filled with 2 mM ethanolic solution of alkanethiols $HS(CH_2)_{11}X$ (X=CH_3, OH, or NH_2, Sigma-Aldrich, purity 97–99 %) and left for self-assembly reaction overnight. The surface of the crystal was subsequently rinsed inside the cell with ethanol and ultra-pure (18.2 MΩ.cm) sterile water.

2.1.3. ATR-FTIR in situ monitoring of alkanethiol adsorption onto surfaces

Infrared spectrometry is based on vibrations of bonds in molecules [141], [260]. Molecules undergo vibrations at frequencies falling in the infrared part of the electromagnetic spectrum. The beam of the infrared radiation passing on the sample is partially absorbed at frequencies resonant to those of specific vibrations in molecules. The likelihood of absorption of the infrared radiation depends essentially on the change in electric dipole of the molecular bond. This is a selection rule of the infrared spectroscopy, according to which polar molecules like water have strong signals in infrared.

The energy of the bonds between different atoms is varying due to intrinsic atom properties such as number of electrons and mass. The change in the interaction between atoms can be viewed as spring-like behaviour (figure 2.4) According to Hooke's law, the force required to extend the spring is directly proportional to its extension with the proportion coefficient k that represents the force constant of the bond.
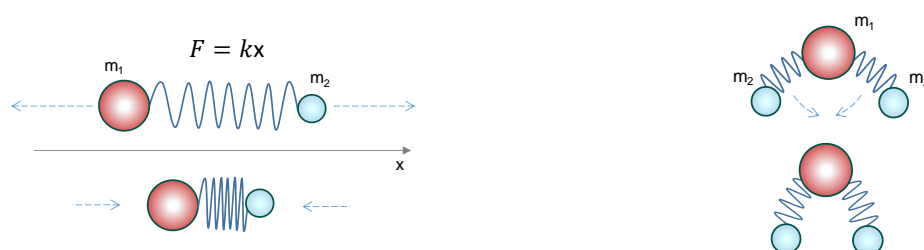
Figure 2.4. Schematic representation of vibration of molecules with atoms of masses m_1 and m_2: left – expanding / contracting (stretching vibration) of the bond with applied force F proportional to the distance x, right – deformation of the angle of the bond (bending vibration)

Then, the following equation relates the frequency of vibration ν of the diatomic molecule, the force constant and the masses of the atoms m_1 and m_2:

$$\nu = \frac{1}{2\pi} \sqrt{k \left(\frac{1}{m_1} + \frac{1}{m_2} \right)}. \tag{2.1}$$

In addition to stretching of molecular bonds, they may undergo bending vibrations that occur when the angle of the bonds is changing (figure 2.4). The energy required for bending vibration is lower than that of stretching vibration, which can be imagined on the example of a simple elastic rod – it is easier to bend it than to stretch it. Bending vibration may occur only in molecules with the number of atoms higher than two. This is due to the vibrational freedom of molecules that depends on the number of atoms. Overall, for the molecule made of N atoms the degree of freedom is equal to 3N, because each atom has three degrees of freedom in the three-dimensional system of coordinates. In this 3N, three degrees of freedom correspond to translation of the entire molecule in space. Furthermore, non-linear molecules rotate around three axes giving the rotational degree of freedom equal to three. The left $3N - 6$ degrees of freedom are vibrational in non-linear molecules. In linear molecules, however, the rotation around one axis does not lead to any changes in the molecule. Thus, the number of rotational degrees in this case are equal to two, leaving $3N - 5$ degrees of vibrational freedom.

Given the fact that molecular vibrations depend on the strength of the bond between atoms, their mass and their environment, one can obtain information on the molecular structure and composition of a substance by analysing vibrations. When the beam of infrared light illuminates the sample, part of its energy is absorbed at frequencies resonant to molecular vibrations. The difference in energy of the incident and final beam is characteristic for the sample molecular structure.

The infrared spectrum is obtained as a result of the ratio of the intensity of the beam obtained from the reference sample (e.g. the solvent without the sample or air) and the intensity of the beam after interaction with the sample. For example, figure 2.5 shows the infrared spectrum of liquid water taken with air as a reference. Two pronounced bands are visible corresponding to stretching and bending vibration of the molecule.
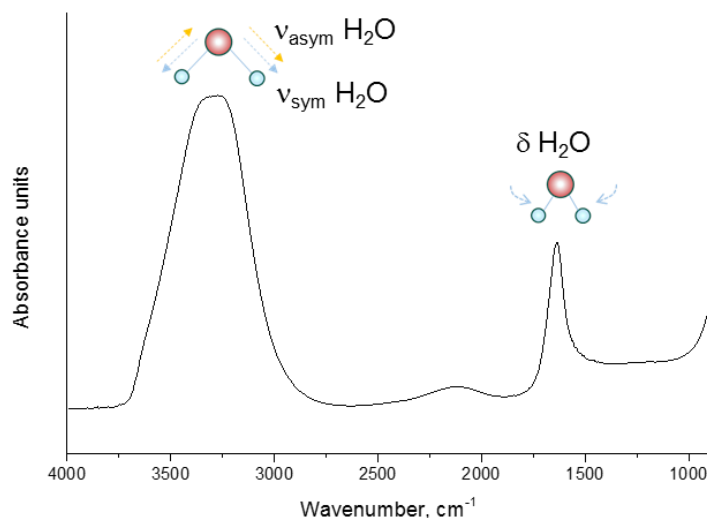
Figure 2.5. Infrared spectrum of water: ν OH and δ OH are stretching and bending vibrations, respectively

The intensity of the bands is measured by detecting the light using, most commonly, pyroelectric detectors. These detectors are based on the measurements of how fast the temperature of the material of the detector (e.g. deuterated-triglycine sulfate) changes upon infrared absorption. It means that ferroelectric crystals comprising the material, change their polarizability with the temperature increase, generating a charge that is detected by electrodes. Alternatively, photoconducting detectors are used when higher sensitivity is needed. They are composed of semiconducting materials that produce electrical current when excited by arrived photons of infrared light. They are more difficult to operate in practice since liquid nitrogen cooling is required to avoid excitation of electrons by thermal motion.

The intensity of the bands is presented as a function of the wavelength of the infrared radiation, expressed through a wavenumber (reciprocal of the wavelength, cm^{-1}). The convenience of the use of wavenumber term is in its proportionality to the energy of the bond. The measurement of the signal intensity as a function of the wavenumber is obtained with the aid of the Michelson interferometer (figure 2.6). When the light is injected from the source, it passes through the beam splitter that transmit half of the light and reflect the other half. The transmitted part arrives to the fixed mirror, from which it is after reflected back to the beam splitter. The reflected part passes to the mirror subjected to a slow move. Moving of the mirror changes the path distance for one half of the light. It means the amplitude of recombined beams changes as a function of distance that the mirror has moved. The amplitude has its maxima points

when both beams travel in the same phase and minima when the beams cancel each other, intermediately giving sinusoidal curve on the detector, the frequency of which is equal to the frequency of the incident infrared beam. The changes in the amplitude of recombined beam as a function of mirror displacement are recorded by the detector and using mathematical operation Fourier transform (FT) transferred into a new function of signal intensity versus wavenumber. The use of FTIR enables fast recording of spectra because all frequencies are analysed at the same time, while a good resolution is maintained (depending on the maximum displacement of the moving mirror).
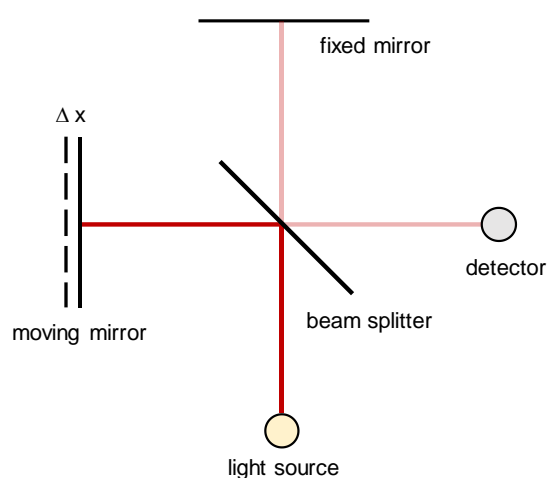
Figure 2.6. Schematic representation of Michelson interferometer (modified from [260])

Infrared spectroscopy can be used in several modes depending on the sample under study: transmission (when the light crosses the sample), reflection-absorption (IRRAS, when the beam is reflected from the sample placed on a mirror), diffuse reflectance (DRIFTS, when multiply scattered IR beam is collected by a spherical mirror), and attenuated total reflection (ATR), the latter being further discussed. ATR and IRRAS have the advantage of being surface-sensitive techniques, whereas ATR additionally allow analysing aqueous samples.

In ATR–FTIR spectroscopy, the sample is placed in contact with a infrared-transparent ATR crystal with high refractive index (figure 2.7). A high index of refraction ensures that the phenomenon of total internal reflection occurs with samples of various nature given the angle of incidence is greater than the critical angle (θ_c) defined as following:

$$\theta_c = \sin^{-1}\left(\frac{n_2}{n_1}\right), \tag{2.2}$$

where n_1 and n_2 are refractive indexes of the ATR crystal and the sample, respectively. The infrared beam is focused onto the edge of the crystal, multiply reflected on the inner surface of the ATR crystal, and then directed to a detector. At each reflection at the sample–crystal interface, an evanescent wave is created and its energy is propagated into the sample. It is absorbed by the sample at resonance with vibration of molecules of the sample.
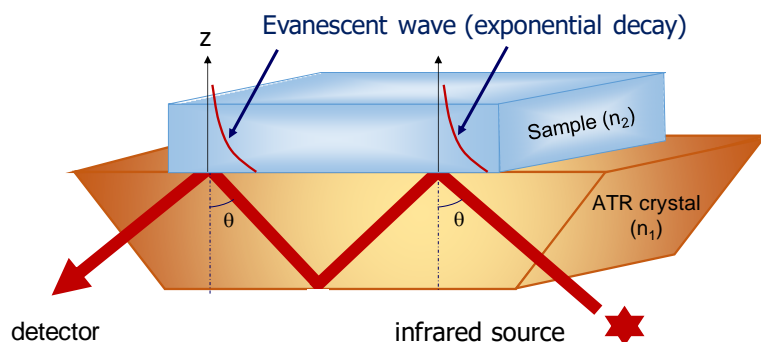
Figure 2.7. schematic representation of the principle of work of ATR–FTIR spectrometer: n_1 and n_2 are refractive indexes ($n_1 > n_2$), θ – angle of incidence at which total internal reflection occurs ($\theta > \theta_c$). Drawn based on [261]

The electric field amplitude of this evanescent wave decays exponentially with the distance from the crystal surface. The penetration depth, d_p, of the evanescent wave is defined as the distance at which the evanescent wave drops to e^{-1} times its intensity:

$$d_p = \frac{\lambda}{2\pi\sqrt{(n_1{}^2 \sin^2 \theta - n_2{}^2)}}, \tag{2.3}$$

where λ is the wavelength of the incident radiation, n_1 is the refractive index of the crystal, n_2 is the refractive index of the sample in contact with the crystal, and θ is the angle of incidence. Common materials used for ATR crystal manufacturing are zinc selenide, germanium, silicon and diamond. For example, in analysis of aqueous samples the penetration depth of ZnSe and diamond is 1.25 µm at 1600 cm^{-1}.

The signal intensity in ATR–FTIR is thus determined by multiple factors including wavelength, refractive index, number of reflections, and quantity of the sample in contact with the ATR crystal.

In this work, the kinetics of self-assembly process of alkanethiols onto the ATR crystal was monitored using Bruker Tensor 27 or Bruker Vertex 70v FTIR spectrometers equipped with beam splitters made of KBr and deuterated triglycine sulfate (DTGS)

thermal detectors. Recording of spectra and their processing were performed using the OPUS 7.5 software (Bruker, Karlsruhe, Germany). The geometry of the used infrared device provided six internal reflections on the upper face of the crystal that is in contact with the alkanethiol solution. The spectrum of ethanol recorded just before the start of each experiment was used as a background (reference spectrum). The infrared device was permanently purged with the nitrogen flow to avoid ethanol vapour contribution in the spectra [262] (Annexe I), which otherwise may appear unpredictably and mistakenly attributed, for example, to bacterial fingerprints [263]. ATR-FTIR spectra of alkanethiols in ethanol were obtained every 1.5 minutes for the first 45 minutes and then every 20 minutes by recording 100 scans per spectrum at a resolution of $4 \, cm^{-1}$. The spectra are presented with an absorbance scale corresponding to $\log(R_{reference}/R_{sample})$, where R is the internal reflectance of the device. All interferograms were Fourier processed using the Mertz phase correction mode and a Blackman-Harris three-term apodization function. Second derivative spectra were used to determine band positions. ATR correction was not performed. Water vapour subtraction was performed and baseline was corrected at 3000 and 2820 or 2780 cm^{-1}.

2.1.4. Contact angle measurements

Contact angle is the angle arising at the intersection of the liquid-solid interface and the liquid-gas interface when the drop of a liquid is placed in contact with a solid substrate (figure 2.8). The contact angle is dependent from the shape of the droplet, which in turn is determined by a surface tension of the liquid and substrate wetting properties in combination with other external forces, such as gravity. A state in which a droplet rests at equilibrium between three interfacial tensions defines the value of contact angle θ, that can be calculated using Young's equation:

$$\gamma_{lg} \cos \theta = \gamma_{sg} - \gamma_{sl}, \tag{2.4}$$

where γ_{lg}, γ_{sg}, and γ_{sl} represent the liquid-gas, solid-gas, and solid-liquid interfacial tensions, respectively [264].
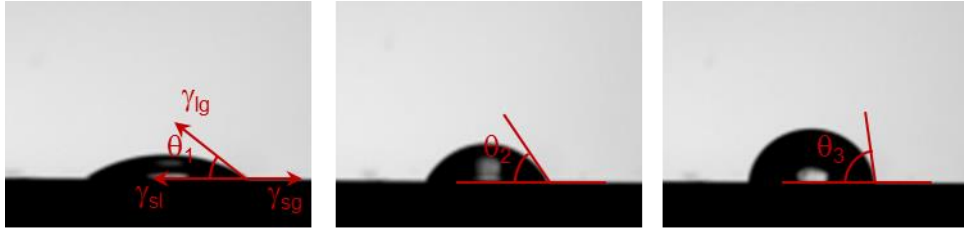
Figure 2.8 Illustration of how a contact angle θ is varying as a function of surface wetting. From left to right: hydrophilic surface to more hydrophobic surface

Several models exist for the calculation of the surface energy of the substrate from contact angle data, for example those based on Zisman, Owens/Wendt, Fowkes or Neumann theories. The debates on the validity of these theories are still ongoing, because none of them model perfectly the reality of the interaction between a solid and a liquid [265]. The choice of the model is often determined by the nature of the substrate (polar / non-polar) and by obtained degree of the fitting error. Thus, it is important to understand that the value of surface energy can be only compared given that the same model for its calculation has been applied. First, Zisman model was tested for estimation of the surface energy of ZnSe functionalised with different SAMs. It did not result in a good estimation of the surface energy due to high fitting error. This model does not take into account polar interactions between solid and liquid, and thus generally works best on non-polar surfaces.

To take into account the polar part of the functionalised ZnSe, Fowkes theory that dissociates polar and nonpolar (dispersive) components was applied [266]:

$$\frac{\gamma_l(\cos\theta + 1)}{2} = \left(\gamma_l^d\right)^{1/2}\left(\gamma_s^d\right)^{1/2} + \left(\gamma_l^p\right)^{1/2}\left(\gamma_s^p\right)^{1/2}, \qquad (2.5)$$

where γ_l^d and γ_l^p are the liquid dispersive and polar components, respectively, and γ_s^d and γ_s^p are the solid dispersive and polar components, respectively. First, the contact angle with diiodomethane ($\gamma_l^d = 50.8 \text{ mJ/m}^2, \gamma_l^p = 0 \text{ mJ/m}^2$) was measured and the dispersive component of the solid surface energy was calculated. Second, water ($\gamma_l^d = 21.8 \text{ mJ/m}^2, \gamma_l^p = 51.0 \text{ mJ/m}^2$) contact angle measurements were performed and the polar component of the solid surface energy was computed. Fowkes theory assumes that the total surface energy is the sum of the dispersive and polar components:

$$\gamma_s = \gamma_s^d + \gamma_s^p.$$

(2.6)

The measurements of contact angles were performed using a Digidrop contact angle meter (GBX Scientific Instruments). A liquid droplet of 0.5 μL was carefully deposited onto the sample surface with a syringe. The syringe was withdrawn and the image of static contact angle was taken immediately after liquid deposition. The reported contact angle values are based on 5 repeats.

2.1.5. X-ray photoelectron spectroscopy

X-ray photoelectron spectroscopy is a method used to determine the composition as well as the chemical state of elements on the topmost (~10 nm) surface of a sample. The method is based on the Einstein's theory of photoelectric effect. In accordance with this theory, an X-ray photon of energy hv ejects an electron from a core level of an element on the sample's surface. Using sufficient energy, the electron leaves its atomic orbital to be emitted from the sample surface. This process is described by the equation of energy conservation in photoemission:

$$E_B = hv - E_k - W,$$

(2.7)

where E_B is binding energy of the electron, hv is the energy of the X-ray photon, E_k is the kinetic energy of the photoelectron, and W is the work function of the spectrometer. Thus, the binding energy can be determined by measuring the kinetic energy of the photoelectron, given that the X-ray energy and the work function are experimental parameters.

The XPS spectrum is a plot of the collected intensity as a function of the binding energy distribution of the electrons. A typical XPS spectrum consists of sharp photoelectron core-level peaks sitting on a relatively low background of inelastically scattered electrons. Since each element has a unique set of binding energies, the surface elemental composition can be determined as well as the information about its electronic structure. In order to avoid the loss of the energy of photoelectrons on the way to the detector, the environment in the experimental chamber is maintained under ultra-high vacuum. The instrumental set up is schematically presented in figure 2.9.
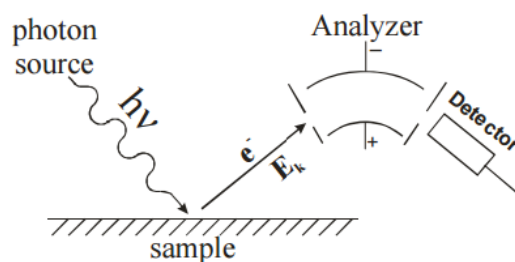
Figure 2.9. Basic scheme of the XPS instrumental set up

XPS measurements were performed using a Kratos Axis Ultra DLD spectrometer (Kratos Analytical, Manchester, UK). Monochromatic source of X-rays (Al Kα, 1486.6eV) was used. The survey spectra were obtained with a pass energy of 160 eV and 1.0 eV step. The data were collected at 90⁰ take-off angle, the analysed spot size was 700×300 µm.

2.1.6. High-energy Rutherford Backscattering Spectrometry

Rutherford backscattering spectrometry (RBS) is a technique that allows the quantitative determination of the composition of a material. A beam of charged particles bombards a sample surface and a small fraction of the incident particles is scattered within a certain solid angle, where the detector is placed (figure 2.10).
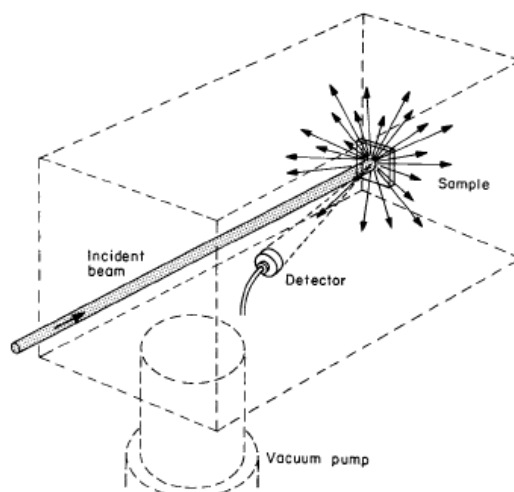
Figure 2.10. Illustration of the analysis chamber in the RBS experiment [267]

The method is based on the elastic binary collision where conservation of energy and momentum holds (figure 2.11) The projectile ion with the mass m will transfer a part of its energy to an atom (in rest) of the sample with the mass M and, hence, will be scattered for each scattering angle θ with a given energy loss.
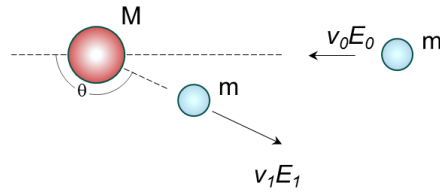
Figure 2.11. Schematic representation of an elastic collision between a projectile ion of mass m, velocity v_0 and energy E_0 and an atom of the sample with the mass M

In the elastic collision, the ratio of the final (E_1) and initial (E_0) energy of the projectile ion is defined as the kinematic factor K, which can be expressed through the equation

$$K_M = \frac{E_1}{E_0} = \left[\frac{(M^2 - m^2 \sin^2 \theta)^{1/2} + m \cos \theta}{M + m}\right]^2 . \qquad (2.8)$$

The scattering angle, the mass and the incident energy of the projectile ion are experimental parameters and, hence, by measuring E_1 one can find the mass M of the sample atom (at the surface). If the scattering event takes place at a certain depth, the corresponding energy loss in the projectile trajectory in the way in and out of the sample should be considered. In this way, compositional profiles can be extracted from the spectra.

Besides the mass, the areal density of the element (in atoms per cm^2) can be determined using the knowledge of its scattering cross-section. The scattering cross-section represents the probability that the scattering will take place for a certain solid angle. The cross-section can also be interpreted as the area around the scattering centre exposed to the incident ion as a function of the scattering angle. RBS is based on the Rutherford cross-section, which can be analytically calculated from the repulsive electrostatic force between the nuclei. In addition, experimental scattering cross-section data are available for the cases when the Rutherford condition cannot be applied to a system. This occurs, for example, when detecting light elements using high energy of incident ions due to overcoming the Coulomb barrier and appearance of nuclear effects. The experimental data on these cross-sections are available in literature and together with theoretical data can be extracted from the SIMNRA software commonly used for the analysis of RBS spectra [268].

As indicated, the detected yield (number of counts or events) in RBS is proportional to the atomic areal density of the material (N_s), which can be calculated from the atomic density (N) and thickness (t) of the sample:

$$N_s = Nt. \tag{2.9}$$

Therefore, the thickness of the analysed sample can be determined only if its density is known and vice versa. In case of SAMs, the calculation of N_s may not be a straightforward procedure due to their monolayer character and possible variations in lateral homogeneity and spatial separation resulting from non-perfectly flat surface of the substrate. Nonetheless, the availability of the data on carbon cross-section and elaboration of the experimental set-up to increase sensitivity for carbon, make RBS an emerging powerful tool for studying SAMs [269].

In this work, carbon coverage values were measured on ZnSe surfaces with different SAMs. The SAMs were obtained on ZnSe disks (Ø 1.8 cm) by overnight exposure to alkanethiol solutions followed by the rinse with ethanol and exposure to physiological water (NaCl 0.9 %) for ~3 hours to remove possible bilayer molecules. High-energy RBS measurements were performed with 5 MV Cockroft–Walton tandetron (HVEE B.V., Amersfoort, The Netherlands) at the Centro de Microanálisis de Materiales (CMAM) from the Universidad Autónoma de Madrid (Spain). To achieve a resonance with the excitation energy of the carbon nucleus, the incident energy of He^+ ions was set at 4265 keV [269]. The incident angle of beam was 50⁰, whereas backscattered ions were detected at a scattering angle of 170⁰ using a silicon detector. The experimental RBS spectra were analysed by comparison with simulated spectra in SIMNRA software (Version 7.02 [268]).

2.1.7. Atomic force microscopy: imaging mode

Atomic force microscopy (AFM) is a method to obtain three-dimensional images of a surface at a nanometre scale. A sharp probe attached to a flexible cantilever is used to approach the surface and the force arising at a close distance between the probe and the surface causes the cantilever to bend. The position of the cantilever is detected using a laser beam sensed with a quadrant diode (figure 2.12). Thus, by detecting the fluctuation in the cantilever bending one can obtain the information on the surface topography of the sample.
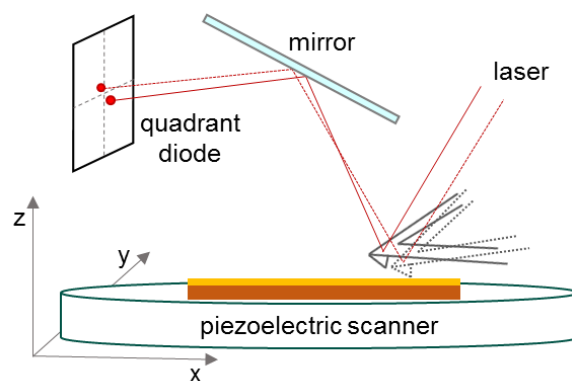
Figure 2.12 Schematic representation of the principle of work of atomic force microscope

The sample is installed on the piezoelectric scanner that adjusts the position of the sample with respect to the measured interaction force. The images are recorded in constant or dynamic modes. In the constant mode, either the force acting on the sample or the distance to the sample surface are set to be constant during the measurement. When the probe is approaching the sample, the changes in z position of the scanner or the deflection of the cantilever, respectively, reflects the information on the sample topography. In the dynamic mode (that is often referred as tapping), the probe is oscillating at a predefined amplitude. This results in intermittent contacts with the sample as the cantilever is brought closer to the surface. The changes in amplitude of the oscillation are correlated with the variation in the sample height. The intermittent contact allows decreasing frictional forces between the sample surface and the probe and associated with it sample damage. However, the resolution of the obtained images is usually lower than in contact mode and higher acquisition time is required.

In this work, ZnSe disks (Ø 1.8 cm, Crystran) were used to obtain AFM images of bare ZnSe after ozone/UV or H_2O_2/HCl treatment, and of gold coating onto ZnSe. The AFM apparatus was an Asylum Research MFP-3D Infinity™ equipped with a 100-µm close-loop scanner (Santa Barbara, USA). The images were recorded in contact mode using silicon nitride probe (MSCT, Bruker).

2.1.8. Scanning transmission electron microscopy

A transmission electron microscope (TEM) enables imaging of the sample using highly accelerated electrons directed by a series of electromagnetic lenses. A magnified contrast image is formed as a projected volume resulted from electron beam absorption, diffusion and diffraction when it passes through a thin specimen (several tenth of nm). Besides morphological and structural properties, the method allows

studying the sample elemental composition by energy dispersive x-ray spectroscopy (EDS). This is achieved by placing a detector of X-ray emission that occurs as a result of an atom relaxation to a ground state after electron loss, and which is characteristic for each element. Scanning TEM (STEM) works under the same principle as TEM, but with the beam of electrons focused at a local spot on the sample surface. Using EDS in STEM instrument allows obtaining maps of sample elemental composition with a resolution down to an atomic scale.

As the thickness of samples must be very low for TEM analysis (few tens of nm), different thinning techniques exist. One of them is based on the use of the focused ion beam for sputter removal of selected parts on the sample. A scheme of FIB sputtering steps and an image of the sample prepared for STEM analysis are shown in figure 2.13
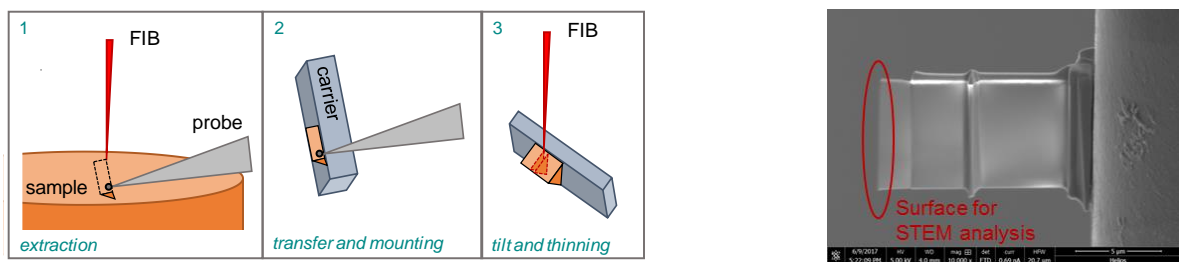
Figure 2.13. Scheme of sample preparation for STEM imaging using FIB (left, modified from [270]) and SEM image of the prepared sample (right)

JEM–ARM 200F Cold FEG TEM/STEM instrument operating at 200 kV and equipped with a spherical aberration (Cs) probe was used for STEM analysis of the surface cross-section.

2.2 Preparation and analysis of bacterial samples: from suspensions to biofilms

2.2.1. Bacterial strains

Two strains were used as main samples in this study, a wild type of *Lactobacillus rhamnosus* GG (LGG, ATCC 53103, University of Antwerp, Belgium) and E2146 strain of *Escherichia coli* (*E. coli*, Institut Pasteur, Paris, France). The AFM images of the bacterial cells and a schematic representation of their cell walls are presented in figure 2.14.

LGG WT, Gram-positive   *E. coli* E2146, Gram-negative
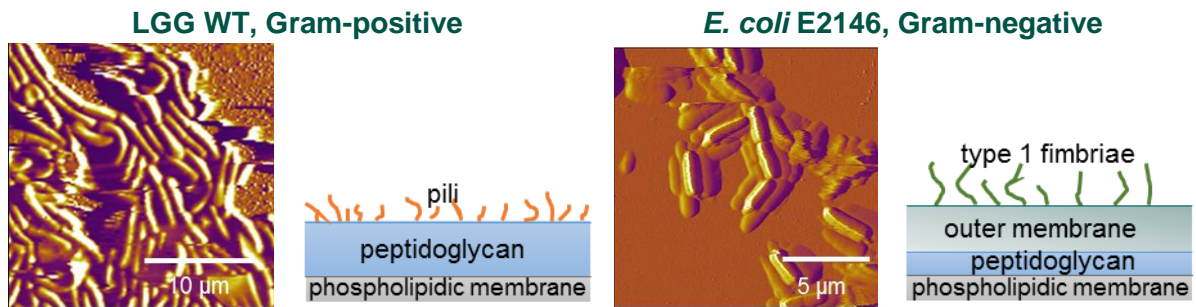
Figure 2.14. AFM deflection images (obtained in PBS) and cell wall schemes of the used bacterial strains

LGG is a Gram-positive, rod-shaped facultative anaerobic bacterium that possess probiotic properties. It was isolated from human stool specimens by Gorbach and Goldin in 1985 (the origin of 'GG' in its name) and is naturally present in the human intestine. It is largely used in food products and in pharmaceutical formulations due to many proofs of clinical benefits reported in literature [83]. It has been consumed in a form of dairy products, juices, cheeses, and capsules in over 40 countries worldwide and is especially popular in Finland thanks to a Finnish dairy company Valio purchasing the rights to use LGG in 1987 [83].

LGG has a strong adhesive capacity to human epithelial cells, but also to abiotic surfaces. This is due to the presence of specific adhesins on its cell wall – pili, playing a key role in promoting adhesive interactions [77]. From 10 to 50 pili can be found on one LGG cell, and their length can reach up to 1 µm [271].

Genetically modified LGG strain kindly provided by S. Lebeer and I. Spacova (University of Antwerp, Belgium) was used in few experiments in this work. This strain, modified from ATCC 53103, expresses blue-fluorescent protein (mTag), which allows observing it without the use of dyes and aids the differentiation of LGG in mixed bacterial biofilms [94].

E. coli is a Gram-negative, rod-shaped facultative anaerobic bacterium, which is also naturally found in the human intestine. Some strains of *E. coli*, however, are pathogenic causing a variety of diseases associated with intestinal (diarrhoea or dysentery) and extra-intestinal (urinary tract, meningitis) infections [272]. Pathogenic *E. coli* strains possess specific adherence factors that allow them to colonize sites, where *E. coli* normally is not present in humans, i.e. small intestine and urethra. The latter niche in particular is colonised by *E.coli* that have type 1 fimbriae on their cell wall acting as

promoters of the adhesion to mannose-containing receptors on uroepithelium. In addition, Type 1 fimbriae were reported to play critical role in attachment of *E. coli* to abiotic surfaces [273]. The strain E2146 used in this work was modified from K12 *E.coli* strain to possess solely type 1 fimbriae on its surface with its length ranging from 1 to 10 µm [112]. Additionally, this strain was modified (Institut Pasteur, Paris, France) to express the green fluorescent protein (*gfp+*) enabling observation of the cells using epifluorescence microscopy without the use of dyes.

2.2.2. Culture conditions

Bacterial strains used in this work were cultivated in Man-Rogosa-Sharpe (MRS, ref. 288130, Difco) for LGG and Lysogeny broth (LB, ref. L3152, Fluka) for *E. coli* (the composition of the media is provided in annexe II).

Both bacterial stocks were stored at -80°C (LGG in MRS with 20 % (v/v) of glycerol, *E. coli* in LB with 25 % (v/v) of glycerol). The working stocks were obtained at 37°C following the growth of bacteria on MRS agar within 48–72 hours or LB agar within 24 hours for LGG and *E. coli*, respectively. Antibiotics, ampicillin (20 µL at 100 mg/mL) and kanamycine (40 µL at 25 mg/mL), were added in 20 mL of LB agar, as selective medium for the E2146 strain.

For monitoring the bacterial growth, the optical density (OD) of the bacterial suspensions was measured at 600 nm using a Cell Density Meter (model 40, Fisher Scientific). The cultures of LGG were prepared in MRS medium at 37°C under static conditions without special caution to avoid oxygen. For LGG (wild type) and LGG (mTag) growth, sub-cultures grown in 20 mL of MRS for 24 hours, were used to incubate cultures in 300 mL or 50 mL of fresh MRS, respectively (initial OD = 0.05 ± 0.01). The cultures of *E. coli* were grown in LB at 37°C under constant agitation (160 rpm). Subcultures of *E. coli* were prepared in 20 mL of LB with added antibiotics (as for LB agar) for 14 hours. The cultures of *E. coli* were incubated in fresh LB without antibiotics with a starting OD of 0.05 ± 0.01. The conditions for bacterial cultivation are gathered in table 1.3.

Table 1.3. Growth conditions for cultivating the bacteria

LGG (wild type or mTag)	E. coli
working stock: MRS agar, 37ºC, 48–72 h	**working stock:** LB agar + antibiotics, 37ºC, 24 h
subculture: 20 mL MRS, 37ºC, 24 h, static	**subculture:** 20 mL LB + antibiotics, 37ºC, 24 h, 160 rpm
culture: 300 mL (WT) or 50 mL (mTag) MRS, 37ºC, 14 h, static	**culture:** 200 mL LB, 37ºC, 2 h, 160 rpm

Both bacteria were collected from suspensions for further analysis at the exponential growth phase (see annexe III for growth curves).

2.2.3. Preparation of bacterial suspensions for biofilm formation

Bacteria were harvested by centrifugation (3000 and 5000 g for LGG and *E. coli* respectively, 10 min, 4°C, Beckman Coulter Allegra 25R) after 14 hours (LGG) or 2 hours (*E. coli*) of incubation in cultures. The pellets were re-suspended in 200 mL of nutritive medium or physiological water (NaCl 0.9 %) by gentle agitation.

When preparing the suspension for LGG biofilms, three nutritive media were tested based on the study of Lebeer et al. (2007), i.e. MRS, Lactobacilli AOAC medium (Difco) and modified trypticase soy broth (mTSB), obtained by mixing 15 g/L of TSB (Fluka) and 20 g/L of Bacto proteose peptone no. 3 (Becton, Dickinson and Co.). The MRS medium is a nutritionally rich medium, specific for lactobacilli species [274]. The AOAC medium contains peptonized milk, and it is a relevant model in terms of industrial conditions. TSB is a general purpose medium, which supports the growth of a wide variety of bacteria.

When biofilms were cultivated using LGG and *E. coli* suspension simultaneously, MRS or mTSB media were used.

All media for biofilm experiments were used at a ten-fold diluted concentration. The low concentration of nutrients reduced interferences of infrared signal from culture medium in the infrared spectra of biofilms during cultivation. It is important to note that the dilution of the medium does not preclude biofilm formation, as has been shown for LGG [94] and other bacterial species [175], [275].

2.2.4. Set-up for monitoring biofilm formation

Through this work biofilms were studied in two key steps: 2.5 hours of initial attachment to the surface (bacterial suspension supply), followed by 24 hours of development of biofilms of bacterial cells adhered onto the surface in the first step (only nutritive medium supply) (figure 2.15). The biofilm development was monitored in real time by recording infrared spectra. The epifluorescence images of biofilms were made at two key times of the experiments: (1) after bacterial suspension flow for 2.5 hours, and (2) after bacterial flow for 2.5 hours followed by sterile medium flow for 24 hours. These biofilms are hereafter called 2.5-hours-old and 26.5-hours-old biofilms. These time conditions were shown to be appropriate for obtaining ATR-FTIR spectra with good signal-to-noise ratios [175].
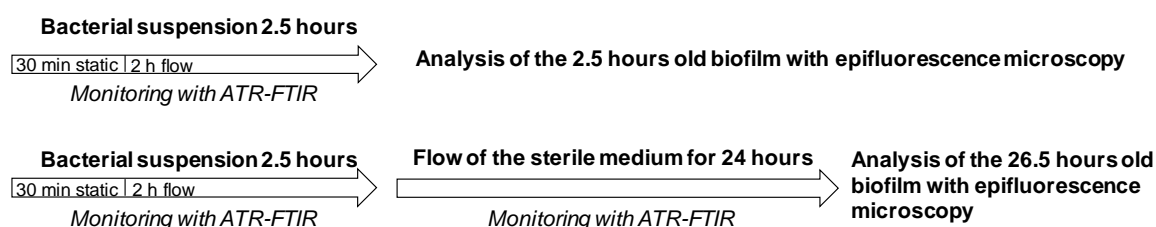
Figure 2.15. Schematic representation of the experimental steps to study biofilm development

As a function of the studied parameter, these conditions were adjusted as presented in figure 2.16. In particular, an effect of the nutritive medium on the development of LGG biofilms was evaluated first. Ten-fold diluted MRS, AOAC or mTSB (hereafter called MRS/10, AOAC/10, and mTSB/10, respectively) media were used in both steps of experiments (2.5 + 24 hours). Further, an impact of the substrate preparation on 2.5-hours-old LGG biofilm formation was investigated. Bare or functionalised $(HS(CH_2)_{11}NH_2)$ ZnSe or gold-coated ZnSe were tested as substrates. Physiological water (NaCl 0.9%) was used as the medium for nascent biofilm cultivation to minimise surface screening with nutrients. ZnSe crystals functionalised with three different alkanethiols were afterwards used as substrates to estimate the influence of surface properties on 2.5-hours- and 26.5-hours-old LGG biofilms. Physiological water was used in the first step of the experiment, whereas mTSB/10 was used for further 24 hours of biofilm cultivation. Finally, the effect of LGG biofilm on the 2.5 hours- and 26.5-hours-old *E. coli* biofilm formation was evaluated. Amino-functionalised ZnSe was used as the substrate and the experiments were performed either in MRS/10 or mTSB/10.

Effect of the medium on the development of LGG biofilm:

LGG on bare ZnSe	2.5 hours MRS/10, AOAC/10, or mTSB/10	+	24 hours MRS/10, AOAC/10, or mTSB/10
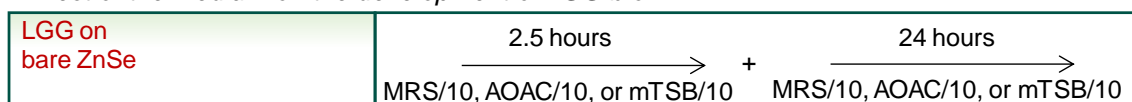
Effect of substrate preparation on LGG attachment:

LGG on ZnSe, Au/ZnSe NH$_2$-ZnSe, NH$_2$-Au/ZnSe	2.5 hours NaCl, 0.9 %	Stop of experiment
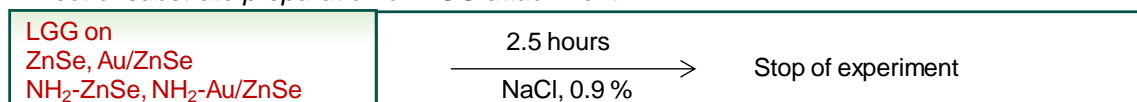
Effect of surface functionalisation on the development of LGG biofilm:

LGG on CH$_3$-ZnSe, OH-ZnSe, NH$_2$-ZnSe	2.5 hours NaCl, 0.9 %	+	24 hours mTSB/10
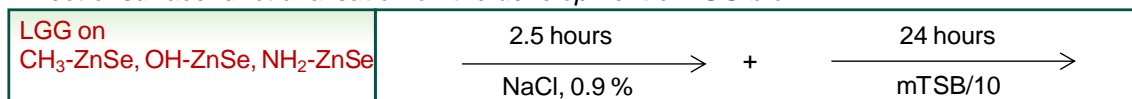
Effect of LGG on the development of E.coli biofilm:

LGG on NH$_2$-ZnSe	2.5 hours NaCl, 0.9 %	+	24 hours mTSB/10	*E. coli flow*	2.5 hours mTSB/10 or MRS/10	+	24 hours mTSB/10 or MRS/10
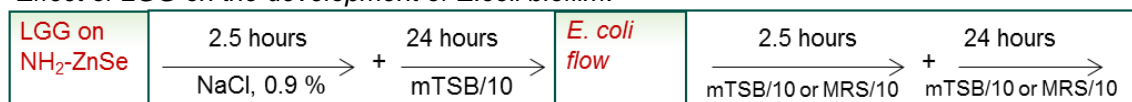
Figure 2.16. A scheme of the change in conditions for biofilm experiments depending on the studied parameter

2.2.5. Flow cell and ATR-FTIR spectral acquisition

Freshly prepared suspensions were put under magnetic stirring (160 rpm) to prevent the sedimentation of the bacterial cells. The suspensions were pumped around a flow cell containing ZnSe crystal using a peristaltic pump (figure 2.17).
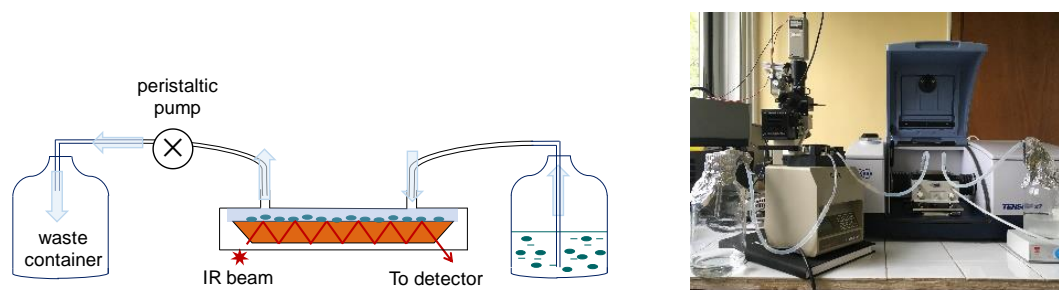
Figure 2.17. Schematic representation and a photo of the experimental set-up for biofilm formation

The spectrum of the bacterial suspension obtained immediately after filling in the flow cell and the spectrum of the sterile medium obtained once it had replaced the bacterial suspension after first 2.5 h of measurements were used as references for first and second step of experiments, respectively (Figure 2.16). The IR spectra were recorded every 10 minutes for the first 2.5 h of the experiment, and every 20 minutes for the 24 h step of the flow of the sterile medium. Water vapour subtraction was performed and the baseline was corrected at 3580, 2750, 1800, and 900 cm^{-1}. All experiments were conducted at 21±1°C in an air-conditioned room.

2.2.6. Curve resolution analysis

A curve resolution analysis was used to estimate the spectral contribution of the various biofilm components during the development of LGG biofilm for 24 hours on bare ZnSe in three different nutritive media.

The vibrational spectra of biofilms are considered to be a weighted sum of the individual spectra (or pure component spectra) of individual species in the mixture. Bayesian positive source separation (BPSS) was used to estimate the variation of pure component spectra from the spectra of the biofilm development during the flow of the sterile nutritive medium. This mixing model assumes that measured data from an evolving system are linear combinations of unknown pure component spectra [181], [182]. The mixing coefficient can then be derived, which is proportional to the concentration of the pure component in the mixture. By assuming a known number of components, the mixture analysis can estimate the pure component spectra and their mixing coefficient profiles (proportional to the concentration) from the mixture spectra without any *a priori* information. All calculations were performed using a custom software in MATLAB. The spectral analysis was performed in the fingerprint region of 1800–900 cm^{-1}, with baseline corrected as a straight line between these two values. The data processing was applied to 67 ATR-FTIR spectra reflecting the period from 1 to 24 hours of biofilm development during the sterile medium supply. The lack of fitting was less than 3% in each series of spectra.

2.2.7. Epifluorescence microscopy

A fluorescence microscope enables imaging of the sample based on the excitation / emission process encountered by specific fluorochromes that are present in the sample volume. All fluorochrome molecules have characteristic excitation / emission wavelengths. The energy of emission is always lower than that of excitation, therefore the observed fluorescence is always at higher wavelengths with respect to excitation range. For example, figure 2.18 presents excitation and emission spectra of three fluorochromes, SYTO 9, SYBR Green and propidium iodide, which have maximum emission wavelengths around 500, 520 and 620 nm, respectively.
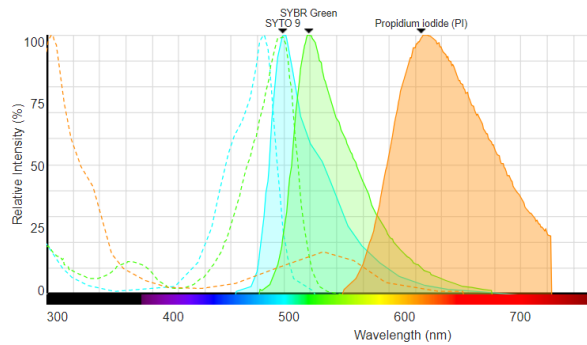
Figure 2.18. Fluorescence spectra of SYBR Green, Syto 9 and propidium iodide fluorochromes (printed with permission of Thermo Fisher Scientific [276])

The key element in the fluorescence microscope is a fluorescent filter cube (figure 2.19). This cube is comprised of optical glass filters that select specific wavelengths from the broader light spectrum passing on and emitted from the sample, and a dichroic mirror allowing the delivery of the signal from the source to the detector. The obtained image is magnified with optical lens (objective), and the microscopes in which the illuminator and objective lens are positioned on the same side of the specimen, are called epifluorescence microscopes.
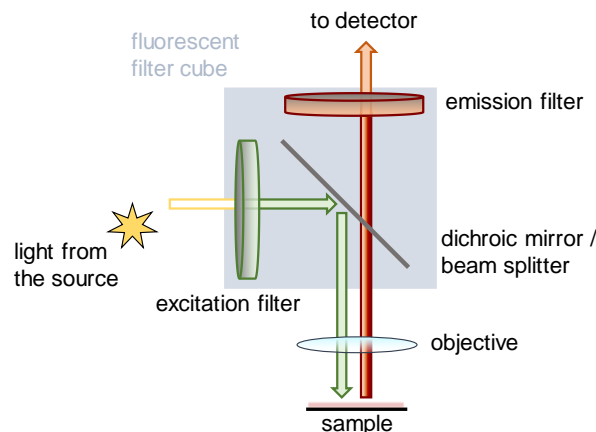
Figure 2.19. Schematic representation of a fluorescence microscope

SYBR Green II (Molecular Probes, ref. S7586) or *Bac*Light™ Live/Dead kit (Molecular Probes, ref. L7012) were used in this work to stain bacterial cells. SYBR Green II stains nucleic acids in bacterial cells, with a higher quantum yield when bound to RNA than to DNA (data from the manufacturer). The *Bac*Light™ kit contains two fluorochromes, green-fluorescent Syto 9 and red-fluorescent propidium iodide, which enable determination of the permeability state of the cell membrane. Syto 9 is able to penetrate into all cells, whereas propidium iodide will enter only the cells with

compromised membrane. Due to higher affinity of propidium iodide to nucleic acids compared to Syto 9, cells with damaged membranes appear red.

At the end of every biofilm experiment, the ATR crystal was carefully demounted from the flow cell and gently rinsed with sterile ultrapure water using pipette (experiments in chapter IV) or dipping into the Petri dish filled with ultrapure water (chapters IV-VI) to remove non-adherent cells. Bacteria attached on the surface were stained with SYBR GREEN II or *Bac*Light™ Live/Dead kit for 30 or 20 minutes, respectively, in the dark at 21±1 °C. The crystal was then gently rinsed with sterile ultrapure water to eliminate excess of the dyes. A series of images (≥60) was recorded at random places of the crystal surface using ×100 and ×10 objectives of an Olympus BX51 microscope. The images were processed with the ImageJ software for calculation of bacterial coverage on the crystal surface.

2.2.8. Atomic force microscopy: force spectroscopy

Force spectroscopy is the mode of utilising AFM for measuring mechanical forces between the probe and the sample. These forces are obtained from the cantilever deflection according to Hooke's law:

$$F = -k_c d, \qquad (2.10)$$

where k_c is the spring constant of the cantilever and d is the extension of the cantilever bend. When the tip is approaching the sample, the force acting on the cantilever from the sample is absent until the point where the probe jumps into contact with the sample surface and the interaction begins. This causes the cantilever to bend until the force (proportional to measured deflection) reaches the value set by the operator. The probe is withdrawn then from the surface and the peaks on the retraction curve (one or multiple depending on the number of interaction sites) are characteristic for the force arising during the interaction of the probe with the sample (figure 2.20). Since the peaks occur at a certain distance regulated by *z* scale of the piezoelectic scanner, the maximum distance at which the probe is still interacting with the sample (rupture distance) can be identified. For example, force-distance curve presented in figure 2.20. shows that the interaction between the probe and the sample occurs at least four times

during retraction of the probe from the sample surface and the rupture distance reaches the value up to 10 µm.
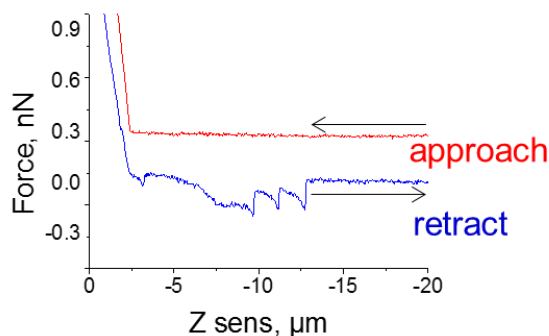
Figure 2.20. An example of the force-distance curve obtained using AFM force spectroscopy mode

In this work, force measurements were made to study the interaction of LGG cell wall with $-CH_3$, OH, and NH_2 functional groups. The experiments were performed at room temperature using Asylum MFP-3D atomic force microscope (Santa Barbara, CA, USA) equipped with a liquid cell and filled with phosphate buffered saline. Gold-coated AFM probes (NPG-10, Bruker) were functionalised with alkanethiols $HS(CH_2)_{11}X$ ($X=CH_3$, OH, or NH_2) by exposure to 1 mM ethanolic solution of corresponding alkanethiol. LGG cells at exponential growth phase suspended in phosphate buffered saline were immobilised (14 hours, 4°C) onto Au/Cr/glass substrates (Sputter Q150T, Quorum technologies) through electrostatic interactions with $-NH_3^+$ terminal groups of SAM of 11-Amino-1-undecanethiol adsorbed on Au/Cr/glass. The interactions between the functionalised probes and the LGG cell wall were quantified by scanning the surface and measuring the deflection of the cantilever as a function of the vertical displacement of the piezoelectric scanner. A total number of 1024 force-distance curves were recorded on the sample spot with the size of 100 µm^2. These curves were analysed using a custom program in MATLAB software for calculation of the frequency of appearance of certain interaction force as a function of probe-sample distance.

2.2.9. CFU counting

To estimate the quantity of *E. coli* cells after cultivation over preliminarily formed LGG biofilm, CFU counting was made. After the extraction of ZnSe crystals with the biofilm from the infrared flow cell, the half of the crystal (as the other half was used for epifluorescence images) was scraped using custom-built sterile spatula composed of polytetrafluoroethylene. The cells were resuspended in 1 mL of phosphate buffered

saline using sonication for 1 minute. The resuspended and subsequently diluted cells were plated on LB agar and let to grow overnight at 37°C. The values of counted colonies were multiplied by two assuming the homogeneous coverage of ZnSe with bacterial cells.

III. Impact of the nutritive medium on the formation of LGG biofilms

The content of this chapter is published in Biofouling:

https://doi.org/10.1080/08927014.2019.1617279

The antipathogenic potential of LGG is correlated with its ability to form biofilms, which might be strongly affected by culture media conditions. Lebeer et al. explored the effect of culture conditions on 72-hours-old LGG biofilms on polystyrene [79]. The choice of the nutritive medium highly modulated the capacity of LGG to develop biofilms, as shown using a microtiter plate biofilm assay. A lack of glucose appeared to be a key factor promoting biofilm formation. More recently, Jiang et al. evaluated the effect of various carbohydrates on the survival and growth of LGG in multispecies simulated oral biofilms [95]. Contrary to the previous study, in the presence of carbohydrates including glucose, LGG grew better on saliva-coated hydroxyapatite, as calculated based on colony forming units from 64.5-hours-old collected biofilms.

The effect of culture conditions on LGG properties have generally been studied for the planktonic form [120], [121], [277] or at the end of the biofilm formation period [79], [95]. The question of how LGG adapts to environmental conditions of different nutritive media from early stages of biofilm development until maturation (i.e. its composition, physiological state, shape) has not yet been investigated and is addressed in this chapter. ATR-FTIR measurements were performed to monitor the changes in molecular fingerprints of LGG biofilms *in situ* in three different nutritive media under flow conditions and in real time. Additionally, the shape of LGG cells and their distribution on the surface were observed using epifluorescence microscopy in nascent and more mature biofilms.

3.1 Results

3.1.1 LGG in planktonic state: impact of the medium on the bacterial growth and the synthesis of lactic acid

First, the influence of the medium on the growth of LGG in planktonic form in diluted nutritive media was verified. The suspensions were adjusted to initial OD of 0.5 (as for biofilm experiments) and the OD measurements were performed over ~8 hours (figure 3.1). The OD gradually increased in MRS/10 and AOAC/10 media, whereas it stayed relatively constant in mTSB/10. This was in line with CFU counts of cultivable LGG cells after 8 hours of incubation in each media, which increased from ~$3 \cdot 10^7$ to ~$9 \cdot 10^7$, ~$8 \cdot 10^7$, and ~$4 \cdot 10^7$ UFC/mL in MRS/10, AOAC/10 and mTSB/10, respectively.
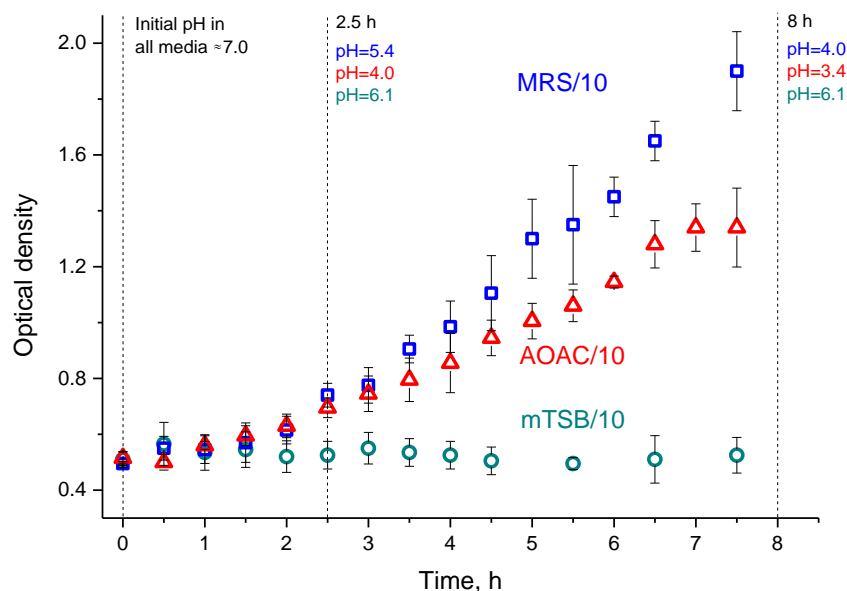
Figure 3.1. Time evolution of optical densities (600 nm) of planktonic LGG in 10-fold diluted MRS, mTSB and AOAC nutritive media after their transfer from MRS medium at the end of their exponential growth phase, and pH values of the suspensions

Besides, the pH values of the nutritive media after 8 hours of LGG incubation were 4.0, 3.4 and 6.1 in MRS/10, AOAC/10 and mTSB/10, respectively, whereas the initial pH of all nutritive media was ~7.0. The increase of the acidity of MRS/10 and AOAC/10 media was probably due to lactic acid production by LGG. The spectra of the cell-free culture supernatants recorded after 2.5 and 8 hours and presented in figure 3.2 were compared with the spectra of lactate recorded at different pH (annexe IV).
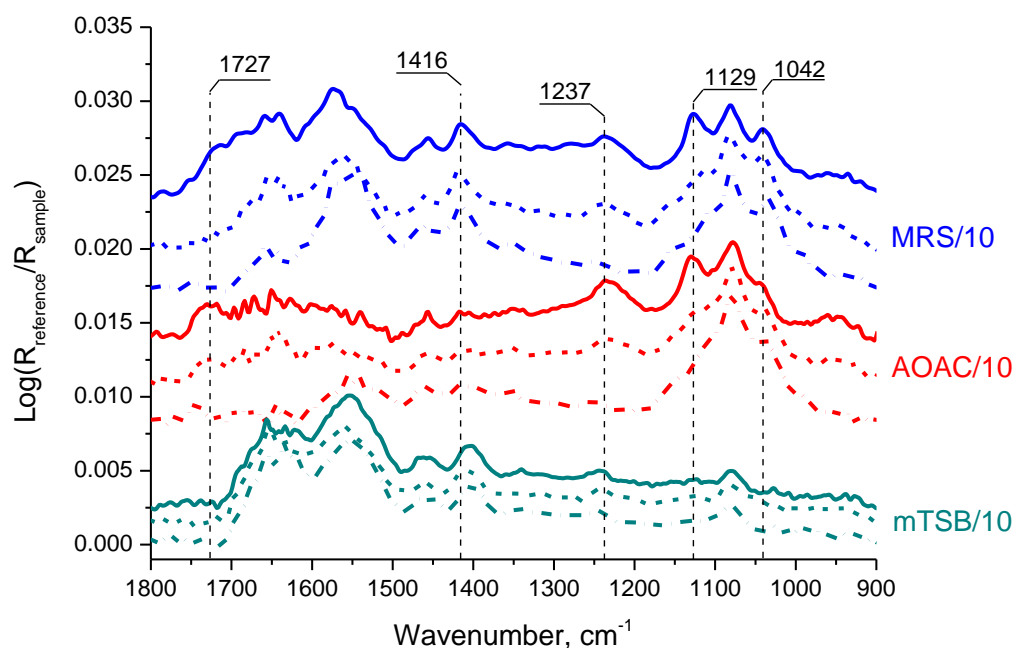
Figure 3.2. ATR-FTIR spectra of nutritive media before (dash dot) and after (dash) 2.5 and (solid) 8 hours of LGG incubation. Sterile Millli-Q water was used as a reference for all spectra. Offsets of spectra are used for clarity

After 2.5 hours of incubation, new bands at 1237, ~1129 and 1042 cm^{-1} appeared in the spectra of MRS/10 and AOAC/10 media. These bands were more intense in the spectra of these media recorded after 8 hours. They were assigned to νCO combined with δOH, ρCH$_3$ combined with νCO, and νC–CH$_3$, respectively, from lactic acid and lactate salt [278]. The occurrence of bands at 1416 cm^{-1} and 1727 cm^{-1} in MRS/10 and AOAC/10, respectively, showed that the lactate and the lactic acid forms were both present in the media, albeit in different ratios. From the spectra, and in accordance with the measured values of pH, the acidic form was more prominent in AOAC/10. The spectrum of filtered mTSB/10 was almost not changed with respect to the initial record neither after 2.5 nor after 8 hours of incubation. The non-significant changes in the spectra are in accordance with the stable optical density measured for LGG suspensions in mTSB/10 (figure 3.1). As glucose is used by LGG to synthesize lactic acid, its higher concentration in MRS/10 (2 g/L) and AOAC/10 (1 g/L) media compared to mTSB/10 (0.25 g/L) support the differences in the observed production of lactic acid. Herein, the higher buffering capacity of MRS /10 due to the presence of citrate and acetate compounds may explain its lower acidity compared to AOAC/10, even though MRS/10 has a higher concentration of glucose. To compare the physiological state of bacterial cells in the three nutritive media, the ATR-FTIR spectra of planktonic LGG after 2.5 hours of incubation were recorded (figure 3.3).
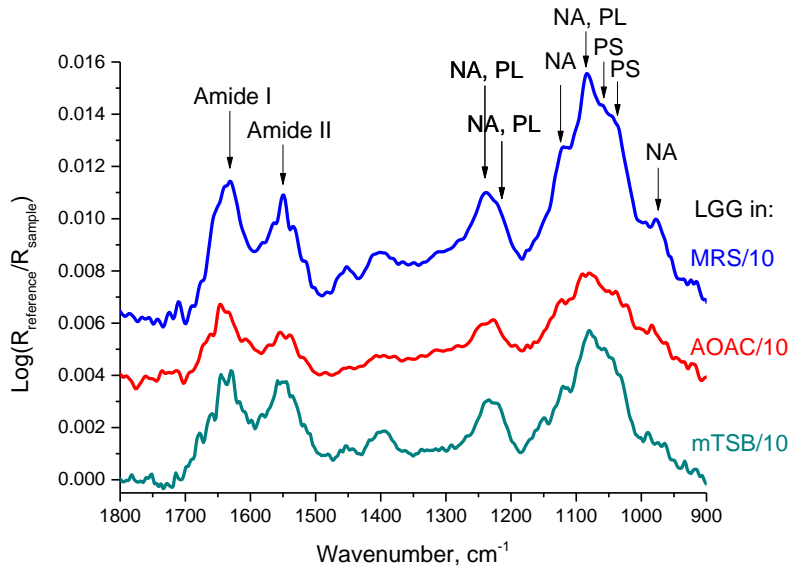
Figure 3.3. ATR-FTIR spectra of LGG collected from bacterial suspensions based on 10-fold diluted MRS, AOAC, and mTSB media after 2.5 hours of incubation; NA – nucleic acids, PL – phospholipids, PS – polysaccharides. Corresponding supernatants from centrifugation were used to obtain the reference spectra. Offsets of spectra are used for clarity.

Differences in relative intensities of the bands assigned to nucleic acids, phospholipids, and polysaccharides [260] can be noticed depending on the medium. The main information derived from these spectra is that LGG produced a higher amount of nucleic acids (bands at 1240 and 1120 cm^{-1} [260]) in MRS/10. This is in line with the growth curves showing higher number of multiplying cells in MRS/10 compared to the other media (figure 3.1).

3.1.2 LGG nascent biofilms (2.5 hours): molecular fingerprints, bacterial shape and distribution on the surface

During the incubation of LGG in the flow cell, the intensity of all bands in the infrared spectra increased in all media suggesting the attachment of bacteria to the crystal surface (figure 3.4).
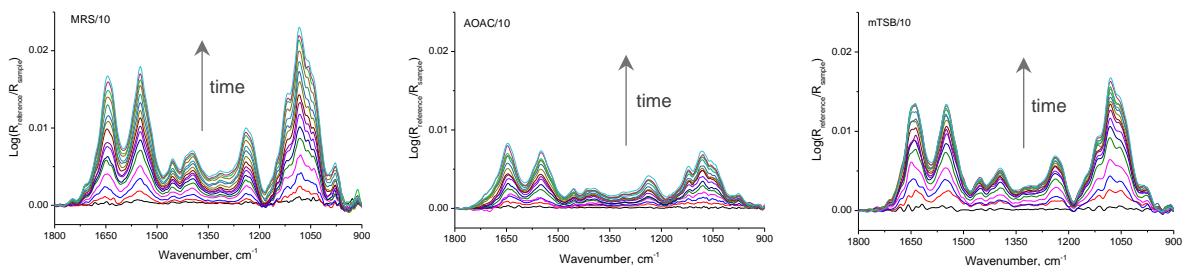
Figure 3.4. Evolution of infrared spectra in ATR mode during the incubation of LGG suspension for 2.5 hours in 10-fold diluted MRS, AOAC, and mTSB media obtained at 10 minutes interval.

Figure 3.5 shows the ATR-FTIR spectra of LGG after 2.5 hours of incubation in the three different nutritive media. The assignment of the infrared bands was realised in accordance with the literature [166], [260], [279], and they are summarized in table 3.1.
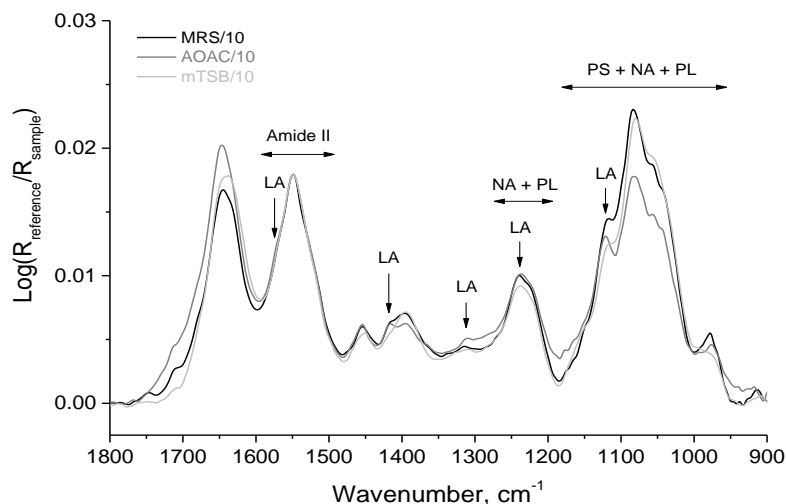
Figure 3.5. ATR-FTIR spectra of LGG in 10-fold diluted MRS, AOAC, and mTSB media after the flow for 2.5 hours over the ATR crystal surface. LA – lactic acid or lactate, NA – nucleic acids, PL – phospholipids, PS – polysaccharides. Spectra were normalised with respect to the amide II band.

The appearance of bands at 1416, 1310 and 1237 cm^{-1} was observed in the spectra of LGG recorded in MRS/10 and AOAC/10 media. These bands were indicative of the production of lactic acid (annexe IV), in accordance with the bacterial behaviour in these two media in the planktonic form. Besides, the region between 1200 and 900 cm^{-1} assigned to polysaccharides, phospholipids and nucleic acids showed slight differences in the bands depending on the medium (figure 3.5). From the data on the planktonic cultures, the rapid decrease of pH in a close biofilm environment can be expected in AOAC/10. This may lead to physico-chemical changes in the external layer of peptidoglycans from the cell wall [113].

Table 3.1. Assignments of principal infrared vibrational bands of 1800–900 cm^{-1} region of the ATR-FTIR spectra of LGG in different nutritive media after 2.5 hours of inoculation

IR wavenumbers (cm^{-1})			Assignments	
LGG in MRS/10	LGG in AOAC/10	LGG in mTSB/10		
1749	1745		νC=O	Esters from lipids
1712	1715	1715	νC=O	Carboxylic acids
1649	1648	1655	Amide I* (Disordered/α-helix)	Proteins
1631 (sh)	1630 (sh)	1634 (sh)	Amide I* (β-sheets)	Proteins
1570–1516	1572–1518	1568–1515	Amide II**	Proteins
1455	1456		δ_aCH$_3$	Lactic acid
		1449	δCH$_2$	Lipids
1417	1418		ν_sCOO$^-$	Amino acids, teichoic acids, lactic acid
1394	1393	1396	ν_sCOO$^-$	Proteins
1316–1274	1313–1283	1311–1284	Amide III***	Proteins
1243	1240	1242	ν_aPO$_2^-$	Phosphodiester, phospholipids, nucleic acids
1220	1221	1219	ν_aPO$_2^-$, δCH (ring)	Ribose, phospholipids
1172–1152	1172–1151	1171–1153	ν_sC–OH, νC–O	Proteins, carbohydrates, esters
1119	1122	1119	νC–O	DNA, RNA
1084	1084	1083	ν_sPO$_2^-$	Phosphodiester, phospholipids, nucleic acids
1055	1056	1052	ν_sC–O–C, ν_sP–O–C (R–O–P–O–R')	Polysaccharides
1038	1041	1033	νC–O	Polysaccharides, RNA ribose
998	988	993	Uracil ring	RNA, phospholipids
968	974	970	νC–C, νP–O–P, Ribose–phosphate skeletal motions	DNA, phospholipids
916	916	915	Ribose–phosphate skeletal motions	DNA

*νC=O with the minor contribution from νC–N, overlapped with the signal of δH$_2$O, 1640 cm^{-1};
δCNH coupled with νC–N; * νC–N, δCNH and νC=O.

To compare the physiological state of bacteria in the nutritive media, ratios of integrated intensities of the main band regions corresponding to proteins, {nucleic acids + phospholipids}, and {nucleic acids + phospholipids + polysaccharides}, were calculated for 2.5-hours-old biofilms (figure 3.6). The values of the ratios were close regardless of the medium. Therefore, it is postulated that the biochemical composition of LGG cells remained similar. Generally, *L. rhamnosus* grows slowly [280], which is in line with low differences in physiological state of LGG cells after short time of biofilm cultivation.
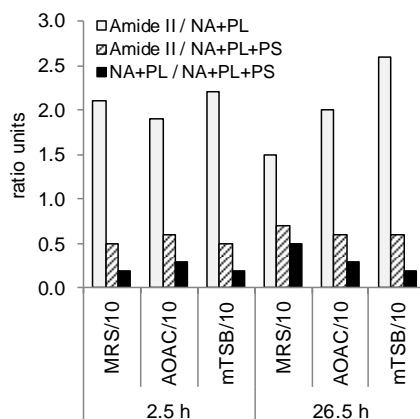
Figure 3.6. Ratios of integrated intensities of the main bands corresponding to the components in bacterial cell calculated from the spectra of 2.5- and 26.5-hours-old biofilms. NA: nucleic acids, PL: phospholipids, PS: polysaccharides. Amide II: $1592-1486$ cm^{-1}, NA+PL: $1271-1188$ cm^{-1}, PS+NA+PL : $1189-956$ cm^{-1}. Amide II band was used for the proteins estimation, as it has less interference with the water signal compared to amide I band.

Images of the bacteria in the 2.5-hours-old biofilms were obtained using epifluorescence microscopy, and the coverage of the crystal with bacteria was estimated (figure 3.7). In all three media the bacterial coverage on the crystal surface was low and heterogeneous as it is shown in the broad distributions in figure 3.7. The lowest coverage was observed in MRS/10. LGG cells, with very few exceptions, preserved their native rod shape. Nonetheless, the length of bacteria varied depending on the nutritive medium, namely being equal to 2.0±0.6, 1.5±0.6, and 0.9±0.3 µm in MRS/10, AOAC/10 and mTSB/10, respectively.
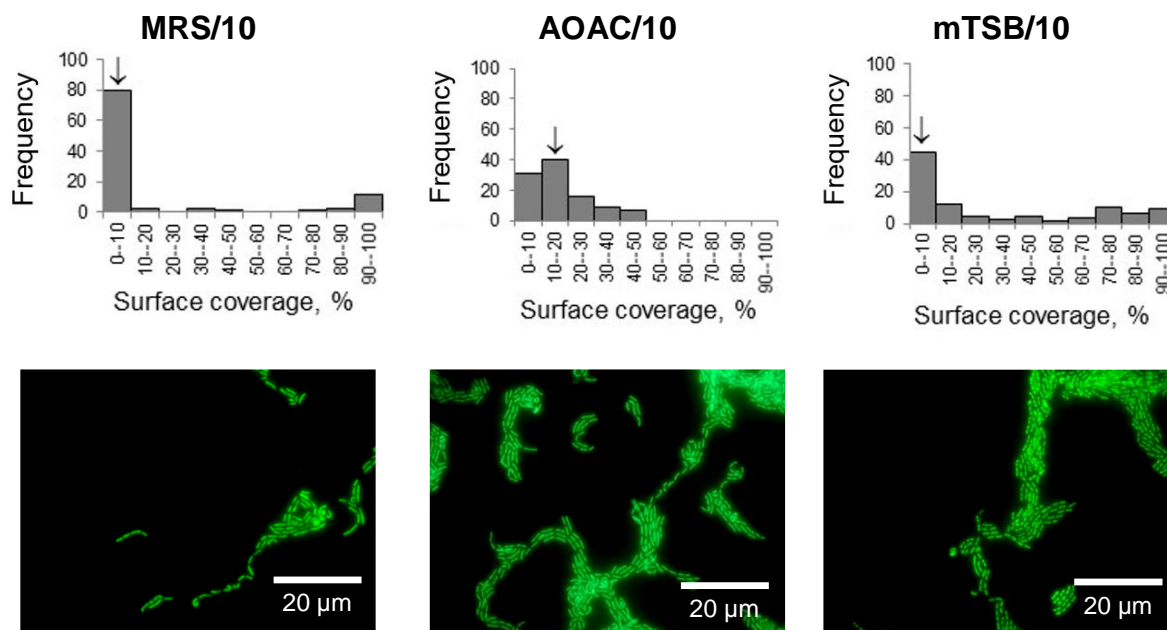
Figure 3.7. Surface coverage distributions and representative epifluorescence images of 2.5-hours-old biofilms obtained in 10-fold diluted MRS, AOAC and mTSB media. Arrows indicate areas of corresponding representative images.

3.1.3 Development of LGG biofilms (26.5 hours): variations in molecular fingerprints during the flow of the sterile nutritive media

Figure 3.8 shows the time-evolution of the ATR-FTIR spectra in the fingerprint region during the flow of each sterile medium over 2.5-hours-old biofilms. The reference spectrum was the spectrum of the 2.5-hours-old nascent biofilm. Hence, spectra in figure 3.8 reflect only information on the development of cells already attached to the crystal by the end of the inoculation period.
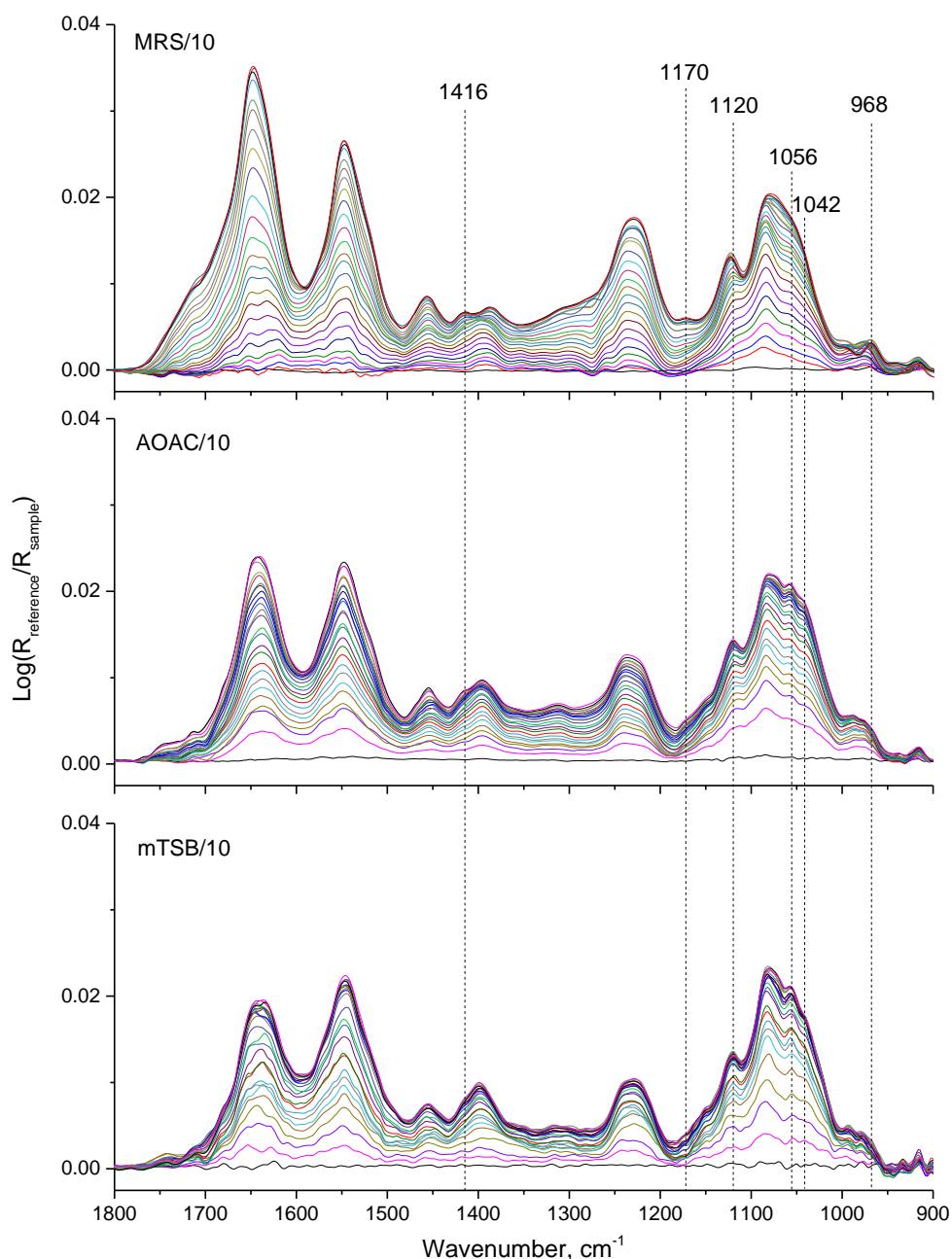
Figure 3.8. Evolution of ATR-FTIR spectra during 24 hours of LGG biofilm development in 10-fold diluted MRS, AOAC and mTSB media obtained at 1 hour interval. The reference spectrum is the spectrum after 2.5 h of flow of suspensions of LGG.

Time-evolution of the integrated intensities of ATR-FTIR spectral regions corresponding to proteins, {nucleic acids + phospholipids}, and {nucleic acids + phospholipids + polysaccharides} are provided in figure 3.9. for each medium. In MRS/10 and AOAC/10, all values of integrated intensities increased during the whole period of measurements. These results suggest the active multiplication of the cells in the vicinity of the surface. In mTSB/10, the increase of all the components was continuous during the first ~15 hours of the flow of the sterile medium over the 2.5-hours-old biofilm, after which a plateau was reached. This result does not necessarily indicate the complete coverage of the crystal surface with bacteria. The stagnation of the infrared intensities might be also a sign of the stationary phase being entered into by the cells or a biofilm growth in excess of the depth of analysis (1.25 µm at 1600 cm⁻¹).
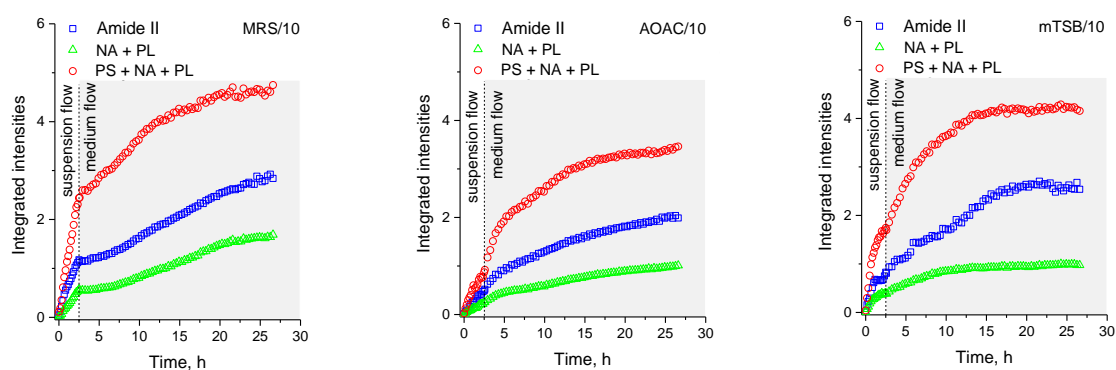
Figure 3.9 Evolution of integrated intensities of the ATR-FTIR bands corresponding to proteins, as derived from the amide II band region at 1592–1486 cm⁻¹, nucleic acids + phospholipids (NA + PL,1271–1188 cm⁻¹), and polysaccharides + nucleic acids + phospholipids (PS + NA + PL, 1189–956 cm⁻¹) during formation of LGG biofilm over 24 hours in MRS/10, AOAC/10, and mTSB/10 after initial 2.5 hours of bacterial flow in same media

The spectral fingerprints of the ATR-FTIR spectra in MRS/10 were very different from those obtained in the two other media (figure 3.8). In the 1100-1000 cm⁻¹ region, the spectra did not clearly show bands at 1072, 1055 and 1036 cm⁻¹ that were present in the other two series of spectra and assigned to polysaccharides. In addition, bands assigned to phospholipids (1745, 1224, 1171, 967 cm⁻¹) were clearly more intense than those from polysaccharides in the spectra of LGG recorded in MRS/10. The ratio of integrated intensities of {nucleic acids + phospholipids} to {nucleic acids + phospholipids + polysaccharides} calculated from the last recorded spectra in each medium was around twice as high for spectra obtained in MRS/10 than in both other media (0.5, 0.3 and 0.2 for MRS/10, AOAC/10 and mTSB/10, respectively, figure 3.6). These data allowed us to conclude that the synthesis of polysaccharides by LGG was lower in MRS/10 than in the other two media.

Figure 3.8 also shows in all spectra the increase of a band at 1416–1417 cm^{-1} assigned to the COO$^-$ symmetric stretching. Besides, a small shift in the band maximum from 1113 to 1123 cm^{-1} as well as a shoulder at 1572 cm^{-1} were observed over the time evolution of the spectra recorded in MRS/10 and AOAC/10. These bands were assigned to the carboxylate and alcohol groups from lactate (annexe IV [278]), indicating the production of lactic acid by LGG during its growth on the surface. The production of lactic acid was higher in MRS/10 than in AOAC/10 and it was very low or absent in mTSB/10, continuing the trend seen in planktonic cultures and nascent biofilms. Of interest, bands indicating the presence of lactate in the biomass were present in the spectra *per se*. It means that the released lactate molecules remain at least partially in a vicinity of the first layers of bacteria.

3.1.4 Spectral contours of the principal components resolved by the chemometric analysis with BPSS during the flow of the media for 24 hours

The BPSS results are presented in two forms: (1) estimated pure components spectra (PC) of individual species present in a biofilm mixture from 3.5-hours to 26.5-hours-old biofilms, and (2) estimated relative contribution (RC) of each individual species, as a function of time. Figure 3.10 (left) shows the pure component spectra extracted from the series of the ATR-FTIR spectra of LGG biofilm development in each medium (i.e. from spectra in figure 3.8). The corresponding relative contributions of individual spectra to the biofilm spectrum are also given in figure 3.10 (right). The assignment of the pure component spectra allowed the relative contribution of the corresponding biomolecules to be traced during biofilm development.

During the first 6 hours of MRS/10 supply, a high production of nucleic acids (PC1 and RC1, figure 3.10a,d) was observed. The predominant synthesis of nucleic acids reflected an activation of a metabolic activity towards cell replication on the surface as had previously been suggested for sessile *Pseudomonas fluorescens* [275]. Another component resolved was a mixture of proteins and nucleic acids (PC3, figure 3.10a), which grew exponentially for the first 9 hours and then stabilised (RC3, figure 3.10a,d). Pure component PC4 (figure 3.10a) showed the features of lactic acid/lactate and proteins. The associated relative contribution of this component increased until the 17th hour of measurements, after which it decreased (RC4, figure 3.10d). The contribution from PC2 (proteins with contribution of polysaccharides, figure 3.10a) increased

continuously and did not plateau by the end of the measurements (RC2, figure 3.10d). This data showed that cells were metabolically active in MRS/10 for the whole period of measurements.
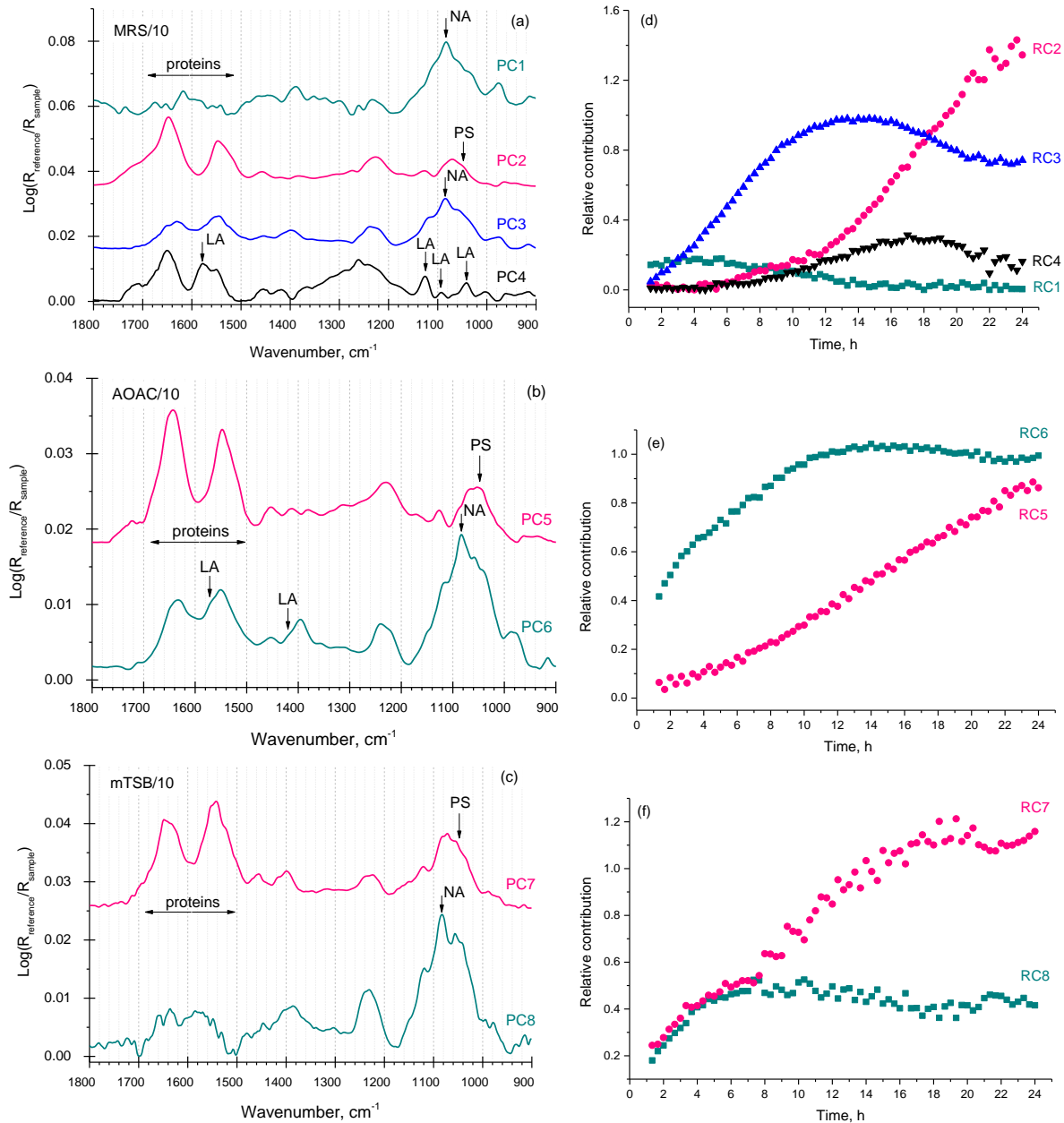
Figure 3.10. Estimated BPSS ATR-FTIR pure component spectra from the spectra recorded during the 24 hours development of LGG biofilm in ten-fold diluted MRS, AOAC and mTSB media. Offsets of spectra are used for clarity (a, b, c). Corresponding relative contribution profiles (d, e, f). LA – lactic acid or lactate, NA – nucleic acids, PS – polysaccharides.

Only two components were resolved in AOAC/10 and mTSB/10 media during the development of the biofilms. As in MRS/10, a high production of nucleic acids was resolved during the first 6 hours of the medium supply (PC6, RC6 and PC8, RC8 figures 3.10c,e,f). In both media the biosynthesis of nucleic acids was accompanied by

the production of proteins, albeit in higher quantity in AOAC/10. The production of these compounds in both media reached a pseudo-plateau weakly decreasing after about 12 hours of flow, indicating a slowdown of the metabolic activity of at least the bottom of the biofilm (RC6 and RC8, figure 3.10e,f). PC5 and PC7 were spectra of a mixture of proteins, polysaccharides, and in case of AOAC/10 also of lactic acid/lactate (figure 3.10b,c). The latter spectrum was not resolved separately as it was in the spectra of the MRS/10 experiment. It reflected the concomitant biosynthesis of proteins, polysaccharides and lactic acid in AOAC/10 whereas only proteins and lactic acid were produced simultaneously in MRS/10. In accordance with the ratios obtained in figure 3.6, a higher synthesis of polysaccharides was observed in mTSB/10 compared to AOAC/10 (PC5 and PC7, figure 3.10b,c). However, the synthesis increased continuously in AOAC/10 whereas it reached a plateau in mTSB/10 (RC5, RC7, figure 3.10e,f) suggesting a steady state of bacteria close to the surface was reached in the latter medium.

3.1.5 Morphology of the LGG cells in the 26.5-hours-old biofilms strongly depends on the nutritive medium

The epifluorescence images of 26.5-hours-old biofilms revealed major differences in bacterial shape depending on the media (figure 3.11). In MRS/10, the cells were characterised with the rod-like appearance typical of lactic-acid bacteria [281]. The average length of the cells in MRS/10 slightly increased in comparison with the cells in the 2.5-hours-old biofilm (2.2±0.7 µm). However, cells were quite heterogeneous in length (1 - 4 µm). This phenomenon was even more pronounced in AOAC/10, where the majority of cells developed a long filamentous shape, with the remainder being characterised by having relatively short and curved shapes. In mTSB/10, the population of bacterial cells had a more homogeneous appearance and length (1.2±0.4 µm). Interestingly, most of bacteria had shapes represented by a curved, "horseshoe" appearance.
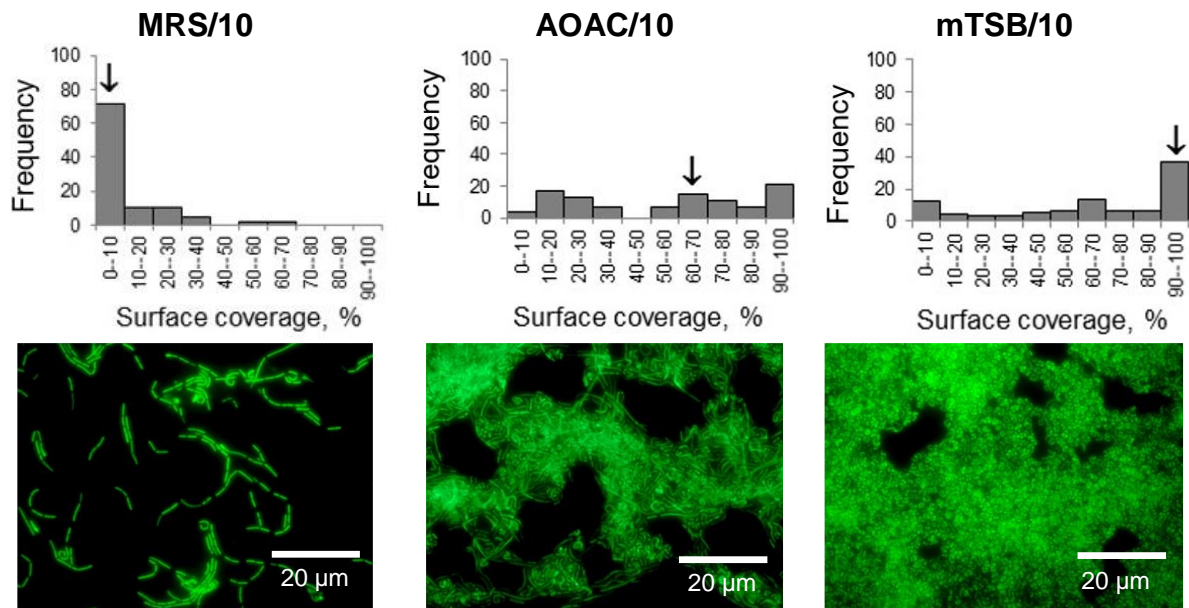
Figure 3.11. Surface coverage distributions and representative epifluorescence images of 26.5-hours-old biofilms obtained in 10-fold diluted MRS, AOAC and mTSB media. Arrows indicate areas of corresponding representative images.

The bacterial coverage of the surface was also medium dependent. It was on average the lowest for biofilms in MRS/10. In AOAC/10 and mTSB/10, the bacterial coverage was higher, but it was broadly distributed on the surface.

3.2 Discussion

In this chapter, changes in the biochemical composition and shape of LGG cells during biofilm formation on an abiotic surface in different nutritive media were monitored over time. Of note, the data were collected in flow conditions that have been rarely addressed until now in studies with LGG [64].

First, it was observed that there was a remarkable difference in growth of planktonic LGG cells depending on the medium. The absence of growth in mTSB/10 could somewhat be expected [282], since this medium is not specific for lactobacilli. However, in AOAC/10 the bacterial growth was also not as high as in MRS/10, although both media are recommended for lactobacilli cultivation. The higher acidity of AOAC/10 compared to MRS/10 led to a lower bacterial growth. Hutkins and Nannen showed that lactobacilli growth occurs optimally at pH > 6 [236]. Koponen et al. suggested that LGG grew favourably at pH=5.8, whereas at pH=4.8 their growth was reduced as a result of an acidic stress [120]. Many lactobacilli are acid-tolerant bacteria [283]. However, lactic acid produced by LGG can easily pass the bacterial cell

membrane, which may lead to the decrease of the intracellular pH and subsequent impairing of the cell functions [120], and hence, presumably to a decrease in the growth of the cells, as was observed in AOAC/10.

The lactic acid/lactate signature was also observed in the IR spectra from biofilm experiments in AOAC/10 and MRS/10. From BPSS analysis it was observed that the lactic acid production was not constant, despite the continuous supply of fresh nutrients. This observation applies at least for the first 1-2 layers of bacteria on the surface (depth of penetration of the IR beam).

Variations in the features of the bands assigned to polysaccharides (950-1100 cm^{-1}) revealed differences in the moieties of the carbohydrates of LGG cells in all three media. Burgain et al. showed that a decrease in pH leads to physico-chemical changes in the external layer of peptidoglycans from the cell wall [113]. The changes in the spectral fingerprints of polysaccharides were more pronounced in the older biofilms. From calculation of the ratios of bands regions (figure 3.6), the biosynthesis of polysaccharides was found to be lower in MRS/10 than in AOAC/10 and mTSB/10. This result was consistent with the study of Lebeer et al., which showed that the production of exopolysaccharides was dramatically lower in MRS than in AOAC or mTSB on 72-hours-old biofilms [79]. However, under the current conditions the production of polysaccharides was higher in mTSB/10 than in AOAC/10, whereas the reverse was observed by Lebeer et al. in these media that were not diluted. BPSS results showed that polysaccharide synthesis was stopped by the end of the measurements in mTSB/10, but not in AOAC/10. Thus, it can be expected that the level of polysaccharides would be higher in biofilms cultivated in AOAC/10 for older biofilms. In addition, due to flow conditions shear forces could also influence EPS production [152]. The nature of extracellular polysaccharides was reported to play an important role in the adhesive properties of LGG [284]. Unfortunately, it was not possible to identify polysaccharides synthesised in biofilms. Nonetheless, differences in bacterial coverage of the surface as a function of the medium were observed. Thus, it would be very interesting to determine in future work the medium dependent nature of EPS molecules produced by LGG in biofilms.

The data of bacterial coverage obtained in this work pointed out an intriguing issue regarding the strength of bacterial attachment to the surface. Although the infrared

signals, directly proportional to the quantity of biomass on the surface, were relatively close to each other in three different media, the numbers of actually attached bacteria seen on the surfaces varied depending on the medium. Apparently, bacteria did not respond in the same manner to the delicate, rinsing step applied before microscopic observation. Even though the experiment was performed under flow conditions, the forces arising during the rinsing step can affect the bacterial retention on the surface [204]. In MRS/10 the eventual coverage of the surface with bacteria was the lowest, suggesting that the cells were weakly attached to the surface. In contrast, in AOAC/10 and especially in mTSB/10 medium, the strength of adhesion to the surface appeared to be stronger. This result is in accordance with observations by Lebeer et al. on 72-hours-old LGG biofilms in media that were not diluted [79]. Based on the infrared data, it is suggested that the percentage of surface covered with LGG was similar regardless of the medium, until the substrate was removed from the flow cell and rinsed. This behaviour appears to be strain specific as it was not observed in the earlier study with *P. fluorescens* [173]. It is noteworthy, that the spectra of biofilms with information on the main biofilm components were obtained *in situ* and non-destructively, therefore highlighting the utility of the ATR-FTIR method for understanding biofilm formation process and its stability.

The differences in bacterial coverage were associated with specific morphological features of LGG cells. In MRS/10, the rod shape of the bacteria was preserved in 26.5-hours-old biofilms. On the contrary, strong morphological modifications (filamentation, curvature) were observed for the cells in AOAC/10 medium in nascent to more mature biofilm. The filamentation of cells was reported as a potential response of cells to various stressful conditions [285]. On *Lactobacillus plantarum*, it was shown that filamentation of cells happens as a result of acidic stress inhibiting cell division while maintaining cell growth [286]. As in AOAC/10 the pH rapidly decreased in the presence of LGG, it is assumed that this filamentous morphology was due to acidic stress experienced by bacteria. The stress caused by acidic conditions accompanied by polysaccharide synthesis may contribute to a better retention of bacteria to the surface in AOAC/10. Yang et al. suggested that curved shape of bacteria facilitates surface colonization [287], as it appeared in 26.5-hours-old biofilms in mTSB/10. The refolding of bacteria into a curved shape was shown as a potential response to prevent the lytic process induced by nutrient deprivation [288]. Nutrient conditions can have a direct

impact on the size of bacteria [289]. In the current study the small size of LGG cells in biofilms in mTSB/10, as well as optical density measurements of planktonic cultures confirm the conditions of nutritive stress present in this medium. Despite this, a dense biofilm was formed in this medium. Overall, the variations in shape of LGG cells in the different nutritive media could be the result of changes in the peptidoglycan layer of bacteria [290], [291]. The differences in the polysaccharide region of the infrared spectra (1100-1000 cm^{-1}, figure 3.8) and the relative amounts of polysaccharides produced in biofilms as a function of the medium are in accordance with this hypothesis.

The use of probiotics as a bio-tool to preserve surfaces and control pathogen growth is a promising strategy and we believe more studies in this field are soon to appear. It is of importance to consider the effect of the environmental conditions on probiotic bacteria when estimating their antimicrobial properties. With the analysis of compositional and morphological changes, our study shows how LGG physiology is affected by different nutrient conditions during biofilm formation. For surface preservation, mTSB medium seems to be a medium of choice as it produced LGG biofilms with a high coverage. However, the absence (or very low quantity) of lactic acid and the nutrient stress expressed in this medium may impact on LGG's antimicrobial potential, which lays the subject of further study in this project.

IV. Substrate role in surface functionalisation and interactions with LGG cells

Having established the role of the medium in LGG biofilms growth, we moved forward to the question of how the substrate properties impact on this process. As the strategy of this project included thiol-based functionalisation chemistry, we studied how substrate properties affect the organisation of SAM and also yield and reproducibility of the self-assembly reaction. In view that the main method used in this PhD project for biofilm analysis was ATR-FTIR spectroscopy, transparent in infrared range ZnSe crystal was used as the base substrate, as previously described. To tune the surface properties of the ZnSe substrate, the grafting of thiol moieties at the surface of ZnSe crystal appeared as a good strategy, as it would lead to a formation of an uniform and dense layer, stable in the conditions relevant for biofilm experiments. While the process of self-assembly of thiols onto gold was addressed in major number of works in last decades [245]–[254], the feasibility of thiol self-assembly onto ZnSe was demonstrated only in one study by Noble-Luginbuhl and Nuzzo [257], as described in part 1.3.2. Hence, the development of full understanding of the thiol self-assembly onto ZnSe still lacks.

In this work, we have then chosen to functionalize ZnSe surface following two different routes. First, the thiol solution was directly applied onto ZnSe substrate, as in the study of Noble-Luginbuhl and Nuzzo [257]. Afterwards, for an improved understanding of the efficiency of SAM functionalisation onto ZnSe and its possible impact on bacterial coverage, self-assembly of thiols was performed onto ZnSe, preliminarily coated with gold nanofilm using PVD method.

The quality of the SAM is affected by the properties of the surface, including its composition, morphology and presence of surface contaminants. The latter point was the subject of study in several works using ZnSe in relation with its use as a substrate for SAMs [257] or other applications [213], [292]–[296]. In particular, many studies have demonstrated the successful cleaning of ZnSe from carbon residues using acid etching [292]–[296]. Therefore, we have tested two methods adapted from the literature to clean ZnSe in order to determine what procedure would result in the

surface maximally free of organic contaminants, i.e. ozone/UV treatment [257] and etching with hydrogen peroxide and hydrochloric acid solutions [213]. The impact of the cleaning procedure on ZnSe surface properties was also analysed.

In the following chapter, we then address the data on LGG spectroscopic fingerprints and its distribution on substrates before and after functionalisation of ZnSe substrates with SAMs. We studied LGG attachment and nascent (2.5 hours) biofilm formation on the amino-terminated surfaces positively charged in physiological water, with the hypothesis of enhanced bacterial attachment due to electrostatic interactions. Using this alkanethiol as a model, we aimed at identifying what method of the substrate preparation is the most suitable for obtaining well-defined SAM on the ZnSe ATR crystal in a reproducible way, and how it affects the behaviour of bacterial cells.

4.1 Results

4.1.1 Control experiments before SAM formation to study the substrate properties and its effect on LGG attachment and spectral fingerprints

First, we performed experiments using substrates prepared in conditions as for thiol functionalisation, but without thiols (blank experiments), and LGG was inoculated on these substrates for 2.5 hours (30 minutes static followed by 2 hours of flow at 50 mL/h).

a) ZnSe properties after different treatments

Figure 4.1 shows AFM topography images of the ZnSe substrates after ozone/UV treatment (a), H_2O_2/HCl treatment (b), and gold coating (c). The morphology of the substrates was dependent on the procedure used for substrate preparation. Long and straight scratches were observed on the surface after ozone/UV treatment. The presence of scratches is characteristic for ZnSe after manufacturing process [297] and therefore, these morphological features can be considered as an intrinsic property of ZnSe after industrial polishing. A drastic change in surface topography was noticed after H_2O_2/HCl etch. Indeed, no clear scratches were anymore seen on the substrates, and instead, sphere-like features with the diameter of ~40 nm appeared homogeneously over the crystal surface (figure 4.1b). In figure 4.1c depicting gold-coated ZnSe (Au/ZnSe), particles of gold with the width of ~15 nm homogeneously

covered the surface of ZnSe. The thickness of gold film was ~2 nm, as it was confirmed by RBS measurements (annexe V).

The roughness also varied depending on the substrate (table 4.1). Here, we use R_a value (arithmetic average of surface heights measured across a surface) to compare the roughness between substrate surfaces. ZnSe cleaned with ozone/UV had R_a around 5 nm due to scratches on the surface. After acidic treatment, the roughness significantly increased to ~15 nm due to appearance of hemispheres on the surface, whereas gold nanofilm homogenised surface topography resulting in the R_a of ~2 nm.
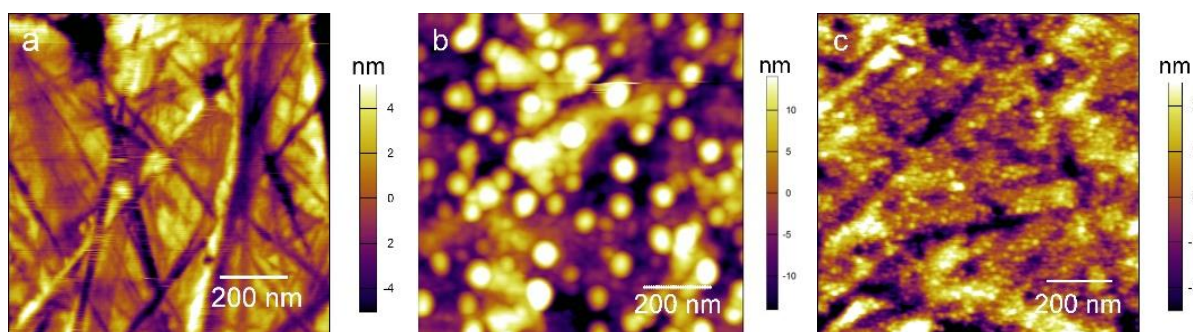
Figure 4.1. AFM topography images of ZnSe substrates after ozone/UV treatment (a), H_2O_2/HCl treatment (b), and gold coating (c)

To obtain the information on hydrophobic / hydrophilic properties of the substrates, water contact angles were measured after cleaning the surfaces and exposure to ethanol overnight (blank experiment with respect to SAM formation). The results showed that all three substrates had similar wetting properties (table 4.1).

Table 4.1. Water contact angles and roughness of the studied substrates

	ZnSe (ozone/UV)	ZnSe (H_2O_2/HCl)	Au/ZnSe
Contact angle	63.5 ± 1.5	72.4 ± 0.2	63.8 ± 2.2
Roughness (R_a), nm	5	15	2

It must be noted that ZnSe immediately after removal from hydrochloric acid was highly hydrophobic (contact angle of 99±1°) due to hydrogen termination of the surface [213]. ZnSe oxidise quickly in ambient air [298], which resulted in a lower contact angle measured after overnight exposure to ethanol. On Au/ZnSe, contact angle was around 64°, in accordance with the values reported for gold [299], [300].

b) Composition of ZnSe after acidic etching

As etching of ZnSe with acids drastically changed the substrate topography, its surface was further characterised using XPS and STEM in EDS mode to determine the impact of etching procedure on the composition of the topmost surface. Figure 4.2 shows XPS spectra obtained on ZnSe before and after acidic treatment.
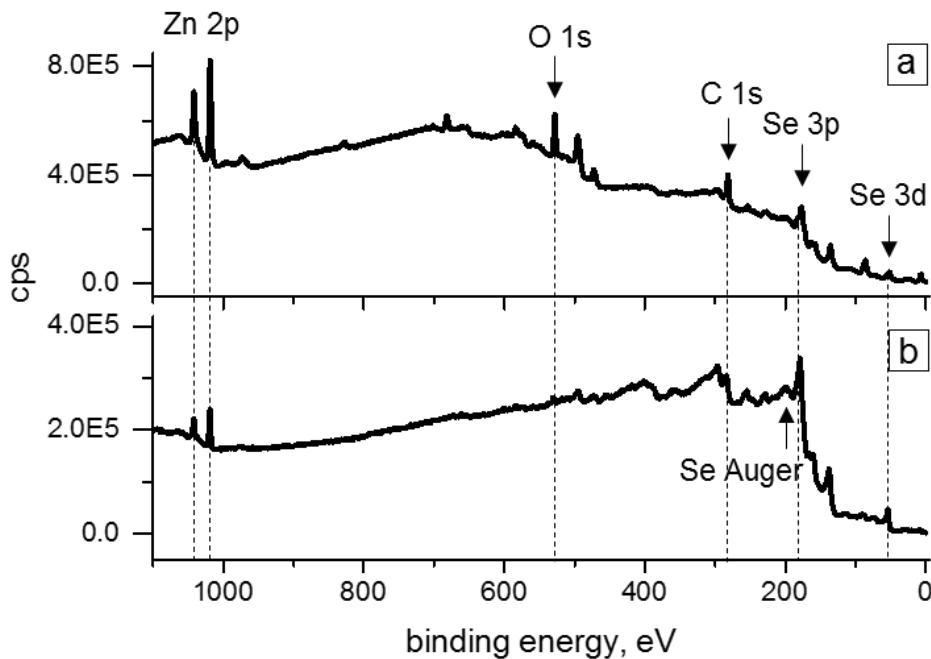
Figure 4.2. Qualitative estimation of the change in composition of ZnSe surface before (a) and after (b) etch with HCl solution as depicted by XPS survey spectra

It was not possible to obtain quantitative information (atomic concentration) from the XPS spectra on ZnSe after acidic treatment. The calibration was complicated by the drastic shift of the baseline, charge effects and a complex background due to appearance of many Auger peaks of selenium. One Auger peak of selenium, in particular, was close to the C 1s (commonly used for calibration of XPS spectra) and modified the shape of the C 1s peak, which would result in the erroneous calibration. It should be mentioned that this problem could potentially be solved, for example, by choosing another peak to calibrate the spectra or by the change of the source of X-ray radiation [293], [301], although it was not tested in the present work. Nonetheless, the spectra obtained were still useful to compare for qualitative estimation of changes in composition. As mentioned above, many Auger peaks of selenium appeared after acidic etch. At the same time, Zn 2p peak decreased in intensity. It suggests that the surface of ZnSe was enriched with selenium after etching. The anomaly in baseline of the spectrum of ZnSe after acidic treatment is in accordance with this result. Indeed,

as the baseline in XPS is formed by inelastically collided electrons, its increased number is related to the high probability for the electrons to lose their energy while passing through selenium layer formed at the surface. It can also be seen that carbon and oxygen are in very low quantity after acidic etching.

The results of XPS were in line with the appearance of reddish colour on ZnSe surface after etching, as this colour is close to the colour of elemental selenium. The phenomenon of the colour change was earlier observed by Liu et al. [292] and Cho et al. [294] on ZnSe treated with the similar protocol.

In view of AFM results showing hemispheres spread over the surface, it was interesting to investigate the elemental composition of the topmost layer at a high lateral resolution. FIB was used to prepare the cross-section of ZnSe after acidic treatment and the sample was analysed with STEM using the EDS mode (figure 4.3).
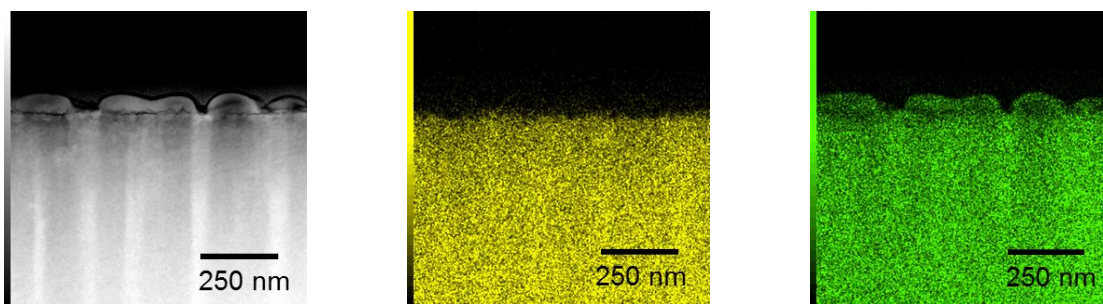
Figure 4.3. STEM analysis of ZnSe after H_2O_2/HCl treatment: SEM photograph of the surface cross-section (left) and EDS maps of the surface cross-section for Zn (middle) and Se (right) elements

The cross-section image and EDS maps depicted nanosized hemispheres. Of interest, these hemispheres had no zinc in the composition and were rich in selenium, in accordance with XPS results. Thus, the acidic treatment resulted in the preferential solubilisation of Zn^{2+} ions from the surface resulting in an Se enriched extreme surface. As this behaviour is beyond the field of this PhD project, we did not conducted deeper investigations about these phenomena.

c) Attachment of LGG cells on the bare ZnSe and Au/ZnSe substrates

Subsequently, the adhesion of LGG cells was studied on ZnSe cleaned with ozone/UV treatment or acidic etching, and on Au/ZnSe. The attachment of bacterial cells in suspension in physiological water was followed using ATR-FTIR spectroscopy and the spectra are presented in figure 4.4.
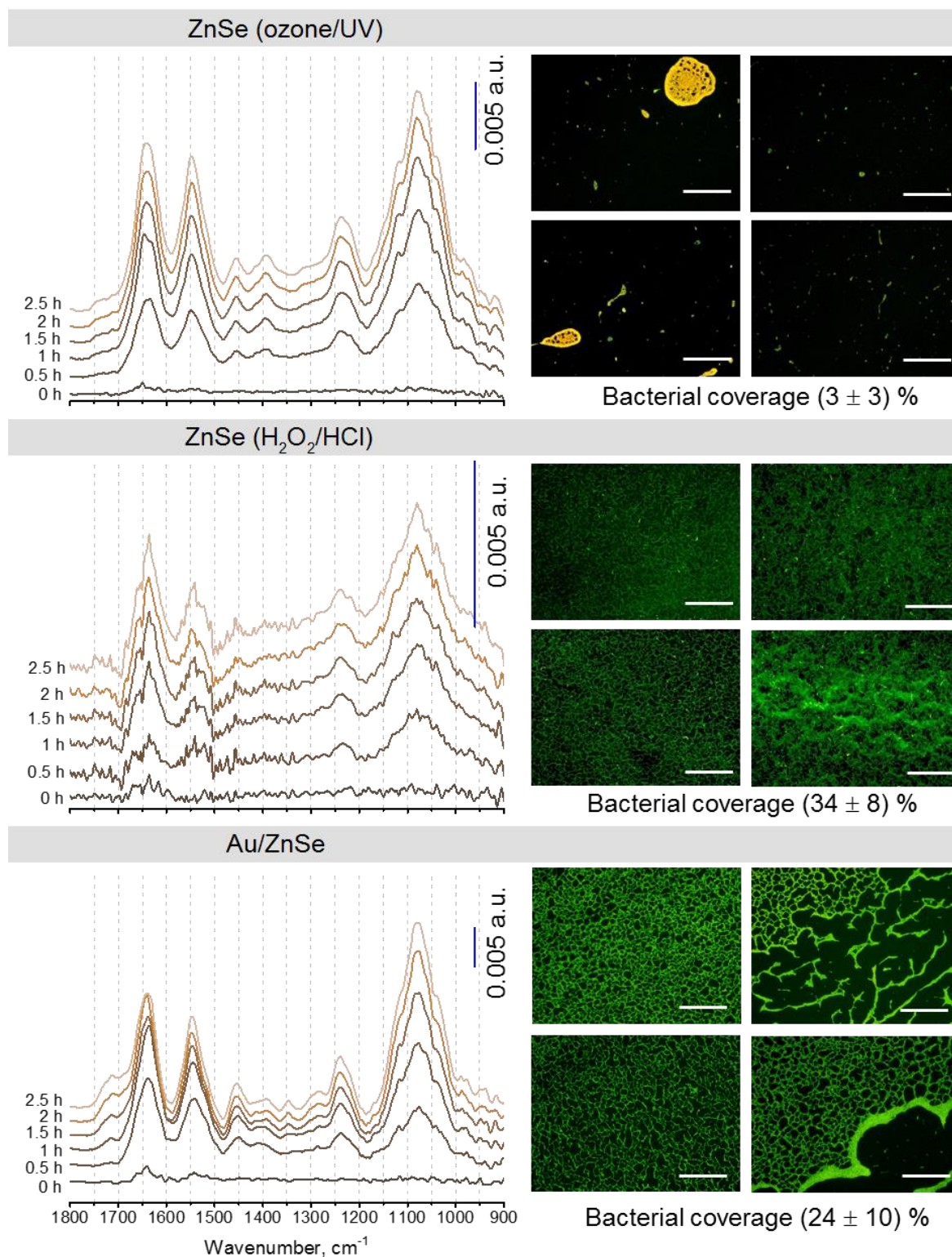
Figure 4.4. LGG spectroscopic fingeprints (offsets) on non-functionalised substrates with corresponding epifluorescence images (BacLight™ staining, scale bar – 200 μm) presenting distribution of bacterial cells on the substrate

The spectra recorded after 2.5 hours of incubation onto ZnSe preliminarily cleaned with ozone/UV were similar to those recorded in various nutritive media (chapter III). This suggests that the biochemical composition of LGG does not change significantly with

respect to the medium in short term experiments (except for the low synthesis of lactic acid in MRS/10 and AOAC/10, as stated in chapter III). However, some peculiarities have to be mentioned for the spectra obtained on ZnSe treated with H_2O_2/HCl and Au/ZnSe. Indeed, overall low signal was obtained on the ZnSe crystal after acidic treatment, and the spectra were characterised with low signal to noise ratio. The close investigation of bacterial distribution on this substrate revealed that LGG cells tended to attach to some interesting micron-sized structures that, apparently, were present on the surface after acidic etch (figure 4.5). The nature of this structures was not investigated in detail, but an earlier study suggests that they were selenium whiskers [292]. They were homogeneously distributed all over the crystal surface, hence partially preventing the direct contact of bacterial cells with the surface of ZnSe. The low signal in the ATR-FTIR spectrum therefore resulted from the distribution of many bacterial cells in excess of the depth of penetration of the infrared light.
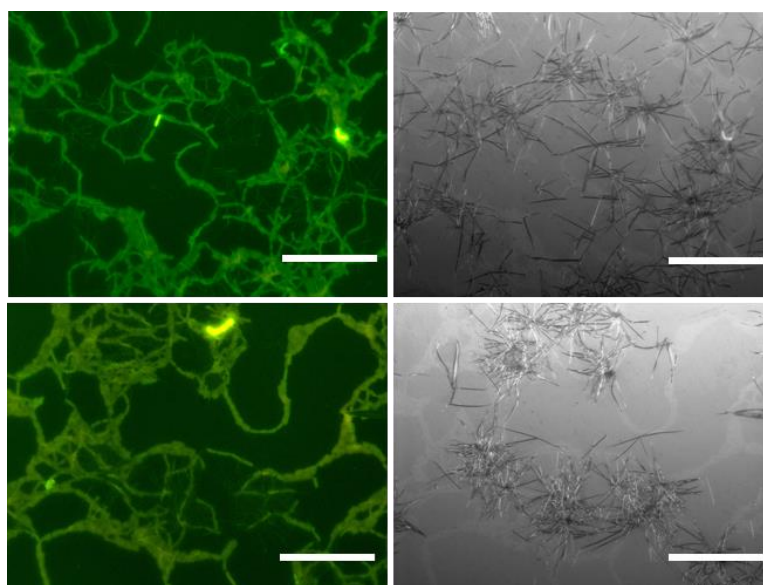
Figure 4.5. Epifluorescence images of LGG on ZnSe preliminarily treated with H_2O_2 and HCl solutions. Bacterial cells stained with BacLight^{TM} (left) and corresponding images of the crystal surface (right). Scale bar - 20 µm

On Au/ZnSe, the fingerprints were different compared to those obtained on ZnSe in a way that the bands between 1700 and 1750 cm^{-1} were significantly more intense, and the region of bands assigned to polysaccharides combined with phospholipids and nucleic acids (950–1200 cm^{-1}) grew more rapidly than other bands in the spectrum (figure 4.4). Besides, the shift of some parts of the spectrum (most pronounced near amide II band, but also amide I and $\nu PO_2^-_{asym}$ at ~1545, ~1650, and ~1220 cm^{-1}, respectively) occurring as a function of time towards negative part of absorbance scale

could be noticed. These changes in the spectrum gave generally an atypical look to the infrared spectrum of bacterial cells. The shift of some parts of the spectrum towards negative absorbance scale (band asymmetry) is a feature that can be associated with changes in the refractive index at the topmost surface of the ATR crystal as a result of gold deposition [302]. Furthermore, it is suggested that bands increasing in intensity at 1700–1750 and 950–1200 cm^{-1} were a contribution from teichoic acids, i.e. surface glycopolymers containing phosphodiester-linked polyol repeat units anchored to bacterial membrane via glycolipid or covalently attached to peptidoglycan [303]. The increase of these bands observed as a function of time might have been reasoned by a rapid synthesis of teichoic acids occurring after the attachment of cells onto Au/ZnSe. This is considered, however, an improbable scenario at such short term measurement. Conversely, the increase in bands tentatively assigned to teichoic acids could be due to the progressive approach of cells to the surface up to a point where the infrared signal can be enhanced. Indeed, thin metal films on ATR crystals were reported to produce the enhanced signal intensities in the infrared spectrum of components in vicinity of the crystal surface (~10 nm) due to changes in the distribution of the electromagnetic field around metal particles [184]. Herein, teichoic acids are located at the periphery of the cell wall of Gram-positive bacteria constituting up to 60% of the cell wall [303], and therefore could be better visualised in the spectra on Au/ZnSe with respect to other components of the cell.

The retention of LGG cells estimated from epifluorescence images after the substrate was extracted from the infrared flow cell and rinsed, was also not the same on different substrates, ranging from ~3 to ~34 % (figure 4.4). LGG did not retain on ZnSe preliminarily cleaned by ozone/UV treatment, suggesting that forces of the interaction with this substrate were weaker in comparison with ZnSe after H_2O_2/HCl treatment and Au/ZnSe. It should also be noted that an all studied substrates LGG cells appeared green after *Bac*Light^{TM} staining, indicating that the membrane of the bacterial cells was not damaged.

4.1.2 The organisation of SAMs on ZnSe and Au/ZnSe, and its impact on the adhesion of LGG

a) SAMs onto ZnSe are less ordered with respect to gold

Freshly prepared substrates were subjected to a solution of amino-terminated alkanethiols and the kinetics of self-assembly was followed *in situ* using ATR-FTIR spectroscopy. The integrated intensities of νCH_2 bands measured as a function of time revealed that the kinetics of the reaction of thiol adsorption was dependant on the substrate, as depicted in figure 4.5a. The experimental values shown in figure 4.5a were fitted using the following equation of Langmuir adsorption and rearrangement model [304]:

$$A = A_0\big(1 - A_{ads}e^{-t/\tau_{ads}} - (1 - A_{ads})e^{-t/\tau_{rea}}\big), \qquad (4.1)$$

where A_0 is the limiting absorbance of a completely organized monolayer, A_{ads} is the adsorption coefficient, τ_{ads} is the rate constant of the adsorption phase, and τ_{rea} is the rate constant of the slow rearrangement phase. It must be noted that other equations based on Langmuir adsorption model can also be used to fit the kinetics of thiol adsorption [305], [306]. The equation 4.1 was selected owing to its consideration of a slow adsorption phase, which is assumed to be strongly substrate dependent based on the shapes of the curves in figure 4.5a.
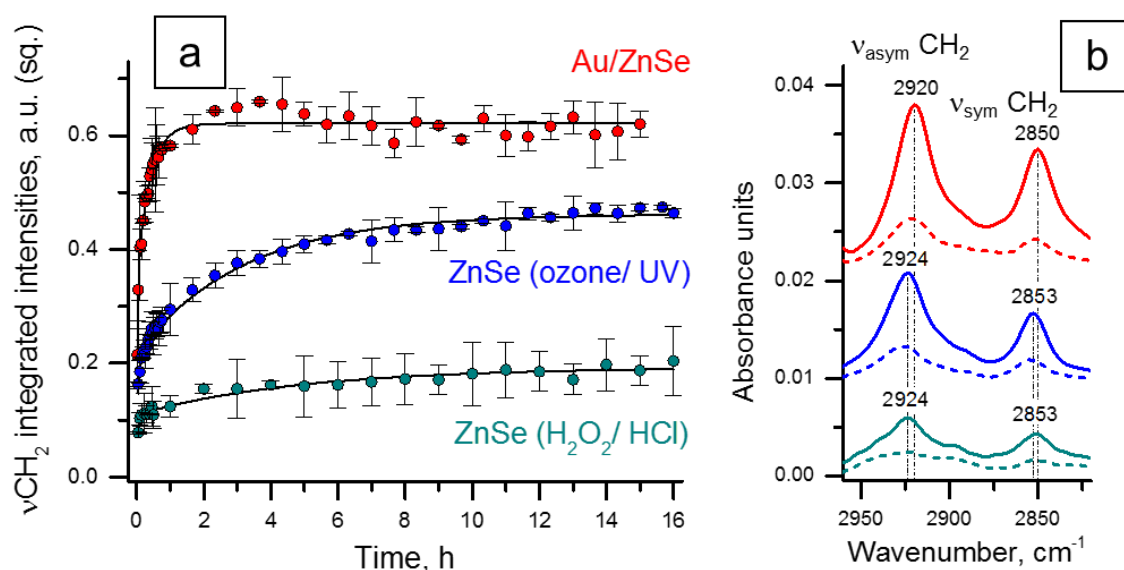
Figure 4.5. Time evolution of the integrated intensities of νCH_2 symmetric and antisymmetric bands (2964–2820 cm^{-1}) of amino-terminated alkanethiol adsorbed on substrates prepared by three different ways (a), and corresponding spectra obtained on these substrates after ~2 min (- - -) and 15 hours (—) of the reaction (b). Reference is the spectrum of ethanol. The lines in a) are fitting curves based on equation 4.1 (r$^2 \geq$0.95)

The values obtained for the fitted curves are gathered in table 4.2. The most pronounced differences were found for τ_{ads} and τ_{rea} obtained on Au/ZnSe and ZnSe substrates. Indeed, the value of τ_{ads} obtained on Au/ZnSe was ≈1.3 and 1.7 times

smaller with respect to ZnSe (H_2O_2/HCl) and ZnSe (ozone/UV), respectively. This result indicated that the adsorption of thiols occurred faster on gold than on ZnSe. The phase of the slow rearrangement was also affected by the substrate (τ_{rea}). Thus, on Au/ZnSe the arrangement of alkanethiol molecules occurred ~8 and ~12 times more rapidly than on ZnSe treated with ozone/UV and ZnSe treated with acids, respectively. It can also be noticed that the value of the limiting absorbance (A_0) was the highest on Au/ZnSe. The obtained values are overall in the same range of those found in the study of Lacour et al. describing the adsorption of alkanethiols onto gallium arsenide (A_{ads}=0.51, τ_{ads}=0.11, and τ_{rea}=2.62).

Table 4.2. Parameters derived from the fitting of adsorption curves of SAM-NH$_2$ on three different substrates

	Au/ZnSe	**ZnSe (ozone/UV)**	**ZnSe (H$_2$O$_2$/HCl)**
A_0	0.62	0.46	0.19
A_{ads}	0.55	0.47	0.57
τ_{ads}	0.03	0.05	0.04
τ_{rea}	0.39	3.16	4.84

The highest infrared intensities on Au/ZnSe can be associated with the highest coverage of thiols on this substrate compared to bare ZnSe. However, the signal on gold could also be enhanced as a result of changes in electric field (as in SEIRAS mentioned in part 1.2.2), that seemed to some extent have occurred in the spectra of LGG (figure 4.1f) and was reported in other studies [184], [307]. Therefore, albeit sensitive to the sample concentration and hence, to the coverage yield, ATR-FTIR could not be used as the only method to estimate the differences in SAM coverage in this particular case of gold-coated and bare ZnSe substrates. The SAM coverage was then estimated based on high energy RBS measurements [269]. The RBS spectra presented in figure 4.6 show that the carbon areal density was higher on Au/ZnSe than on ZnSe (prepared with ozone/UV treatment), namely ~103 and ~75 atoms/nm^2 corresponding to ~9.4 and ~6.8 alkanethiol molecules per nm^2, respectively. Interestingly, the ratio of the SAM coverage on Au/ZnSe to ZnSe was found to be 1.4 based on RBS data and 1.3 based on ATR-FTIR (after overnight reaction), showing a close accordance between the results obtained by both techniques.
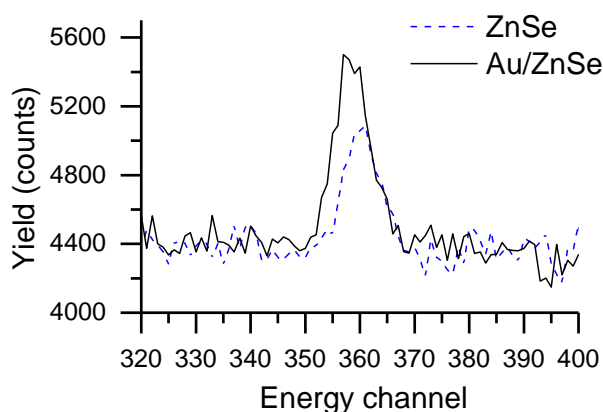
Figure 4.6. Rutherford backscattering spectra showing carbon counts for NH$_2$-terminated thiol on bare ZnSe and gold-coated ZnSe. Incident beam energy = 4265 keV

The ATR-FTIR spectra of νCH$_2$ bands region (figure 4.5b) appeared with lower wavenumbers on gold-coated ZnSe (2920 and 2850 cm^{-1}) with respect to those that were on bare ZnSe (2924 and 2853 cm^{-1}) after overnight reaction. It suggests that the lower number of conformational defects occurred in SAMs on gold-coated ZnSe [304], [308]–[314], in accordance with the higher coverage yield on this substrate. The steady increase of ordering in SAMs over time was observed from shifts of the νCH$_{2asym}$ band equal to 2922 cm^{-1} and 2926 cm^{-1} on Au/ZnSe and ZnSe, respectively, at the start of self-assembly process, as depicted also in figure 4.5b.

b) LGG attachment onto amino-terminated surfaces is similar regardless of the substrate

After the functionalisation with amino-terminated SAMs, ZnSe and Au/ZnSe substrates were subjected to a flow of bacterial suspension. The attachment of cells was monitored using ATR-FTIR spectroscopy and the coverage of the crystal with bacteria was calculated from epifluorescence images of the crystal surface after its removal from the infrared cell (figure 4.7).
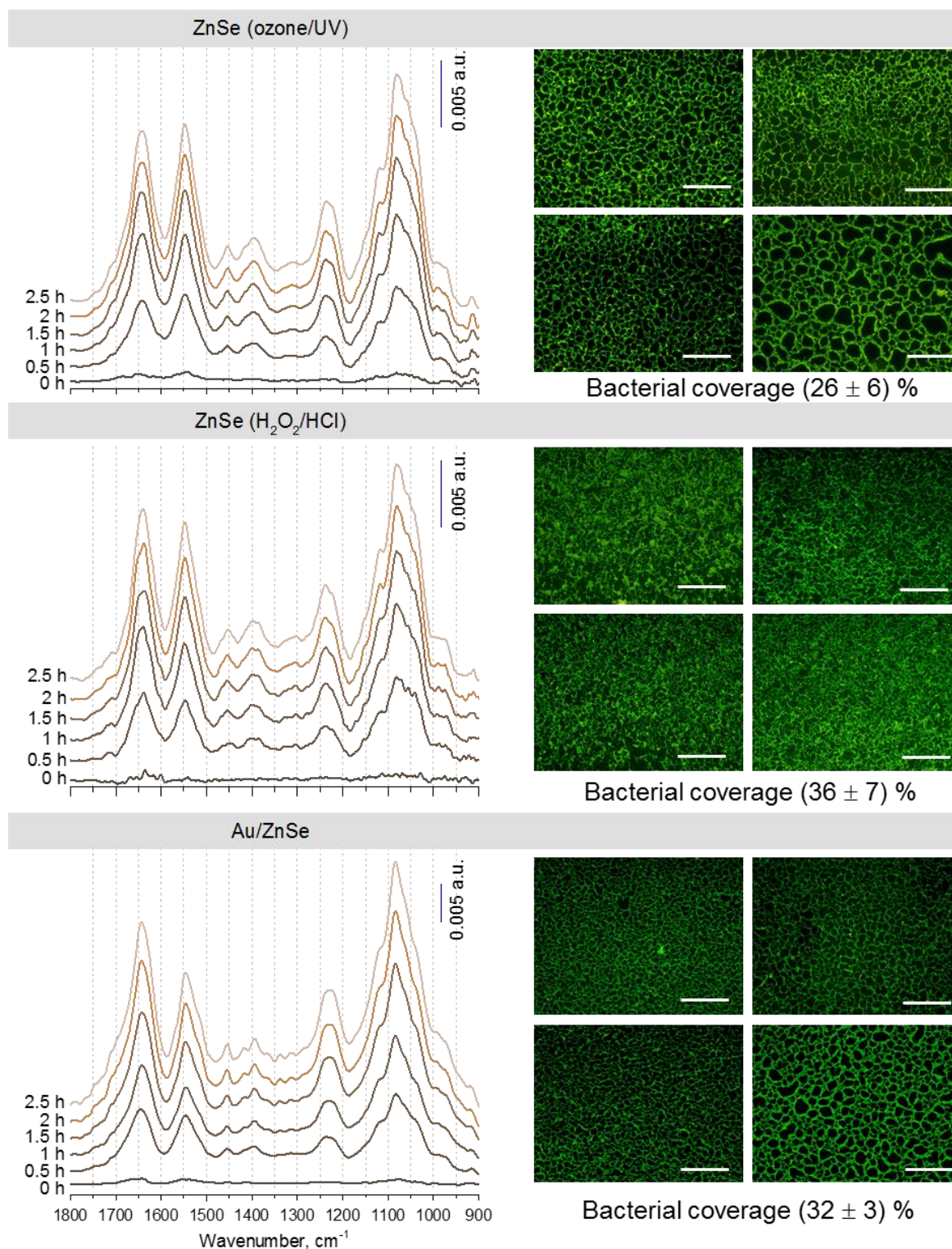
Figure 4.7. LGG spectroscopic fingerprints (offsets) on functionalised substrates (SAM-NH$_3$+) with corresponding epifluorescence images (BacLight^{TM} staining, scale bar – 200 µm) presenting distribution of bacterial cells on the substrate

As it can be seen, ATR-FTIR spectra were similar regardless of the substrate, except the band region corresponding to polysaccharides, phospholipids and nucleic acids (950–1200 cm^{-1}). This region was characterised with a less pronounced band at 1040 cm^{-1} assigned to νC–O vibration from polysaccharides and nucleic acids on Au/ZnSe.

Also on Au/ZnSe, although less pronounced than in the blank experiment, the growth of bands at 1700–1750 and 950–1200 cm^{-1} was more rapid with respect to other bands in the spectrum. The coverage of the substrates with LGG was similar on the three substrates varying from 26 to 36 %, suggesting that the functionalisation with thiols had impact on the strength of the interaction of attached cells with the surface and consequently, on the retention of cells. Bacteria were homogeneously distributed over the surfaces with characteristic chain-like pattern, which was especially pronounced on ZnSe preliminarily treated with ozone/UV and on Au/ZnSe surfaces. Besides, LGG cells appeared green after the *Bac*Light^{TM} staining, which suggested the integrity if their membrane.

4.2 Discussion

This study presents the role of the substrate properties in the processes of self-assembly of alkanethiols and interactions with bacterial cells. The results on bare ZnSe treated by ozone/UV or acids for removal of organic contaminants showed important aspects on how a surface cleaning procedure may drastically change the outcome of the experiment, both in case of SAM formation and bacterial attachment. The data of XPS and STEM revealed an enrichment of ZnSe surface with selenium after H$_2$O$_2$/HCl etching, in accordance with previously reported works on ZnSe etching [293], [295], [315]. Thus, the etching of ZnSe is selective for the atoms of zinc on the surface. Zinc in the form of a nanopowder was reported to be easily dissolved in acidic solutions [316], whereas the bulk zinc is passivated with a hydroxide layer. In case of ZnSe, it appears that selenium plays the role of a passivation layer, possibly due to a higher strength of Se–Se bonds compared to Zn–Se [317]. Strong Se-Se bonds might also be the reason for the formation of selenium nanosized hemispheres and micron-sized whiskers on the surface after treatment with hydrochloric acid. The latter ones were also observed by Liu et al. after ZnSe was etched with hydrofluoric acid [292]. To our knowledge, our study is the first to provide a link between the change in composition and morphology of ZnSe after acid etch at the nanoscale. The enrichment of ZnSe with selenium could cause the lowest yield of thiol adsorption among three studied substrates. Indeed, Noble-Luginbuhl and Nuzzo hypothesised that thiols bind to Zn on ZnSe surface [257], and our results are in accordance with this hypothesis.

The gold nanofilm on ZnSe was represented by homogeneously distributed grains despite its nanoscale thickness of ~2 nm. The morphology of the homogeneous film composed of nanosized particles is in accordance with previously reported results of 3 nm gold physical vapour deposited onto silicone [318]–[320] and glass [321]. It is interesting to note that such small thickness of metallic nanofilm is expected to be below so called percolation threshold, which means that the gold film can be pictured as isolated capacitively coupled metal clusters, and not as a continuous conductive film [318]. This is important, as the electric field distribution must be considered in the interpretation of the infrared spectra, in particular on metal surfaces [318], [319]. Indeed, thin metal films can be the origin of the enhanced infrared signal due to an enhanced localized electromagnetic field developed around small metal particles that comprise these films, the phenomenon on which surface enhanced infrared absorption spectroscopy (SEIRAS) relies [183]. The surface enhancement, in such case, is limited to the first ~10 nm above the ATR crystal, and only for bands that arise from a change in dipole moment perpendicular to the surface [322]. The degree of enhancement is expected to be approximately of 100-1000 fold, but this value changes drastically as a function of the morphology of a metal nanofilm. Did SEIRAS effect occur in the present study in infrared measurements on gold-coated ZnSe? This question remains difficult to answer unequivocally due to several reasons. First, it should be stated that the features of spectra recorded during LGG flow over Au/ZnSe suggest that some effects that unlikely originated from actual changes in the sample indeed were present. The high signal intensity of bands tentatively assigned to teichoic acids was observed in the measurements using bare Au/ZnSe and, albeit to a less extent, amino-terminated Au/ZnSe. We believe it was due to progressive approach/attachment of bacteria onto the surface and subsequent enhancement of the bands assigned to teichoic acids in close contact with the gold nanofilm. Herein, the interaction with gold could potentially occur through thiol groups of amino-acids present on the cell wall of bacteria, e.g. cysteine as reported for *Lactobacillus helveticus* [323]. Then, the less pronounced enhancement of the bands corresponding to teichoic acids on functionalised Au/ZnSe could possibly be due to a "screening" of the gold surface with SAM in a sense that it falls in the region of the enhancement in SEIRAS. Hereby, the SAM expands the distance between the gold surface and LGG cells, which leads to a lower enhancement of bands associated with LGG.

Here, one would also expect to have the enhancement of the intensity of bands assigned to alkanethiol molecules on Au/ZnSe. Infrared results indeed showed that the intensities were higher on Au/ZnSe with respect to ZnSe, albeit much lower than would typically be expected in SEIRAS. RBS data suggest that the difference in IR intensities of bands for SAMs on Au/ZnSe and ZnSe was probably not associated with SEIRAS effect. Indeed, according to RBS measurements the ratio of the coverage on Au/ZnSe to ZnSe (after ozone/UV) was found to be in a good agreement with the one obtained from the ATR-FTIR spectra. In the work of Bieri and Bürgi it was also demonstrated using germanium crystal coated with ~2 nm thick gold film that the asymmetry of bands and surface selection rule for metals hold in these conditions, but the enhancement of IR intensities with respect to bare germanium was not claimed [324]. In any way at present, the possibility of SEIRAS effect to occur in the conditions used in the present work remains ambiguous and further experiments should be performed. Here, phospholipids layers can be used as a model sample to further elucidate the possible enhancement of the signal due to SEIRAS conditions. These structures are on average around 10 nm thick, taking fully the enhancement area in case of SEIRAS effect, and are well oriented on surfaces including ATR crystals [239], which means if SEIRAS effect occurs, it should be pronounced.

The values of the coverage of surfaces of Au/ZnSe and ZnSe (cleaned with ozone and UV) with alkanethiol molecules were found to be higher in this work than those usually found for a monolayer of alkanethiols on gold packed with the maximal density (4.5 molecules/nm^2 [245]). This difference in results can be explained by two factors, i.e. the increased surface roughness of substrates compared to those typically used in studies with alkanethiol SAMs (e.g. mica, silicon, glass), hence more surface area available for grafting of thiol molecules (i), and by formation of partial bilayer of molecules (ii), as schematically shown in figure 1.10. The latter problem for amino-terminated SAMs is usually solved by thorough rinsing and sonication of the substrate in solvents such as acetic acid [256]. These procedures could not be applied in the present study due to poor ZnSe mechanical and chemical stability. Nonetheless, a care has been taken to perform equal manipulations with SAMs before subjecting them to bacterial inoculation. An extend rinse with ethanol and distilled water resulted in approximately twice less intensities (as presented and discussed in chapter V) with

respect to those presented in Figure 4.5 after overnight reaction, which indicated that physically and hydrogen-bonded molecules must have been removed.

The high roughness of substrates used in this work somewhat complicated the analysis of the results on SAM coverage. On the one hand, as mentioned above, higher surface roughness is associated with higher surface area for SAM formation. On the other hand, it also leads to a higher disordering of SAMs on the substrates and consequently, less packed SAMs. Considering the lowest roughness of Au/ZnSe among three studied substrates, the latter point was in line with RBS results showing higher carbon areal density on Au/ZnSe, and with infrared measurements indicating lower number of conformational defects on Au/ZnSe substrate. Indeed, the wavenumbers of νCH_{2asym} and νCH_{2sym} bands found for SAM on ZnSe in this work were found to be very close to those found by Noble-Luginbuhl and Nuzzo for 1-dodecanethiol onto ZnSe, i.e. 2923 and 2853 cm^{-1}, respectively. At the same time, on Au/ZnSe these values were few units lower, indicating formation of the well ordered SAM, as suggested by many authors in studies with different substrates [304], [308]–[314].

The kinetics of SAM formation estimated through the increase of the intensities of infrared signal was also substrate-dependent. The reaction has occurred most rapidly on Au/ZnSe and was slower on ZnSe cleaned with ozone/UV and H_2O_2/HCl. The increase in infrared bands on all studied substrates was progressive for the first ~30 minutes and after slowed down. This result, in accordance with the shift of νCH_2 wavenumbers towards lower values as a function of time, suggests two stages of adsorption process, i.e. first, rapid adsorption of molecules with alkanethiol chains being strongly entangled, and further straightening of the chains leading to a densely packed monolayer. This mechanism was generally accepted for SAMs obtained on other substrates [247], [305]. In addition, the increase of the intensity of bands as a function of time can also be contributed by a progressive exchange of near-surface solvent with thiol molecules [248].

The results of bacterial retention at surfaces obtained from epifluorescence images after the rinsing step have pointed interesting differences between the substrates in blank experiments (without the thiol SAM). ZnSe cleaned with ozone/UV had very poor interaction with bacterial cells, whereas on ZnSe enriched with selenium and Au/ ZnSe bacteria attached stronger. The difference in water contact angles between the three

substrates was low suggesting that the wettability of the substrate is not the main factor affecting LGG retention. On ZnSe after acidic treatment, the higher bacterial retention is suggested to be associated with the formation of selenium whiskers, on which LGG appear to attach preferentially. These structures could play a role of the physical barrier, on which LGG might have "clung" during the flow. Indeed, the characteristic chain-like look of LGG biofilm was slightly perturbed on the selenium-enriched substrate, in line with this hypothesis. It is interesting to note that this chain-like appearance of LGG at a surface seems to be dependent on pili presence. This was demonstrated in the work of Tripathi et al. using LGG mutants devoid of pili, which spread on the substrate with a random character losing the ability to form chains [325]. Another interesting thing to note is that nanostructured selenium deposited on a substrate was reported to render the substrate antibacterial (specifically for *S. aureus*) [326]. However, the nanosized hemispheres observed in the present work on ZnSe substrate after acidic etch did not seem to be toxic for LGG, as LGG cells appeared green after *Bac*Light[TM] staining.

On gold-coated ZnSe before thiol functionalisation, high retention of LGG cells may be explained by the interaction of thiol groups in proteins on bacterial cell wall with gold, as mentioned above and as previously suggested by Kesel and co-authors in the study of *B. subtilis* adhesion on gold [327]. In a recent work of Jarosz et al. it was demonstrated that LGG does not adhere to gold [328]. Here, it must be mentioned that Jarosz et al. used LGG from the probiotic product available on the market and thus, the properties of LGG strain could have been modified during the industrial formulation. Moreover, the authors performed adhesion tests in MRS medium, the nutritive components of which can screen the effect of the surface. LGG has poor adhesive properties in MRS, as it was shown previously in chapter III, and in the study of Lebeer et al. [79].

Interestingly, on functionalised substrates the difference in SAM ordering and coverage did not have strong impact on bacterial retention at surface, which was around 30 % on all the studied substrates. Possibly, this effect was attributed to the fact that lower number of amine groups on ZnSe without gold coating was still sufficient to maintain electrostatically attached cells at the rinsing step. The 10-fold increase of LGG

retention on functionalised ZnSe (ozone/UV) with respect to the one without SAM additionally confirms successful assembly of alkanethiols onto ZnSe.

Conclusions

Taken together, the results presented here show that the understanding of the surface properties is critical for understanding of bacterial attachment and retention at surfaces. In order to control the bacterial retention at surface, the control of the surface properties is important. Thiols formed more ordered and dense SAMs on the gold-coated ZnSe substrate than on ZnSe without the gold nanofilm. Nonetheless, bacterial retention was similar regardless of the efficiency of thiol self-assembly. We thus conclude that for reasons of simplicity and cost-efficiency, it is more convenient to perform the study of the formation of LGG biofilm on ZnSe directly functionalised with thiols, without preliminary deposition of gold. We further suggest that ozone/UV is a more suitable cleaning procedure than acidic etch, in relevance with ZnSe used as a substrate to study bacterial cells. Albeit very efficient to remove organic contaminants, acidic etch is an aggressive treatment that damages drastically the surface of ZnSe crystal resulting in a low detected energy of the infrared beam, which makes difficult to perform experiments routinely. However, the phenomena of high adhesion and retention of LGG on gold and selenium-rich substrates are interesting on itself and could be applied in other research projects with LGG (e.g. bioelectrodes based on gold or antipathogenic selenium-based substrates with probiotic biofilms). Finally, we postulate that LGG indeed is able to retain on positively charged substrates and that its membrane stays intact after a short time of incubation onto this surface.

V. Impact of surface chemistry on the development and retention of LGG biofilms

In the previous chapter, we have shown that LGG attaches well on the amino-terminated substrate. The next step in the project was associated with the questions of (i) whether LGG cells stay intact on the amino-functionalised surface in a long term (ii) and if there could be thiols with other terminal groups that would aid to maintain LGG on the surface with similar or higher efficiency with respect to amino-terminated surface.

The first question raised from the fact that positively-charged surfaces were earlier reported as not supportive for the long-term growth of bacteria [216], as high density of positive charges could result in the disruption of bacterial membrane [217]. Besides, ammonium compounds are known as common disinfectants as they induce leakage of intracellular components by damaging the membrane of the bacterial cell [329]–[331]. It must be mentioned, however, that the action of biocidal compounds varies drastically as a function of bacterial species, and in particular depends on the Gram-status of the bacterium that is defined by the difference in the bacterial cell wall (annexe VI). On the one hand, some Gram-positive bacteria were shown to be more resistant to positive charges due to their thick peptidoglycan layer [218], [219]. On the other hand, it was postulated by others that Gram-positive bacteria are more susceptible to cationic biocide action, as they, unlike Gram-negative cells, do not possess an outer membrane composed of lipopolysaccharides, phospholipids, and special pore/channel-like proteins (porins), which permits the selective diffusion of nutrients across the cell wall and acts as a barrier for biocidal components [329], [330]. Hence, the effect of the amino-terminated substrate, which is mostly positively charged under physiological conditions (pKa ≈6.5–7.5 [332], [333]), on the viability of LGG cells remains difficult to predict.

Considering the high risk to impair LGG functionality with electrostatic interactions on the positively charged substrate, other types of interactions between LGG and its support are of interest to explore. As described in part 1.3.2, variation in wetting properties of the substrate can tune significantly the degree of bacterial retention.

Therefore, hydrophilic and hydrophobic surfaces are relevant in terms of investigation of the mechanisms of the formation of LGG biofilm. In this regard, alkanethiol SAMs represent a convenient approach to vary the surface properties by choosing different terminal groups of the alkanethiol chain. Many works have validated the utility of these systems in research of bacterial attachment and biofilm development [78], [139], [140], [207], [259].

In this chapter, alkanethiol molecules terminated with methyl (SAM-CH$_3$), hydroxyl (SAM-OH) or amine (SAM-NH$_2$/NH$_3^+$) groups were grafted onto ZnSe substrate preliminarily cleaned with ozone/UV treatment, to obtain hydrophobic non-charged, hydrophilic non-charged and hydrophilic positively charged substrates in the aqueous media used, respectively. Similarly to the protocol presented in chapter IV, LGG suspended in physiological water was then inoculated over functionalised substrates for 2.5 hours and the attachment of cells on the surface was followed in situ using ATR-FTIR spectroscopy. Furthermore, the growth of LGG on CH$_3$- and NH$_3^+$-functionalised substrates was studied for additional 24 hours with the constant supply of nutrients. As the most favourable medium for LGG biofilm formation was mTSB/10 (presented in chapter III), this medium was chosen for biofilms formation here.

5.1 Results

5.1.1 Functionalisation of ZnSe with alkanethiols and characterisation of the obtained surfaces

The functionalisation of the surface with three different alkanethiols was performed on the ZnSe crystal mounted into the infrared cell and the process of thiol adsorption onto the surface was monitored *in situ* using ATR-FTIR spectroscopy. Figure 5.1 shows ATR-FTIR spectra recorded during self-assembly reaction from alkanethiol solutions.
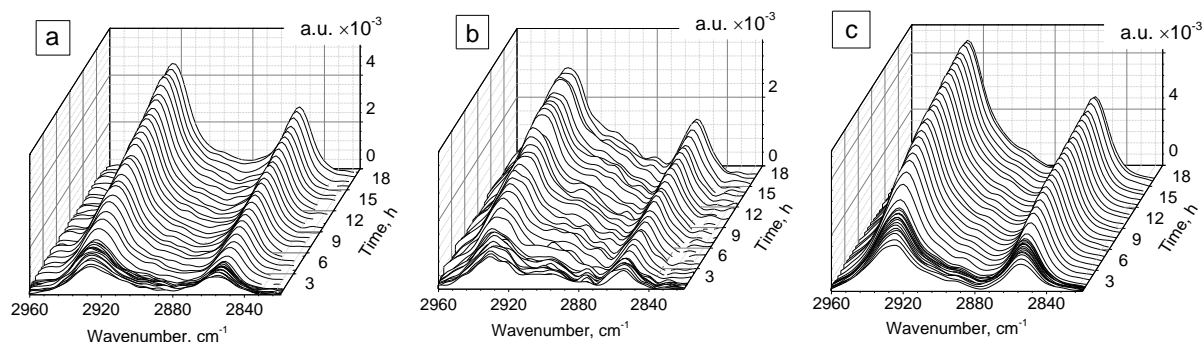
Figure 5.1. ATR-FTIR spectra depicting νCH_2 bands of alkanethiol molecules terminated with CH_3 (a), OH (b), and NH_3^+ (c) groups, suspended in ethanolic solution and presented as a function of time. The spectrum of ethanol recorded immediately before the inflow of alkanethiol solution served as a reference.

The growth of νCH_2 bands indicated the adsorption of thiol molecules onto the surface. Interestingly, the positions of these bands were varying as a function of time and with respect to the terminal group of the alkanethiol molecules (table 5.1). The position of νCH_{2asym} band provides insight into the intermolecular environment of the alkyl chains [308]. Lower frequencies of vibrations indicate lower number of conformational defects, whereas the position at ~2918 cm^{-1} is considered to be representative for crystalline-like structure [308]. As can be seen in table 5.1 from the decrease of the wavenumber for νCH_{2asym} band over time, all studied alkanethiols increased the degree of ordering in SAMs from the initial adsorption until the end of recording period. Moreover, it can be noticed that the SAM-OH had the least ordered organisation, as this value was 3 cm^{-1} higher than for the other two SAMs by after 16 hours of reaction.

Table 5.1. Position of νCH_2 antisymmetric and symmetric bands for alkanethiols with different functional groups at the beginning and at the end of the reaction

	SAM-CH$_3$		SAM-OH		SAM-NH$_2$	
	νCH_{2asym}	νCH_{2sym}	νCH_{2asym}	νCH_{2sym}	νCH_{2asym}	νCH_{2sym}
~2 min	2927	2855	2929	2855	2926	2854
~16 hours	2924	2853	2927	2854	2924	2853

The low degree of the organisation in SAMs is usually associated with less packed monolayers. To compare the surface coverage with SAMs as a function of the terminal group the intensities of νCH_{2sym} band in the spectra recorded regularly over time of the reaction were integrated, and the values obtained were used as indicators of the kinetics of the reaction process (figure 5.2). As estimated from these integrated intensities, the surface coverage was higher in the order "SAM-NH$_2$ > SAM-CH$_3$ > SAM-OH". In particular, 2.8 and 5.8 fold higher intensities were observed at the end of the measurements and before rinse with water for SAM-NH$_2$ compared to SAM-CH$_3$

and SAM-OH, respectively. Here, it must be noted that amino-terminated SAMs tend to form a bilayer due to hydrogen bonding, as mentioned in chapter IV and chapter I (figure 1.10). In the case with SAM-OH, the formation of a bilayer can also be expected via hydrogen bonds. However, it was earlier demonstrated in the work of te Riet et al. using nanografting method and the analysis of friction maps of the AFM probe that SAM-OH, somewhat surprisingly, did not appear to form interlayer hydrogen bonds, whereas SAM-NH$_2$ clearly showed a bilayer configuration [334]. As suggested by the authors, this result could be explained by an unfavourable competition with the formation of strong hydrogen bonds between the molecules within the SAM-OH, or an unfavourable competition with the solvent for hydrogen bonding. Based on these findings and from our observations of the low intensities obtained for SAM-OH (figure 5.2), it could be suggested that the organisation of SAM-OH was represented by a monolayer on ZnSe. However, the scenario in which the low intensity is obtained as a result of very low packing density and some hydrogen-bonded molecules lying on top cannot be excluded. The definitive conclusion on the possible bilayer formation is complicated by the fact that the intensities obtained for SAM-OH were very low. However, the contribution of a bilayer into the intensity for SAM-NH$_2$ can be further estimated.
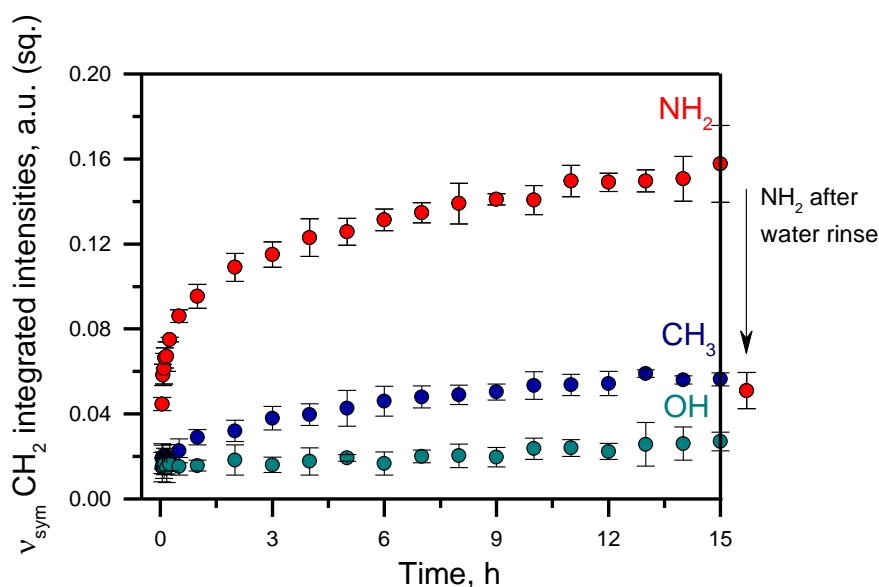
Figure 5.2. Time evolution of the integrated intensities of νCH_2 symmetric band (2874–2814 cm^{-1}) of alkanethiol SAMs terminated with amine (NH$_2$), methyl (CH$_3$) and hydroxyl (OH) groups. Error bars represent standard deviations between three measurements. νCH_2 symmetric band was chosen for calculation as it was found to be less affected by variation of ethanol bands.

To estimate the contribution from the bilayer formation into obtained infrared intensities the spectra of the SAM-NH$_2$ and, for comparison, the SAM-CH$_3$, were recorded after

rinsing the substrates with ethanol and distilled water (figure 5.3). It must be noted that the contribution from ethanol to the spectra of SAMs was not constant along the measurements of the self-assembly reaction (see annexe VII), sometimes resulting in a modification of $\nu_{asym}CH_2$ band by the end of recording period. The problem associated with the removal of ethanol bands that overlapped with the bands of alkanethiol SAMs has also been mentioned in the study of Enders et al. [335]. In particular, the variation in the intensity of the band at ~2973 cm^{-1} corresponding to νCH_{3asym} from ethanol precluded an accurate estimation of the intensity of νCH_{2asym} band in the spectra obtained after the rinsing the substrates with ethanol and water. Therefore, only νCH_{2sym} band was used for comparison of surface coverage with SAMs in the spectra obtained after rinsing (figure 5.3) and those recorded in situ during alkanethiol adsorption (figure 5.2).
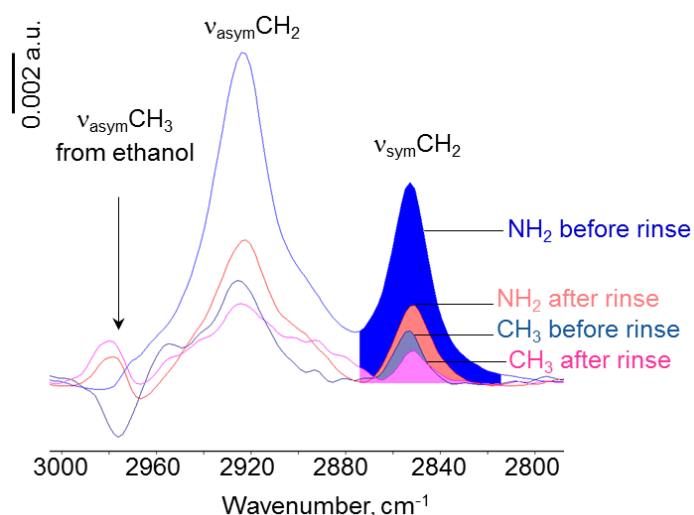
Figure 5.3. ATR-FTIR spectra depicting νCH_2 bands region of amino- and methyl-terminated SAMs at the end of the overnight reaction (before rinse) and after subsequent rinse with ethanol and water. The area marked is a result of calculating the intergated intensity of $\nu_{sym}CH_2$ band. Reference spectrum is the spectrum of ethanol recored immediately before the inflow of alkanthiol solution in the infrared cell

Owing to the limitation associated with ethanol bands, the integrated intensity of $\nu_{sym}CH_2$ band for SAM-NH$_3^+$ and SAM-CH$_3$ before and after rinse with ethanol and distilled water could be roughly compared. Based on the results depicted in figure 5.3, it is estimated that ~60–70% of the intensity of the spectra of SAM-NH$_3^+$ before rinse is contributed from bilayer and/or physically sorbed molecules, whereas in the spectrum of SAM-CH$_3$ before rinse it was found that ~20–30% of the intensity was presumably due to physically sorbed molecules. Thus, considering that integrated

intensities for actual self-assembled monolayer corresponded to 30–40 % from the intensities in the spectra of SAM-NH$_2$ and 70–80 % in the spectra of SAM-CH$_3$ presented in figure 5.2, the surface coverage proportional to band intensities was recalcualted to be 1.6 fold higher for SAM-NH$_2$ than for SAM-CH$_3$ (if the values are taken as 40 % and 70 % from initial intensities after 15 hours of reaction, for SAM-NH$_2$ and SAM-CH$_3$ respectively) or equal on both substrates (if the values are taken as 30 % and 80 % from the intensities of SAM-NH$_2$ and SAM-CH$_3$, respectively).

To further elucidate the difference in surface coverages between SAMs, high energy Rutherford backscattering spectrometry measurements were performed. As described in part 2.1.6, the counts in RBS is a function of both atomic density and thickness, and this method was successfully applied earlier to study the surface coverage with alkanethiol SAMs based on the signal from carbon [269]. Figure 5.4 shows RBS spectra of alkanethiol SAMs terminated with CH$_3$, OH, and NH$_2$ groups. The energy of the backscattered ion is decreasing with the atomic number, therefore carbon signal lies atop of the strong signal from ZnSe substrate. The insert in figure 5.4 depicts the difference in carbon counts for the three different SAMs. The highest signal was observed in case of the SAM terminated with amine group and somewhat lower counts were obtained on SAMs with methyl and hydroxyl groups.
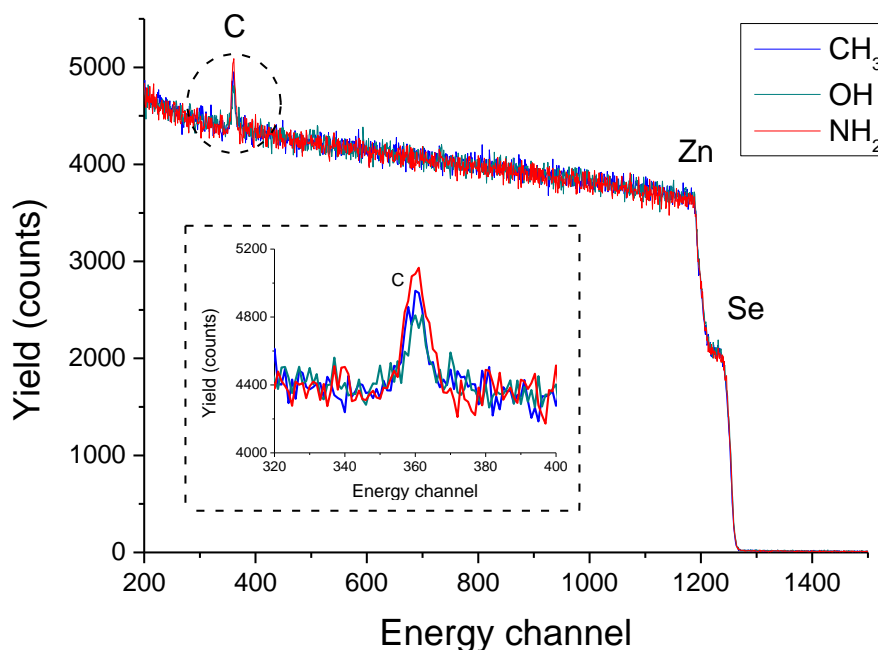
Figure 5.4. Rutherford backscattering spectra of alkanethiol SAMs terminated with CH$_3$, OH, and NH$_2$ groups. Incident beam energy = 4265 keV

The experimental RBS spectra were further analysed by comparison with the simulated spectra in SIMNRA software [268], allowing one to extract the data on the areal density of the elements. As shown in table 5.2, the results of RBS measurements on carbon coverage indicated that the surface coverage with alkanethiol molecules was 1.6 and 1.7 fold higher in SAM-NH$_2$ than in SAM-CH$_3$ and SAM-OH, respectively. The values of coverages corresponding to SAM-NH$_2$ and SAM-CH$_3$ were in agreement with the results obtained from ATR-FTIR spectra after the rinsing step.

Table 5.2. Surface coverage with SAMs and surface energy of the functionalised substrates

		SAM-CH$_3$	SAM-OH	SAM-NH$_2$
Carbon coverage	atoms/nm^2	52	45	75
	molecules/nm^2	4.3	4.0	6.8
Contact angle H$_2$O		89.8	70.4	68.5
Contact angle CH$_2$I$_2$		40.1	35.0	41.0
Surface energy, mN/m		40.6	48.7	47.4

In the perspective of the study of bacterial attachment, the surface energy of functionalised substrates was determined based on the contact angle measurements (table 5.2). Two solvents, water and diiodomethane, were used for the measurements, following the Fowkes theory as described in part 2.1.4. The obtained values showed the lowest surface energy value among three studied surfaces for SAM-CH$_3$, as expected from the lack of the polar component, whereas the values obtained on surfaces with SAM-NH$_2$ and SAM-OH were similar to each other.

5.1.2 LGG attachment, biochemical composition and retention on functionalised substrates

a) Biochemical composition and attachment degree of LGG cells as a function of substrate functional groups

The functionalised substrates were subjected to a flow of LGG suspended in physiological water for 2.5 hours (30 minutes at static mode and 2 hours flowing at the rate of 50 mL/h). The kinetics of LGG adhesion to the substrates was monitored based on the growth of amide II band intensities during the inoculation of LGG suspension (figure 5.5). The use of this band as an indicator for biomass quantity has been earlier validated [161], [336]. It is important to note that the obtained growth curves represent

the lateral increase of the biomass amount, since the absorbance is measured only 1-2 µm above the substrate. The growth of amide II band was very close on the substrates with SAM-CH$_3$ and SAM-OH, whereas on SAM-NH$_3^+$ it occurred faster with higher obtained values for the integrated intensities (0.8, 0.7 and 0.7 for SAM-NH$_3^+$, SAM-CH$_3$ and SAM-OH, respectively) after 2.5 hours of bacterial flow. According to Kang et al. [337], the kinetics of bacterial attachment may fit the following equation:

$$A = A_{max}(1 - e^{-kt}), \tag{5.1}$$

where A_{max} is the amide II band integrated intensity corresponding to a complete single layer of bacteria, k is the rate constant, and t is the time of bacterial incubation. It is important to note, that such adsorption rate constant is dependent on the accessory optics and the suspension concentration, but it is useful for comparing the results obtained using the same ATR crystal and ATR-FTIR accessory. As presented in figure 5.5, the results corresponding to LGG attachment onto three differently functionalised substrates fit well this model of adsorption (regression coefficient $r^2 > 0.99$ for all curves). The rate constant values were 0.64, 0.86, and 0.99 h^{-1} for LGG attachment on ZnSe functionalised with CH$_3$, OH and NH$_3^+$ groups, respectively. Thus, the highest rate of LGG attachment was observed onto amino-terminated surface. However, it must be noted that the difference between the values was not drastic, and the obtained values indicated that LGG was able to attach onto substrates regardless of their functionalisation properties.
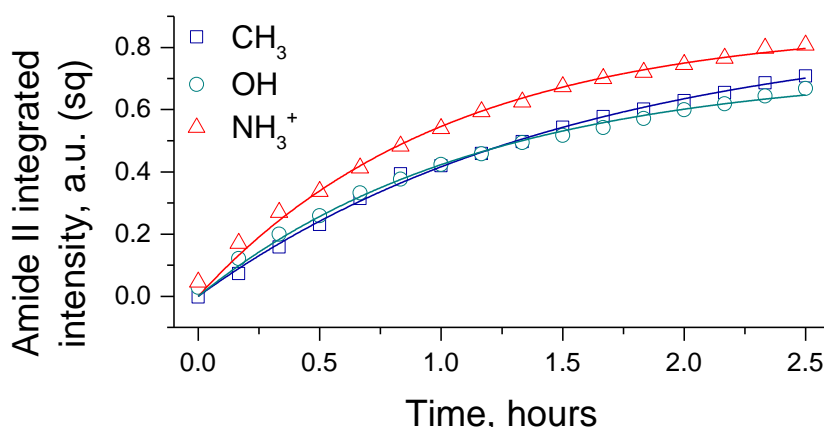
Figure 5.5. Time-evaluation of amide II band integrated intensities during inoculation of LGG suspension over ZnSe functionalised with alkanethiol SAM terminated by CH$_3$, OH or NH$_3^+$-functional groups. The curves are fitted using equation 5.1

The ATR-FTIR spectra obtained after 2.5 hours of LGG incubation on the substrates with SAM-CH$_3$, SAM-OH, and SAM-NH$_3^+$ are shown in figure 5.6a. The spectral features were overall similar on all studied substrates resembling common biochemical components of bacterial cells [260], [336] (see also table 3.1). Nonetheless, a slight difference can be noticed for νC=O (~1710 cm^{-1}) and νCOO$^-$ (~1415 cm^{-1}) bands, which were more intense on NH$_3^+$-functionalised substrate. These bands were assigned to carboxylic acids, which could be specifically linked to NH$_3^+$ moieties of the surface. The analysis of the ratios of main components of bacterial cells (figure 5.6b) suggests that the ratio of nucleic acids and phospholipids to a sum of nucleic acids, phospholipids and polysaccharides (NA+PL / NA+PL+PS) was similar regardless of the substrate. At the same time, the protein content was higher with respect to nucleic acids, phospholipids and polysaccharides (Amide II / NA+PL, Amide II / NA+PL+PS) on the substrate with SAM-NH$_3^+$. Therefore, based on the calculated ratios it can be suggested that the higher intensities of νC=O and νCOO$^-$ bands on the surface with SAM-NH$_3^+$ were due to the higher interaction of proteins from the peptidoglycan layer with NH$_3^+$ groups.
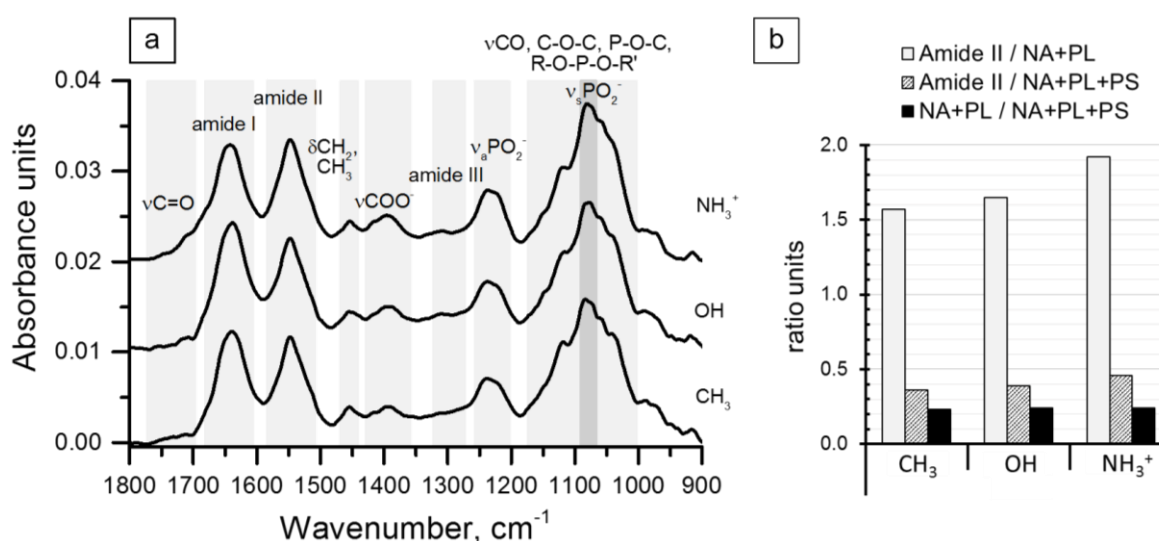
Figure 5.6. a) ATR-FTIR spectra of LGG suspended in physiological water after 2.5 hours of incubation on ZnSe functionalised with alkanethiol SAMs terminated with -CH$_3$, -OH, and -NH$_3^+$ groups. Offsets are used for clarity. The regions in grey correspond to main assignments of biochemical components. The reference spectrum was obtained immediately after filling in the infrared cell with LGG suspension. b) Ratios of integrated intensities of bands corresponding to proteins (amide II, 1592 – 1486 cm^{-1}), nucleic acids + phospholipids (NA + PL, 1271–1188 cm^{-1}), and a combinateion of NA, PL and polysaccharides (NA+PL+PS, 1189–956 cm^{-1}). Amide II band was used for proteins estimation, as it has little interference with the signal for δH$_2$O at 1640 cm^{-1}

b) The degree of retention of LGG cells and its membrane integrity on functionalised substrates

After inoculation of the bacterial suspension for 2.5 hours, the crystals were extracted from the flow cells, and the cells on surfaces were stained using the *Bac*Light^{TM} kit after a gentle rinse. As it can be seen in figure 5.7, the retention of cells on the substrates after the rinsing step was strongly substrate dependent. The retention was very poor on CH_3- and OH-functionalised substrates, whereas on NH_3^+-functionalised substrate the cells retained and the coverage with bacteria was homogeneously spread on the crystal, as it was presented in chapter IV. As mentioned before, the chain-like pattern observed on the latter substrate (figure 5.7c) can be associated with the presence of pili on LGG cell wall, as the cells devoid of them were shown to attach onto surfaces as randomly distributed and non-connected with each other [325]. Similar chain-like pattern of bacterial distribution at surfaces was demonstrated in the study of Jarosz et al. on LGG [328], and Leccese Terraf et al. on the vaginal strain of *L. rhamnosus* CRL 1332 [338].
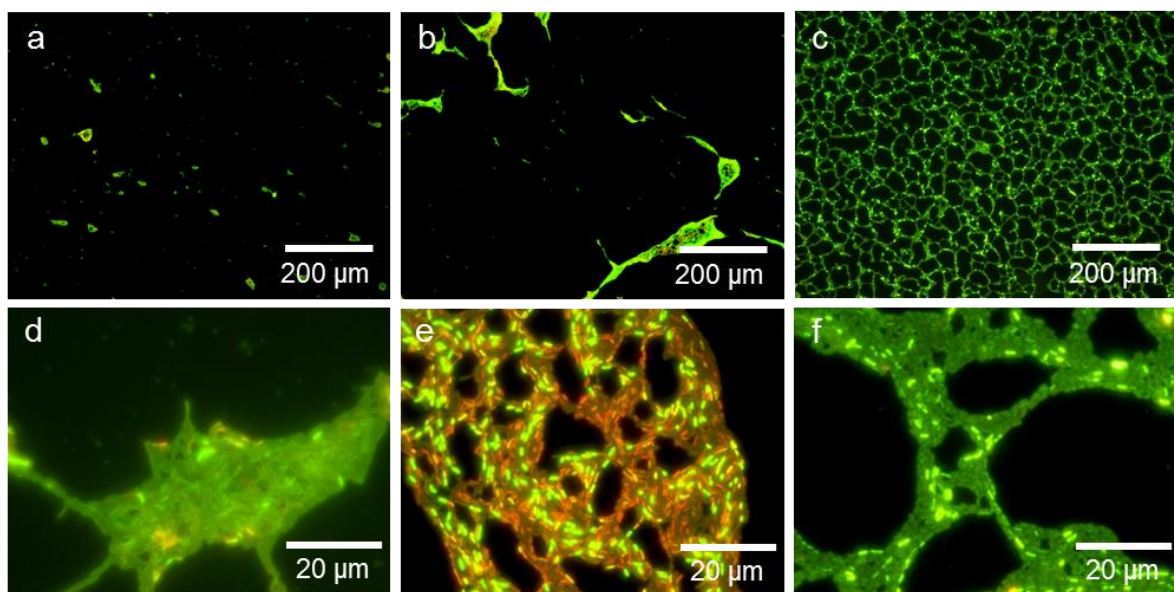
Figure 5.7. Epifluorescence images presenting LGG cell distributions after 2.5 hours incubation on the substrates functionalised with SAM-CH3 (a,d), SAM-OH (b,e), and SAM-NH2 (c,f). The substrates were rinsed by dipping into ultrapure water before staining with BacLight^{TM}

The cells left after the rinsing step on the substrates with SAM-CH_3 and SAM-OH were packed into batches of various shapes (figure 5.7a,b). Based on the observations of (i) how the crystal surface was dried after the rinsing step and (ii) droplet-like features of cell batches, in which many cells were densely packed on the borders of these droplets (as if being pulled), it is postulated that the distribution of cells on CH_3 and OH-functionalised surfaces is determined by the motion and the surface tension of the aqueous medium surrounding bacterial cells (in this case water). In simple terms, this

phenomenon can be imagined as a coffee stain on a surface, in which a border is formed by the particles of coffee as a result of water evaporation and the principle of maintaining a low surface energy [339]. Water at the edge of the droplet evaporates more quickly than in the middle because higher quantity of molecules are exposed to air there. Hence, in the case of bacterial suspension the water molecules from the middle of the droplet would arrive to replace evaporated molecules at the edge of the droplet, pulling bacteria (as if it would be coffee particles) suspended in it towards edges. As water continued to evaporate, bacterial cells stayed at the edges.

As the surfaces with SAM-CH$_3$ and SAM-OH were drastically affected by the rinsing step, the estimation of the membrane integrity using *Bac*Light^{TM} staining was complicated on these surfaces. For example, on the CH$_3$-functionalised surface the aqueous solution containing dyes tended to gather in large droplets on the crystal surface due to the low wetting properties of the substrate. This difficulty of spreading the staining solution led to the use of higher volume of this solution with respect to other surfaces. In addition, there was very low number of cells on these substrates (~0.5% coverage on SAM-CH$_3$ and ~7% coverage on SAM-OH), and many of them were gathered in overlaying patches. These phenomena could bring biases in the estimation of the impact of the surface on the membrane integrity. Nonetheless, as it can be estimated from the images (b, e) in figure 5.7, the incubation of LGG on the surface with SAM-OH resulted in a somewhat higher number of cells with damaged membrane compared to other two substrates. On the surface with SAM-CH$_3$ and, as already shown in chapter IV, on the surface with SAM-NH$_3^+$, the majority of cells appeared green, indicating the integrity of their membrane. It could also be noticed that the cells were not homogeneously stained on all substrates, but especially those with SAM-OH and SAM-NH$_3^+$ that showed some cells being highly fluorescent. This result may indicate differences in the physiological state of these cells.

c) The impact of the surface functionalisation on the adhesive forces of LGG

The results presented above showed that LGG appeared to attach on all studied substrates in the infrared flow cells, but did not respond in the same manner to a rinsing step. To further illustrate the effect of the substrate on LGG stability onto the surface, it was attempted to evaluate the detachment of bacterial cells *in situ* in the infrared flow cell based on variations of signal intensity under various mechanical stresses. In a first

assay, the cells attached onto the substrate after 2.5 hours of inoculation were subjected to a flow with an increased rate (15 mL/min with respect to normally applied ~0.8 mL/min). It did not result in a loss of the infrared intensities with respect to those that were obtained after 2.5 hours of bacterial inoculation on the substrate with SAM-CH3, on which the retention of LGG cells was very low after rinsing. It was then suggested that the force arising at the air-liquid interface, when this interface is in contact with the bacterial cell (as in the rinsing step), is a determining factor in the detachment of bacteria from the substrates. To verify this hypothesis, an experiment using a continuous flow of nitrogen bubbles (volume ~0.2 cm^3, ~15 bubbles per minute) in physiological water at 15 mL/min was set up, in which the effect of these bubbles on the attached bacteria was monitored *in situ* in the infrared flow cell. Figure 5.8 presents the time evolution of amide II band integrated intensities during bubble flow over LGG cells attached on three different substrates for 3.5 hours. Amide II band was chosen, as proteins are the most abundant molecules in bacterial cells considered as the marker of the biomass quantity [340]. For example, the linear correlation between amide II band and biomass quantity was reported in the study of *P. fluorescens* by Quilès et al. [336].
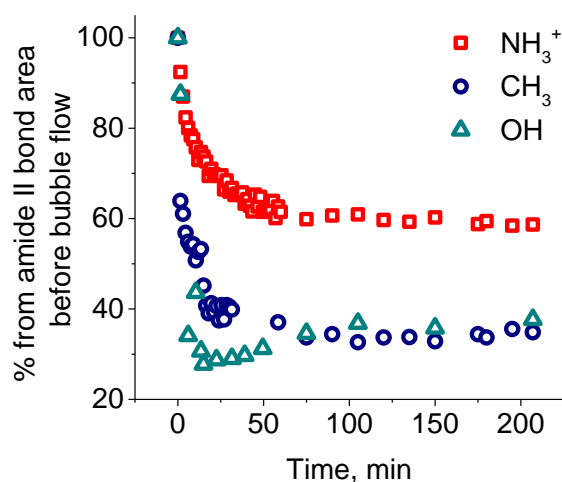
Figure 5.8. Time-evolution of amide II band integrated intensity during nitrogen bubble flow over LGG cells after 2.5 hour of preliminary inoculation on substrates functionalised with alkanethiol molecules terminated with CH$_3$, OH and NH$_3^+$ groups

Thus, the prominent decrease in amide II band integrated intensity suggested the removal of cells from the substrates under the mechanical stress exerted. The integrated intensities reached a pseudo-plateau after ~1 hour and then stayed constant for the following 2.5 hours of measurements on all substrates. The highest values of integrated intensity on the substrate with SAM-NH$_3^+$ seen after continuous

flow of bubbles suggested that the interaction forces were the highest between this substrate and LGG cells.

To estimate quantitatively the interaction forces between LGG cells and the three functional groups ($-CH_3$, $-OH$, $-NH_3^+$), single molecule force spectroscopy based on AFM measurements were performed. The dense carpet formed from bacterial cells taken at an exponential growth phase was immobilised on NH_3^+-functionalised Au/Cr/glass substrate. The immobilised bacteria were intermittently approached with AFM probes functionalised with CH_3-, OH- or NH_3^+-terminated alkanethiol molecules. The force curves of the interaction between LGG and functionalised probes were then recorded and analysed using MATLAB software with the program developed earlier in the laboratory. The values of adhesion forces that have occurred at various rupture distances between LGG and alkanethiol molecules with different terminal groups were extracted from the force curves and plotted as maps presenting the probability of adhesive events (figure 5.9).
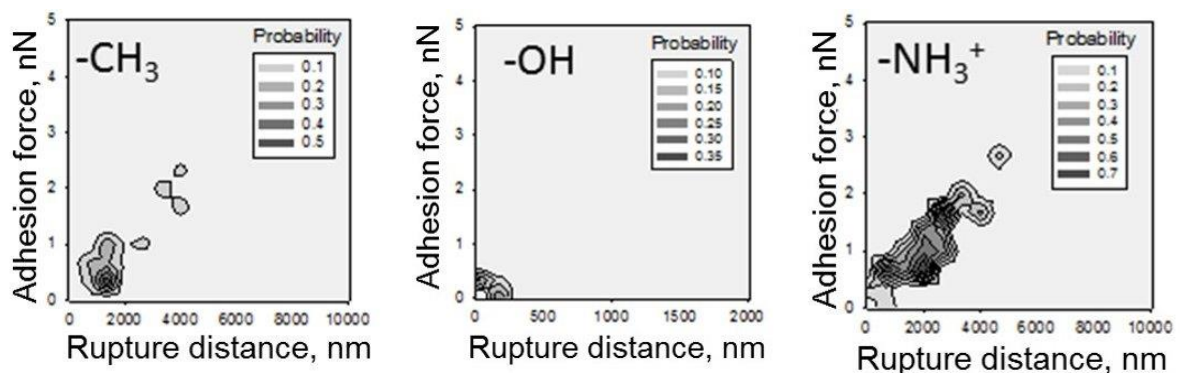
Figure 5.9. Force-distance maps for the interactions between LGG cell wall and AFM probes functionalized with alkanethiols terminated by CH_3, OH, and NH_3^+ groups recorded in phosphate buffered saline

The rupture distance here represents the longest distance at which the interaction between the probe and the wall of the bacterial cell still occurs as the probe retracts upwards from the sample surface. As can be seen in figure 5.9, the interaction was the weakest between LGG and -OH functional group, reaching maximum 0.5 nN at the rupture distance of 250 nm. The adhesive forces between the $-CH_3$ group and LGG were spread in a larger spectrum of values (more frequently being around 0.3 nN with rare events over 2 nN) and occurring at larger rupture distances (mostly between 1 and 2 µm, but present up to 4 µm). The highest interaction forces at longer rupture distances were found between LGG and $-NH_3^+$ group: high probability interactions

were between 0.5 and 2 nN, reaching up to 2.5–3 nN at rupture distances up to 5 µm. The strongest interaction forces observed between LGG and the amino-functionalised AFM probe were in a good agreement with the results obtained with ATR-FTIR spectroscopy and epifluorescence microscopy.

The impact of the substrate on LGG nascent biofilm was thus expressed predominantly as differences of adhesive forces of bacterial cells in the layer adjacent to the substrate.

d) Long-term development of LGG biofilms on functionalised substrates

The growth and membrane integrity of LGG cells on two selected substrates presenting the stronger interactions (SAM-NH$_3^+$ and SAM-CH$_3$) were studied in a long-term experiment in order to find out how important the substrate functionality is in the maturation process of the biofilm and the mechanical stability of the biofilm. Figure 5.10 shows the evolution of ATR-FTIR spectra depicting the LGG biofilm formation as a function of the time on both substrates in mTSB/10.
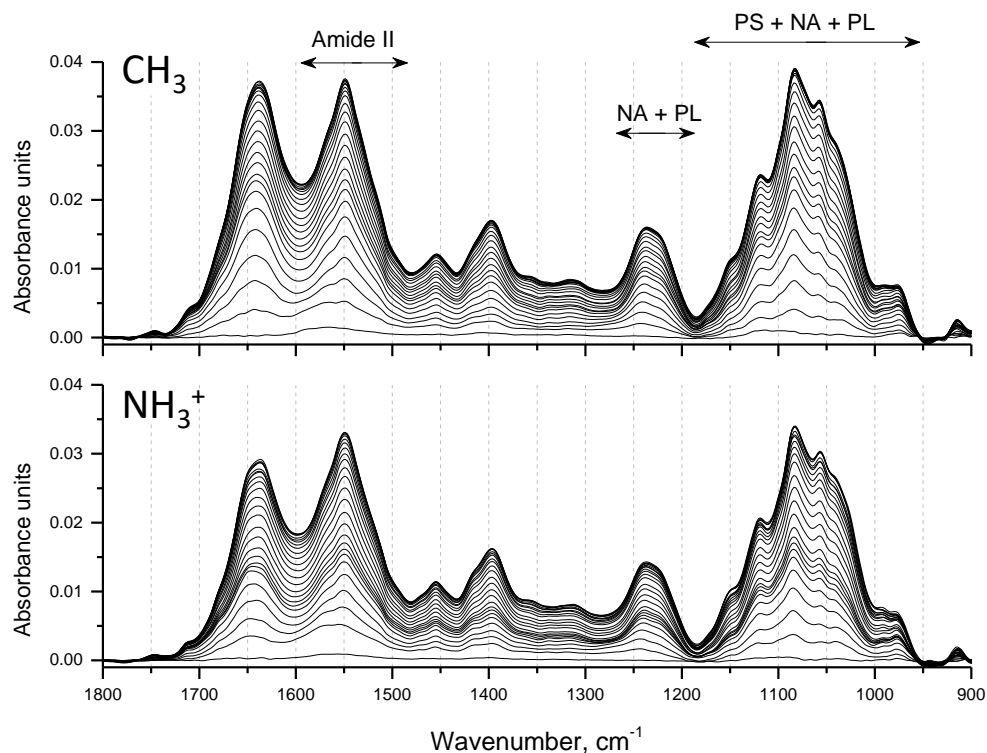
Figure 5.10. Evolution of ATR-FTIR spectra during 24 hours of LGG biofilm development in 10-fold diluted mTSB medium on CH$_3$- and NH$_3^+$-functionalised substrates, obtained at 1 hour interval. The reference spectrum is the spectrum obtained immediately after the nutritive medium had replaced bacteria suspended in physiological water preliminarily inoculated for 2.5 h hours. Bands used for the estimation of changes in the biochemical composition are marked: NA+PL = nucleic acids + phospholipids; PS = polysaccharides

The spectral features were very similar on both substrates, suggesting little impact of the substrate functionality on the biochemical composition of the LGG biofilm. At the same time, some differences in the kinetics of the growth of the bands intensities could be noticed depending on the substrate. The intensities of main bands marked in figure 5.10 were calculated for each spectrum and the results are shown in figure 5.11.
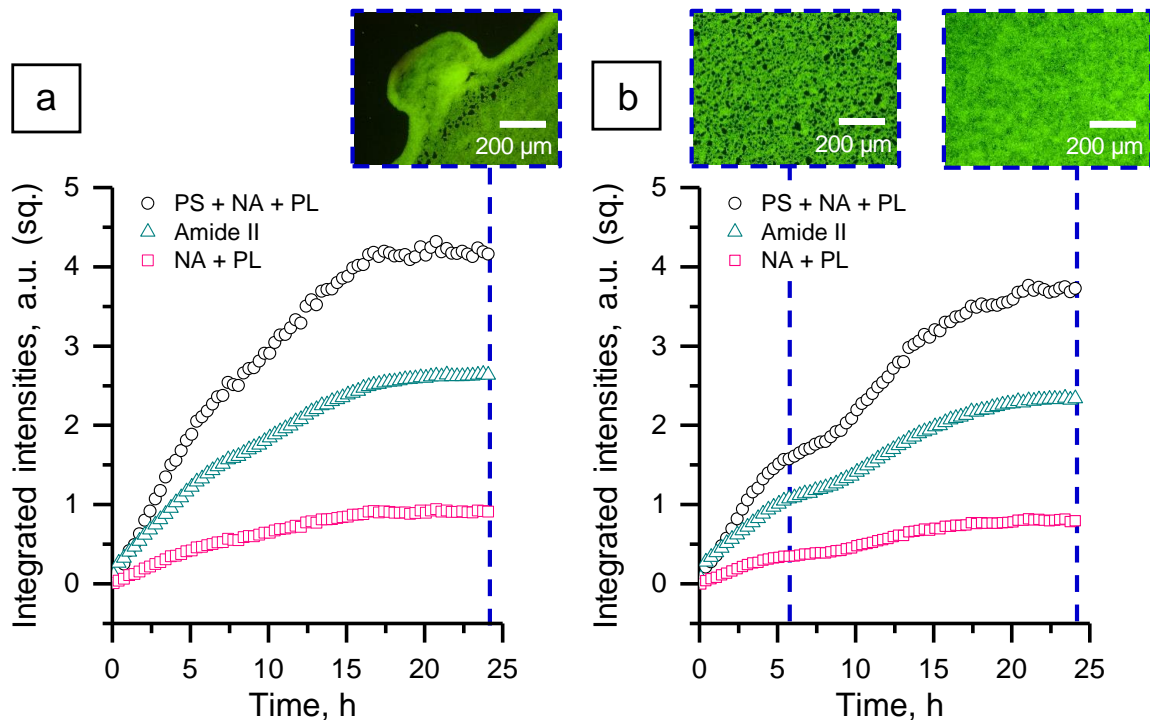
Figure 5.11. Evolution of integrated intensities of the ATR-FTIR bands corresponding to proteins, as derived from the amide II band region at 1592–1486 cm^{-1}, nucleic acids + phospholipids (NA + PL,1271–1188 cm^{-1}), and polysaccharides + nucleic acids + phospholipids (PS + NA + PL, 1189–956 cm^{-1}) during formation of LGG biofilm over 24 hours in mTSB/10 on CH$_3$- (a) and NH$_3^+$-functionalised (b) substrates after initial 2.5 hours of bacterial flow in physiological water

Indeed, the kinetics of the growth of infrared bands intensities were substrate-dependent. On the substrate with SAM-CH$_3$ (figure 5.11a), the integrated intensities of all studied band regions grew steadily until a plateau was reached after ~15 hours of incubation. On the substrate with SAM-NH$_3^+$, the kinetics of the growth of integrated intensities was, surprisingly, represented by a two-step process. The bands were growing with a similar rate compared to CH$_3$-functionalised substrate for the first 6 hours, after which the first plateau was reached. It was followed by the second stage of the prominent increase in infrared band intensities that was slowly declined in period from 15th till 24th hour of the incubation. It was hypothesised that such two-step kinetics can be explained by layer-by-layer fouling process, in such a way that the first layer of bacteria covered fully the substrate, provoking the first saturation of band intensities,

and then continued to grow upwards until the next plateau could be reached due to the limits of the depths of the analysis in ATR-FTIR spectroscopy. To verify this hypothesis, the epifluorescence images were made on the NH_3^+-functionalised substrate at times of incubation corresponding to the beginning of first plateau of the infrared signal (6 hours) and after 24 hours of the incubation (figure 5.11b). As can be seen, the surface after 6 hours of the incubation was not fully covered with bacterial cells (surface coverage 64 ± 15 %). Therefore, the hypothesis regarding the signal plateau reached as a result of full surface coverage by the first layer of bacteria was not confirmed by the epifluorescence images, and at present, the origin of two-step kinetics process remains unknown. Here, it is important to mention that the images were obtained after the removal of the crystal from the infrared cell and delicate rinsing. For an appropriate verification of this hypothesis, it would be advantageous to observe the fouling of the surface with LGG cells *in situ* using, for example, a microfluidic cell under optical microscope.

Interestingly, after 24 hours of the incubation of LGG cells the distribution of cells on the substrates functionalised with SAM-CH_3 and SAM-NH_3^+ was very different. On the CH_3-functionalised substrate the half of the crystal was covered fully with bacterial cells (coverage 97 ± 2 %), whereas the other half was completely empty (coverage 2 ± 2 %). The epifluorescence image in figure 5.11a shows the border between the half of the crystal fully covered with bacteria and the empty half. It was observed by the naked eye that the crystal surface was fully covered with bacteria after its removal from the infrared cell (bacteria formed a white film on the ATR crystal). However, during the rinsing step half of the crystal left without water due to low wetting properties of the hydrophobic crystal surface and water surface tension. It thus appeared that during this water reorganisation at the crystal surface, attached bacterial cells were lifted from the surface and moved following water towards the part of the crystal surface that was still covered with water (figure 5.12a). This behaviour at the three-contact interface between air, liquid and bacteria clearly demonstrates that the surface coverage, in this case, depends on a complex number of parameters that are defined by the rinsing step conditions. Indeed, the geometry of the sample, the volume of rinsing solution, the chosen procedure for rinsing (pipetting, dipping, etc.) and drying the sample (exposure to air, to gas flow, the use of absorbing paper, etc) may strongly impact on the resulting surface coverage with bacterial cells. Hence, the results on bacterial attachment from

aqueous suspensions on hydrophobic substrates should be analysed with great care towards these small details.

On the substrate functionalised with SAM-NH$_3^+$, the majority of the surface was densely covered with bacteria (surface coverage >90 %) (figure 5.11b and 5.12b). The distribution of bacteria was different as a function of the area analysed. Thicker biofilm was observed in the middle of the crystal surface and thinner one on the edges (figure 5.12b). This variation in the biofilm thickness could be associated with the gradient of forces as a function of the infrared cell geometry arising under flow conditions.
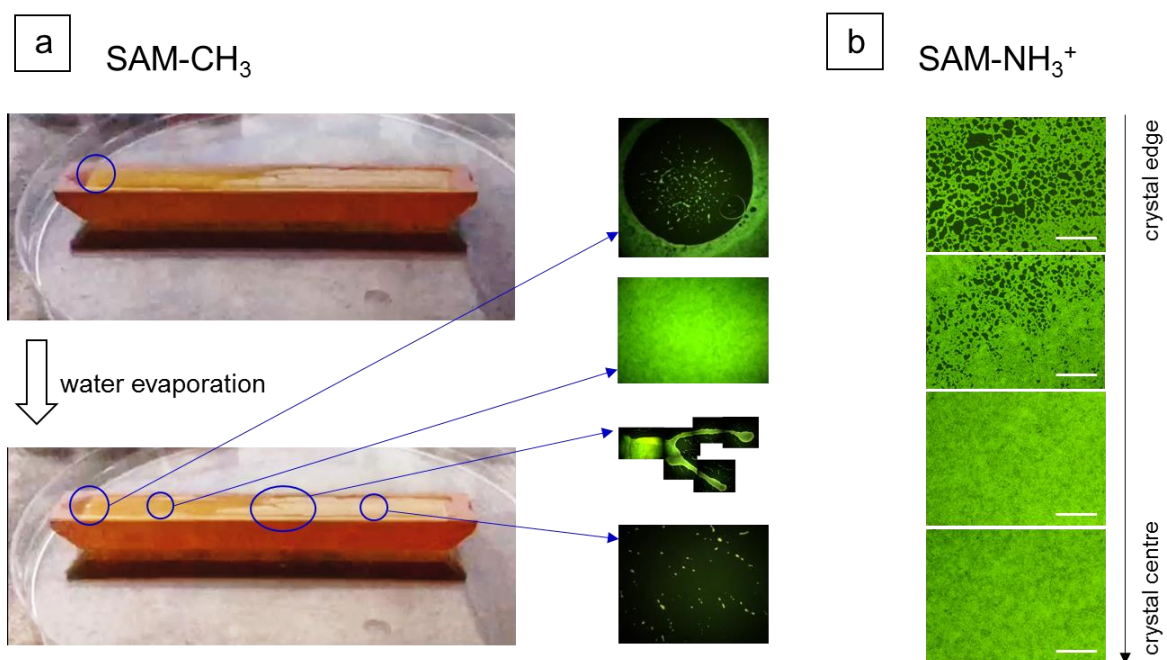
Figure 5.12. a) Functionalised with SAM-CH$_3$ ZnSe crystal after formation of LGG biofilm for 26.5 hours. The photos present the crystal surface after rinsing and staining with BacLight^{TM} and corresponding epifluorescence images that were reconstructed to present the features marked on the photos. Note the absence of the dry circle area before water evaporation, and its appearance after water evaporation, and the correspondence of the bacterial distribution in a circle alignment to this feature of water drying pattern. b) Examples of epifluorescence images of 26.5-hours-old LGG biofilm on functionalised with SAM-NH$_3^+$ ZnSe substrate, showing the difference in the density of the biofilm as a function of the place along the length of the crystal surface. Scale bar is 200 µm

Therefore, the combination of the results obtained using ATR-FTIR spectroscopy and epifluorescence microscopy demonstrated a strong implication of the substrate properties in the mechanical stability of LGG biofilm, even after long-term development.

5.2 Discussion

The substrates with well-defined surface chemistry are important for understanding the process of bacterial attachment and biofilm development, and their precise characterisation is necessary for deriving reliable correlation between surface properties and bacterial fate. In this study, we used ZnSe ATR crystals functionalised with three different alkanethiol molecules that possess either methyl, hydroxyl or amine functional groups. The results obtained with ATR-FTIR spectroscopy and high energy RBS revealed small differences between the SAM surface coverage depending on the terminal group of the alkanethiol molecule. Amino-terminated alkanethiols formed the densest SAMs, with the coverage of around 6.8 molecules/nm^2. This value is 1.5 fold higher than the one expected for the well-ordered SAM on the atomically flat gold surface (4.5 molecules/nm^2 [245]). As described in chapter IV, this difference may be a consequence of the high surface area of the relatively rough ZnSe substrate, and a possible bilayer formation (figure 1.10), which could partially be left at the surface after rinsing. Based on the RBS results, surface coverage of SAM-CH_3 and SAM-OH were found to be comparable (4.3 and 4.0 molecules/nm^2, respectively). Slightly higher values of the surface coverage for SAM-CH_3 and high density coverage with SAM-NH_2 were in accordance with the ATR-FTIR results showing lower number of conformational defects in these SAMs when compared with the SAM-OH. Herein, the low organisation of SAM-OH comparatively to SAM-CH_3 has been earlier demonstrated in the study of te Riet et al. on atomically flat gold surfaces [341]. As the authors suggested, the lower degree of packing in SAM-OH compared to SAM-CH_3, could be reasoned by the differences in the terminal group size. The definitive nature of the defects in SAM-OH seem not to be clear, but apparently, they can be expected regardless of the substrates nature, as they were previously observed on gold [341], gallium arsenide [304], and were found in this work on ZnSe.

The results of contact angle measurements evidenced differences in the surface energy as a function of the terminal group of alkanethiol molecules in SAMs. As expected, the lowest surface energy was found for the substrate functionalised with CH_3 groups, as it presents very low component for polar interactions. Herein, SAM-OH and SAM-NH_2 were characterised with similar values of the surface energy, as they both contain polar groups at the surface. The values of the surface energy are difficult

to compare with those reported in literature due to the differences in models used for the calculation and applied solvents [265]. Nonetheless, the values of water contact angles obtained in this work are in good agreement with the results of Noble-Luginbuhl and Nuzzo obtained for the SAM terminated with CH_3 group ($\approx 85°$ for the SAM with the same length of alkanethiol chain) [257]. For the SAM-NH_2, the values obtained here were somewhat higher than those expected from literature on SAMs formed on gold (~40–50° [332], [342], [343]). This can be attributed to the lower degree of ordering in SAMs obtained on ZnSe than on Au (as concluded from the results of ATR-FTIR measurements), and hence more methylene groups at the outmost surface of SAMs onto ZnSe leading to a lower hydrophilic character of the surface. For SAM-OH, the values usually reported are below 30° [332], [343]. Since SAM-OH obtained in the present study was with defects in the structure, it could result in the inclining of the alkanethiol chains and looser structure. The results of contact angle on SAM-OH corresponds well to the one reported by Berron and Jennings for loosely packed hydroxyl-terminated alkanethiol SAMs on gold ($\approx 68°$) [344]. However, in this case the results of RBS do not agree well with this conclusion, as the coverage was found to be comparatively close on SAM-CH_3 and SAM-OH. The higher values of water contact angles on SAM-OH (and those obtained on SAM-NH_2) could then be explained by the higher roughness of ZnSe with respect to, for example, gold-coated glass commonly used as a substrate in studies of SAMs, as aforementioned.

Does the substrate matter in the development of LGG biofilm?

Having a good vision of the surface properties, it can be reasonably questioned to what extent these differences between the substrates affect the fate of LGG cells in the process of biofilm development. The results obtained by multiple approaches in the present work put in evidence several important factors regarding the role of substrate functionality in LGG attachment and growth. It must be emphasized that further conclusions are valid for LGG biofilms cultivated under flow conditions in relatively highly concentrated suspensions, and thus if generalised, these arguments should be considered accordingly. Indeed, the effects of mass transport and sedimentation processes, dependent from both bacterial concentration and flow rate, will ultimately influence the adhesion of cells and biofilm properties.

- Substrate functionality plays moderate role in the kinetics of LGG attachment, but affects strongly the kinetics of biofilm growth

Based on ATR-FTIR results obtained in this work, it can be suggested that LGG tends to attach quicker on positively charged substrates, than on hydroxyl and hydrophobic ones. Overall, this result is in accordance with other works demonstrating faster adhesion rates of different bacterial species on SAMs terminated with amine groups [140], [206], [342]. The difference in rates found in the present study, however, was rather small. It has been claimed that bacterial cells attach preferentially to hydrophobic materials (materials with low surface energy) owing to a mismatch between their surface energy and a typically higher surface energy of liquids in which cells are suspended [345]. However, recently it was suggested that the surface energy alone is not a good predictor for bacterial attachment, as this process is governed by multiple mechanisms including the surface interaction of extending from cells appendages molecules and gene regulation [346]. In addition, besides actual forces between bacterial cells and solid support mediating the adhesion (Van der Waals, electrostatic, acid-base and hydrophobic interactions) one should consider other mechanisms as Brownian motion, sedimentation and hydrodynamic flow, also impacting the number of attached cells [197]. In the present study, within the similar time scale LGG was able to attach and grow on the surfaces regardless of their functional properties and measured surface energy. It therefore appears that under the chosen conditions the process of LGG attachment was little governed by thermodynamics, but rather by aforementioned hydrodynamic forces and sedimentation process.

It is important to note that LGG was able to grow on substrates regardless of their surface energy and functional properties, as demonstrated by the study of 24 hours growth on surfaces with SAM-CH_3 and SAM-NH_3^+. The kinetics of growth of the attached bacterial cells, however, was strongly affected by substrate properties. Thus, a slow-down in the growth of LGG on SAM-NH_3^+ was present, suggesting a two-stage kinetics on this substrate. In the same conditions, the growth on CH_3-functionalised substrate was continuous. Apparently, -NH_3^+ groups to some extent slow down the formation of LGG biofilm. The inhibiting effect of positively charged substrates towards biofilm formation by other bacteria was reported [216]–[218].

- Substrate has no or little impact on the biochemical composition of LGG biofilms and the membrane integrity of the cells

The difference in the kinetics of biofilm growth was not associated neither with strong changes in biochemical composition, within the limits of the ATR-FTIR sensitivity, nor it was due to the damage of the membrane of LGG cells. Based on the results of bacterial staining, LGG cell were intact after 26.5 hours of incubation on both CH_3- and, importantly, NH_3^+-functionalised surfaces. The membrane integrity of bacterial cells on positively charged substrates is put under risk due to possible ion exchange process [347] or strong electrostatic interactions with molecules that are essential for the survival of bacterial cells [348], leading to the disruption of the bacterial cell wall. The results of AFM force spectroscopy obtained in this work indeed showed that LGG has very strong interaction forces that occur at long rupture distances on NH_3^+-surface. Herein, the extended rupture lengths and multiple force peaks could be a result of stretching and unfolding of cell surface proteins, as suggested in the study of Beaussart et al. on *L. plantarum* [349]. However, these strong forces did not lead to the damage of LGG cell wall. It is possible that the membrane of the cell was not disrupted due to the presence of a thick peptidoglycan layer, in accordance with the hypothesis of Terada et al. [218] and Gottenbos et al. [219]. In addition, as the density of positive charges in SAM-NH_3^+ is expected to be lower on ZnSe than, for example, on gold (chapter IV), it may be below the threshold of charges required for a coating to possess biocidal properties [347].

- Substrate plays critical role in the retention of attached LGG cells

Based on earlier findings on *P. fluorescens* [336] and on *E. coli* [175], it was expected that high and similar infrared integrated intensities observed for LGG on all studied substrates would result in similar surface coverages with bacteria measured by epifluorescence microscopy. Therefore, it was surprising to see nearly empty substrates after 2.5-hours of LGG inoculation, when these substrates were functionalised with SAM-OH and Sam-CH_3 preliminarily to LGG flow. Based on repetitive observations of how LGG biofilm responds to the rinsing step, and use of multiple approach to study the strength of interaction between LGG and different functional groups, it is postulated that LGG do not retain on substrates with SAM-CH_3 and SAM-OH due to weak interaction and strong lifting forces arising at the interface

between bacteria, liquid and air during rinsing. Indeed, AFM force spectroscopy measurements revealed significantly weaker interactions of LGG with -CH$_3$ and even lower with –OH groups when compared to -NH$_3^+$ groups. Herein, higher adhesive forces at longer rupture distances between LGG and –CH$_3$ group with respect to –OH, can be due to unfolding and stretching of proteins that expose fresh hydrophobic groups for the interaction leading to the increase of the rupture distance, whereas single force peaks at low rupture distance when interacting with hydrophilic groups can be attributed to glycopolymer stretching, as suggested for *L. plantarum* [349].

The forces induced during washing/rinsing of a biofilm can reach up to 10^{-7} N and are perpendicularly oriented with respect to the substrate. This is a much larger force than hydrodynamic shear forces acting parallel to the substrate [198]. This phenomenon was well illustrated with the results of ATR-FTIR measurements that showed a drastic response of LGG attached cells to a continuous passage of nitrogen bubbles. Of note, this response was substrate dependent, in line with the nanoscale measurements of forces between LGG and functional groups using AFM probes. Thus, subjecting of LGG biofilm to an air-liquid interface creates a strong impulse for biofilm detachment. Similar observations of bacterial removal from surfaces as a result of contact with air-liquid interface were reported in the study of Gómez-Suárez et al. on the response of several bacterial species to an air bubble flow [204]. Of interest, as pointed by Frickmann et al. [69], the difference in counting of cells as a function of conditions/species involved in biofilm formation may lead to a confusion in the interpretation of the data as to what the observed effect should be attributed. That means the question – is the lower/higher number of recovered cells from the surface a function of lower/higher retention of the biofilm at washing before counting, or an actual decrease/increase of the number of cells in the biofilm? From the results of the present study, these effects seem to be of special concern when the support for biofilm formation is hydrophobic (figure 5.12). Considering that vast amount of biofilm studies are conducted on polystyrene microtitre plates (as listed with examples in table 1.1), which are hydrophobic substrates, the greatest attention must be paid when rinsing biofilms. The implication of this procedure in the obtained results should also be carefully analysed.

One may be wondering then why a biofilm retains well on the one substrate, but not on another one. As the results obtained in this study showed weak retention on SAM-CH$_3$ and SAM-OH, the terminal groups of these SAMs at the surface may be at the origin of repelling effects. Hydroxyl-terminated substrates are known for its ability to prevent bacterial attachment not only for bacterial cells, but also for proteins [198], [350]. This effects have been proposed to be associated with steric excluded volume effects and entropic and osmotic repulsion [351], as well as with the decrease of hydrophobic interactions due to an interfacial layer of water [352]. For hydrophobic substrates, on the one hand, it is claimed that they are more favourable for bacterial adhesion due to removal of water from the interphase of the interacting bacterial cell and a substrate enhancing the possibility of bridging [197]. On the other hand, the retention on hydrophobic substrates might be low, particularly on rough surfaces, due to trapped air in vicinity of the surface, which prevents its wetting and provokes easy rolling off of the water droplet and any particles residing in it. Although this phenomenon is considered to be valid more for surfaces with very high contact angles (superhydrophobic), as for example a surface of a lotus flower that have self-cleaning ability owing to the mechanisms described above [202], [203], it appears that similar effects may occur even on surfaces with lower contact angle, as it was observed on SAM-CH$_3$ in the present study (figure 5.12). Furthermore, this effect was observed not only after short attachment step, but also in a longer-term measurement (>24 hours) of LGG biofilm formation. This shows that bacterial cells did not succeed to develop strong interaction with CH$_3$-terminated substrate given longer times of incubation and changes in biofilm composition with respect to early attached cells (as it was presented in chapter III). It thus highlights the critical role of the interaction forces between the layer of bacteria adjacent to a surface in response of the whole biofilm to mechanical stress.

Conclusions

Multiple approaches were applied in this work to study the role of the substrate properties in the attachment of LGG cells, biofilm formation and its stability on the surface. It was shown that LGG attached and grew on the surfaces with different functional properties, but did not retain as equally on all studied substrates. In a global perspective, it means that the substrate does represent a crucial influencing factor for

LGG biofilm, until mechanical stress conditions are changed from those in which the biofilm was formed. The strongest interaction were observed between LGG and $-NH_3^+$ groups, which then resulted in formation of the dense biofilm with full surface coverage after 26.5 hours of incubation on thus functionalised substrates. LGG cells stayed intact on the amino-terminated surfaces in a long-term experiment, which allows further application of this substrate in the studies involving LGG biofilms.

VI. Behaviour of *E. coli* during incubation over LGG biofilm: an exclusion assay

As it was shown in chapter V, LGG cells form dense and stable biofilms on amino-terminated surfaces, in which the bacterial membrane is not damaged and cells are physiologically active. Hence, this substrate was chosen to test the antagonistic potential of LGG biofilms against *E. coli* adhesion and growth. The non-pathogenic strain *E. coli 2146* was chosen for the assays in this work. Albeit non-pathogenic, this strain is characteristic for its ability to overproduce type 1 fimbriae, which are the only appendages present on its cell wall. These fimbriae were reported as one of the virulence factors of *E. coli* [353]. This *E. coli* strain has thus appeared as a fairly good model micro-organism to have a first insight on possible antipathogenic action of LGG biofilms.

This chapter presents the preliminary results of the cultivation of biofilms of LGG and *E. coli* under flow conditions. Biofilms were formed in the infrared cell in the exclusion set up, which means that LGG biofilm was preformed during 26.5 hours preliminarily to the addition of the *E. coli* suspension and further incubation for 26.5 hours (as schematically presented in figure 2.16 of part 2.2.4). Biofilms were obtained under continuous nutrient supply. It was hypothesised that biofilms of LGG with full surface coverage would result in the most efficient prevention of *E. coli* adhesion. Therefore, mTSB/10 was used as the nutritive source during the cultivation of LGG biofilms, as it was shown to provide the most favourable conditions for obtaining dense biofilms (chapter III and chapter IV). However, it was also found that this medium exerted stress conditions on LGG cells due to poor nutritive quality, and it did not induce the significant biosynthesis of lactic acid. Herein, lactic acid was proposed as one of the main factors contributing directly or indirectly to antipathogenic activity of probiotic lactobacilli species [75], [96], [97]. Therefore, the possible influence of the nutritive medium on the antipathogenic effect of LGG was of interest to study. The use of MRS/10 for the LGG biofilm cultivation resulted in the observation of the highest amounts of the produced lactic acid among all tested nutritive media (chapter III). Besides, this medium contains the highest amount of glucose among three media studied in this work (annexe II).

Herein, it was reported that *E. coli* ability to form biofilm is inhibited by glucose when it is the sole source of carbon in a medium [273]. However, the ability of *E. coli* to form biofilms could also be influenced by LGG. Therefore, we studied the behaviour of *E. coli* cells during incubation over the established LGG biofilm in both media, i.e. MRS/10 and mTSB/10. In the first period when only LGG was inoculated, mTSB/10 was used to obtain dense biofilms, and in the second period of time when *E. coli* was added, the medium was either kept or changed for MRS/10 to induce the synthesis of lactic acid by LGG (as depicted in figure 2.16).

Results and discussion

6.1 Development of the biofilm of *E. coli* as single species or over preformed LGG biofilm in MRS/10

For estimation of the effect of MRS/10 medium on *E. coli* biofilm formation it was cultivated in under conditions that were used in chapter III and V to cultivate LGG (2.5.h of bacterial suspension flow followed by 24 h of growth under constant supply of the sterile nutritive medium at 50 mL/h). To follow the growth of *E. coli* biofilm *in situ* ATR-FTIR measurements were made. The ATR-FTIR spectra showed specific bands corresponding to the components of *E. coli* cells [273] (figure 6.2). However, the overall intensity of the bands was extremely small when *E. coli* cells were incubated in MRS/10 compared to those obtained in LB/10 medium [273]. This result suggests that this medium was not favourable for *E. coli* biofilm development, in accordance with earlier mentioned study on the inhibiting effect of glucose in the medium [273]. Interestingly, MRS/10 medium appeared to supress the growth of *E. coli* in a biofilm, but not the growth in the planktonic form (annexe VIII). It was shown that the glucose inhibiting effect against *E. coli* biofilm formation is associated specifically with its influence onto quorum sensing (QS) mechanism [354], [355]. As mentioned in part 1.1.2, QS is an important mechanism in biofilm formation, which coordinates gene expression in bacteria in accordance with their density and takes part in the regulation of virulence factors [37]. QS is regulated by specific molecules called autoinducers. The increased concentration of autoinducers in bacterial biofilms promotes the synthesis of a biofilm matrix, such as adhesion proteins and polysaccharides, which are required for the maintenance of the biofilm structure [356]. There are several categories of

autoinducer molecules, one important among which is so called autoinducer-2 (AI-2). It was reported that AI-2 control the formation of the biofilm by *E. coli* [354], [355]. Herein, Xavier and Bassler reported that glucose affects the amount of measurable AI-2 in *E. coli* [357]. Therefore, the low growth of *E. coli* biofilm in MRS/10 observed in our study is in accordance with these previously reported results.
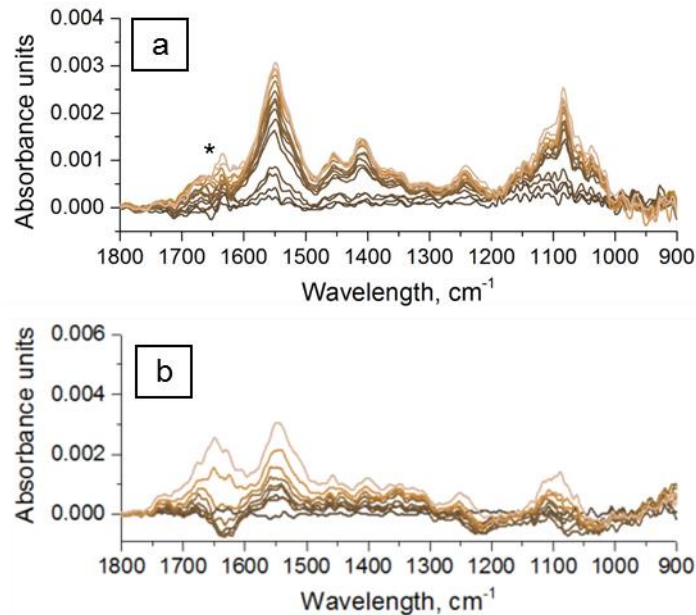
Figure 6.1. Time-evolution of ATR-FTIR spectra depicting the evolution of E. coli on -NH₃⁺ functionalised ZnSe in MRS/10: a) ATR-FTIR spectra recorded during the 2.5 hours flow of E. coli suspension; spectra showing the evolution from bottom to up every 10 minutes; the reference is the spectrum recorded immediately after filling in the cell with E. coli suspension. b) ATR-FTIR spectra during 24 hours of E. coli biofilm development from bottom to up every 3 hours. The reference the spectrum obtained immediately after the nutritive medium had replaced E. coli suspension after 2.5 hours flow. * indicates a bad compensation of δH₂O band.

Since the ability of *E. coli* to form biofilm might be influenced by LGG, the development of *E. coli* biofilm in MRS/10 medium was also studied in the exclusion assay with LGG. Figure 6.2 shows the ATR-FTIR spectra obtained during the incubation *of E. coli* in MRS/10 over the preformed 26.5-hours-old LGG biofilm. The spectra recorded during the first 2.5 hours (figure 6.2a), were difficult to interpret due to the mixture of appearing positive and negative bands. Nonetheless, the small increase of intensities of bands in the region at ~1160–1320 cm^{-1} and 1050–1150 cm^{-1} could be noticed. It is possible that these regions were growing mainly from the contribution of $\nu_a PO_2^-$ and $\nu_s PO_2^-$ groups. These groups are constituents of nucleic acids and phospholipids.
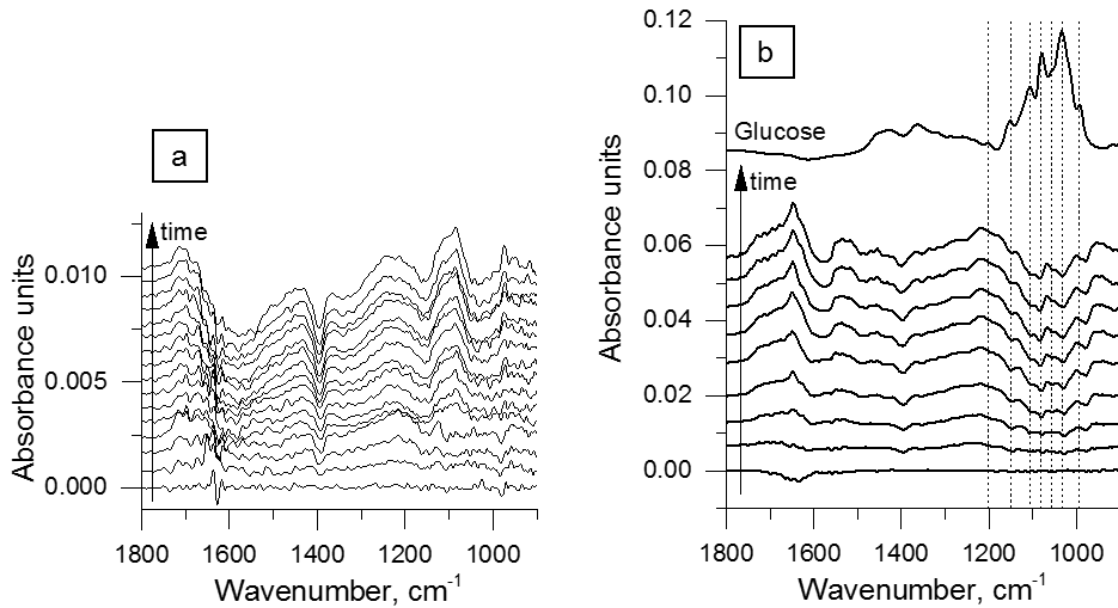
Figure 6.2. ATR-FTR spectra depicting E. coli development in MRS/10 over preliminary formed biofilm of LGG: a) flow of E. coli suspension over LGG biofilm; spectra every 10 min; b) flow of MRS/10 after removal of E. coli suspension, spectra every 3 hours, and the spectrum of glucose. The reference in a) is the spectrum obtained immediately after filling in the cell with E. coli suspension. The reference in b) is the spectrum obtained after the flow of E. coli suspension on the established LGG biofilm; The spectrum of glucose solution is referenced to water.

After removal of the *E. coli* suspension and continuation of the flow of MRS/10 medium several negative bands appeared progressively in the spectrum (figure 6.2b). It was interesting to notice that the bands in the region corresponding to carbohydrate molecules (950–1170 cm^{-1}) were mainly corresponding to the bands of glucose. It could then be suggested that LGG and/or *E. coli* bacterial cells consumed glucose from the nutritive medium, which have resulted in the negative peaks in the spectrum. Possibly, the starvation of LGG in mTSB/10 led to a rapid uptake of the sugars from MRS/10 once it had replaced mTSB/10 in the cell. In addition, it could be a result of the preferential consuming of glucose also by *E. coli*, as in many conditions it is the first sugar that *E. coli* utilises for growth [358]. Besides, *E. coli* grow much more rapidly in comparison with LGG. The hypothesis of the glucose utilisation by bacterial cells can be confirmed by the continuous small growth of bands assigned to bacterial fingerprints, such as amide I (~1648 cm^{-1}) and amide II (~1534 cm^{-1}), phospholipids (~1730 cm^{-1}, 1220 cm^{-1}) and nucleic acids (1220 cm^{-1}). However, an additional study is required to obtain the confirmation of these preliminary results and such possible interpretation.

To verify whether *E. coli* was growing on the biofilm of LGG, CFU of *E. coli* were counted after cultivation of *E. coli* biofilm over LGG in MRS/10. The results suggested that *E. coli* cells were absent in the biofilm or could not form colonies, as there were no countable colonies on the LB agar plates. This result was in accordance with very low intensities observed during ATR-FTIR monitoring (figure 6.2b). It means either *E. coli* did not attach and grow on LGG in MRS/10 or the growth was inhibited by the medium and/or LGG cells. Due to the difficulty of distinguishing between the effect of the medium and LGG onto *E. coli* biofilms and suppressing effect of MRS/10 on the ability of *E. coli* to form biofilms, we did not continue further study using this medium.

6.2 Development of the biofilm of *E. coli* as single species or over preformed LGG biofilm in mTSB/10

Similarly as described for MRS/10 (figure 6.1), the impact of mTSB/10 on the ability of *E. coli* to form biofilm was verified. Figure 6.3 shows the ATR-FTIR spectra recorded the period of E. coli suspension inoculation (a) and the period of the sterile mTSB/10 medium flow over attached *E. coli* cells (b). As it can be seen, the growth of bands during the period of the attachment of cells from the suspension and further growth of the biofilm was intense in mTSB/10. The bands were indicative for bacterial cell components, as previously described by Freudenthal et al. in the study of the same *E. coli* strain using ATR-FTIR spectroscopy [175]. The rapid growth of *E. coli* biofilm occurred in this medium, as it can be estimated from the evolution of amide II band integrated intensities (figure 6.3c).
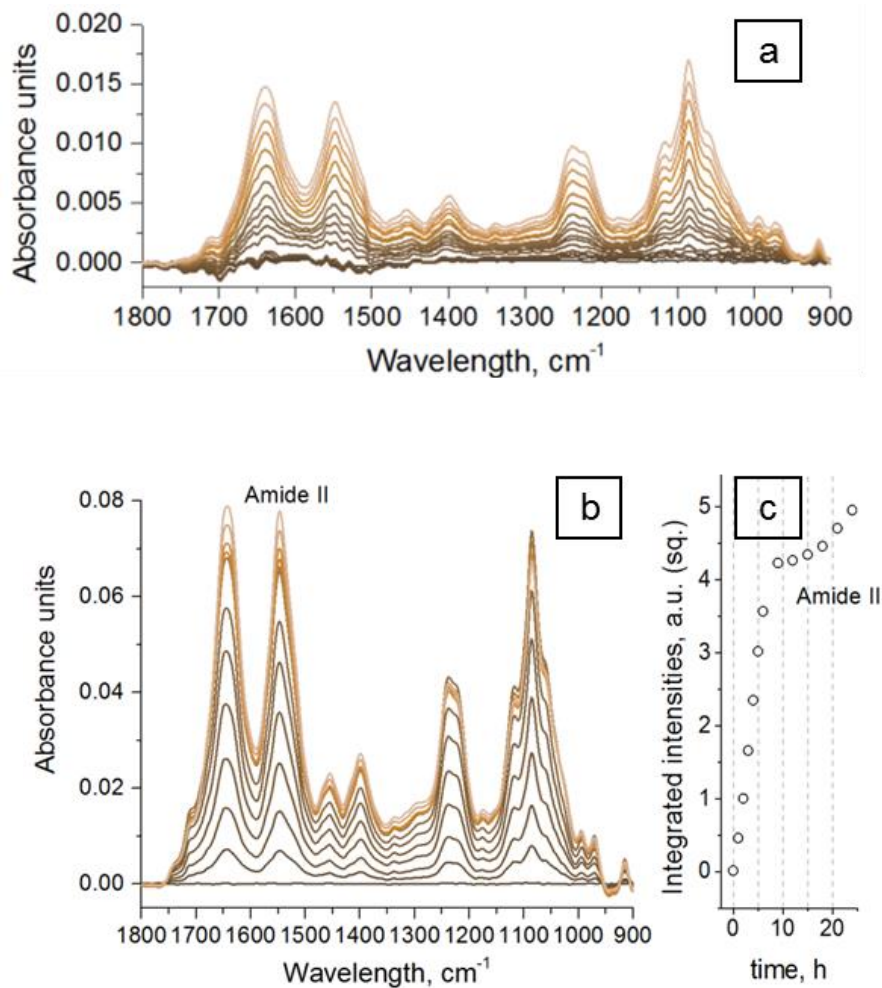
Figure 6.3. Time-evolution of ATR-FTIR spectra depicting the evolution of E. coli on NH$_3^+$-functionalised ZnSe in mTSB/10: a) ATR-FTIR spectra recorded during the flow of E. coli suspension for 2.5 hours; spectra showing the evolution from bottom to up every 10 minutes; the reference is the spectrum recorded immediately after filling in the cell with E. coli suspension. b) ATR-FTIR spectra during the flow of mTSB/10 for 24 hours showing the evolution from bottom to up at 0, 1, 2, 3, 4, 5, 6, 9, 12, 15, 18, 21, and 24 hours of the cultivation. The reference the spectrum obtained immediately after the nutritive medium had replaced E. coli suspension after 2.5 hours flow; c) evolution of the amide II band integrated intensities calculated from the spectra in b)

The biofilm of *E. coli* was cultivated in mTSB/10 medium on the preformed 26.5-hours-old LGG biofilm under the same conditions as those used for obtaining the spectra in figure 6.3. Figure 6.4 shows ATR-FTIR spectra obtained during the cultivation *of E. coli* in mTSB/10 over the preformed 26.5-hours-old LGG biofilm. In the first 2.5 hours, when the spectra were recorded during the flow of *E. coli* suspended in mTSB/10 over the established LGG biofilm, not many changes in the spectra occurred over time (figure 6.4a). This observation can either mean that *E. coli* did not adhere on the biofilm of LGG or that the adhesion took place beyond the depth of the penetration of the infrared beam. Conversely, the spectral features obtained after the flow of the *E. coli* suspension was exchanged to sterile mTSB/10 medium revealed the growth of the

bands assigned to bacterial components with much higher intensities than those observed in MRS/10 (figure 6.4b, 6.2b). It thus appeared that LGG and/or *E. coli* were growing within the 1-2 µm above the crystal surface. Herein, the features of the first spectrum in the series in figure 6.4b were similar to those observed earlier for *E. coli* (figure 6.3). To estimate the quantity of *E. coli* present in the biofilm, CFU were counted after the biofilm was scraped and dispersed for plating. Many colonies were seen on the plates where *E. coli* were grown after cultivation on LGG biofilm in mTSB/10 medium. The estimated concentration of *E. coli* cells on the biofilm of LGG was ~6×10^6 CFU/mL. Therefore, from the bands of the spectra in figure 6.4b that reflected the feature of *E. coli* cells and CFU values, it can be concluded that *E. coli* cells adhered on the LGG biofilm.
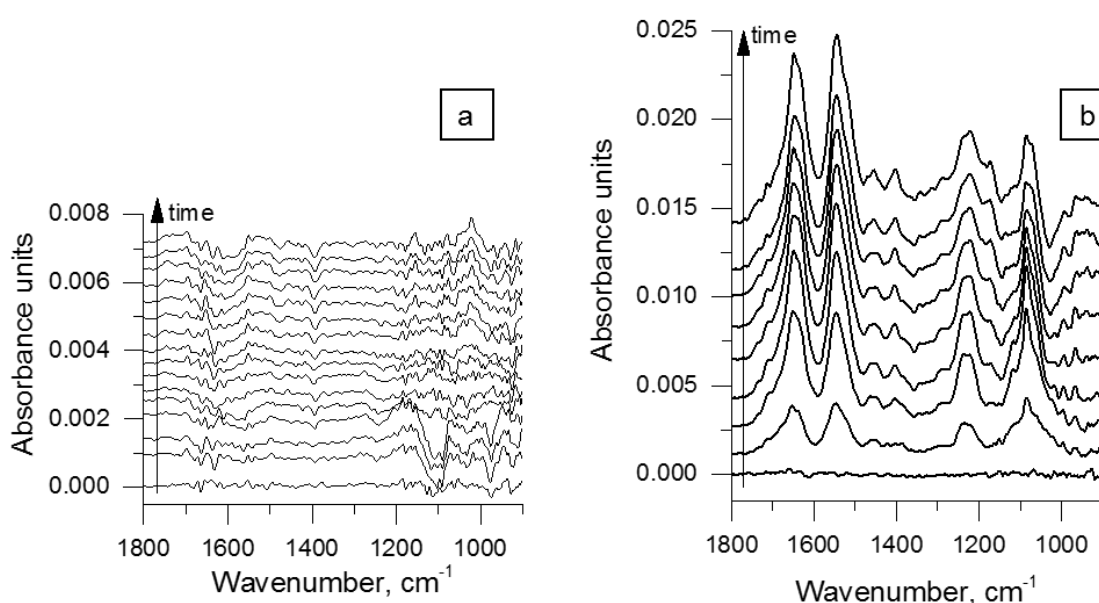
Figure 6.4. ATR-FTR spectra depicting E. coli development in mTSB/10 over preliminary formed biofilm of LGG: a) flow of E. coli suspension over LGG biofilm; spectra every 10 min; b) flow of mTSB/10 after removal of E. coli suspension, spectra every 3 hours. The reference in a) is the spectrum obtained immediately after filling in the cell with E. coli suspension. The reference in b) is the spectrum obtained after the flow of E. coli suspension on the established LGG biofilm

It must be noted that the signature from the region corresponding to polysaccharides, nucleic acids and phospholipids (950–1150 cm^{-1}) had an atypical evolution with characteristic narrowing of the area under the bands and the shift towards negative values especially pronounced around the band at 1030 cm^{-1}. These spectral features did not correspond to those commonly observed in LGG biofilms previously in this project, nor it was expected for the growing *E. coli* biofilm. In addition, the growth of bands at 1284 and 1174 cm^{-1} was observed over time, which were also not observed earlier neither during LGG nor *E. coli* biofilm development. This result could then be

explained by two hypothesises: the biochemical composition and metabolism of LGG/*E. coli* was changed under conditions of co-cultivation, and/or by the presence of both bacteria in the vicinity of the crystal surface resulting in the complex interfering infrared fingerprints.

6.3 Different approaches for the differentiation of LGG and *E. coli* in epifluorescence images

To observe LGG and *E. coli* cells in the obtained biofilm, the epifluorescence images of the biofilm, in which two species of bacteria could be distinguished, were necessary to obtain. We have conducted multiple experiments for optimising the conditions to stain LGG and *E. coli* differentially. The first approach that was attempted was based on the fluorescent in-situ hybridisation (FISH) protocol. FISH is a genetic technique that allows staining bacterial cells based on their DNA differences. As described in part 1.2.1, FISH is based on the molecular hybridization between the target DNA or RNA sequences and artificially constructed and fluorescently-labelled probe matching the sequence under question. We have adapted the protocol for FISH analysis from the study of Lebeer et al. [109], and carried successful trials on the staining of LGG and *E. coli* cells in conditions where the cells were present as single species (figure 6.5). Herein, FISH was used to stain *E. coli* expressing *gfp* due to the fact that *E. coli* cells were damaged under conditions of FISH used to stain LGG, and *gfp* was not visible enough anymore. We encountered difficulties in the staining simultaneously both strains with FISH protocol when they were co-cultivated in biofilms, and due to the complexity and time-consumption of this protocol, we did not go further in the elaboration of this method.
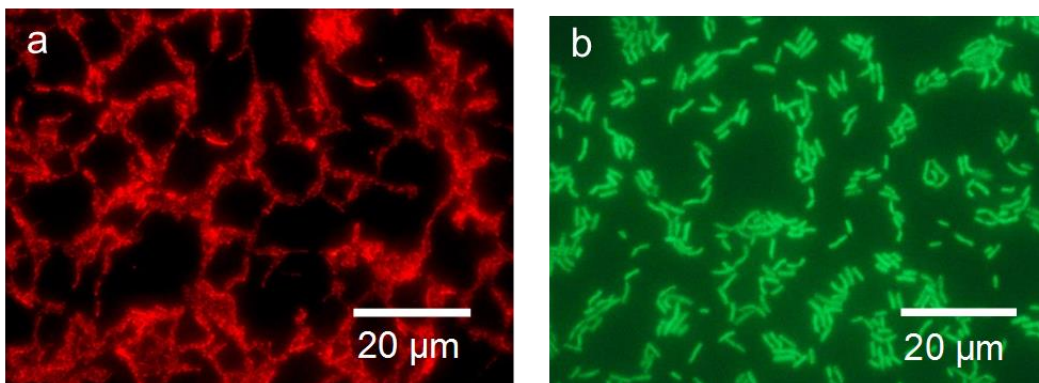
Figure 6.5. Epifluorescence images of LGG (a) and E. coli (b) stained with oligonucleotide probes conjugated with Cy3 and AlexaFluor488 dyes, respectively

Less specific but more simple to handle, two approaches to differentiate bacteria based on their Gram-status were tested. The first one is based on the affinity of wheat germ agglutinin (WGA) to N-acetylglucosamine in the peptidoglycan layer of the cell wall. It was reported that due to the fact that Gram-negative bacteria, unlike Gram-positive ones, have a layer of lipopolysaccharide covering the cell wall, they are not stained with the dye-conjugated WGA [359]. However, the trials performed in our study have shown that WGA (conjugated with the dye Alexa 594) stained both LGG and *E. coli* cells. We then proceeded to another approach also based on the Gram-status differentiation, i.e. utilisation of hexidium iodide and Syto group dyes. It was reported that while Syto group dyes (Syto 9, Syto 24, Syto 12, etc.) stain all bacterial cells, hexidium iodide stains preferentially only gram-positive cells [360]–[362]. Nonetheless despite trying several experimental conditions (varying the time of exposing and the concentration of dyes), in the present work it was not possible to differentiate LGG and *E. coli* using these dyes, as hexidium iodide also stained *E. coli* cells.

6.4 Evolution of *E. coli* biofilm on the biofilm made of LGG expressing fluorescent protein

Following the unsuccessful trials of differential staining of LGG and *E. coli* in the biofilm, the group of Prof. S. Lebeer (University of Antwerp, Belgium) kindly provided their recently developed strain of LGG that expresses protein mTagBFP2 (excitation peak at 399 nm and an emission peak at 454 nm) [94]. This strain hereafter referred as LGG mTag. LGG mTag and *E. coli* could therefore be distinguished in the biofilm based on the differences of the emission region of mTAGBFP2 protein expressed by LGG mTag and *gfp* expressed by *E. coli* without an additional dye staining.

The biofilm of LGG mTag and *E. coli* were then cultivated under conditions identical to the biofilms described in paragraph 6.2, in mTSB/10 medium. As shown in figure 6.6, first 2.5 hours of *E. coli* suspension flow over preliminarily established LGG mTag biofilm did not reflect changes within the depth of penetration of the infrared beam. Perhaps, only slight beginning of the growth of amide I (~1640 cm^{-1}) and amide II (~1540 cm^{-1}) bands can be noticed by the end of 2.5 hours. This results is in accordance with the previously observed spectra in figure 6.4.
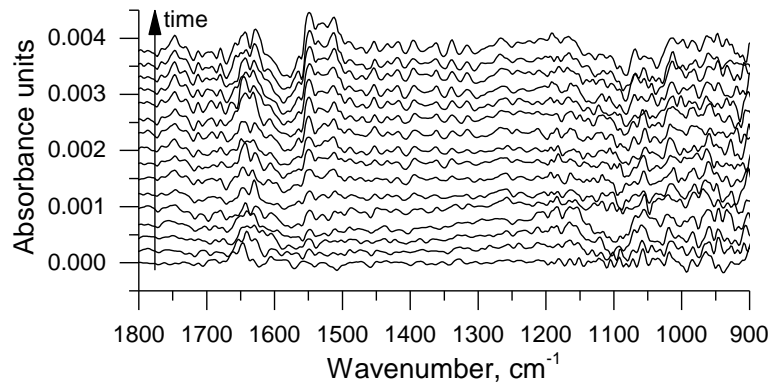
Figure 6.6. ATR-FTIR spectra (offsets) recorded during the flow of E. coli suspended in mTSB/10 over preliminarily formed LGG mTag biofilm, spectra every 10 min. The reference is the spectrum obtained immediately after filling in the cell with E. coli suspension

Afterwards, the suspension of *E. coli* was replaced by the flow of sterile mTSB/10 for additional 24 hours. The spectra recorded during this period are shown in figure 6.7a. They showed similar bands with respect to those that were in the spectra presented in figure 6.7b. To further interpret these spectra, we compared them with those obtained for 26.5-hours-old biofilms of LGG mTag and *E. coli* in single species biofilm (figure 6.7c,d, conditions presented in figure 2.16). It was found by comparing these spectra with those presented in figure 6.7a that the spectra in figure 6.7a did not reflect clearly neither the features of LGG mTag nor *E. coli*. It therefore meant that, as in the case with the spectra in figure 6.7, the spectra in figure 6.7a reflected the changes in the biochmecial composition of the bacterial cells, and/or were showing mixed fingerprints of the cells, where the bands were interfering. To analyse the contribution of the LGG mTag and *E. coli* into the spectra in figure 6.7a, it was tried to sum and subtract the spectra of single species (figure 6.7c,d) to fit the spectral fingerprints in figure 6.7a. It was very interesting to notice that the bands at ~1294 and 1177 cm^{-1} growing in the series of spectra in figure 6.7a matched the bands around same wavenumbers in the spectrum obtained as a result of subtraction of LGG mTag spectrum (figure 6.7d) from the spectrum of *E. coli* (figure 6.7c), as shown in figure 6.7b. In addition the spectra in figure 6.7a and 6.7b were similar in a way that the shoulder around 1060 cm^{-1} was smoothed, unlike in the spectra of single species biofilms (figure 6.7c,d). These observations therefore pointed on the increase of *E. coli* cells in the vicinity of ZnSe surface, which were probably partially replacing LGG mTag. Indeed, it is suggested from these results that *E. coli* cells penetrated LGG mTag biofilm, and slowly entered into the depth of the analysis of the infrared beam, as such

explaining the lack of bands in the spectra recorded in the beginning of *E. coli* suspension flow (figure 6.6 and 6.4a) and their appearance afterwards.
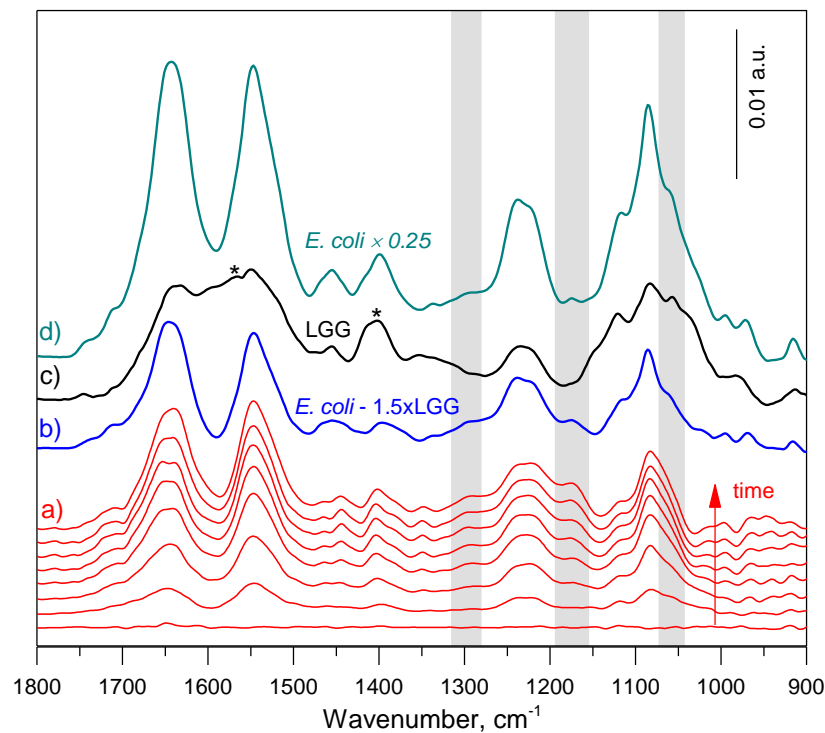
*Figure 6.7. Evolution of E. coli biofilm on the preliminary established biofilm of LGG mTag: a) ATR-FTIR spectra obtained after replacement of E. coli suspension to a flow of mTSB/10 over the cells of E. coli and LGG mTag adhered in preliminary steps of cultivation, spectra every 3 hours; The reference in a) is the spectrum obtained after the flow of E. coli suspension on the established LGG mTag biofilm b)Subtraction spectrum of 26.5h-old E. coli biofilm obtained in mTSB/10 (depicted in c) and 26.5h-old LGG mTag biofilm obtained in mTSB/10 (depicted in d). * indicates contribution of mTSB/10 medium in the spectrum of LGG mTag presumably due to the high thickness of the biofilm. The regions in grey mark the key features for comparison of the spectra.*

The epifluorescence images showed that *E. coli* cells and LGG were both present in the biofilm (figure 6.8a). *E. coli* could be observed in depth of the LGG biofilm by changing the focus of the observation under the microscope. The obtained biofilm was thick, and the observation using confocal epifluorescence microscope would be advantageous. Additionally, it can be noticed that the number of *E. coli* cells was directly correlated with the number of LGG mTag cells (figure 6.8b). Therefore, it was probable that LGG mTag and *E. coli* cells co-aggregated in the biofilm. This result can be explained by the presence of fimbriae type 1 on the cell wall of *E. coli* strain used here, and mannose on the cell wall of LGG cells [284]. Fimbriae type 1 are known for their affinity to mannose residues [194]. This hypothesis would be interesting to verify in the future work, for example using α-Methyl-D-mannoside, which blocks the

mannose-sensitive adhesive sites on the fimbriae type 1 resulting in the reduction of the adhesion (co-aggregation) if it is governed by mannose-fimbriae interactions.
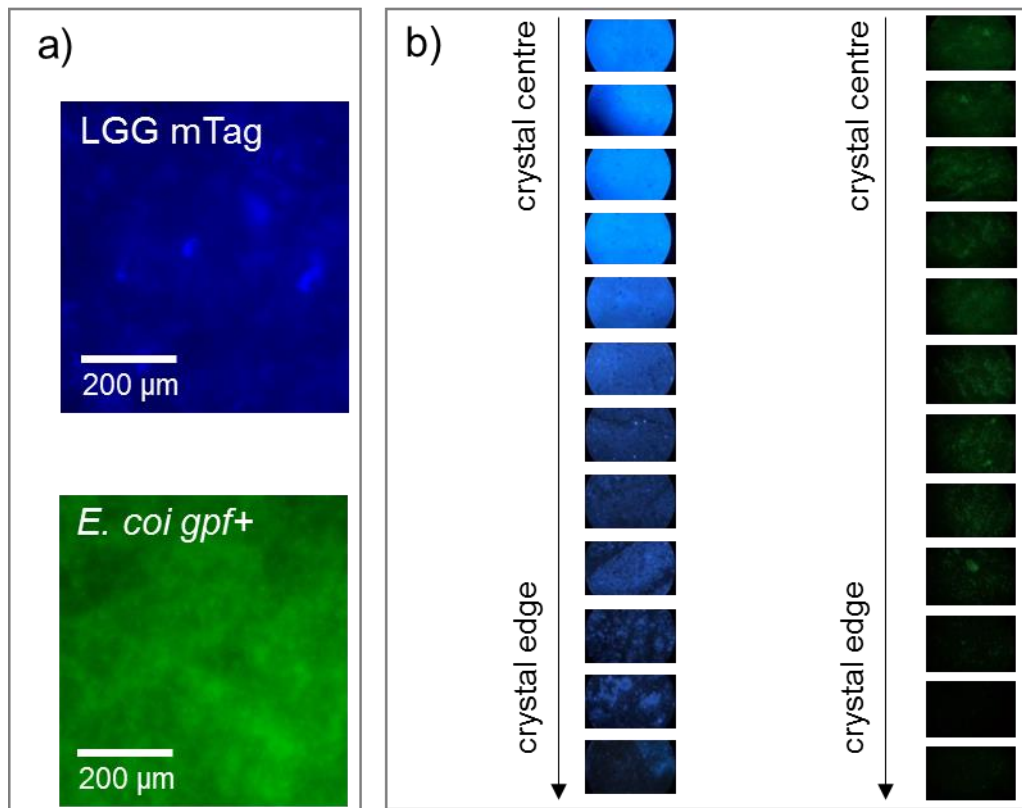
Figure 6.8. a) Epifluorescence images obtained at the same spot on the surface with the filter for LGG mTag and the filter for E. coli. b) Eye view of the surface under the microscope, depicting direct correlation between number of LGG mTag and E. coli in the biofilm. The brightness of the photos was intentionally not changed to reflect the differences in the quantities between LGG and E. coli.

This first assay did not evidence an antagonistic effect of LGG against the *E. coli* strain chosen as a model under conditions used here. It has been shown that this property is strain dependent. For example, LGG did not inhibit the growth of Staphylococci species in the study of Frickmann et al. [69]. Lectin-like proteins isolated from LGG did not have the inhibiting influence on the growth of *S. aureus*, *E. coli* K12, and *P. auroginosa*, but had strong antagonistic action against *Salmonella spp.* and *E. coli* uropathogenic strain [81]. *E. coli* 2146 strain used in this work is genetically modified from *E. coli* K12. It can then be suggested that LGG did not impact this strain, similarly to as it did not impact *E. coli* K12 strain in the study of Petrova et al., but may potentially impact other strains of *E. coli* or other pathogenic species. Moreover, the absence of the impact on the adhesion and growth of *E. coli* does not necessarily indicate the absence of the LGG antipathogenic effect. Indeed, in the study of Park et al. it was shown that *Lactobacillus sakei* did not inhibit the viability of the pathogenic *E. coli* O157:H7 strain,

although it reduced its pathogenicity via inhibition of AI-2 molecules [66]. Therefore, the possible implication of LGG biofilms in the virulence of pathogenic bacteria requires further in-depth analysis.

VII. General conclusions

The objective of this work was to study in situ the development and the possible control of bacterial biofilms by probiotic *Lactobacillus rhamnosus* GG on surfaces with controlled physico-chemical properties. The advantage to control the properties of probiotic biofilms is associated with the strategy to utilise biofilms of non-pathogenic bacterial species as a bio-based method to preserve surfaces from the contamination with unwanted microorganisms. Therefore, the development of surfaces with properties favourable for LGG growth, and the understanding the interactions between LGG and the surface is of great interest, and was in the focus of this project.

Our approach was based on the *in-situ* monitoring of the response of LGG cells to different environments, such as different nutritive media or substrates with various surface properties using infrared spectroscopy. Herein, major attention was paid to the properties of the substrate, as they have influence on the critically important step in biofilm formation process, i.e. bacterial adhesion. Compatible with infrared spectroscopy measurements, a ZnSe ATR crystal was used as a substrate for biofilm formation. Its functional properties were tuned using the self-assembly reaction with alkanethiol SAMs terminated by $-CH_3$, $-OH$, or $-NH_2$ groups on bare ZnSe or ZnSe coated with gold for obtaining substrates with different surface energy and charge. To study the changes in surface functional properties as well as to study the properties of ZnSe surface lying underneath the SAMs, a combination of several techniques including AFM, ATR-FTIR, contact angle measurements, XPS, and high energy RBS, were applied. The substrates with well-defined surface properties were then used to monitor the adhesion and the biofilm growth of LGG using ATR-FTIR measurements. In addition, epifluorescence images of the biofilms were obtained at early and more mature stages of the biofilm development to analyse the physiological properties of bacterial cells under different environmental conditions.

As bacterial cells are living objects, their fate strongly depends on the availability and quality of nutrients. Different type of nutrients consumed by bacteria lead to different composition of cells as such affecting their physiological properties and possible antipathogenic action. Therefore, the first part of this project was aimed at investigating the influence of three nutritive media on the process of biofilm development by LGG.

Two of these media are recommended for the cultivation of *lactobacilli* (MRS, AOAC), and a third medium supports the growth of many types of bacterial strains (mTSB). Spectroscopic fingerprints recorded during LGG biofilm formation revealed a medium-dependent content of nucleic acids, phospholipids and polysaccharides in LGG biofilms. In addition, time-dependent synthesis of lactic acid was observed in MRS/10 and AOAC/10. Polysaccharides were produced to the highest extent in mTSB/10, and the biofilms obtained were the densest in this medium. Strong changes in the shape of bacteria were observed due to acidic or nutrient stress in AOAC/10 and mTSB/10, respectively. Despite the conditions of poor nutritive quality, mTSB medium was chosen in the following for the cultivation of LGG biofilms as this medium provided conditions for the highest substrate coverage with bacterial cells.

Having established the role of the medium in the growth of LGG on ZnSe, we switched the attention towards the role of the substrate in this process. As the strategy included thiol-based functionalisation chemistry, we studied how the substrate properties affected the organisation of SAM and yield and reproducibility of the self-assembly reaction. The important implication of the surface cleaning process prior to both the alkanethiol self-assembly process and the adhesion of LGG was shown. The results obtained in this part of the study allowed us also to conclude that SAMs were more ordered and dense on the gold-coated ZnSe than on ZnSe without gold nanofilm. This difference in SAM properties, however, did not show strong influence on the behaviour of LGG, which was similar on bare ZnSe and Au/ZnSe regardless of the efficiency of thiol self-assembly. The next experiments were then carried out only using ZnSe, i.e. without performing gold deposition.

The effect of the substrate functional properties on the biochemical composition and the strength of attachment of LGG biofilms was addressed further in the work. It was shown that LGG attached and grew on the surfaces with different functional properties, but did not retain equally on all studied substrates. The strongest interaction were observed between LGG and $-NH_3^+$ groups, which then resulted in formation of a dense biofilm with full surface coverage after incubation for 26.5 hours. Notably, the membrane of LGG cells stayed intact despite strong electrostatic interaction observed on the latter substrate. In perspective, other molecules baring positive charges are interesting to study in order to expand the application of LGG biofilms, as for example

it was recently demonstrated with a cationic dextran derivative used to attach LGG cells on gold electrodes[328]. The understanding of the bacterial development on the surface can be further advanced using SAMs associated from molecules with different functional groups, as it would allow to vary surface energy of the substrate. Moreover, these functional groups can be used to graft other, more complex molecules, such as proteins (mucin, β-lactoglobulin) for understanding the interaction of LGG with biological tissues or food matrices. In addition, using surface functionalisation with thiols one can obtain patterned surfaces, on which it would be interesting to study bacterial adhesion for elucidating the biofilm response and cell-cell interactions with respect to surfaces constraints. It should also be mentioned that the treatment of surfaces by physical methods presents a convenient complementary step to chemical functionalisation procedure, as for example the activation of surfaces by plasma [363].

The final step in this project was dedicated to estimating the potential of LGG to prevent the growth of pathogenic biofilms using as a model a genetically modified strain of *E. coli*. Several attempts were performed to differentiate bacteria in the epifluorescence images, which unfortunately, did not lead to success. A LGG strain genetically modified to express a fluorescent protein, was then used in this part of the project. Interestingly, it was found that the nutritive medium itself had possibly a strong impact on the ability of *E. coli* to develop a biofilm on a pre-formed LGG biofilm. This observation illustrates the importance of the proper choice of the medium in bacterial interference assays. The difficulty to choose a medium supporting the growth of bacteria belonging to different genera were earlier addressed [282], suggesting that selected components can be added in the standard nutritive media to facilitate the growth of bacteria. This approach can be used in future works. Furthermore, ATR-FTIR spectroscopy combined with epifluorescence microscopy have proven to be a powerful approach to follow the dynamics of changes in mixed LGG and *E. coli* biofilms. The results obtained revealed a penetration of *E. coli* in the LGG biofilm, suggesting more complex mechanisms of LGG antipathogenic action, than a simple prevention of the adhesion. These findings point on the interesting interplay between bacterial cells that deserves additional study, despite being out of the concept of this work. The effect of LGG biofilms on other microorganisms should be also interesting to check. Besides, since probiotics are an important part of the human microbiome and many industrial formulations are currently being developed, it could be relevant to conduct the study in

the inverse set up when the effect of pathogenic species on the properties of the probiotic bacteria are explored.

Biofilms have a very complex nature, which makes it challenging, yet extremely interesting to study. As living systems, they can be analysed from different perspectives covering multiple physical and chemical phenomena of biotic and abiotic origins. The life cycle of a biofilm is governed by various biological processes and chemical reactions occurring both in cells and surrounding matrix. Furthermore, as being closely linked with each other, bacterial cells in biofilms represent a micron-to-millimetre scale object that is subjected to the influence of physical phenomena describing soft matter. Adhesive and lifting forces exerted on the biofilm under mechanical stresses, and viscoelasticity of the biofilm lie within this field of research competence. It is, finally, evident that without knowing the properties of substrates on which biofilms develop, the full picture of these systems will not be drawn. Biofilms therefore represent a great exploration area, the understanding of which demands the cooperation between microbiologists, chemists, physicists and material scientists, and fascinating perspectives of its research lie across the borders between these scientific domains.

Annexes

AI. ATR-FTIR spectrum of ethanol vapour
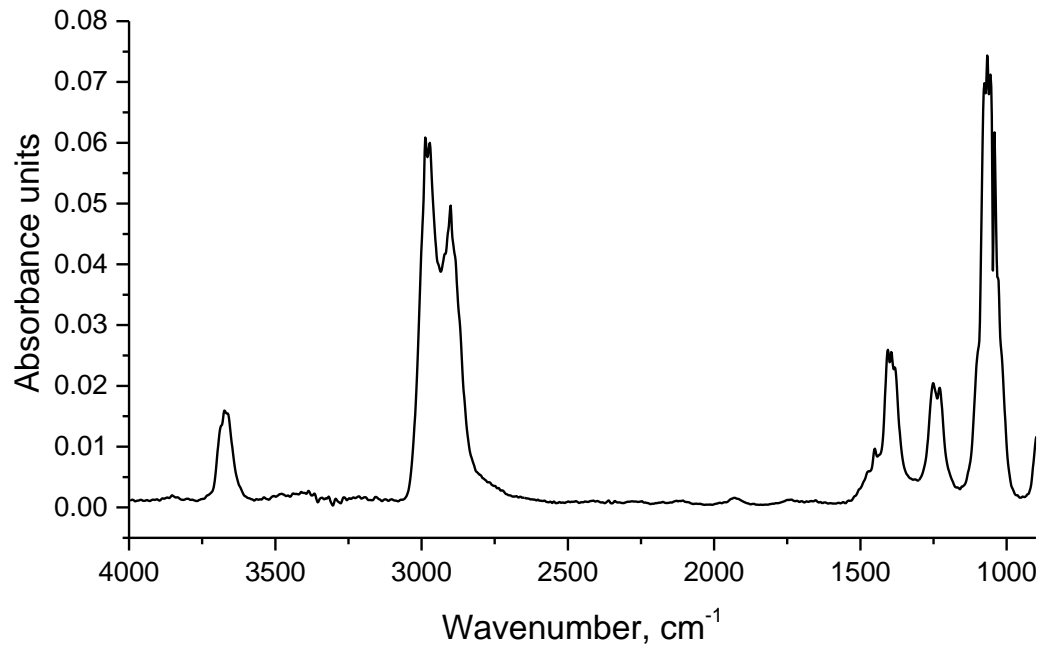
Figure A1. ATR-FTIR spectrum of ethanol vapour

AII. Composition of the nutritive media

Table A1. Composition of the nutritive media used in this work, g/L

MRS medium:	AOAC medium:	Modified TSB:	LB :
proteose peptone no. 3 – 10 beef extract – 10 yeast extract – 5 dextrose – 20 Polysorbate 80 – 1 ammonium citrate – 2 sodium acetate – 5 magnesium sulfate – 0.1 manganese sulfate – 0.05 dipotassium phosphate – 2	peptonized milk – 15 yeast extract – 5 dextrose – 10 tomato juice – 5 monopotassium phosphate – 2 Tween 80 – 1	pancreatic digest of casein – 17 enzymatic digest of soybean meal – 3 sodium chloride – 5 dipotassium phosphate – 2.5 dextrose – 2.5 Bacto proteose peptone no. 3 – 20	tryptone – 10 NaCl – 10 yeast extract – 5

AIII. Growth curves of LGG and *E. coli*
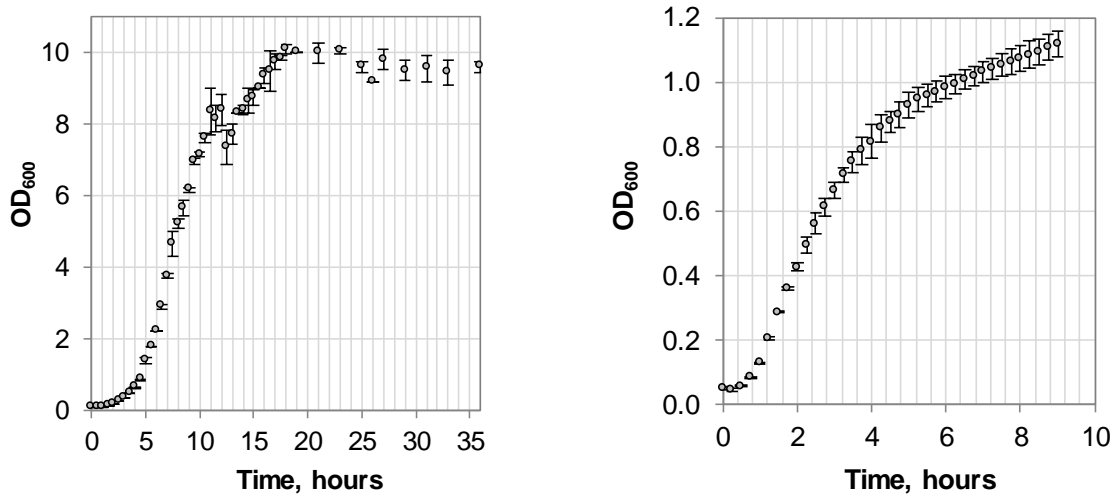
Figure A2. Growth curves of LGG (left) and E. coli (right) obtained in MRS and LB, respectively

AIV. ATR-FTIR spectra of lactic acid in water at different pH
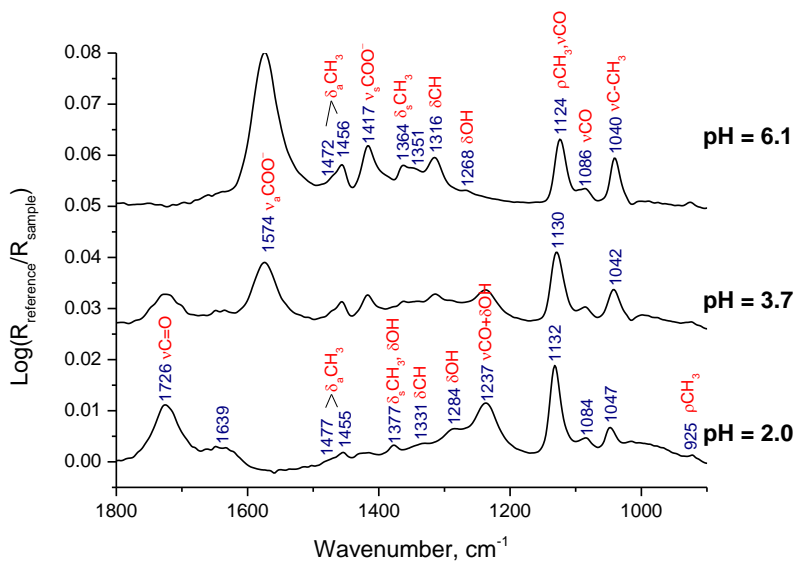
Figure A3. ATR-FTIR spectra of 0.1 M aqueous solution of sodium L-lactate recorded at pH equal to 2.0, 3.7 (pKa), and 6.1. Assignments were made in accordance with Cassanas et al. [278]

AV. RBS results on the thickness of gold coating
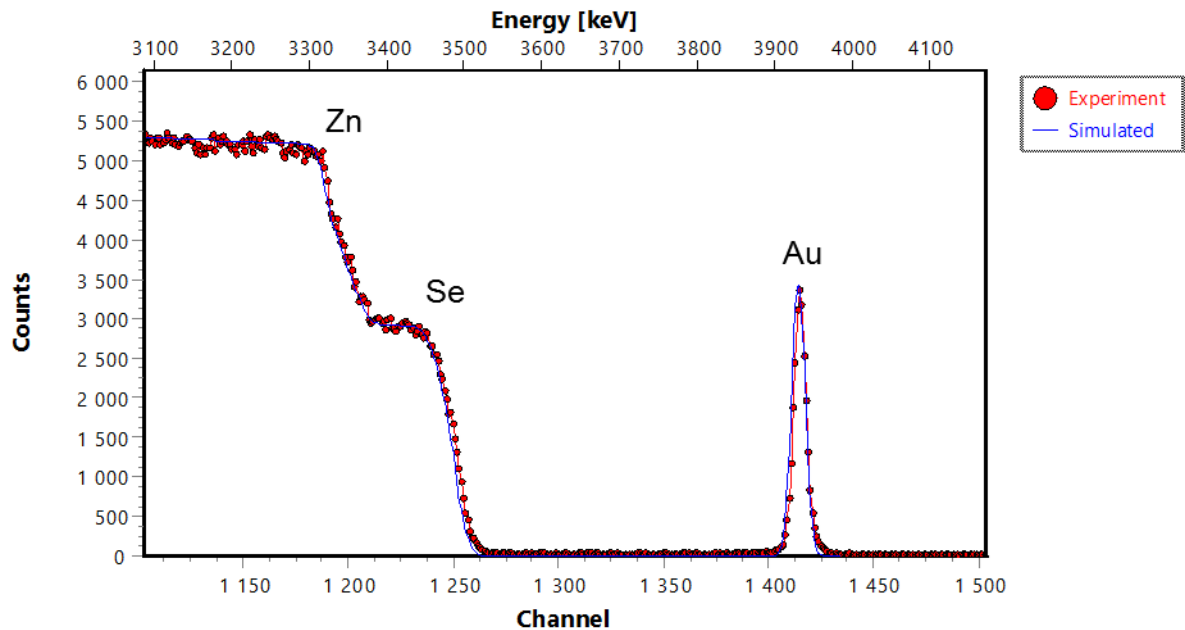
Figure A4. Rutherford backscattering spectrum showing experimental and simulated curves for the yield of Zn, Se and Au counts on Au-coated ZnSe. The area of the peak corresponds to the areal density of the material (atoms/cm^2), which can be recalculated into the thickness given the density is known. The thickness of gold is ~2.3 nm.

AVI. Schemes of cell walls of Gram-positive and Gram-negative bacteria
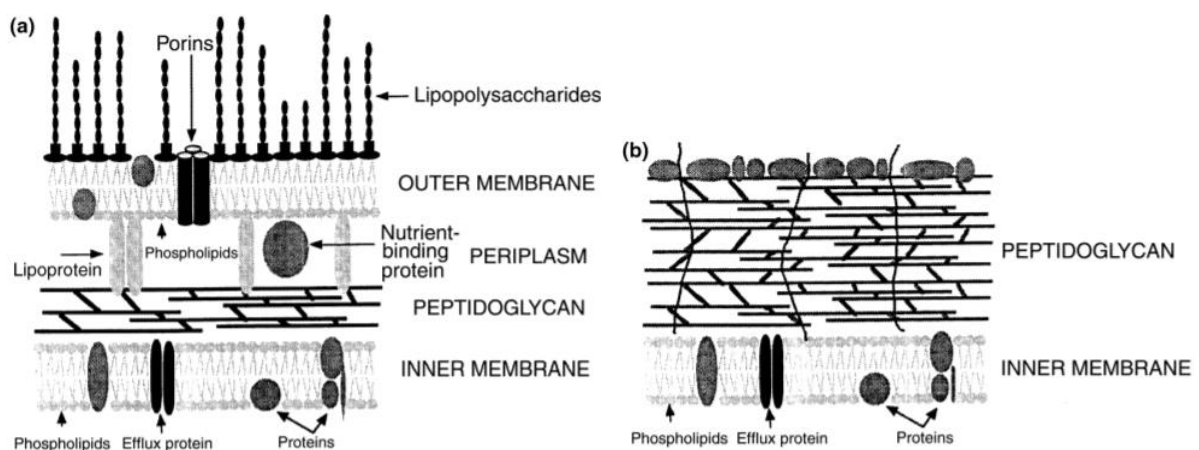
Figure A5. Schemes of the cell wall of Gram-negtaive (a) and Gram-positive (b) bacteria [329]

AVII. Time-evolution of ethanol bands in ATR-FTIR spectra
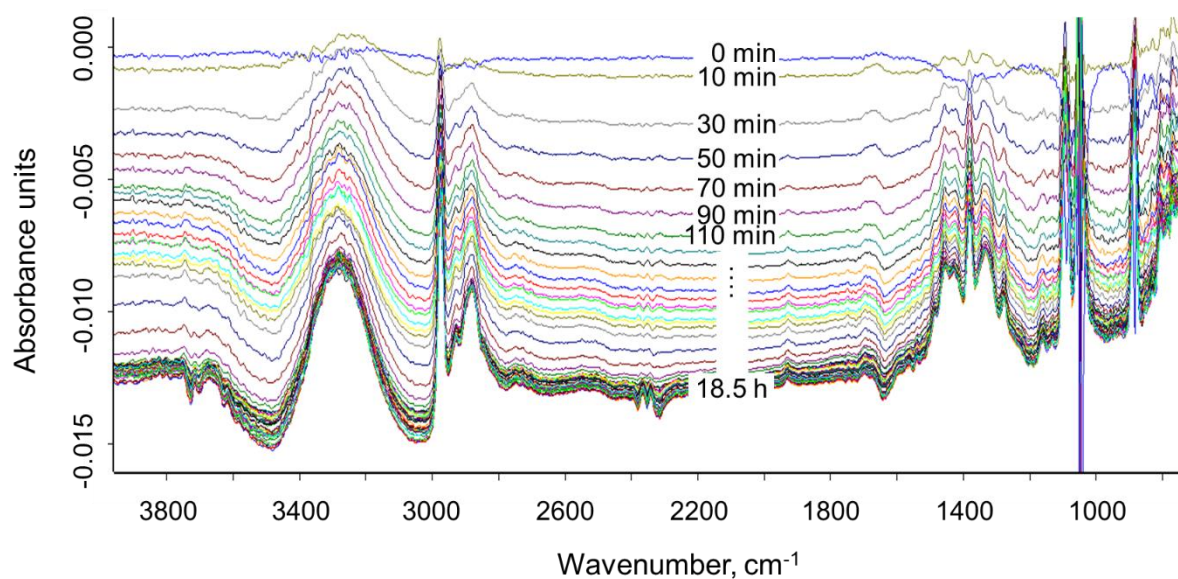
Figure A6. Time-evolution of ethanol spectra recorded on ZnSe crystal and referenced to ethanol

AVIII. The growth of *E. coli* in the planktonic form in MRS/10 and mTSB/10
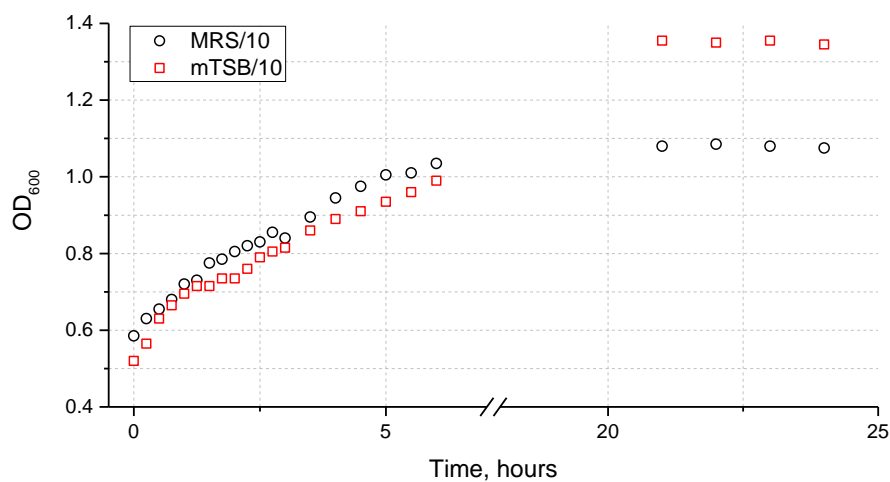
Figure A7. Growth curves of E. coli obtained in MRS/10 and mTSB/10 after transfer of the cells from the LB culture

AIX. Scientific communications

Publication:

E. Yunda, F. Quilès. *In situ* spectroscopic analysis of *Lactobacillus rhamnosus* GG flow on an abiotic surface reveals a role for nutrients in biofilm development. Biofouling, 2019, in press. DOI: 10.1080/08927014.2019.1617279.

Conferences:

- The 17th European conference on applications of surface and interface analysis – ECASIA'17, 24-29 September, Montpellier, France (oral communication: "*Surface functionalization of zinc selenide for control and monitoring of biofilm growth*"), Biointerphases Student Award for the best presentation,

- NANOinBIO 2018, 22-27 May, Le Gosier, Guadeloupe, French Caribbean (oral communication: *"A probiotic bacterium in the abiotic environment: a multiscale study of surface dependent adhesion"*)

- International symposium on biophysics of microbial adhesion 'BioPhysAdh' 2018, 10-11 September, Toulouse, France (oral communication: *"Effect of the nutritive medium choice on the formation of Lactobacillus rhamnosus GG biofilms on an abiotic surface"*)

References

[1] R. M. Donlan, "Biofilms: microbial life on surfaces," *Emerging infectious diseases*, vol. 8, no. 9, pp. 881–890, 2002.

[2] H.-C. Flemming and S. Wuertz, "Bacteria and archaea on Earth and their abundance in biofilms," *Nature Reviews Microbiology*, vol. 17, no. 4, pp. 247–260, 2019.

[3] R. Sender, S. Fuchs, and R. Milo, "Revised estimates for the number of human and bacteria cells in the body," *PLOS Biology*, vol. 14, no. 8, p. e1002533, 2016.

[4] L. M. Feazel, L. K. Baumgartner, K. L. Peterson, D. N. Frank, J. K. Harris, and N. R. Pace, "Opportunistic pathogens enriched in showerhead biofilms," *Proc Natl Acad Sci USA*, vol. 106, no. 38, p. 16393, 2009.

[5] L. Neu, C. Bänziger, C. R. Proctor, Y. Zhang, W.-T. Liu, and F. Hammes, "Ugly ducklings—the dark side of plastic materials in contact with potable water," *npj Biofilms and Microbiomes*, vol. 4, no. 1, p. 7, 2018.

[6] S. Yoshida *et al.*, "A bacterium that degrades and assimilates poly(ethylene terephthalate)," *Science*, vol. 351, no. 6278, p. 1196, 2016.

[7] L. Chaves Simões and M. Simões, "Biofilms in drinking water: problems and solutions," *RSC Adv.*, vol. 3, no. 8, pp. 2520–2533, 2013.

[8] H.-C. Flemming, J. Wingender, U. Szewzyk, P. Steinberg, S. A. Rice, and S. Kjelleberg, "Biofilms: an emergent form of bacterial life," *Nature Reviews Microbiology*, vol. 14, p. 563, 2016.

[9] N. Høiby, "A personal history of research on microbial biofilms and biofilm infections," *Pathogens and Disease*, vol. 70, no. 3, pp. 205–211, 2014.

[10] H.-C. Flemming and J. Wingender, "The biofilm matrix," *Nature Reviews Microbiology*, vol. 8, p. 623, 2010.

[11] G. A. O'Toole and G. C. Wong, "Sensational biofilms: surface sensing in bacteria," *Current Opinion in Microbiology*, vol. 30, pp. 139–146, 2016.

[12] P. Stoodley, K. Sauer, D. G. Davies, and J. W. Costerton, "Biofilms as complex differentiated communities," *Annu. Rev. Microbiol.*, vol. 56, no. 1, pp. 187–209, 2002.

[13] "National Institute of Health. Research on microbial biofilms: PA Number: PA-03-047. [http://grants.nih.gov/grants/guide/pa-files/PA-03-047.html]." 2002.

[14] W. M. Dunne Jr, "Bacterial adhesion: seen any good biofilms lately?" *Clinical microbiology reviews*, vol. 15, no. 2, pp. 155–166, 2002.

[15] G. B. Pier *et al.*, "Human monoclonal antibodies to *Pseudomonas aeruginosa* alginate that protect against Infection by both mucoid and nonmucoid Strains," *J. Immunol.*, vol. 173, no. 9, p. 5671, 2004.

[16] S. Ramírez-Estrada, B. Borgatta, and J. Rello, "*Pseudomonas aeruginosa* ventilator-associated pneumonia management," *Infection and drug resistance*, vol. 9, pp. 7–18, 2016.

[17] N. Safdar, C. Dezfulian, H. Collard, and S. Saint, "Clinical and economic consequences of ventilator-associated pneumonia: a systematic review," *Critical Care Medicine*, vol. 33, no. 10, pp. 2184–2193, 2005.

[18] D. A. Rosen, T. M. Hooton, W. E. Stamm, P. A. Humphrey, and S. J. Hultgren, "Detection of intracellular bacterial communities in human urinary tract infection," *PLoS medicine*, vol. 4, no. 12, pp. e329–e329, 2007.

[19] "Department of Health and Human Services. Centers for Disease Control and Prevention, USA. https://www.cdc.gov/." 06-May-2019.

[20] M. J. Soto-Giron *et al.*, "Biofilms on hospital shower hoses: characterization and implications for nosocomial infections," *Applied and environmental microbiology*, vol. 82, no. 9, pp. 2872–2883, 2016.

[21] H. Whiley, J. Hinds, J. Xi, and R. Bentham, "Real-time continuous surveillance of temperature and flow events presents a novel monitoring approach for hospital and healthcare water distribution systems," *International Journal of Environmental Research and Public Health*, vol. 16, no. 8, 2019.

[22] Y. Zhang and W.-T. Liu, "The application of molecular tools to study the drinking water microbiome – current understanding and future needs," *Critical Reviews in Environmental Science and Technology*, vol. 49, no. 13, pp. 1188–1235, 2019.

[23] "Annual epidemiological reports of French National Public Health agency, http://invs.santepubliquefrance.fr/." 23-Apr-2019.

[24] A. A. Latorre *et al.*, "Biofilm in milking equipment on a dairy farm as a potential source of bulk tank milk contamination with *Listeria monocytogenes*," *Journal of Dairy Science*, vol. 93, no. 6, pp. 2792–2802, 2010.

[25] S. Galié, C. García-Gutiérrez, E. M. Miguélez, C. J. Villar, and F. Lombó, "Biofilms in the food industry: health aspects and control methods," *Frontiers in microbiology*, vol. 9, pp. 898–898, 2018.

[26] J. Whitehead and B. Lake, "Recent trends in unpasteurized fluid milk outbreaks, legalization, and consumption in the United States," *PLoS currents*, vol. 10, p. ecurrents.outbreaks.bae5a0fd685616839c9cf857792730d1, 2018.

[27] R. C. Santos Mendonça, A. M. F. Morelli, J. A. M. Pereira, M. M. de Carvalho, and N. L. de Souza, "Prediction of *Escherichia coli* O157:H7 adhesion and potential to form biofilm under experimental conditions," *Food Control*, vol. 23, no. 2, pp. 389–396, 2012.

[28] J. Denny, M. Bhat, and K. Eckmann, "Outbreak of *Escherichia coli* O157:H7 associated with raw milk consumption in the Pacific Northwest," *Foodborne Pathogens and Disease*, vol. 5, no. 3, pp. 321–328, 2008.

[29] "Alerte sanitaire. « La Fromagerie Alpine » : informations complémentaires sur les fromages au lait cru concernés par le rappel. Site du Ministère de l'Agriculture et d'Alimentation." 08-May-2019.

[30] N. Marouani-Gadri, O. Firmesse, D. Chassaing, D. Sandris-Nielsen, N. Arneborg, and B. Carpentier, "Potential of Escherichia coli O157:H7 to persist and form viable but non-culturable cells on a food-contact surface subjected to cycles of soiling and chemical treatment," *International Journal of Food Microbiology*, vol. 144, no. 1, pp. 96–103, 2010.

[31] L. L. Nesse *et al.*, "Potentially pathogenic *Escherichia coli* can form a biofilm under conditions relevant to the food production chain," *Appl. Environ. Microbiol.*, vol. 80, no. 7, p. 2042, 2014.

[32] S. Singh, S. K. Singh, I. Chowdhury, and R. Singh, "Understanding the mechanism of bacterial biofilms resistance to antimicrobial agents," *The open microbiology journal*, vol. 11, pp. 53–62, 2017.

[33] W. Hengzhuang, H. Wu, O. Ciofu, Z. Song, and N. Høiby, "In vivo pharmacokinetics/pharmacodynamics of colistin and imipenem in *Pseudomonas aeruginosa* biofilm infection," *Antimicrobial agents and chemotherapy*, vol. 56, no. 5, pp. 2683–2690, 2012.

[34] D. Campoccia, L. Montanaro, and C. R. Arciola, "A review of the biomaterials technologies for infection-resistant surfaces," *Biomaterials*, vol. 34, no. 34, pp. 8533–8554, 2013.

[35] F. Achouri *et al.*, "ZnO nanorods with high photocatalytic and antibacterial activity under solar light irradiation," *Materials (Basel, Switzerland)*, vol. 11, no. 11, p. 2158, 2018.

[36] H. A. Foster, I. B. Ditta, S. Varghese, and A. Steele, "Photocatalytic disinfection using titanium dioxide: spectrum and mechanism of antimicrobial activity," *Applied Microbiology and Biotechnology*, vol. 90, no. 6, pp. 1847–1868, 2011.

[37] H. Wu, C. Moser, H.-Z. Wang, N. Høiby, and Z.-J. Song, "Strategies for combating bacterial biofilm infections," *International journal of oral science*, vol. 7, no. 1, pp. 1–7, 2014.

[38] C. T. O'Loughlin, L. C. Miller, A. Siryaporn, K. Drescher, M. F. Semmelhack, and B. L. Bassler, "A quorum-sensing inhibitor blocks *Pseudomonas aeruginosa* virulence and biofilm formation," *Proc Natl Acad Sci USA*, vol. 110, no. 44, p. 17981, 2013.

[39] T. Bjarnsholt *et al.*, "Garlic blocks quorum sensing and promotes rapid clearing of pulmonary *Pseudomonas aeruginosa* infections," *Microbiology*, vol. 151, no. 12, pp. 3873–3880, 2005.

[40] Z. Song *et al.*, "Panax ginseng has anti-infective activity against opportunistic pathogen *Pseudomonas aeruginosa* by inhibiting quorum sensing, a bacterial communication process critical for establishing infection," *Phytomedicine : international journal of phytotherapy and phytopharmacology*, vol. 17, no. 13, pp. 1040–1046, 2010.

[41] K. LoVetri and S. Madhyastha, "Antimicrobial and antibiofilm activity of quorum sensing peptides and peptide analogues against oral biofilm bacteria," in *Antimicrobial Peptides: Methods and Protocols*, A. Giuliani and A. C. Rinaldi, Eds. Totowa, NJ: Humana Press, 2010, pp. 383–392.

[42] U. Römling, M. Y. Galperin, and M. Gomelsky, "Cyclic di-GMP: the first 25 years of a universal bacterial second messenger," *Microbiology and molecular biology reviews : MMBR*, vol. 77, no. 1, pp. 1–52, 2013.

[43] R. M. Dedrick *et al.*, "Engineered bacteriophages for treatment of a patient with a disseminated drug-resistant Mycobacterium abscessus," *Nature Medicine*, vol. 25, no. 5, pp. 730–733, 2019.

[44] S. K. Hansen, P. B. Rainey, J. A. J. Haagensen, and S. Molin, "Evolution of species interactions in a biofilm community," *Nature*, vol. 445, p. 533, 2007.

[45] S. Elias and E. Banin, "Multi-species biofilms: living with friendly neighbors," *FEMS Microbiology Reviews*, vol. 36, no. 5, pp. 990–1004, 2012.

[46] C. Hill *et al.*, "The International Scientific Association for Probiotics and Prebiotics consensus statement on the scope and appropriate use of the term probiotic," *Nature Reviews Gastroenterology &Amp; Hepatology*, vol. 11, p. 506, 2014.

[47] M. E. Sanders, "How do we know when something called 'probiotic' is really a probiotic? A guideline for consumers and health care professionals," *Functional Food Reviews*, vol. 1, pp. 1–12, 2009.

[48] V. Hancock, M. Dahl, and P. Klemm, "Probiotic *Escherichia coli* strain Nissle 1917 outcompetes intestinal pathogens during biofilm formation," *Journal of Medical Microbiology*, vol. 59, no. 4, pp. 392–399, 2010.

[49] I. Y. Hwang *et al.*, "Engineered probiotic *Escherichia coli* can eliminate and prevent *Pseudomonas aeruginosa* gut infection in animal models," *Nature Communications*, vol. 8, p. 15028, 2017.

[50] K. Fang, X. Jin, and S. H. Hong, "Probiotic *Escherichia coli* inhibits biofilm formation of pathogenic *E. coli* via extracellular activity of DegP," *Scientific Reports*, vol. 8, no. 1, p. 4939, 2018.

[51] Q. Chen *et al.*, "Probiotic *E. coli* Nissle 1917 biofilms on silicone substrates for bacterial interference against pathogen colonization," *Acta Biomaterialia*, vol. 50, pp. 353–360, 2017.

[52] K. Lohith and K. A. Anu-Appaiah, "Antagonistic effect of *Saccharomyces cerevisiae* KTP and *Issatchenkia occidentalis* ApC on hyphal development and adhesion of *Candida albicans*," *Medical Mycology*, vol. 56, no. 8, pp. 1023–1032, 2018.

[53] E. Metchnikoff, "The Prolongation of Life. Optimistic Studies," New York : Putnam., 1908, p. 96 p.

[54] P. A. Mackowiak, "Recycling metchnikoff: probiotics, the intestinal microbiome and the quest for long life," *Frontiers in public health*, vol. 1, pp. 52–52, 2013.

[55] "Probiotics Market Size, Share & Trends Analysis Report By Application (Food & Beverages, Dietary Supplements, Animal Feed), By End-use, By Region, And Segment Forecast, 2018 - 2024."

[56] M. Bermudez-Brito, J. Plaza-Díaz, S. Muñoz-Quezada, C. Gómez-Llorente, and A. Gil, "Probiotic mechanisms of action," *Annals of Nutrition and Metabolism*, vol. 61, no. 2, pp. 160–174, 2012.

[57] M. Surendran Nair, M. A. Amalaradjou, and K. Venkitanarayanan, "Chapter One - Antivirulence properties of probiotics in combating microbial pathogenesis," in *Advances in Applied Microbiology*, vol. 98, S. Sariaslani and G. M. Gadd, Eds. Academic Press, 2017, pp. 1–29.

[58] F. Ben Taheur *et al.*, "Anti-bacterial and anti-biofilm activity of probiotic bacteria against oral pathogens," *Microbial Pathogenesis*, vol. 97, pp. 213–220, 2016.

[59] C. M. C. Chapman, G. R. Gibson, and I. Rowland, "Effects of single- and multi-strain probiotics on biofilm formation and in vitro adhesion to bladder cells by urinary tract pathogens," *Anaerobe*, vol. 27, pp. 71–76, 2014.

[60] T. Fiedler, C. Riani, D. Koczan, K. Standar, B. Kreikemeyer, and A. Podbielski, "Protective mechanisms of respiratory tract Streptococci against *Streptococcus pyogenes* biofilm formation and epithelial cell infection," *Applied and environmental microbiology*, vol. 79, no. 4, pp. 1265–1276, 2013.

[61] E. G. Lopes, D. A. Moreira, P. Gullón, B. Gullón, A. Cardelle-Cobas, and F. K. Tavaria, "Topical application of probiotics in skin: adhesion, antimicrobial and antibiofilm in vitro assays," *Journal of Applied Microbiology*, vol. 122, no. 2, pp. 450–461, 2017.

[62] P. Varma, N. Nisha, K. R. Dinesh, A. V. Kumar, and R. Biswas, "Anti-infective properties of *Lactobacillus fermentum* against *Staphylococcus aureus* and *Pseudomonas aeruginosa*," *Journal of Molecular Microbiology and Biotechnology*, vol. 20, no. 3, pp. 137–143, 2011.

[63] E. Ciandrini, R. Campana, and W. Baffone, "Live and heat-killed *Lactobacillus* spp. interfere with *Streptococcus mutans* and *Streptococcus oralis* during biofilm development on titanium surface," *Archives of Oral Biology*, vol. 78, pp. 48–57, 2017.

[64] F. Schwendicke, F. Korte, C. E. Dörfer, S. Kneist, K. Fawzy El-Sayed, and S. Paris, "Inhibition of *Streptococcus mutans* growth and biofilm formation by probiotics in vitro," *Caries Research*, vol. 51, no. 2, pp. 87–95, 2017.

[65] R. D. Rossoni *et al.*, "Inhibitory effect of probiotic *Lactobacillus* supernatants from the oral cavity on *Streptococcus mutans* biofilms," *Microbial Pathogenesis*, vol. 123, pp. 361–367, 2018.

[66] H. Park *et al.*, "Autoinducer-2 associated inhibition by *Lactobacillus sakei* NR28 reduces virulence of enterohaemorrhagic *Escherichia coli* O157:H7," *Food Control*, vol. 45, pp. 62–69, 2014.

[67] D. Bujnakova, E. Strakova, and V. Kmet, "In vitro evaluation of the safety and probiotic properties of Lactobacilli isolated from chicken and calves," *Anaerobe*, vol. 29, pp. 118–127, 2014.

[68] R. Ben Slama, B. Kouidhi, T. Zmantar, K. Chaieb, and A. Bakhrouf, "Anti-listerial and anti-biofilm activities of potential probiotic *Lactobacillus* strains isolated from Tunisian traditional fermented food," *Journal of Food Safety*, vol. 33, no. 1, pp. 8–16, 2013.

[69] H. Frickmann, C. Klenk, P. Warnke, S. Redanz, and A. Podbielski, "Influence of probiotic culture supernatants on in vitro biofilm formation of staphylococci," *European Journal of Microbiology and Immunology*, vol. 8, no. 4, pp. 119–127, 2018.

[70] J. Woo and J. Ahn, "Probiotic-mediated competition, exclusion and displacement in biofilm formation by food-borne pathogens," *Letters in Applied Microbiology*, vol. 56, no. 4, pp. 307–313, 2013.

[71] E. Turhan, Z. Erginkaya, M. Hatice, and E. Ozer, "Inactivation effect of probiotic biofilms on growth of Listeria monocytogenes," *Journal of the Faculty of Veterinary Medicine, Kafkas University*, vol. 23, no. 4, pp. 541–546, 2017.

[72] N. C. Gómez, J. M. P. Ramiro, B. X. V. Quecan, and B. D. G. de Melo Franco, "Use of potential probiotic lactic acid bacteria (LAB) biofilms for the control of *Listeria monocytogenes*, *Salmonella Typhimurium*, and *Escherichia coli* O157:H7 biofilms formation," *Frontiers in Microbiology*, vol. 7, p. 863, 2016.

[73] P. Ommen, N. Zobek, and R. L. Meyer, "Quantification of biofilm biomass by staining: Non-toxic safranin can replace the popular crystal violet," *Journal of Microbiological Methods*, vol. 141, pp. 87–89, 2017.

[74] B. W. Trautner *et al.*, "Nanoscale surface modification favors benign biofilm formation and impedes adherence by pathogens," *Nanomedicine : nanotechnology, biology, and medicine*, vol. 8, no. 3, pp. 261–270, 2012.

[75] M. E. Segers and S. Lebeer, "Towards a better understanding of *Lactobacillus rhamnosus* GG - host interactions," *Microbial Cell Factories*, vol. 13, no. 1, p. S7, 2014.

[76] A. Tarrah *et al.*, "Probiotic potential and biofilm inhibitory activity of *Lactobacillus casei* group strains isolated from infant feces," *Journal of Functional Foods*, vol. 54, pp. 489–497, 2019.

[77] M. Kankainen *et al.*, "Comparative genomic analysis of *Lactobacillus rhamnosus* GG reveals pili containing a human- mucus binding protein," *Proceedings of the National Academy of Sciences of the United States of America*, vol. 106, no. 40, pp. 17193–17198, 2009.

[78] R. M. A. Sullan *et al.*, "Single-cell force spectroscopy of pili-mediated adhesion," *Nanoscale*, vol. 6, no. 2, pp. 1134–1143, 2014.

[79] S. Lebeer, T. L. A. Verhoeven, M. Perea Vélez, J. Vanderleyden, and S. C. J. De Keersmaecker, "Impact of environmental and genetic factors on biofilm formation by the probiotic strain *Lactobacillus rhamnosus* GG," *Applied and Environmental Microbiology*, vol. 73, no. 21, pp. 6768–6775, 2007.

[80] R. Lu, N. Madayiputhiya, N. P. Morin, J. Nataro, and A. Fasano, "Isolation, identification, and characterization of small bioactive peptides from *Lactobacillus* GG conditional media that exert both anti-Gram-negative and Gram-positive bactericidal activity," *Journal of Pediatric Gastroenterology and Nutrition*, vol. 49, no. 1, pp. 23–30, 2009.

[81] M. I. Petrova *et al.*, "Lectin-Like molecules of *Lactobacillus rhamnosus* GG inhibit pathogenic *Escherichia coli* and *Salmonella* biofilm formation," *PloS one*, vol. 11, no. 8, pp. e0161337–e0161337, 2016.

[82] C. N. Allonsius *et al.*, "Inhibition of *Candida albicans* morphogenesis by chitinase from *Lactobacillus rhamnosus* GG," *Scientific Reports*, vol. 9, no. 1, p. 2900, 2019.

[83] S. Doron, D. R. Snydman, and S. L. Gorbach, "*Lactobacillus* GG: bacteriology and clinical applications," *Gastroenterol Clin North Am.*, vol. 34, no. 3, pp. 483–498, 2005.

[84] M. Kalliomäki, S. Salminen, T. Poussa, and E. Isolauri, "Probiotics during the first 7 years of life: A cumulative risk reduction of eczema in a randomized, placebo-controlled trial," *Journal of Allergy and Clinical Immunology*, vol. 119, no. 4, pp. 1019–1021, 2007.

[85] R. Berni Canani *et al.*, "Extensively hydrolyzed casein formula containing *Lactobacillus rhamnosus* GG reduces the occurrence of other allergic manifestations in children with cow's milk allergy: 3-year randomized controlled trial," *Journal of Allergy and Clinical Immunology*, vol. 139, no. 6, pp. 1906-1913.e4, 2017.

[86] G. Harata *et al.*, "Probiotics modulate gut microbiota and health status in Japanese cedar pollinosis patients during the pollen season," *European Journal of Nutrition*, vol. 56, no. 7, pp. 2245–2253, 2017.

[87] L. Näse *et al.*, "Effect of Long–Term Consumption of a Probiotic Bacterium, *Lactobacillus rhamnosus* GG, in Milk on Dental Caries and Caries Risk in Children," *Caries Research*, vol. 35, no. 6, pp. 412–420, 2001.

[88] A. Toiviainen *et al.*, "Impact of orally administered lozenges with *Lactobacillus rhamnosus* GG and *Bifidobacterium animalis* subsp. lactis BB-12 on the number of salivary mutans streptococci, amount of plaque, gingival inflammation and the oral microbiome in healthy adults," *Clinical oral investigations*, vol. 19, no. 1, pp. 77–83, 2015.

[89] E. Bruzzese *et al.*, "Effect of *Lactobacillus* GG supplementation on pulmonary exacerbations in patients with cystic fibrosis: A pilot study," *Clinical Nutrition*, vol. 26, no. 3, pp. 322–328, 2007.

[90] L. E. Morrow, M. H. Kollef, and T. B. Casale, "Probiotic prophylaxis of ventilator-associated pneumonia: a blinded, randomized, controlled trial," *American journal of respiratory and critical care medicine*, vol. 182, no. 8, pp. 1058–1064, 2010.

[91] S. W. Seow *et al.*, "*Lactobacillus rhamnosus* GG induces tumor regression in mice bearing orthotopic bladder tumors," *Cancer Science*, vol. 101, no. 3, pp. 751–758, 2010.

[92] M. Kandasamy, B.-H. Bay, Y.-K. Lee, and R. Mahendran, "Lactobacilli secreting a tumor antigen and IL15 activates neutrophils and dendritic cells and generates cytotoxic T lymphocytes against cancer cells," *Cellular Immunology*, vol. 271, no. 1, pp. 89–96, 2011.

[93] K. Laitinen, T. Poussa, and E. Isolauri, "Probiotics and dietary counselling contribute to glucose regulation during and after pregnancy: a randomised controlled trial," *British Journal of Nutrition*, vol. 101, no. 11, pp. 1679–1687, 2008.

[94] I. Spacova *et al.*, "Expression of fluorescent proteins in *Lactobacillus rhamnosus* to study host–microbe and microbe–microbe interactions," *Microbial Biotechnology*, vol. 11, no. 2, pp. 317–331, 2018.

[95]   Q. Jiang, V. Kainulainen, I. Stamatova, R. Korpela, and J. H. Meurman, "*Lactobacillus rhamnosus* GG in experimental oral biofilms exposed to different carbohydrate sources," *Caries Research*, vol. 52, no. 3, pp. 220–229, 2018.

[96]   S. C. J. De Keersmaecker, T. L. A. Verhoeven, J. Desair, K. Marchal, J. Vanderleyden, and I. Nagy, "Strong antimicrobial activity of *Lactobacillus rhamnosus* GG against *Salmonella typhimurium* is due to accumulation of lactic acid," *FEMS Microbiology Letters*, vol. 259, no. 1, pp. 89–96, 2006.

[97]   L. Makras *et al.*, "Kinetic analysis of the antibacterial activity of probiotic lactobacilli towards *Salmonella enterica* serovar Typhimurium reveals a role for lactic acid and other inhibitory compounds," *Research in Microbiology*, vol. 157, no. 3, pp. 241–247, 2006.

[98]   G. Schaule, T. Griebe, and H.-C. Flemming, "Steps in biofilm sampling and characterization in biofouling cases," in *Biofilms: Investigative Methods and Applications*, 2000, 268 p.

[99]   C. Hannig, M. Hannig, O. Rehmer, G. Braun, E. Hellwig, and A. Al-Ahmad, "Fluorescence microscopic visualization and quantification of initial bacterial colonization on enamel in situ," *Archives of Oral Biology*, vol. 52, no. 11, pp. 1048–1056, 2007.

[100] A. Delille, F. Quilès, and F. Humbert, "In situ monitoring of the nascent *Pseudomonas fluorescens* biofilm response to variations in the dissolved organic carbon level in low-nutrient water by Attenuated Total Reflectance-Fourier Transform Infrared Spectroscopy," *Applied and Environmental Microbiology*, vol. 73, no. 18, pp. 5782–5788, 2007.

[101] L. Drago, S. Agrappi, M. Bortolin, M. Toscano, C. L. Romanò, and E. De Vecchi, "How to study biofilms after microbial colonization of materials used in orthopaedic implants," *International journal of molecular sciences*, vol. 17, no. 3, pp. 293–293, 2016.

[102] A. Fahs, F. Quilès, D. Jamal, F. Humbert, and G. Francius, "In situ analysis of bacterial extracellular polymeric substances from a *Pseudomonas fluorescens* biofilm by combined vibrational and single molecule force spectroscopies," *J. Phys. Chem. B*, vol. 118, no. 24, pp. 6702–6713, 2014.

[103] M. M. Baum *et al.*, "Characterization of structures in biofilms formed by a *Pseudomonas fluorescens* isolated from soil," *BMC microbiology*, vol. 9, pp. 103–103, 2009.

[104] C. Wilson *et al.*, "Quantitative and qualitative assessment methods for biofilm growth: a mini-review," *Research & reviews. Journal of engineering and technology*, vol. 6, no. 4, p. http://www.rroij.com/open-access/quantitative-and-qualitative-assessment-methods-for-biofilm-growth-a-minireview-.pdf, 2017.

[105] M. V. Berridge, P. M. Herst, and A. S. Tan, "Tetrazolium dyes as tools in cell biology: New insights into their cellular reduction," in *Biotechnology Annual Review*, vol. 11, Elsevier, 2005, pp. 127–152.

[106] S. Ullrich, B. Karrasch, H. Hoppe, K. Jeskulke, and M. Mehrens, "Toxic effects on bacterial metabolism of the redox dye 5-cyano-2,3-ditolyl tetrazolium chloride.," *Appl. Environ. Microbiol.*, vol. 62, no. 12, p. 4587, 1996.

[107] S. N. Rampersad, "Multiple applications of Alamar Blue as an indicator of metabolic function and cellular health in cell viability bioassays," *Sensors (Basel, Switzerland)*, vol. 12, no. 9, pp. 12347–12360, 2012.

[108] J. R. Lawrence, D. R. Korber, and T. R. Neu, "Analytical Imaging and Microscopy Techniques," in *Manual of Environmental Microbiology, Third Edition*, American Society of Microbiology, 2007, pp. 40–68.

[109] S. Lebeer *et al.*, "FISH analysis of *Lactobacillus* biofilms in the gastrointestinal tract of different hosts," *Letters in Applied Microbiology*, vol. 52, no. 3, pp. 220–226, 2011.

[110] K. S. Brandenburg *et al.*, "Development of *Pseudomonas aeruginosa* Biofilms in Partial-Thickness Burn Wounds Using a Sprague-Dawley Rat Model," *Journal of burn care & research : official publication of the American Burn Association*, vol. 40, no. 1, pp. 44–57, 2019.

[111] S. Srey, I. K. Jahid, and S.-D. Ha, "Biofilm formation in food industries: A food safety concern," *Food Control*, vol. 31, no. 2, pp. 572–585, 2013.

[112] G. Francius *et al.*, "Bacterial surface appendages strongly impact nanomechanical and electrokinetic properties of *Escherichia coli* cells subjected to osmotic stress," *PloS one*, vol. 6, no. 5, pp. e20066–e20066, 2011.

[113] J. Burgain *et al.*, "Impacts of pH-mediated EPS structure on probiotic bacterial pili–whey proteins interactions," *Colloids and Surfaces B: Biointerfaces*, vol. 134, pp. 332–338, 2015.

[114] J. Guerin *et al.*, "Adhesion of *Lactobacillus rhamnosus* GG surface biomolecules to milk proteins," *Food Hydrocolloids*, vol. 82, pp. 296–303, 2018.

[115] S. Lebeer *et al.*, "Functional analysis of *Lactobacillus rhamnosus* GG pili in relation to adhesion and immunomodulatory interactions with intestinal epithelial cells," *Applied and environmental microbiology*, vol. 78, no. 1, pp. 185–193, 2012.

[116] R. R. Burgess, "Chapter 32 Elution of proteins from gels," in *Methods in Enzymology*, vol. 463, R. R. Burgess and M. P. Deutscher, Eds. Academic Press, 2009, pp. 565–572.

[117] T. Mahmood and P.-C. Yang, "Western blot: technique, theory, and trouble shooting," *N Am J Med Sci*, vol. 4, no. 9, pp. 429–434, 2012.

[118] I. J. J. Claes *et al.*, "Genetic and biochemical characterization of the cell wall hydrolase activity of the major secreted protein of *Lactobacillus rhamnosus* GG," *PLOS ONE*, vol. 7, no. 2, p. e31588, 2012.

[119] R. Diez, M. Herbstreith, C. Osorio, and O. Alzate, "Chapter 42-D fluorescence difference gel electrophoresis (DIGE) in neuroproteomics," in *Neuroproteomics*, Boca Raton (FL): CRC Press/Taylor & Francis, 2010.

[120] J. Koponen *et al.*, "Effect of acid stress on protein expression and phosphorylation in *Lactobacillus rhamnosus* GG," *Journal of Proteomics*, vol. 75, no. 4, pp. 1357–1374, 2012.

[121] K. Koskenniemi *et al.*, "Proteome analysis of *Lactobacillus rhamnosus* GG using 2-D DIGE and mass spectrometry shows differential protein production in laboratory and industrial-type growth media," *J. Proteome Res.*, vol. 8, no. 11, pp. 4993–5007, 2009.

[122] N. Ali, R. de Cássia Pontello Rampazzo, A. Dias Tavares Costa, and M. Aurelio Krieger, "Current nucleic acid extraction methods and their implications to point-of-care diagnostics," *BioMed Research International*, vol. 2017, p. ID 9306564, 2017.

[123] G. Schochetman, C.-Y. Ou, and W. K. Jones, "Polymerase chain reaction," *The Journal of Infectious Diseases*, vol. 158, no. 6, pp. 1154–1157, 1988.

[124] L. Garibyan and N. Avashia, "Research techniques made simple: polymerase chain reaction (PCR)," *J Invest Dermatol*, vol. 133, no. 3, pp. 1–4, 2013.

[125] S. A. Barghouthi, "A universal method for the identification of bacteria based on general PCR primers," *Indian J Microbiol*, vol. 51, no. 4, pp. 430–444, 2011.

[126] A. Endo, J. Aakko, and S. Salminen, "Evaluation of strain-specific primers for identification of *Lactobacillus rhamnosus* GG," *FEMS Microbiology Letters*, vol. 337, no. 2, pp. 120–125, 2012.

[127] P. Treven, V. Mrak, B. Bogovič Matijašić, S. Horvat, and I. Rogelj, "Administration of probiotics *Lactobacillus rhamnosus* GG and *Lactobacillus gasseri* K7 during pregnancy and lactation changes mouse mesenteric lymph nodes and mammary gland microbiota," *Journal of Dairy Science*, vol. 98, no. 4, pp. 2114–2128, 2015.

[128] T. Ahlroos and S. Tynkkynen, "Quantitative strain-specific detection of *Lactobacillus rhamnosus* GG in human faecal samples by real-time PCR," *Journal of Applied Microbiology*, vol. 106, no. 2, pp. 506–514, 2009.

[129] S. S. Nielsen, "Phenol-sulfuric acid method for total carbohydrates," in *Food Analysis Laboratory Manual*, Food Science Texts Series. Springer., Boston, MA: Nielsen S.S., 2010, pp. 47–53.

[130] P. M. Bales, E. M. Renke, S. L. May, Y. Shen, and D. C. Nelson, "Purification and characterization of biofilm-associated EPS exopolysaccharides from ESKAPE organisms and other pathogens," *PLoS One*, vol. 8, no. 6, pp. e67950–e67950, 2013.

[131] S. Jachlewski, W. D. Jachlewski, U. Linne, C. Bräsen, J. Wingender, and B. Siebers, "Isolation of extracellular polymeric substances from biofilms of the thermoacidophilic *Archaeon Sulfolobus acidocaldarius*," *Front Bioeng Biotechnol*, vol. 3, pp. 123–123, 2015.

[132] C. N. Allonsius *et al.*, "Interplay between *Lactobacillus rhamnosus* GG and *Candida* and the involvement of exopolysaccharides," *Microb Biotechnol*, vol. 10, no. 6, pp. 1753–1763, 2017.

[133] P. Stoodley *et al.*, "5 - Biofilms, Biomaterials, and device-related infections," in *Handbook of Polymer Applications in Medicine and Medical Devices*, K. Modjarrad and S. Ebnesajjad, Eds. Oxford: William Andrew Publishing, 2013, pp. 77–101.

[134] C. Hannig, M. Follo, E. Hellwig, and A. Al-Ahmad, "Visualization of adherent micro-organisms using different techniques," *Journal of Medical Microbiology*, vol. 59, no. 1, pp. 1–7, 2010.

[135] M. A. Auty *et al.*, "Direct in situ viability assessment of bacteria in probiotic dairy products using viability staining in conjunction with confocal scanning laser microscopy," *Appl Environ Microbiol*, vol. 67, no. 1, pp. 420–425, 2001.

[136] F. Ou, C. McGoverin, S. Swift, and F. Vanholsbeeck, "Absolute bacterial cell enumeration using flow cytometry," *Journal of Applied Microbiology*, vol. 123, no. 2, pp. 464–477, 2017.

[137] M. Erriu, G. Genta, E. Tuveri, G. Orrù, G. Barbato, and R. Levi, "Microtiter spectrophotometric biofilm production assay analyzed with metrological methods and uncertainty evaluation," *Measurement*, vol. 45, no. 5, pp. 1083–1088, 2012.

[138] O. Zagorodko *et al.*, "Surface Plasmon Resonance (SPR) for the Evaluation of Shear-Force-Dependent Bacterial Adhesion," *Biosensors (Basel)*, vol. 5, no. 2, pp. 276–287, 2015.

[139] J.-S. Guo *et al.*, "Microbial attachment and adsorption–desorption kinetic of tightly bound extracellular polymeric substances on model organic surfaces," *Chemical Engineering Journal*, vol. 279, pp. 516–521, 2015.

[140] A. Pranzetti *et al.*, "Model organic surfaces to probe marine bacterial adhesion kinetics by surface plasmon resonance," *Advanced Functional Materials*, vol. 22, no. 17, pp. 3672–3681, 2012.

[141] P. Larkin, *Infrared and Raman Spectroscopy: Principles and Spectral Interpretation*. Elsevier, 2011.

[142] W. E. Huang, R. I. Griffiths, I. P. Thompson, M. J. Bailey, and A. S. Whiteley, "Raman Microscopic Analysis of Single Microbial Cells," *Anal. Chem.*, vol. 76, no. 15, pp. 4452–4458, 2004.

[143] M. Myintzu Hlaing, B. Wood, D. McNaughton, D. Ying, and M. A. Augustin, "Raman spectroscopic analysis of *Lactobacillus rhamnosus* GG in response to dehydration reveals DNA conformation changes," *Journal of Biophotonics*, vol. 10, no. 4, pp. 589–597, 2017.

[144] V. Emmanuel, B. Odile, and R. Céline, "FTIR spectroscopy of woods: A new approach to study the weathering of the carving face of a sculpture," *Spectrochimica Acta Part A: Molecular and Biomolecular Spectroscopy*, vol. 136, pp. 1255–1259, 2015.

[145] M. J. Baker *et al.*, "Using Fourier transform IR spectroscopy to analyze biological materials," *Nat Protoc*, vol. 9, no. 8, pp. 1771–1791, 2014.

[146] Paulina Zarnowiec, Lukasz Lechowicz, and Grzegorz Czerwonka and Wiesław Kaca, "Fourier Transform Infrared Spectroscopy (FTIR) as a Tool for the Identification and Differentiation of Pathogenic Bacteria," *Current Medicinal Chemistry*, vol. 22, no. 14, pp. 1710–1718, 2015.

[147] H. J. Busscher and H. C. van der Mei, "Microbial adhesion in flow displacement systems," *Clin Microbiol Rev*, vol. 19, no. 1, pp. 127–141, 2006.

[148] P. R. Rutter and B. Vincent, "Attachment mechanisms in the surface growth of microorganisms," in *Physiological models in microbiology*, CRC Press, Boca Raton, Fla: M.J. Bazin and J.I. Prosser, pp. 87–107.

[149] N. Mohamed, T. R. Rainier Jr., and J. M. Ross, "Novel experimental study of receptor-mediated bacterial adhesion under the influence of fluid shear," *Biotechnology and Bioengineering*, vol. 68, no. 6, pp. 628–636, 2000.

[150] W. E. Thomas, E. Trintchina, M. Forero, V. Vogel, and E. V. Sokurenko, "Bacterial adhesion to target cells enhanced by shear force," *Cell*, vol. 109, no. 7, pp. 913–923, 2002.

[151] P. Qi, W. Wang, and Z. Qi, "Effect of shear stress on biofilm morphological characteristics and the secretion of extracellular polymeric substances," in *2008 2nd International Conference on Bioinformatics and Biomedical Engineering*, 2008, pp. 3438–3441.

[152] J. Hou, D. H. Veeregowda, B. van de Belt-Gritter, H. J. Busscher, and H. C. van der Mei, "Extracellular polymeric matrix production and relaxation under fluid shear and mechanical pressure in *Staphylococcus aureus* Biofilms," *Applied and Environmental Microbiology*, vol. 84, no. 1, 2018.

[153] M. Lemos, F. Mergulhão, L. Melo, and M. Simões, "The effect of shear stress on the formation and removal of *Bacillus cereus* biofilms," *Food and Bioproducts Processing*, vol. 93, pp. 242–248, 2015.

[154] K. P. Norris, "Infra-red spectroscopy and its application to microbiology," *J Hyg (Lond)*, vol. 57, no. 3, pp. 326–345, 1959.

[155] R. H. Bordner, P. W. Kabler, B. A. Kenner, J. W. Riddle, S. W. Rockwood, and H. J. Stevenson, "Bacterial identification by infrared spectrophotometry," *J Bacteriol*, vol. 72, no. 5, pp. 593–603, 1956.

[156] D. E. Nivens, J. Q. Chambers, T. R. Anderson, A. Tunlid, J. Smit, and D. C. White, "Monitoring microbiol adhesion and biofilm formation by attenuated total reflection/Fourier transform infrared spectroscopy," *Journal of Microbiological Methods*, vol. 17, no. 3, pp. 199–213, 1993.

[157] D. C. White, A. A. Arrage, D. E. Nivens, R. J. Palmer, J. F. Rice, and G. S. Sayler, "Biofilm ecology: On-line methods bring new insights into mic and microbial biofouling," *Biofouling*, vol. 10, no. 1–3, pp. 3–16, 1996.

[158] D. E. Nivens, D. E. Ohman, J. Williams, and M. J. Franklin, "Role of alginate and its O acetylation in formation of Pseudomonas aeruginosa microcolonies and biofilms," *J Bacteriol*, vol. 183, no. 3, pp. 1047–1057, 2001.

[159] J. Schmitt, D. Nivens, D. C. White, and H.-C. Flemming, "Changes of biofilm properties in response to sorbed substances - an FTIR-ATR study," *Water Science and Technology*, vol. 32, no. 8, pp. 149–155, 1995.

[160] P. A. Suci, G. G. Geesey, and B. J. Tyler, "Integration of Raman microscopy, differential interference contrast microscopy, and attenuated total reflection Fourier transform infrared spectroscopy to investigate chlorhexidine spatial and temporal distribution in *Candida albicans* biofilms," *Journal of Microbiological Methods*, vol. 46, no. 3, pp. 193–208, 2001.

[161] P. A. Suci, J. D. Vrany, and M. W. Mittelman, "Investigation of interactions between antimicrobial agents and bacterial biofilms using attenuated total reflection Fourier transform infrared spectroscopy," *Biomaterials*, vol. 19, no. 4, pp. 327–339, 1998.

[162] R. M. Donlan *et al.*, "Model system for growing and quantifying *Streptococcus pneumoniae* biofilms in situ and in real time," *Applied and Environmental Microbiology*, vol. 70, no. 8, pp. 4980–4988, 2004.

[163] M. Boualam, F. Quilès, L. Mathieu, and J.-C. Block, "Monitoring the effect of organic matter on biofilm growth in low nutritive waters by ATR/FT-IR Spectroscopy," *Biofouling*, vol. 18, no. 1, pp. 73–81, 2002.

[164] S. J. Parikh and J. Chorover, "FTIR spectroscopic study of biogenic Mn-Oxide formation by *Pseudomonas putida* GB-1," *Geomicrobiology Journal*, vol. 22, no. 5, pp. 207–218, 2005.

[165] J. J. Ojeda, M. E. Romero-Gonzalez, H. M. Pouran, and S. A. Banwart, "In situ monitoring of the biofilm formation of *Pseudomonas putida* on hematite using flow-cell ATR-FTIR spectroscopy to investigate the formation of inner-sphere bonds between the bacteria and the mineral," *Mineralogical Magazine*, vol. 72, no. 1, pp. 101–106, 2008.

[166] F. Quilès, F. Humbert, and A. Delille, "Analysis of changes in attenuated total reflection FTIR fingerprints of *Pseudomonas fluorescens* from planktonic state to nascent biofilm state," *Spectrochimica Acta Part A: Molecular and Biomolecular Spectroscopy*, vol. 75, no. 2, pp. 610–616, 2010.

[167] J.-H. Huang, E. J. Elzinga, Y. Brechbuehl, A. Voegelin, and R. Kretzschmar, "Impacts of *Shewanella putrefaciens* strain CN-32 cells and extracellular polymeric substances on the sorption of As(V) and As(III) on Fe(III)-(Hydr)oxides," *Environ. Sci. Technol.*, vol. 45, no. 7, pp. 2804–2810, 2011.

[168] G. S. Lorite, C. M. Rodrigues, A. A. de Souza, C. Kranz, B. Mizaikoff, and M. A. Cotta, "The role of conditioning film formation and surface chemical changes on *Xylella fastidiosa* adhesion and biofilm evolution," *Journal of Colloid and Interface Science*, vol. 359, no. 1, pp. 289–295, 2011.

[169] G. S. Lorite, A. A. de Souza, D. Neubauer, B. Mizaikoff, C. Kranz, and M. A. Cotta, "On the role of extracellular polymeric substances during early stages of *Xylella fastidiosa* biofilm formation," *Colloids and Surfaces B: Biointerfaces*, vol. 102, pp. 519–525, 2013.

[170] L. Giotta *et al.*, "Reversible binding of metal ions onto bacterial layers revealed by protonation-induced ATR-FTIR difference spectroscopy," *Langmuir*, vol. 27, no. 7, pp. 3762–3773, 2011.

[171] H. Wang, S. Ding, G. Wang, X. Xu, and G. Zhou, "In situ characterization and analysis of *Salmonella* biofilm formation under meat processing environments using a combined microscopic and spectroscopic approach," *International Journal of Food Microbiology*, vol. 167, no. 3, pp. 293–302, 2013.

[172] S. J. Parikh, F. N. D. Mukome, and X. Zhang, "ATR–FTIR spectroscopic evidence for biomolecular phosphorus and carboxyl groups facilitating bacterial adhesion to iron oxides," *Colloids and Surfaces B: Biointerfaces*, vol. 119, pp. 38–46, 2014.

[173] F. Quilès, S. Saadi, G. Francius, J. Bacharouche, and F. Humbert, "In situ and real time investigation of the evolution of a *Pseudomonas fluorescens* nascent biofilm in the presence of an antimicrobial peptide," *Biochimica et Biophysica Acta (BBA) - Biomembranes*, vol. 1858, no. 1, pp. 75–84, 2016.

[174] S. Kumari, N. Mangwani, and S. Das, "Interaction of Pb(II) and biofilm associated extracellular polymeric substances of a marine bacterium *Pseudomonas pseudoalcaligenes* NP103," *Spectrochimica Acta Part A: Molecular and Biomolecular Spectroscopy*, vol. 173, pp. 655–665, 2017.

[175] O. Freudenthal, F. Quilès, and G. Francius, "Discrepancies between cyclic and linear antimicrobial peptide actions on the spectrochemical and nanomechanical fingerprints of a young biofilm," *ACS Omega*, vol. 2, no. 9, pp. 5861–5872, 2017.

[176] L. Zhou *et al.*, "Surface interaction between metazeunerite and an indigenous microorganism *Kocuria rosea*: Implications for bioremediation of As-U tailings," *Chemical Engineering Journal*, vol. 359, pp. 393–401, 2019.

[177] A. Fanesi, A. Zegeye, C. Mustin, and A. Cébron, "Soil particles and phenanthrene interact in defining the metabolic profile of *Pseudomonas putida* G7: a vibrational spectroscopy approach," *Frontiers in Microbiology*, vol. 9, p. 2999, 2018.

[178] M. Pousti and J. Greener, "Altered biofilm formation at plasma bonded surfaces in microchannels studied by attenuated total reflection infrared spectroscopy," *Surface Science*, vol. 676, pp. 56–60, 2018.

[179] R. Davis and L. J. Mauer, "Fourier tansform infrared (FT-IR) spectroscopy: A rapid tool for detection and analysis of foodborne pathogenic bacteria," in *Current Research, Technology and Education Topics in Applied Microbiology and Microbial Biotechnology*, Formatex Research Center., A. Méndez-Vilas, 2010.

[180] Kochan Kamila *et al.*, "In vivo atomic force microscopy–infrared spectroscopy of bacteria," *Journal of The Royal Society Interface*, vol. 15, no. 140, p. 20180115, 2018.

[181] S. Moussaoui, C. Carteret, D. Brie, and A. Mohammad-Djafari, "Bayesian analysis of spectral mixture data using Markov Chain Monte Carlo Methods," *Chemometrics and Intelligent Laboratory Systems*, vol. 81, no. 2, pp. 137–148, 2006.

[182] N. Dobigeon, S. Moussaoui, J.-Y. Tourneret, and C. Carteret, "Bayesian separation of spectral sources under non-negativity and full additivity constraints," *Signal Processing*, vol. 89, no. 12, pp. 2657–2669, 2009.

[183] A. Hartstein, J. R. Kirtley, and J. C. Tsang, "Enhancement of the Infrared Absorption from Molecular Monolayers with Thin Metal Overlayers," *Phys. Rev. Lett.*, vol. 45, no. 3, pp. 201–204, 1980.

[184] M. Osawa and M. Ikeda, "Surface-enhanced infrared absorption of p-nitrobenzoic acid deposited on silver island films: contributions of electromagnetic and chemical mechanisms," *J. Phys. Chem.*, vol. 95, no. 24, pp. 9914–9919, 1991.

[185] G. T. Merklin and P. R. Griffiths, "Influence of chemical interactions on the surface-enhanced infrared absorption spectrometry of nitrophenols on copper and silver films," *Langmuir*, vol. 13, no. 23, pp. 6159–6163, 1997.

[186] J. P. Busalmen, A. Esteve-Nuñez, A. Berná, and J. M. Feliu, "ATR-SEIRAs characterization of surface redox processes in G. sulfurreducens," *Bioelectrochemistry*, vol. 78, no. 1, pp. 25–29, 2010.

[187] Y. Liu, A. Berná, V. Climent, and J. M. Feliu, "Real-time monitoring of electrochemically active biofilm developing behavior on bioanode by using EQCM and ATR/FTIR," *Sensors and Actuators B: Chemical*, vol. 209, pp. 781–789, 2015.

[188] P.-M. Toziou, P. Barmpalexis, P. Boukouvala, S. Verghese, and I. Nikolakakis, "Quantification of live *Lactobacillus acidophilus* in mixed populations of live and killed by application of attenuated reflection Fourier transform infrared spectroscopy combined with chemometrics," *Journal of Pharmaceutical and Biomedical Analysis*, vol. 154, pp. 16–22, 2018.

[189] R. Tareb, M. Bernardeau, C. Amiel, and J. P. Vernoux, "Usefulness of FTIR spectroscopy to distinguish rough and smooth variants of *Lactobacillus farciminis* CNCM-I-3699," *FEMS Microbiology Letters*, vol. 364, no. 2, 2017.

[190] G. Deepika, R. J. Green, R. A. Frazier, and D. Charalampopoulos, "Effect of growth time on the surface and adhesion properties of *Lactobacillus rhamnosus* GG," *Journal of Applied Microbiology*, vol. 107, no. 4, pp. 1230–1240, 2009.

[191] G. Posselt, S. Backert, and S. Wessler, "The functional interplay of *Helicobacter pylori* factors with gastric epithelial cells induces a multi-step process in pathogenesis," *Cell Communication and Signaling*, vol. 11, no. 1, p. 77, 2013.

[192] J. M. Koczan, B. R. Lenneman, M. J. McGrath, and G. W. Sundin, "Cell surface attachment structures contribute to biofilm formation and xylem colonization by *Erwinia amylovora*," *Appl Environ Microbiol*, vol. 77, no. 19, pp. 7031–7039, 2011.

[193] Y. Hong and D. G. Brown, "Electrostatic behavior of the charge-regulated bacterial cell surface," *Langmuir*, vol. 24, no. 9, pp. 5003–5009, 2008.

[194] G. Capitani, O. Eidam, R. Glockshuber, and M. G. Grütter, "Structural and functional insights into the assembly of type 1 pili from *Escherichia coli*," *Microbes and Infection*, vol. 8, no. 8, pp. 2284–2290, 2006.

[195] J.-H. Ryu, H. Kim, J. F. Frank, and L. R. Beuchat, "Attachment and biofilm formation on stainless steel by *Escherichia coli* O157:H7 as affected by curli production," *Letters in Applied Microbiology*, vol. 39, no. 4, pp. 359–362, 2004.

[196] C. I. Pereni, Q. Zhao, Y. Liu, and E. Abel, "Surface free energy effect on bacterial retention," *Colloids and Surfaces B: Biointerfaces*, vol. 48, no. 2, pp. 143–147, 2006.

[197] N. P. Boks, W. Norde, H. C. van der Mei, and H. J. Busscher, "Forces involved in bacterial adhesion to hydrophilic and hydrophobic surfaces," *Microbiology*, vol. 154, no. 10, pp. 3122–3133, 2008.

[198] D. Cunliffe, C. A. Smart, C. Alexander, and E. N. Vulfson, "Bacterial adhesion at synthetic surfaces," *Appl Environ Microbiol*, vol. 65, no. 11, pp. 4995–5002, 1999.

[199] B. Li and B. E. Logan, "Bacterial adhesion to glass and metal-oxide surfaces," *Colloids and Surfaces B: Biointerfaces*, vol. 36, no. 2, pp. 81–90, 2004.

[200] X.-Q. Dou, D. Zhang, C. Feng, and L. Jiang, "Bioinspired Hierarchical Surface Structures with Tunable Wettability for Regulating Bacteria Adhesion," *ACS Nano*, vol. 9, no. 11, pp. 10664–10672, 2015.

[201] Y. Yuan, M. P. Hays, P. R. Hardwidge, and J. Kim, "Surface characteristics influencing bacterial adhesion to polymeric substrates," *RSC Adv.*, vol. 7, no. 23, pp. 14254–14261, 2017.

[202] X. Zhang, L. Wang, and E. Levänen, "Superhydrophobic surfaces for the reduction of bacterial adhesion," *RSC Adv.*, vol. 3, no. 30, pp. 12003–12020, 2013.

[203] W. Barthlott and C. Neinhuis, "Purity of the sacred lotus, or escape from contamination in biological surfaces," *Planta*, vol. 202, no. 1, pp. 1–8, 1997.

[204] C. Gómez-Suárez, H. J. Busscher, and H. C. van der Mei, "Analysis of Bacterial Detachment from Substratum Surfaces by the Passage of Air-Liquid Interfaces," *Appl. Environ. Microbiol.*, vol. 67, no. 6, p. 2531, 2001.

[205] W. G. Pitt, M. O. McBride, A. J. Barton, and R. D. Sagers, "Air-water interface displaces adsorbed bacteria," *Biomaterials*, vol. 14, no. 8, pp. 605–608, 1993.

[206] J. K. Oh *et al.*, "The influence of surface chemistry on the kinetics and thermodynamics of bacterial adhesion," *Scientific Reports*, vol. 8, no. 1, p. 17247, 2018.

[207] C. Valotteau *et al.*, "Nanoscale antiadhesion properties of sophorolipid-coated surfaces against pathogenic bacteria," *Nanoscale Horiz.*, 2019.

[208] J. Verran, A. Packer, P. J. Kelly, and K. A. Whitehead, "Use of the Atomic Force Microscope to Determine the Strength of Bacterial Attachment to Grooved Surface Features," *Journal of Adhesion Science and Technology*, vol. 24, no. 13–14, pp. 2271–2285, 2010.

[209] S. J. Parikh and J. Chorover, "ATR-FTIR spectroscopy reveals bond formation during bacterial adhesion to iron oxide," *Langmuir*, vol. 22, no. 20, pp. 8492–8500, 2006.

[210] M. J. McWhirter, A. J. McQuillan, and P. J. Bremer, "Influence of ionic strength and pH on the first 60 min of *Pseudomonas aeruginosa* attachment to ZnSe and to TiO2 monitored by ATR-IR spectroscopy," *Colloids and Surfaces B: Biointerfaces*, vol. 26, no. 4, pp. 365–372, 2002.

[211] S. E. Glassford, B. Byrne, and S. G. Kazarian, "Recent applications of ATR FTIR spectroscopy and imaging to proteins," *Biochimica et Biophysica Acta (BBA) - Proteins and Proteomics*, vol. 1834, no. 12, pp. 2849–2858, 2013.

[212] J. Schartner *et al.*, "Chemical functionalization of germanium with dextran brushes for immobilization of proteins revealed by Attenuated Total Reflection Fourier Transform Infrared Difference Spectroscopy," *Anal. Chem.*, vol. 87, no. 14, pp. 7467–7475, 2015.

[213] C. S. Riccardi, D. W. Hess, and B. Mizaikoff, "Surface-modified ZnSe waveguides for label-free infrared attenuated total reflection detection of DNA hybridization," *Analyst*, vol. 136, no. 23, pp. 4906–4911, 2011.

[214] I. C. Stefan, D. Mandler, and D. A. Scherson, "In Situ FTIR-ATR studies of functionalized self-assembled bilayer interactions with metal ions in aqueous solutions," *Langmuir*, vol. 18, no. 18, pp. 6976–6980, 2002.

[215] B. A. Jucker, H. Harms, and A. J. Zehnder, "Adhesion of the positively charged bacterium *Stenotrophomonas* (*Xanthomonas*) *maltophilia* 70401 to glass and Teflon," *J Bacteriol*, vol. 178, no. 18, pp. 5472–5479, 1996.

[216] B. Gottenbos, H. C. Van der Mei, and H. J. Busscher, "Initial adhesion and surface growth of *Pseudomonas aeruginosa* on negatively and positively charged poly(methacrylates)," *Journal of Materials Science: Materials in Medicine*, vol. 10, pp. 853–855, 1999.

[217] C. Chen, T. Petterson, J. Illergård, M. Ek, and L. Wågberg, "Influence of cellulose charge on bacteria adhesion and viability to PVAm/CNF/PVAm-modified cellulose model surfaces," *Biomacromolecules*, vol. 20, no. 5, pp. 2075–2083, 2019.

[218] A. Terada, A. Yuasa, T. Kushimoto, S. Tsuneda, A. Katakai, and M. Tamada, "Bacterial adhesion to and viability on positively charged polymer surfaces," *Microbiology*, vol. 152, no. 12, pp. 3575–3583, 2006.

[219] B. Gottenbos, D. W. Grijpma, H. C. van der Mei, J. Feijen, and H. J. Busscher, "Antimicrobial effects of positively charged surfaces on adhering Gram-positive and Gram-negative bacteria," *Journal of Antimicrobial Chemotherapy*, vol. 48, no. 1, pp. 7–13, 2001.

[220] J. L. Clement and P. S. Jarrett, "Antibacterial silver," *Met Based Drugs*, vol. 1, no. 5–6, pp. 467–482, 1994.

[221] M. G. Schmidt *et al.*, "Copper surfaces are associated with significantly lower concentrations of bacteria on selected surfaces within a pediatric intensive care unit," *American Journal of Infection Control*, vol. 44, no. 2, pp. 203–209, 2016.

[222] K. A. Whitehead, J. Colligon, and J. Verran, "Retention of microbial cells in substratum surface features of micrometer and sub-micrometer dimensions," *Colloids and Surfaces B: Biointerfaces*, vol. 41, no. 2, pp. 129–138, 2005.

[223] J. Verran, A. Packer, P. Kelly, and K. A. Whitehead, "The retention of bacteria on hygienic surfaces presenting scratches of microbial dimensions," *Letters in Applied Microbiology*, vol. 50, no. 3, pp. 258–263, 2010.

[224] D. Perera-Costa, J. M. Bruque, M. L. González-Martín, A. C. Gómez-García, and V. Vadillo-Rodríguez, "Studying the influence of surface topography on bacterial adhesion using spatially organized microtopographic surface patterns," *Langmuir*, vol. 30, no. 16, pp. 4633–4641, 2014.

[225] M. Lorenzetti *et al.*, "The influence of surface modification on bacterial adhesion to titanium-based substrates," *ACS Appl. Mater. Interfaces*, vol. 7, no. 3, pp. 1644–1651, 2015.

[226] G. Feng, Y. Cheng, S.-Y. Wang, D. A. Borca-Tasciuc, R. W. Worobo, and C. I. Moraru, "Bacterial attachment and biofilm formation on surfaces are reduced by small-diameter nanoscale pores: how small is small enough?," *Npj Biofilms And Microbiomes*, vol. 1, p. 15022, 2015.

[227] A. Bhattacharjee, M. Khan, M. Kleiman, and A. I. Hochbaum, "Effects of growth surface topography on bacterial signaling in coculture biofilms," *ACS Appl. Mater. Interfaces*, vol. 9, no. 22, pp. 18531–18539, 2017.

[228] B. Derjaguin and L. Landau, "Theory of the stability of strongly charged lyophobic sols and of the adhesion of strongly charged particles in solutions of electrolytes," *Acta physicochimica URSS*, vol. 14, pp. 633–662, 1941.

[229] J. H. Adair, E. Suvaci, and J. Sindel, "Surface and colloid chemistry," in *Encyclopedia of Materials: Science and Technology*, K. H. J. Buschow, R. W. Cahn, M. C. Flemings, B. Ilschner, E. J. Kramer, S. Mahajan, and P. Veyssière, Eds. Oxford: Elsevier, 2001, pp. 1–10.

[230] S. Perni, E. C. Preedy, and P. Prokopovich, "Success and failure of colloidal approaches in adhesion of microorganisms to surfaces," *Advances in Colloid and Interface Science*, vol. 206, pp. 265–274, 2014.

[231] M. J. Salas-Jara, E. A. Sanhueza, A. Retamal-Díaz, C. González, H. Urrutia, and A. García, "Probiotic *Lactobacillus fermentum* UCO-979C biofilm formation on AGS and Caco-2 cells and *Helicobacter pylori* inhibition," *Biofouling*, vol. 32, no. 10, pp. 1245–1257, 2016.

[232] N. Aoudia *et al.*, "Biofilms of *Lactobacillus plantarum* and *Lactobacillus fermentum*: Effect on stress responses, antagonistic effects on pathogen growth and immunomodulatory properties," *Food Microbiology*, vol. 53, pp. 51–59, 2016.

[233] M. J. McShane and Y. M. Lvov, "Electrostatic self-assembly: layer-by-layer," in *Dekker Encyclopedia of Nanoscience and Nanotechnology, Third Edition*, Marcel Dekker, Inc., J.A. Schwarz, S.E. Lyshevski, C.I. Contescu, 2014.

[234] *Layer-by-Layer Films for Biomedical Applications*, Wiley-VCH Verlag GmbH & Co. KGaA. C. Picart, F. Caruso J.-C. Voegel, 2015.

[235] D. Gundogdu, V. Bütün, and I. Erel-Göktepe, "Preparation of layer-by-layer films with remarkably different pH-stability and release properties using dual responsive block copolymer micelles," *Macromolecular Chemistry and Physics*, vol. 219, no. 15, p. 1800128, 2018.

[236] R. W. Hutkins and N. L. Nannen, "pH Homeostasis in lactic acid bacteria," *Journal of Dairy Science*, vol. 76, no. 8, pp. 2354–2365, 1993.

[237] S. A. Hussain, B. Dey, D. Bhattacharjee, and N. Mehta, "Unique supramolecular assembly through Langmuir – Blodgett (LB) technique," *Heliyon*, vol. 4, no. 12, p. e01038, 2018.

[238] D. Y. Takamoto *et al.*, "Stable Ordering in Langmuir-Blodgett Films," *Science*, vol. 293, no. 5533, p. 1292, 2001.

[239] O. Freudenthal *et al.*, "Nanoscale investigation of the interaction of colistin with model phospholipid membranes by Langmuir technique, and combined infrared and force spectroscopies," *Biochimica et Biophysica Acta (BBA) - Biomembranes*, vol. 1858, no. 11, pp. 2592–2602, 2016.

[240] N. Kumar, L. Wang, I. Siretanu, M. Duits, and F. Mugele, "Salt dependent stability of stearic acid Langmuir–Blodgett films exposed to aqueous electrolytes," *Langmuir*, vol. 29, no. 17, pp. 5150–5159, 2013.

[241] S.-S. Feng, K. Gong, and J. Chew, "Molecular interactions between a lipid and an antineoplastic drug Paclitaxel (Taxol) within the lipid monolayer at the air/water interface," *Langmuir*, vol. 18, no. 10, pp. 4061–4070, 2002.

[242] J. B. Brzoska, I. B. Azouz, and F. Rondelez, "Silanization of solid substrates: a step toward reproducibility," *Langmuir*, vol. 10, no. 11, pp. 4367–4373, 1994.

[243] J. Böhmler, A. Ponche, K. Anselme, and L. Ploux, "Self-assembled molecular platforms for bacteria/material biointerface studies: importance to control functional group accessibility," *ACS Appl. Mater. Interfaces*, vol. 5, no. 21, pp. 10478–10488, 2013.

[244] A. R. Yadav, R. Sriram, J. A. Carter, and B. L. Miller, "Comparative study of solution-phase and vapor-phase deposition of aminosilanes on silicon dioxide surfaces," *Mater Sci Eng C Mater Biol Appl*, vol. 35, pp. 283–290, 2014.

[245] J. C. Love, L. A. Estroff, J. K. Kriebel, R. G. Nuzzo, and G. M. Whitesides, "Self-assembled monolayers of thiolates on metals as a form of nanotechnology," *Chem. Rev.*, vol. 105, no. 4, pp. 1103–1170, 2005.

[246] M. Kind and C. Wöll, "Organic surfaces exposed by self-assembled organothiol monolayers: Preparation, characterization, and application," *Progress in Surface Science*, vol. 84, no. 7–8, pp. 230–278, 2009.

[247] C. D. Bain, E. B. Troughton, Y. T. Tao, J. Evall, G. M. Whitesides, and R. G. Nuzzo, "Formation of monolayer films by the spontaneous assembly of organic thiols from solution onto gold," *J. Am. Chem. Soc.*, vol. 111, no. 1, pp. 321–335, 1989.

[248] C. Vericat, M. E. Vela, G. Benitez, P. Carro, and R. C. Salvarezza, "Self-assembled monolayers of thiols and dithiols on gold: new challenges for a well-known system," *Chem. Soc. Rev.*, vol. 39, no. 5, pp. 1805–1834, 2010.

[249] L. G. Dubois and R. G. Nuzzo, "Synthesis, structure, and properties of model organic surfaces," *Annual Review of Physical Chemistry*, vol. 43, no. 1, pp. 437–463, 1992.

[250] A. Ulman, "Formation and structure of self-assembled monolayers," *Chem. Rev.*, vol. 96, no. 4, pp. 1533–1554, 1996.

[251] G. M. Whitesides and P. E. Laibinis, "Wet chemical approaches to the characterization of organic surfaces: self-assembled monolayers, wetting, and the physical-organic chemistry of the solid-liquid interface," *Langmuir*, vol. 6, no. 1, pp. 87–96, 1990.

[252] D. K. Schwartz, "Mechanisms and kinetics of self-assembled monolayer formation," *Annu. Rev. Phys. Chem.*, vol. 52, no. 1, pp. 107–137, 2001.

[253] G. Yang and G. Liu, "New insights for self-assembled monolayers of organothiols on Au(111) revealed by scanning tunneling microscopy," *J. Phys. Chem. B*, vol. 107, no. 34, pp. 8746–8759, 2003.

[254] G. E. Poirier, "Characterization of organosulfur molecular monolayers on Au(111) using scanning tunneling microscopy," *Chem. Rev.*, vol. 97, no. 4, pp. 1117–1128, 1997.

[255] L. J. Cristina, G. Ruano, R. Salvarezza, and J. Ferrón, "Thermal stability of self-assembled monolayers of n-Hexanethiol on Au(111)-(1 × 1) and Au(001)-(1 × 1)," *J. Phys. Chem. C*, vol. 121, no. 50, pp. 27894–27904, 2017.

[256] H. Wang, S. Chen, L. Li, and S. Jiang, "Improved method for the preparation of carboxylic acid and amine terminated self-assembled monolayers of alkanethiolates," *Langmuir*, vol. 21, no. 7, pp. 2633–2636, 2005.

[257] A. R. Noble-Luginbuhl and R. G. Nuzzo, "Assembly and characterization of SAMs formed by the adsorption of alkanethiols on zinc selenide substrates," *Langmuir*, vol. 17, no. 13, pp. 3937–3944, 2001.

[258] T. M. McIntire, O. Ryder, and B. J. Finlayson-Pitts, "Secondary ozonide formation from the ozone oxidation of unsaturated self-assembled monolayers on zinc selenide Attenuated Total Reflectance crystals," *J. Phys. Chem. C*, vol. 113, no. 25, pp. 11060–11065, 2009.

[259] K. M. Wiencek and M. Fletcher, "Effects of substratum wettability and molecular topography on the initial adhesion of bacteria to chemically defined substrata," *Biofouling*, vol. 11, no. 4, pp. 293–311, 1997.

[260] B. Stuart, *Infrared spectroscopy : fundamentals and applications*. Chichester, West Sussex, England ; Hoboken, NJ : J. Wiley, 2004.

[261] F. Humbert and F. Quilès, "In-situ study of early stages of biofilm formation under different environmental stresses by ATR-FTIR spectroscopy," in *Science against microbial pathogens: communicating current research and technological advances*, Méndez-Vilas A., 2011.

[262] E. K. Plyler, "Infrared spectra of methanol, ethanol, and n-propanol," *Journal of Research of the National Bureau of Standards*, vol. 48, no. 4, p. Research Paper: 2314, 1952.

[263] J. P. Maity *et al.*, "Identification and discrimination of bacteria using Fourier transform infrared spectroscopy," *Spectrochimica Acta Part A: Molecular and Biomolecular Spectroscopy*, vol. 116, pp. 478–484, 2013.

[264] Y. Yuan and T. R. Lee, "Contact angle and wetting properties," in *Surface Science Techniques*, G. Bracco and B. Holst, Eds. Berlin, Heidelberg: Springer Berlin Heidelberg, 2013, pp. 3–34.

[265] "KRÜSS Technical Note: So you want to measure surface energy? Models for surface free energy calculation. https://www.kruss-scientific.com/services/education-theory/literature/application-reports/.

[266] F. M. Fowkes, "Additivity of intermolecular forces at intefaces. I. Determination of the contribution to surface and interfacial tensions of dispersion forces in vatious liquids," *J. Phys. Chem.*, vol. 67, no. 12, pp. 2538–2541, 1963.

[267] W.-K. Chu, J. W. Mayer, and M.-A. Nicolet, "Chapter 1 - Introduction," in *Backscattering Spectrometry*, W.-K. Chu, J. W. Mayer, and M.-A. Nicolet, Eds. Academic Press, 1978, pp. 1–20.

[268] M. Mayer, "Improved physics in SIMNRA 7," *Nuclear Instruments and Methods in Physics Research Section B: Beam Interactions with Materials and Atoms*, vol. 332, pp. 176–180, 2014.

[269] A. T. Demissie, G. Haugstad, and C. D. Frisbie, "Quantitative surface coverage measurements of self-assembled monolayers by Nuclear Reaction Analysis of Carbon-12," *J. Phys. Chem. Lett.*, vol. 7, no. 17, pp. 3477–3481, 2016.

[270] J. Mayer, L. A. Giannuzzi, T. Kamino, and J. Michael, "TEM sample preparation and FIB-induced damage," *MRS Bulletin*, vol. 32, no. 5, pp. 400–407, 2007.

[271] P. Tripathi *et al.*, "Towards a nanoscale view of lactic acid bacteria," *Micron*, vol. 43, no. 12, pp. 1323–1330, 2012.

[272] J. B. Kaper, J. P. Nataro, and H. L. T. Mobley, "Pathogenic *Escherichia coli*," *Nature Reviews Microbiology*, vol. 2, no. 2, pp. 123–140, 2004.

[273] L. A. Pratt and R. Kolter, "Genetic analysis of *Escherichia coli* biofilm formation: roles of flagella, motility, chemotaxis and type I pili," *Molecular Microbiology*, vol. 30, no. 2, pp. 285–293, 1998.

[274] De Man J. C., Rogosa M., and Sharpe M. Elisabeth, "A medium for the cultivation of Lactobacilli," *Journal of Applied Bacteriology*, vol. 23, no. 1, pp. 130–135, 1960.

[275] F. Quilès and F. Humbert, "On the production of glycogen by *Pseudomonas fluorescens* during biofilm development: an in situ study by attenuated total reflection-infrared with chemometrics," *Biofouling*, vol. 30, no. 6, pp. 709–718, 2014.

[276] "ThermoFisher Scientific. Fluorescence SpectraViewer. https://www.thermofisher.com/fr/en/home/life-science/cell-analysis/labeling-chemistry/fluorescence-spectraviewer.html." .

[277] B. M. Corcoran, C. Stanton, G. F. Fitzgerald, and R. P. Ross, "Survival of probiotic Lactobacilli in acidic environments is enhanced in the presence of metabolizable sugars," *Appl. Environ. Microbiol.*, vol. 71, no. 6, p. 3060, 2005.

[278] G. Cassanas, M. Morssli, E. Fabrègue, and L. Bardet, "Vibrational spectra of lactic acid and lactates," *Journal of Raman Spectroscopy*, vol. 22, no. 7, pp. 409–413, 1991.

[279] P. J. Bremer and G. G. Geesey, "An evaluation of biofilm development utilizing non-destructive attenuated total reflectance Fourier transform infrared spectroscopy," *Biofouling*, vol. 3, no. 2, pp. 89–100, 1991.

[280] A. R. Berry, C. M. M. Franco, W. Zhang, and A. P. J. Middelberg, "Growth and lactic acid production in batch culture of *Lactobacillus rhamnosus* in a defined medium," *Biotechnology Letters*, vol. 21, no. 2, pp. 163–167, 1999.

[281] V. Bottazzi, "An introduction to rod-shaped lactic-acid bacteria," *Biochimie*, vol. 70, no. 3, pp. 303–315, 1988.

[282] T. F. Cálix-Lara, T. Duong, and T. M. Taylor, "Addition of a surfactant to tryptic soy broth allows growth of a Lactic Acid Bacteria food antimicrobial, *Escherichia coli* O157:H7, and *Salmonella enterica*," *Letters in Applied Microbiology*, vol. 54, no. 5, pp. 392–397, 2012.

[283] H. Siegumfeldt, K. Björn Rechinger, and M. Jakobsen, "Dynamic changes of intracellular pH in individual lactic acid bacterium cells in response to a rapid drop in extracellular pH," *Applied and Environmental Microbiology*, vol. 66, no. 6, pp. 2330–2335, 2000.

[284] S. Lebeer *et al.*, "Identification of a gene cluster for the biosynthesis of a long, galactose-rich exopolysaccharide in *Lactobacillus rhamnosus* GG and functional analysis of the priming glycosyltransferase," *Appl Environ Microbiol*, vol. 75, no. 11, pp. 3554–3563, 2009.

[285] K. D. Young, "The Selective value of bacterial shape," *Microbiology and Molecular Biology Reviews*, vol. 70, no. 3, pp. 660–703, 2006.

[286] C. J. Ingham, M. Beerthuyzen, and J. van Hylckama Vlieg, "Population heterogeneity of *Lactobacillus plantarum* WCFS1 microcolonies in response to and recovery from acid stress," *Applied and environmental microbiology*, vol. 74, no. 24, pp. 7750–7758, 2008.

[287] D. C. Yang, K. M. Blair, and N. R. Salama, "Staying in shape: the impact of cell shape on bacterial survival in diverse environments," *Microbiol. Mol. Biol. Rev.*, vol. 80, no. 1, p. 187, 2016.

[288] E. Cefalì *et al.*, "Morphologic variations in bacteria under stress conditions: Near- field optical studies," *Scanning*, vol. 24, no. 6, pp. 274–283, 2002.

[289] A.-C. Chien, N. S. Hill, and P. A. Levin, "Cell size control in bacteria," *Current Biology*, vol. 22, no. 9, pp. R340–R349, 2012.

[290] A. Typas, M. Banzhaf, C. A. Gross, and W. Vollmer, "From the regulation of peptidoglycan synthesis to bacterial growth and morphology," *Nature Reviews Microbiology*, vol. 10, p. 123, 2011.

[291] A. J. F. Egan, R. M. Cleverley, K. Peters, R. J. Lewis, and W. Vollmer, "Regulation of bacterial cell wall growth," *The FEBS Journal*, vol. 284, no. 6, pp. 851–867, 2016.

[292] L. Liu, G. Lindauer, W. B. Alexander, and P. H. Holloway, "Surface preparation of ZnSe by chemical methods," *Journal of Vacuum Science & Technology B: Microelectronics and Nanometer Structures Processing, Measurement, and Phenomena*, vol. 13, no. 6, pp. 2238–2244, 1995.

[293] A. Kita, M. Ozawa, and C. D. Gutleben, "XPS analysis of chemically etched II–VI semiconductor surfaces," *Applied Surface Science*, vol. 100, pp. 652–655, 1996.

[294] M. W. Cho *et al.*, "Surface treatment of znse substrate and homoepitaxy of znse," *Journal of Electronic Materials*, vol. 26, no. 5, pp. 423–428, 1997.

[295] T. F. McGee and H. J. Cornelissen, "X-ray photoelectron spectroscopy of etched ZnSe," *Applied Surface Science*, vol. 35, no. 3, pp. 371–379, 1989.

[296] J. L. Meléndez and C. R. Helms, "Wet chemical cleaning and surface analysis of ZnSe," *Journal of The Electrochemical Society*, vol. 141, no. 7, pp. 1973–1976, 1994.

[297] *The crystran handbook of infra-red and ultra-violet optical materials*. Crystran Ltd, 2016.

[298] H. Gong, H. Huang, L. Ding, M. Wang, and K. Liu, "Characterization and optical properties of ZnSe prepared by hydrothermal method," *Journal of Crystal Growth*, vol. 288, no. 1, pp. 96–99, 2006.

[299] S. Joshi, P. Pellacani, T. A. van Beek, H. Zuilhof, and M. W. F. Nielen, "Surface characterization and antifouling properties of nanostructured gold chips for imaging surface plasmon resonance biosensing," *Sensors and Actuators B: Chemical*, vol. 209, pp. 505–514, 2015.

[300] W. Shen *et al.*, "Blocking agent optimization for nonspecific binding on phage based magnetoelastic biosensors," *Journal of The Electrochemical Society*, vol. 159, no. 10, pp. B818–B823, 2012.

[301] Z. Hussain, M. A. Salim, M. A. Khan, and E. E. Khawaja, "X-ray photoelectron and auger spectroscopy study of copper-sodium-germanate glasses," *Journal of Non-Crystalline Solids*, vol. 110, no. 1, pp. 44–52, 1989.

[302] R. G. Greenler, "Infrared study of adsorbed molecules on metal surfaces by reflection techniques," *J. Chem. Phys.*, vol. 44, no. 1, pp. 310–315, 1966.

[303] S. Brown, J. P. Santa Maria Jr, and S. Walker, "Wall teichoic acids of gram-positive bacteria," *Annu Rev Microbiol*, vol. 67, pp. 313–336, 2013.

[304] V. Lacour, K. Moumanis, W. M. Hassen, C. Elie-Caille, T. Leblois, and J. J. Dubowski, "Formation kinetics of mixed self-assembled monolayers of alkanethiols on GaAs(100)," *Langmuir*, vol. 35, no. 13, pp. 4415–4427, 2019.

[305] M. R. Kosuri, R. Cone, Q. Li, S. M. Han, B. C. Bunker, and T. M. Mayer, "Adsorption kinetics of 1-alkanethiols on hydrogenated Ge(111)," *Langmuir*, vol. 20, no. 3, pp. 835–840, 2004.

[306] S. S. Cheng, D. A. Scherson, and C. N. Sukenik, "In situ observation of monolayer self-assembly by FTIR/ATR," *J. Am. Chem. Soc.*, vol. 114, no. 13, pp. 5436–5437, 1992.

[307] N. Goutev and M. Futamata, "Attenuated Total Reflection Surface-Enhanced Infrared Absorption Spectroscopy of carboxyl terminated self-assembled monolayers on gold," *Appl Spectrosc*, vol. 57, no. 5, pp. 506–513, 2003.

[308] M. D. Porter, T. B. Bright, D. L. Allara, and C. E. D. Chidsey, "Spontaneously organized molecular assemblies. 4. Structural characterization of n-alkyl thiol monolayers on gold by optical ellipsometry, infrared spectroscopy, and electrochemistry," *J. Am. Chem. Soc.*, vol. 109, no. 12, pp. 3559–3568, 1987.

[309] R. Arnold, W. Azzam, A. Terfort, and C. Wöll, "Preparation, modification, and crystallinity of aliphatic and aromatic carboxylic acid terminated self-assembled monolayers," *Langmuir*, vol. 18, no. 10, pp. 3980–3992, 2002.

[310] M. I. Béthencourt, L. Srisombat, P. Chinwangso, and T. R. Lee, "SAMs on gold derived from the direct adsorption of alkanethioacetates are inferior to those derived from the direct adsorption of alkanethiols," *Langmuir*, vol. 25, no. 3, pp. 1265–1271, 2009.

[311] M. R. Anderson, M. N. Evaniak, and M. Zhang, "Influence of solvent on the interfacial structure of self-assembled alkanethiol monolayers," *Langmuir*, vol. 12, no. 10, pp. 2327–2331, 1996.

[312] Sabina Hillebrandt, Tobias Glaser, and Annemarie Pucci, "Investigation of self-assembled monolayer formation using infrared-reflection-absorption-spectroscopy," presented at the Proc.SPIE, 2014, vol. 9137.

[313] T. Baum, S. Ye, and K. Uosaki, "Formation of self-assembled monolayers of alkanethiols on GaAs surface with in situ surface activation by ammonium hydroxide," *Langmuir*, vol. 15, no. 25, pp. 8577–8579, 1999.

[314] A. Urakawa, T. Buergi, and A. Baiker, "Modulation Excitation PM-IRRAS: a new possibility for simultaneous monitoring of surface and gas species and surface properties," *Chimia*, vol. 60, no. 4, pp. 231–233, 2006.

[315] J. Zhao, M. H. Na, E. H. Lee, H. C. Chang, J. A. Gardella, and H. Luo, "Surface chemistry of II–VI semiconductor ZnSe studied by time of flight secondary ion mass spectrometry and x-ray photoelectron spectroscopy," *Journal of Vacuum Science & Technology B: Microelectronics and Nanometer Structures Processing, Measurement, and Phenomena*, vol. 16, no. 6, pp. 3048–3054, 1998.

[316] S. Skoglund, J. Hedberg, E. Yunda, A. Godymchuk, E. Blomberg, and I. Odnevall Wallinder, "Difficulties and flaws in performing accurate determinations of zeta potentials of metal nanoparticles in complex solutions—Four case studies," *PLOS ONE*, vol. 12, no. 7, p. e0181735, 2017.

[317] M. Shenasa, S. Sainkar, and D. Lichtman, "XPS study of some selected selenium compounds," *Journal of Electron Spectroscopy and Related Phenomena*, vol. 40, no. 4, pp. 329–337, 1986.

[318] M. Hövel, B. Gompf, and M. Dressel, "Dielectric properties of ultrathin metal films around the percolation threshold," *Phys. Rev. B*, vol. 81, no. 3, p. 035402, 2010.

[319] B. Gompf, J. Beister, T. Brandt, J. Pflaum, and M. Dressel, "Nanometer-thick Au-films as antireflection coating for infrared light," *Opt. Lett.*, vol. 32, no. 11, pp. 1578–1580, 2007.

[320] A. Klimovskaya, A. Sarikov, Y. Pedchenko, A. Voroshchenko, O. Lytvyn, and A. Stadnik, "Study of the formation processes of gold droplet arrays on Si substrates by high temperature anneals," *Nanoscale Res Lett*, vol. 6, no. 1, pp. 151–151, 2011.

[321] E. N. Aybeke, Y. Lacroute, C. Elie-Caille, A. Bouhelier, E. Bourillot, and E. Lesniewska, "Homogeneous large-scale crystalline nanoparticle-covered substrate with high SERS performance," *Nanotechnology*, vol. 26, no. 24, p. 245302, 2015.

[322] K. Ataka, S. T. Stripp, and J. Heberle, "Surface-enhanced infrared absorption spectroscopy (SEIRAS) to probe monolayers of membrane proteins," *Biochimica et Biophysica Acta (BBA) - Biomembranes*, vol. 1828, no. 10, pp. 2283–2293, 2013.

[323] S. Lortal, M. Rousseau, P. Boyaval, and J. Van Heijenoort, "Cell wall and autolytic system of Lactobacillus helveticus ATCC 12046," *Microbiology*, vol. 137, no. 3, pp. 549–559, 1991.

[324] M. Bieri and T. Bürgi, "Adsorption kinetics, orientation, and self-assembling of N-Acetyl-l-cysteine on gold: a combined ATR-IR, PM-IRRAS, and QCM Study," *J. Phys. Chem. B*, vol. 109, no. 47, pp. 22476–22485, 2005.

[325] P. Tripathi *et al.*, "Adhesion and nanomechanics of pili from the probiotic *Lactobacillus rhamnosus* GG," *ACS Nano*, vol. 7, no. 4, pp. 3685–3697, 2013.

[326] Q. Wang and T. J. Webster, "Nanostructured selenium for preventing biofilm formation on polycarbonate medical devices," *Journal of Biomedical Materials Research Part A*, vol. 100A, no. 12, pp. 3205–3210, 2012.

[327] S. Kesel, A. Mader, P. H. Seeberger, O. Lieleg, and M. Opitz, "Carbohydrate coating reduces adhesion of biofilm-forming *Bacillus subtilis* to gold surfaces," *Appl. Environ. Microbiol.*, vol. 80, no. 19, p. 5911, 2014.

[328] M. Jarosz *et al.*, "Novel bioelectrodes based on polysaccharide modified gold surfaces and electrochemically active *Lactobacillus rhamnosus* GG biofilms," *Electrochimica Acta*, vol. 296, pp. 999–1008, 2019.

[329] J.-Y. Maillard, "Bacterial target sites for biocide action," *Journal of Applied Microbiology*, vol. 92, no. s1, pp. 16S-27S, 2002.

[330] P. Maris, "Modes of action of disinfectants," *Scientific and Technical Review of the Office International des Epizooties (Paris)*, vol. 14, no. 1, pp. 47–55, 1995.

[331] C. P. Gerba, "Quaternary ammonium biocides: efficacy in application," *Appl. Environ. Microbiol.*, vol. 81, no. 2, p. 464, 2015.

[332] K. P. Fears, S. E. Creager, and R. A. Latour, "Determination of the surface pK of carboxylic- and amine-terminated alkanethiols using surface plasmon resonance spectroscopy," *Langmuir*, vol. 24, no. 3, pp. 837–843, 2008.

[333] T. H. Degefa, P. Schön, D. Bongard, and L. Walder, "Elucidation of the electron transfer mechanism of marker ions at SAMs with charged head groups," *Journal of Electroanalytical Chemistry*, vol. 574, no. 1, pp. 49–62, 2004.

[334] J. te Riet *et al.*, "AFM topography and friction studies of hydrogen-bonded bilayers of functionalized alkanethiols," *Soft Matter*, vol. 6, no. 15, pp. 3450–3454, 2010.

[335] D. Enders, T. Nagao, A. Pucci, T. Nakayama, and M. Aono, "Surface-enhanced ATR-IR spectroscopy with interface-grown plasmonic gold-island films near the percolation threshold," *Phys. Chem. Chem. Phys.*, vol. 13, no. 11, pp. 4935–4941, 2011.

[336] F. Quilès, F. Humbert, and A. Delille, "Analysis of changes in attenuated total reflection FTIR fingerprints of *Pseudomonas fluorescens* from planktonic state to nascent biofilm state," *Spectrochimica Acta Part A: Molecular and Biomolecular Spectroscopy*, vol. 75, no. 2, pp. 610–616, 2010.

[337] S.-Y. Kang, P. J. Bremer, K.-W. Kim, and A. J. McQuillan, "Monitoring metal ion binding in single-layer *Pseudomonas aeruginosa* biofilms using ATR−IR spectroscopy," *Langmuir*, vol. 22, no. 1, pp. 286–291, 2006.

[338] M. C. Leccese Terraf, M. S. Juárez Tomás, L. Rault, Y. Le Loir, S. Even, and M. E. F. Nader-Macías, "Biofilms of vaginal *Lactobacillus reuteri* CRL 1324 and *Lactobacillus rhamnosus* CRL 1332: kinetics of formation and matrix characterization," *Archives of Microbiology*, vol. 198, no. 7, pp. 689–700, 2016.

[339] H. Czerski, "Small is beautiful: Surface tension and viscosity," in *Storm in a Teacup: The Physics of Everyday Life*, Penguin Random House UK, 2016, pp. 83–85.

[340] M. V. Zubkov, B. M. Fuchs, H. Eilers, P. H. Burkill, and R. Amann, "Determination of total protein content of bacterial cells by SYPRO staining and flow cytometry," *Appl. Environ. Microbiol.*, vol. 65, no. 7, p. 3251, 1999.

[341] J. te Riet *et al.*, "Molecular friction as a tool to identify functionalized alkanethiols," *Langmuir*, vol. 26, no. 9, pp. 6357–6366, 2010.

[342] M. M. T. Khan, L. K. Ista, G. P. Lopez, and A. J. Schuler, "Experimental and theoretical examination of surface energy and adhesion of nitrifying and heterotrophic bacteria using self-assembled monolayers," *Environ. Sci. Technol.*, vol. 45, no. 3, pp. 1055–1060, 2011.

[343] Y. Arima and H. Iwata, "Effects of surface functional groups on protein adsorption and subsequent cell adhesion using self-assembled monolayers," *J. Mater. Chem.*, vol. 17, no. 38, pp. 4079–4087, 2007.

[344] B. Berron and G. K. Jennings, "Loosely packed hydroxyl-terminated SAMs on gold," *Langmuir*, vol. 22, no. 17, pp. 7235–7240, 2006.

[345] D. R. Absolom, F. V. Lamberti, Z. Policova, W. Zingg, C. J. van Oss, and A. W. Neumann, "Surface thermodynamics of bacterial adhesion.," *Appl. Environ. Microbiol.*, vol. 46, no. 1, p. 90, 1983.

[346] M. R. Alexander and P. Williams, "Water contact angle is not a good predictor of biological responses to materials," *Biointerphases*, vol. 12, no. 2, p. 02C201, 2017.

[347] R. Kügler, O. Bouloussa, and F. Rondelez, "Evidence of a charge-density threshold for optimum efficiency of biocidal cationic surfaces," *Microbiology*, vol. 151, no. 5, pp. 1341–1348, 2005.

[348] A. M. Bieser and J. C. Tiller, "Mechanistic considerations on contact-active antimicrobial surfaces with controlled functional group densities," *Macromolecular Bioscience*, vol. 11, no. 4, pp. 526–534, 2011.

[349] A. Beaussart *et al.*, "Single-cell force spectroscopy of probiotic bacteria," *Biophys J*, vol. 104, no. 9, pp. 1886–1892, 2013.

[350] M. V. Riquelme, H. Zhao, V. Srinivasaraghavan, A. Pruden, P. Vikesland, and M. Agah, "Optimizing blocking of nonspecific bacterial attachment to impedimetric biosensors," *Sensing and Bio-Sensing Research*, vol. 8, pp. 47–54, 2016.

[351] R. Konradi, B. Pidhatika, A. Mühlebach, and M. Textor, "Poly-2-methyl-2-oxazoline: a peptide-like polymer for protein-repellent surfaces," *Langmuir*, vol. 24, no. 3, pp. 613–616, 2008.

[352] M. Heuberger, T. Drobek, and N. D. Spencer, "Interaction forces and morphology of a protein-resistant Poly(ethylene glycol) layer," *Biophysical Journal*, vol. 88, no. 1, pp. 495–504, 2005.

[353] I. Connell, W. Agace, P. Klemm, M. Schembri, S. Mărild, and C. Svanborg, "Type 1 fimbrial expression enhances *Escherichia coli* virulence for the urinary tract," *Proc Natl Acad Sci U S A*, vol. 93, no. 18, pp. 9827–9832, 1996.

[354] T. K. Wood, "Insights on *Escherichia coli* biofilm formation and inhibition from whole-transcriptome profiling," *Environ Microbiol*, vol. 11, no. 1, pp. 1–15, 2009.

[355] A. F. González Barrios, R. Zuo, Y. Hashimoto, L. Yang, W. E. Bentley, and T. K. Wood, "Autoinducer 2 controls biofilm formation in *Escherichia coli* through a novel motility quorum-sensing regulator (MqsR, B3022)," *J Bacteriol*, vol. 188, no. 1, pp. 305–316, 2006.

[356] M. Guo, S. Gamby, Y. Zheng, and H. O. Sintim, "Small molecule inhibitors of AI-2 signaling in bacteria: state-of-the-art and future perspectives for anti-quorum sensing agents," *Int J Mol Sci*, vol. 14, no. 9, pp. 17694–17728, 2013.

[357] K. B. Xavier and B. L. Bassler, "Regulation of uptake and processing of the quorum-sensing autoinducer AI-2 in *Escherichia coli*," *J Bacteriol*, vol. 187, no. 1, pp. 238–248, 2005.

[358] G. Aidelberg, B. D. Towbin, D. Rothschild, E. Dekel, A. Bren, and U. Alon, "Hierarchy of non-glucose sugars in *Escherichia coli*," *BMC Syst Biol*, vol. 8, pp. 133–133, 2014.

[359] C. Holm and L. Jespersen, "A flow-cytometric gram-staining technique for milk-associated bacteria," *Appl Environ Microbiol*, vol. 69, no. 5, pp. 2857–2863, 2003.

[360] D. J. Mason, S. Shanmuganathan, F. C. Mortimer, and V. A. Gant, "A fluorescent Gram stain for flow cytometry and epifluorescence microscopy," *Appl Environ Microbiol*, vol. 64, no. 7, pp. 2681–2685, 1998.

[361] A. H. P. Anvarian, Y. Cao, S. Srikumar, S. Fanning, and K. Jordan, "Flow cytometric and 16S sequencing methodologies for monitoring the physiological status of the microbiome in powdered infant formula production," *Front Microbiol*, vol. 7, pp. 968–968, Jun. 2016.

[362] J. D. Durtschi *et al.*, "Increased sensitivity of bacterial detection in cerebrospinal fluid by fluorescent staining on low-fluorescence membrane filters," *Journal of Medical Microbiology*, vol. 54, no. 9, pp. 843–850, 2005.

[363] A. I. Lopez, A. Kumar, M. R. Planas, Y. Li, T. V. Nguyen, and C. Cai, "Biofunctionalization of silicone polymers using poly(amidoamine) dendrimers and a mannose derivative for prolonged interference against pathogen colonization," *Biomaterials*, vol. 32, no. 19, pp. 4336–4346, 2011.